PB-239 618

AN EXPERIMENTAL HIGH ASH PAPERMILL SLUDGE LANDFILL

SECOND ANNUAL REPORT

MICHIGAN STATE UNIVERSITY

PREPARED FOR
NATIONAL ENVIRONMENTAL RESEARCH CENTER

DECEMBER 1974

DISTRIBUTED BY:
NTIS
National Technical Information Service
U. S. DEPARTMENT OF COMMERCE

PB-239 618

071179

EPA-670/2-74-076b
December 1974

AN EXPERIMENTAL HIGH ASH PAPERMILL SLUDGE LANDFILL

Second Annual Report

By

O. B. Andersland, Wayne A. Charlie, and Robert P. Vallee
Division of Engineering Research
Michigan State University
East Lansing, Michigan 48824

Duane W. Marshall
National Council of the Paper Industry for
Air and Stream Improvement, Inc.
New York, New York 10016

Program Element No. 1DB064
Grant No. R-801282

Project Officer

Norbert B. Schomaker
Solid and Hazardous Waste Research Laboratory
National Environmental Research Center
Cincinnati, Ohio 45268

Reproduced by
NATIONAL TECHNICAL
INFORMATION SERVICE
US Department of Commerce
Springfield, VA. 22151

NATIONAL ENVIRONMENTAL RESEARCH CENTER
OFFICE OF RESEARCH AND DEVELOPMENT
U.S. ENVIRONMENTAL PROTECTION AGENCY
CINCINNATI, OHIO 45268

TECHNICAL REPORT DATA

(Please read Instructions on the reverse before completing)

1. REPORT NO. EPA-670/2-74-076b	2.	3. PB 239 618
4. TITLE AND SUBTITLE AN EXPERIMENTAL HIGH ASH PAPERMILL SLUDGE LANDFILL: Second Annual Report		5. REPORT DATE December 1974-Issuing Date 6. PERFORMING ORGANIZATION CODE
7. AUTHOR(S) O. B. Andersland, Wayne A. Charlie, Robert P. Vallee, and Duane W. Marshall		8. PERFORMING ORGANIZATION REPORT NO.
9. PERFORMING ORGANIZATION NAME AND ADDRESS Division of Engineering Research Michigan State University East Lansing, Michigan 48824		10. PROGRAM ELEMENT NO. 1DB064; ROAP 24ALH;Task02 11. ~~CONTRACT/~~GRANT NO. R-801282
12. SPONSORING AGENCY NAME AND ADDRESS National Environmental Research Center Office of Research and Developnent U. S. Environmental Protection Agency Cincinnati, Ohio 45268		13. TYPE OF REPORT AND PERIOD COVERED Final 14. SPONSORING AGENCY CODE

15. SUPPLEMENTARY NOTES

See "AN EXPERIMENTAL HIGH ASH PAPERMILL SLUDGE LANDFILL: First Annual Report," EPA-670/2-74-076a.

16. ABSTRACT

The second annual report investigated slope stability by removal of one dike from the sludge landfill. The landfill was excavated to form a 3:4 slope and trimmed to 1:8 slope. Prior to construction, vane shear strength and Dutch cone resistance data were obtained. Slope indicator and piezometers were installed. Laboratory studies and analysis were also conducted. Leachate sampling and analysis documented changes occurring during the project period.

Reproduced by
NATIONAL TECHNICAL
INFORMATION SERVICE
US Department of Commerce
Springfield, VA. 22151

17. KEY WORDS AND DOCUMENT ANALYSIS

a. DESCRIPTORS	b. IDENTIFIERS/OPEN ENDED TERMS	c. COSATI Field/Group
Lysimeters Sludge Leaching Papermills Soils Soil mechanics	Sludge landfill Solid waste management Landfill	13B

PRICES SUBJECT TO CHANGE

18. DISTRIBUTION STATEMENT Release to Public	19. SECURITY CLASS *(This Report)* Unclassified	21. NO. OF PAGES 247
	20. SECURITY CLASS *(This page)* Unclassified	22. PRICE 7.50 - 2.25

i.

EPA Form 2220-1 (9-73)

REVIEW NOTICE

The National Environmental Research Center--Cincinnati has reviewed this report and approved its publication. Approval does not signify that the contents necessarily reflect the views and policies of the U.S. Environmental Protection Agency, nor does mention of trade names or commercial products constitute endorsement or recommendation for use.

FOREWORD

Man and his environment must be protected from the adverse effects of pesticides, radiation, noise and other forms of pollution, and the unwise management of solid waste. Efforts to protect the environment require a focus that recognizes the interplay between the components of our physical environment--air, water, and land. The National Environmental Research Centers provide this multidisciplinary focus through programs engaged in

- studies on the effects of environmental contaminants on man and the biosphere, and
- a search for ways to prevent contamination and to recycle valuable resources.

This research was supported by EPA to further understand the real time effects of environmental factors on papermill sludge landfills.

A. W. Breidenbach, Ph.D.
Director
National Environmental
Research Center, Cincinnati

ABSTRACT

For the slope stability study conducted during the second year of the project, the experimental papermill sludge landfill was altered by removal of the north dike. Next the landfill was excavated to form a 3:4 slope and two weeks later was trimmed to a 1:8 slope. Prior to the above construction, vane shear strength and Dutch cone resistance data were obtained at one foot intervals of depth. Seven slope indicator casings and additional piezometers were installed in preparation for the slope stability study. Earlier instrumentation remained operative and monitoring was continued throughout the year. Undisturbed block samples of consolidated sludge and field water contents were taken at the time of slope excavation. Laboratory work included consolidation tests on undisturbed sludge samples. Triaxial tests were run on fresh sludge samples using istropic consolidation and on undisturbed sludge samples using anisotropic consolidation. Unconfined compression tests were run with the sample axis oriented at 0, 45, and 90 degrees to the horizontal so as to provide information on the anisotropy of the consolidated sludge. Leachate sampling and analysis documented changes occurring during the second year of the project.

It was shown that soil mechanics theory can be used to predict the stability of slopes excavated in a sludge landfill. The significant increase in shear strength of the papermill sludge as a direct consequence of consolidation resulted in a stable 3:4 slope with small observed lateral movements. This behavior was in contrast to the very soft, almost fluid behavior of the fresh sludge placed in the landfill during construction. Lateral movements increased rapidly after excavation to the 1:8 slope. Rate of movement decreased with time suggesting that creep behavior was responsible for a large portion of the final 6 inches of movement at the surface. Development of failure zones for the 1:8 slope was studied using the finite element method of analysis and laboratory triaxial test data. Stability analysis of the 1:8 slope, using Janbu's method for a composite failure surface, gave excellent agreement between the actual factor of safety and the computed factor of safety. The vane shear strength, corrected for deformation rate and sludge anisotropy effects, appeared to give the better representation of the undrained field shear strength for the sludge.

Additional information on physical properties of the sludge shows the dependence of liquid and plastic limits on the organic content of the sludge. The papermill sludge has properties in many respects similar to peaty soils. The low permeability of the high ash papermill sludge together with a decreasing rate of leachate flow associated with fill consolidation exerted a moderating effect on the quantity of leachate leaving the landfill. The leachate analyses showed that the quantities of sulfate, Kjeldahl nitrogen, phosphorous, iron, and chloride were well below values cited for municipal refuse. Concentrations of mineral salts and hardness were similar to those for leachate originating in landfills of municipal refuse.

PREFACE

This annual report covers phase (2) of an experimental high ash papermill sludge landfill project. Data for phase (1), not available during preparation of the first annual report, are also presented, analyzed, and discussed in this report. The work described was made possible by Research Grant R801282 from the U. S. Environmental Protection Agency, under agreement with Michigan State University.

Wayne A. Charlie and Robert P. Vallee, research assistants in soil mechanics, were responsible for the supervision of construction at the site, instrumentation and monitoring of the landfill, and carried out experimental laboratory work in the Soil Mechanics Laboratory of the Department of Civil Engineering at Michigan State University. Timothy A. Armstrong, Research Associate for the National Council of the Paper Industry for Air and Stream Improvement, Inc., performed the leachate analysis. Dr. O. B. Andersland, Professor of Civil Engineering, supervised the research and preparation of this report. The B. G. Danis Company, Dayton, Ohio, carried out construction for the project and the Bowser-Morner Testing Laboratories, Inc., Dayton, Ohio, provided equipment and services needed to install additional instrumentation.

The opinions, findings and conclusions expressed in this publication are those of the authors and not necessarily those of the U. S. Environmental Protection Agency.

TABLE OF CONTENTS

Page

ABSTRACT iv

PREFACE. vi

LIST OF TABLES x

LIST OF FIGURES xii

LIST OF SYMBOLS xvi

Chapter I. INTRODUCTION. 1

Need for study. 1
Objectives of study 2
Nature and scope of study 3

Chapter II. PAPERMILL SLUDGE LANDFILLS--LITERATURE REVIEW 5

Consolidation theories and normally consolidated soils 5
Fill movement and stability 11
Methods of analyses. 14
  Rotational movement 15
  Composite sliding surface. 16
  Failure zones around slopes during excavation 17

Chapter III. ENGINEERING PROPERTIES OF PAPERMILL SLUDGE 23

Physical properties 23
Stress-deformation characteristics 23
  Consolidation of undisturbed samples. 23
  Triaxial shear tests 24
    Sample preparation. 25
    Undrained test 26
    Consolidated undrained test 27

Chapter IV. INSTRUMENTATION, MONITORING, AND EXCAVATION 31

Instrumentation and monitoring 31
  Horizontal movement 31
    Slope indicator casings. 31
    Surface measurements 32
  Vertical movement. 32
  Piezometers 32
  Total pressure cells and temperature sensors. 33
  Leachate sampling and analysis. 33
Excavation for the experimental slope 34

TABLE OF CONTENTS (continued)

Page

Chapter V. EXPERIMENTAL RESULTS 43

Physical properties of the papermill sludge . . . 43
Stress-deformation behavior of the sludge 43
  Consolidation of undisturbed samples 43
  Shear strength 44
    Fresh sludge samples 44
    Undisturbed sludge samples 45
    Unconfined compression tests 46
    In-place vane shear tests 46
Slope behavior 47
  Lateral movement 47
  Vertical movement 48
  Pore water pressures 48
  Temperature 49
  Total pressure cells 49
  Surface observations 49
Leachate analysis 50

Chapter VI. DISCUSSION AND INTERPRETATION OF RESULTS 94

Physical properties 94
Consolidation and field settlement 95
  Laboratory consolidation. 95
  Field settlement 97
Slope stability for the papermill sludge. 99
  Laboratory and field shear strengths 99
  Observed slope movements 102
  Development of failure zones 102
  Slope failure 105
  Analysis for the composite failure surface . . 106
Leachate analysis 107

Chapter VII. SUMMARY AND CONCLUSIONS 134

Engineering properties of the sludge 134
Sludge landfill settlement 135
Slope stability of consolidated sludge 136
Leachate analysis 137
Practical implications of the investigation 138

REFERENCES 140

TABLE OF CONTENTS (continued)

Page

APPENDICES

A. Surface movements 143

B. Slope indicator data 145

C. Settlement plate data 166

D. Piezometer data 170

E. Temperature data 173

F. Vane shear and Dutch cone data 174

G. Total pressure cell data 177

H. Undisturbed consolidation data 178

I. Triaxial test data 184

J. Average daily temperature and precipitation 219

K. Computer program for solution of the equations in the theory of Gibson and Lo . 226

LIST OF TABLES

Table		Page
4. 1	Leachate samples	36
5. 1	Physical properties of the papermill sludge, October, 1972	52
5. 2	Variation in water contents for one cubic foot block samples	53
5. 3	Summary of consolidation characteristics, undisturbed sludge samples	54
5. 4	Summary of triaxial test results	56
5. 5	Summary of $\overline{\phi}$ values for the triaxial tests	58
5. 6	Analysis of leachate quality	59
6. 1	Material numbers and properties for the finite element analysis	111
A- 1	Surface movements	143
B- 1 through B- 21	Slope indicator data	145-165
C- 1	Settlement plate elevations at the bottom sand blanket	166
C- 2	Settlement plate elevations at the middle sand blanket	167
C- 3	Settlement plate elevations at the top sand blanket	168
C- 4	Settlement plate elevations at the mid-points of the lower and upper sludge layers	169
D- 1	Pore water pressures for the lower and upper 1/4 points of the lower and upper sludge layers	170
D- 2	Pore water pressures for the center of the lower and upper sludge layers	171
D- 3	Pore water pressures for the lower and middle sand blankets	172
E- 1	Temperature data for the papermill sludge landfill	173
F- 1	Vane shear strength data, September 7, 1972	174
F- 2	Vane shear strength data, October 6, 1972	175
F- 3	Dutch cone penetration results, September 7, 1972	176
G- 1	Total pressure cell data	177
H- 1	Undisturbed consolidation data, rapid load increments.	178
H- 2	Undisturbed consolidation data, sample B- 3	180
H- 3	Undisturbed consolidation data, sample B- 4	181

LIST OF TABLES (continued)

Table Page

H-4 Undisturbed consolidation data, sample F-3. 182

H-5 Undisturbed consolidation data, sample F-4. 183

I-1 through
I-35 Triaxial test data 184-218

J-1 Average daily temperature and precipitation 219

LIST OF FIGURES

Figure Page

2.1 Models for the consolidation process. (a) Gibson and Lo (1961). (b) Wahls (1962) 19

2.2 Void ratio-effective stress relationships for a normally consolidated clay (Leonards, 1962) 20

2.3 Equations and definitions for shear strength theory, effective stress basis. 21

2.4 (a) Forces in the circular arc analysis (after Bishop, 1954). (b) Notation to Janbu's (1957) analytical procedure 22

3.1 (a) Undisturbed block sample of consolidated sludge. (b) Sample preparation using a high speed rotary saw 29

3.2 Triaxial tests. (a) Mounting the cylindrical sample. (b) Anisotropic consolidation in the triaxial cell. (c) Newly prepared sample left, failed and oven dry sample right 30

4.1 Slope indicator casing locations, A through G, and 3:4 slope, plan view 37

4.2 Horizontal control stake locations, plan view 38

4.3 Distribution of settlement plates, piezometers, and total pressure cells in the instrument groups . . . 39

4.4 Experimental slope cross-sections. (a) 3:4 slope. (b) 1:8 slope 40

4.5 3:4 slope preparation. (a) Sludge removal by dragline. (b) Slope cross-section, October 13, 1972. 41

4.6 1:8 slope preparation. (b) Trimming the upper sludge layer. (b) Sludge removal using a dozer, October 24, 1972 42

5.1 Field water contents of the sludge in the landfill, October, 1972. 60

5.2 Void ratio-effective stress relationships, undisturbed sludge samples 61

5.3 Consolidation characteristics for the undisturbed sludge samples. (a) Coefficient of consolidation, c_v. (b) Primary compression ratio, r. (c) Coefficient of secondary compression, C_α 62

5.4 Stress-strain behavior of fresh sludge in undrained shear, sample U-3-7 63

5.5 Consolidated undrained triaxial test results for sludge sample U-3. (a) K_f line. (b) Water content. (c) Undrained strength 64

LIST OF FIGURES (continued)

Figure Page

5.6 Consolidated undrained triaxial test results for sludge sample U-1. (a) K_f line. (b) Water content. (c) Undrained strength 65

5.7 Stress-strain behavior of consolidated sludge in undrained shear, sample G-5 66

5.8 Consolidated undrained triaxial test results for block G, anisotropic consolidation, vertical axis. (a) K_f line. (b) Water content. (c) Undrained strength 67

5.9 Stress-strain behavior of consolidated sludge in undrained shear, sample G-10 with the major principal axis horizontal 68

5.10 Consolidated undrained triaxial test results for block G, isotropic consolidation, and horizontal axis. (a) K_f line. (b) Water content. (c) Undrained strength 69

5.11 Stress-strain behavior of consolidated sludge in undrained shear, sample G-20 with a vertial axis, σ_1 constant and σ_3 decreasing 70

5.12 Variation of unconfined compressive strength with direction of compression 71

5.13 Experimental landfill, immediately before slope excavation. (a) Vane shear strength. (b) Dutch cone resistance 72

5.14 Lateral movement. (a) Slope indicator casing A. (b) Slope indicator casing B. (c) Slope indicator casing C. (d) Slope indicator casing D. (e) Slope indicator casing A and D. (f) Slope indicator casing E and F. (g) Slope indicator casing G 73-79

5.15 Settlement in the top, ⑤ - ③ , and bottom, ③ - ①, sludge layers. (a) Instrument groups 4, 6, and 8 (b) Instrument groups 3, 5, and 7 80-81

5.16 Pore pressure versus time curves. (a) Instrument group 4 82
(b) Instrument group 5 83

5.17 Temperature versus time. (a) Thermistors 1, 3,5,7, and 9. Thermistors 4,6,8, and 0. 84

5.18 Horizontal and vertical total stresses, bottom sludge layer 85

LIST OF FIGURES (continued)

Figure		Page
5.19	Tension cracks. (a) Photo. (b) Crack locations on October 25, 1972	86
5.20	(a) Initial slope failure, October 29, 1972. (b) Slope condition on November 21, 1972	87
5.21	Cross-section of 1:8 slope, before and after failure	88
5.22	Biochemical oxygen demand (BOD) and chemical oxygen demand (COD) for leachate samples	89
5.23	Total iron for leachate samples	90
5.24	Specific conductance for leachate samples	90
5.25	Dissolved solids for leachate samples	91
5.26	Color for leachate samples	91
5.27	Turbidity for leachate samples	92
5.28	Total hardness and alkalinity for leachate samples .	92
5.29	Chloride concentration for leachate samples	93
6.1	Weight loss versus temperature for a papermill sludge sample from block C	112
6.2	Relationships between ash content and consistency limits	113
6.3	Plasticity chart (Unified Soil Classification System) with data points for several fresh pulp and papermill sludges	114
6.4	Comparison of actual and predicted time-settlement curves, upper sludge layer. (a) Theory of Gibson and Lo (1961)	115
	(b) Wahl's theory (1962)	116
6.5	Comparison between the predicted and measured time-settlement curves, lower sludge layer, Terzaghi procedure for a linearly increasing load . .	117
6.6	Influence of organic content on the angle of internal friction, effective stress basis	118
6.7	Undrained stress-strain behavior of a normally consolidated papermill sludge with σ_1 constant and σ_3 decreasing	119
6.8	Casing movements at elevation 94.6 ft during and after excavation for the experimental slope	120

LIST OF FIGURES (continued)

Figure Page

6.9 Time-rate of lateral movement. (a) Slope indicator casing A. (b) Slope indicator casing B. (c) Slope indicator casing C. (d) Slope indicator casing D. (e) Slope indicator casing E and F. (f) Slope indicator casing G 121-126

6.10 (a) Excavated slope showing the section to be analyzed. (b) Finite element idealization of slope cross-section. (c) Typical finite element configuration of the slope showing the excavation sequence 127

6.11 Development of failure zones for the 1:8 slope, $s_u/p = 3.45$ and $K = 0.4$ 128

6.12 Correction factor for converting vane shear strengths to field shear strengths (after Bjerrum, 1972) 129

6.13 Stability calculations using Janbu's (1954, 1957) method, total stress basis 130

6.14 Biochemical oxygen demand (BOD) versus chemical oxygen demand (COD) 131

6.15 Mass of leachate constituents 132

6.16 Magnitude of leachate flow 133

A-1 Slope failure areas, plan view 144

LIST OF SYMBOLS

a = primary compressibility of the soil skeleton, in^2/lb

a_v = coefficient of compressibility

$\overline{a}$ = y intercept, effective stress basis

A = pore pressure parameter

A_n = spring constant

b = secondary compressibility of the soil skeleton, in^2/lb

b = slice width

B_n = dashpot constant

c = cohesion

c = distance to the midpoint of a doubly drained clay layer at $t = 0$

c_u = total stress strength parameter

c_v = coefficient of consolidation

$\overline{c}$ = cohesion, effective stress basis

C_c = compression index

C_n = dashpot constant of the nth secondary dashpot

C_α = coefficient of secondary compression

e = void ratio

E = Young's modulus

E = normal force on slice sides

f = strain in spring element

F = factor of safety

H = Henry's coefficient of solubility

H = thickness of sludge layer or sample

H_p = thickness of sludge layer or sample at the end of primary consolidation

I_p = plasticity index

LIST OF SYMBOLS (continued)

k = coefficient of permeability
K = total stress earth pressure coefficient
K_f-line = line through $\overline{p}_f$ versus q_f
K_o = coefficient of earth pressure at rest
ℓ = length
L_w = liquid limit
N = normal force
p = consolidation pressure
p_o = initial pressure; present overburden pressure
p_c = preconsolidation pressure
$\overline{p}$ = $\frac{1}{2}(\overline{\sigma}_1 + \overline{\sigma}_3)$
$\overline{p}_f$ = $\overline{p}$ at failure
P = force
q_o = applied surface load
$\overline{q}$ = $\frac{1}{2}(\overline{\sigma}_1 - \overline{\sigma}_3)$
$\overline{q}_f$ = $\overline{q}$ at failure
Q = line load
r = primary compression ratio
R = radius
s = shearing resistance
S = shear force
$S(t)$ = settlement as a function of time
S_o = initial degree of saturation
t = time
t_p = time assumed for the end of primary compression
T = temperature

LIST OF SYMBOLS (continued)

T = shear force

T_v = time factor

u = pore water pressure

u_{a_o} = initial air pressure

u_{a_s} = pressure necessary for full saturation

w = water content

W = total weight

x = distance

z = depth to a point in a soil layer

α = inclination angle of force

$\bar{\alpha}$ = slope of $\bar{p}_f$ versus $\bar{q}_f$

γ = unit weight

γ_w = unit weight of water

Δ = increment

δ_1 = settlement at time t_1

δ_2 = settlement at time t_2

ϵ = strain

σ = normal stress

$\bar{\sigma}$ = effective normal stress

$\bar{\sigma}_{ff}$ = normal stress on failure surface at failure

$\sigma_1, \sigma_3, \bar{\sigma}_1, \bar{\sigma}_3$ = principal stresses

τ = dummy variable

τ_{ff} = shear stress on failure surface at failure

μ = correction factor

$\bar{\phi}$ = friction angle based on effective stresses

ϕ_u = total stress strength parameter

$1/\lambda$ = viscosity of the soil structure, lb-sec/in^2

AN EXPERIMENTAL HIGH ASH PAPERMILL SLUDGE LANDFILL
Second Annual Report

O. B. Andersland,[+] Wayne A. Charlie,[+] Robert P. Vallee,[+]
and Duane W. Marshall[*]

CHAPTER I. INTRODUCTION

Need for Study

Solid wastes resulting from the pulp or paper making process are removed from effluent streams by treatment devices designed to protect the nation's surface water resources. The great majority of these sludges are disposed of in some form of landfill. Literature cited in the First Annual Report indicated that sludge disposal on land, in most cases, lacks long-range planning, hence disposal is achieved on a temporary rather than a permanent basis. Guidelines or recommendations for the efficient and safe disposal of pulp and papermill sludge are incomplete. Sludge disposal in landfills must include the application of sound engineering and environmental principles to all stages of site selection, design, and completed use. Possible uses of a sludge landfill include conversion into a green area or a design for recreational, agricultural, or light construction purposes.

Design for completed use and regulation of solid pulp and papermill waste landfills requires an understanding of the many variables that affect volume change and settlement, slope stability and bearing capacity, drainage of the waste material, and leachate characteristics. Consideration of the overall impact on the environment must be included. The First Annual Report showed that large volume changes do occur under a relatively small earth surcharge and indicated that a rather significant increase in shear strength occurs as a result of consolidation. Settlement rates gave a good estimate of the flow rate for leachate

---

[+] Department of Civil Engineering, Michigan State University, East Lansing.

[*] National Council of the Paper Industry for Air and Stream Improvement, Inc.

draining from the papermill sludge. Field and laboratory work were not complete at the time of writing the First Annual Report, hence this report continues the effort to verify with field observations the accuracy of predictions of settlement and slope stability based on laboratory data. Continued leachate sampling and analysis documented changes occurring during the second year of the project.

Objectives of Study

The general objective of the study, as set forth in the First Annual Report, was to contribute--through field observations on an experimental landfill, laboratory work, and analysis--basic information relative to sludge behavior which is needed for developing guidelines and recommendations for the design, operation, and regulation of landfills for pulp and papermill solid wastes. It is desirable that a completed sludge landfill be stable and have the potential for a number of uses, including recreation purposes or as a foundation for light construction. Pursuant to this general objective the research program for the second year was directed to completing work on the consolidation behavior, proceeding with work on the stability of the landfill, and continuing the sampling and analysis of leachate from the landfill. More specific items relative to the stability of the landfill include:

1. Surcharge loads in combination with drainage blankets made possible a large reduction in water content of the fresh papermill sludge during the first year of the project. Effectiveness of this drainage in improving the shear strength of the sludge has been presented in terms of both field and laboratory data.

2. Undrained shear strength data obtained by means of the vane borer are compared with shear strength data from laboratory triaxial tests on both fresh sludge samples and undisturbed block samples taken from the landfill during preparation for the experimental slope. Suitability of the shear strength data for the stability calculations has been discussed.

3. Removal of the dike on one side and excavation to a 3:4 slope was followed two weeks later by trimming to a 1:8 slope. This excavation involved unloading of forces within the sludge mass in a manner similar to that occurring in soils during an excavation. Data on the observed lateral and vertical movements within the sludge mass resulting from unloading have been summarized and discussed.

4. Failure zones develop in excavated slopes when the maximum shear stress values approach the shear strength of the papermill sludge. Development of these failure zones in the 1:8 slope was studied using the finite element method of analysis and laboratory triaxial test data.

5. Slope failure occurred shortly after excavation of the 1:8 slope. The slope stability was analyzed so as to compare field behavior with predicted behavior on the basis of soil mechanics theory and laboratory shear strength data.

6. Pore water pressure observations taken during the slope preparation, before and after slope failure, and during the remainder of the year have been summarized. Implications relative to the slope behavior are reviewed.

7. The exposed sludge slope was observed during the remainder of the year in terms of movements and the effect of the environment including high rainfall, snow, and freezing temperature.

8. The leachate analysis was continued on samples obtained from the landfill during the year so as to document changes during the life of the project.

Specific items relative to the consolidation behavior and the leachate analysis and lysimeter study were included in the First Annual Report.

Nature and Scope of Study

As described in the First Annual Report, the research program was designed to be conducted in two essentially sequential phases: (1) landfill consolidation plus leachate analysis and lysimeter study, and (2) the stability study. The first phase involved construction of the experimental sludge landfill, placement and monitoring of instrumentation, laboratory work for determination of physical properties and certain stress-deformation characteristics of the sludge, and the leachate analysis and lysimeter study. The First Annual Report was written during the summer of 1972 using data available at that time. Additional laboratory and field consolidation data has since been obtained so that some parts of phase (1) of the study are incorporated into this report.

The stability study portion of the project was initiated in early September, 1972. The field work involved installation of slope indicator casings and additional piezometers, removal of the dike on the north side, excavating the experimental slope in two increments, taking undisturbed block samples and field water contents at several levels in the exposed cut, and monitoring of field instrumentation as needed to provide a continuous record of the slope performance. Laboratory work included tests to determine changes in physical properties of the sludge, which have been described in the First Annual Report, and triaxial tests for measurement of stress-deformation properties of both fresh and undisturbed sludge samples. Leachate samples were analyzed by NCASI staff at their Central-Lake States Regional Center, Kalamazoo, Michigan, so as to document any changes in the leachate composition during the second year of the project. Parameters evaluated were those consistent with the nature of the landfill material and considered to be of significance to groundwater quality. Data analysis was continued throughout the year with the Second Annual Report being prepared during the late summer and fall of 1973.

CHAPTER II. PAPERMILL SLUDGE LANDFILLS--LITERATURE REVIEW

Information on current practice for papermill sludge disposal, settlement resulting from consolidation, and groundwater protection have been reviewed in the first annual report. To help explain the observed settlement behavior of the experimental papermill sludge landfill, consolidation theories and normally consolidated soils are reviewed below. Fill movement, stability, and methods of analyses are discussed with reference to the experimental slope reported on in subsequent chapters of this report.

Consolidation Theories and Normally Consolidated Soils

In the first annual report Terzaghi's (1943) theory was used to model the consolidation behavior of the sludge landfill. This theory does not account for secondary consolidation, hence it was desirable to consider other theories which appear to provide a more realistic mathematical formulation. Two consolidation theories which include secondary compression in their formulation are reviewed below and have been included in the sludge landfill settlement analysis.

The theory proposed by Gibson and Lo (1961) for the consolidation of soils exhibiting secondary compression involves the representation of the soil skeleton by the mathematical model shown in Figure 2. 1a. In this rheological model, primary compression is represented by the transfer of stress from the pore water to the soil skeleton with drainage resulting in an effective stress, $\bar{\sigma}(t)$, which causes compression of the Hookean spring a. This effective stress is also applied to the Kelvin element, but its compression is retarded because of the presence of the dashpot 'λ'. The effective stress is thus initially carried entirely by the viscous dashpot, but as time passes the stress is transferred to spring b, resulting in secondary compression. Since the transfer of stress from pore water to soil skeleton is delayed due to the low permeability of the soil, the effective stress $\bar{\sigma}(t)$ increases gradually and hence the compression of spring a is also gradual. Secondary compression is controlled by the viscous resistance of the soil skeleton and can occur simultaneously with primary compression, thus eliminating

Terzaghi's assumption that time lag of compression is caused exclusively by the low permeability of the material.

Gibson and Lo (1961) consider stress and compatibility conditions in the Kelvin element, yielding

$$\frac{f}{b} + \frac{1}{\lambda}\frac{df}{dt} = \bar{\sigma}(t) \qquad (2.1)$$

where b is the secondary compressibility, f is the strain in spring b, $\frac{1}{\lambda}$ is the viscosity of the soil structure (dashpot 'λ'), and t is the time after load application. Solving this equation gives the stress-strain relationship

$$\epsilon = a\bar{\sigma}(t) + \int_0^t \bar{\sigma}(\tau)e^{-\frac{\lambda}{b}(t-\tau)}\,d\tau \qquad (2.2)$$

where a is the primary compressibility, and τ is a dummy variable. Considering continuity of flow of water through an element of soil, Gibson and Lo (1961) write

$$\frac{k}{\gamma_w}\frac{\partial^2\bar{\sigma}(t)}{\partial Z^2} = \frac{\partial\epsilon}{\partial t} \qquad (2.3)$$

where k is the permeability of the soil, ϵ is the vertical strain at a point, γ_w the unit weight of water, and Z is the distance from the surface of a soil layer with an impermeable base. Combining equations 2.2 and 2.3 yields the one-dimensional equation of consolidation

$$\frac{k}{\gamma_w}\frac{\partial^2\bar{\sigma}(t)}{\partial Z^2} = a\frac{\partial\bar{\sigma}(t)}{\partial t} + \lambda\bar{\sigma}(t) - \frac{\lambda^2}{b}\int_0^t \bar{\sigma}(Z,\tau)e^{-\frac{\lambda}{b}(t-\tau)}\,d\tau \qquad (2.4)$$

Gibson and Lo (1961) solved this equation, for the appropriate boundary conditions, by the use of Laplace Transforms and the Convolution Theorem. The solution for a step (instantaneous) load, q_o, yields the following expression for settlement:

$$S(t) = (a+b)q_oH\left(1 + \frac{8}{\pi^2}\sum_{n=odd}^{\infty}\frac{1}{n^2}\left[\left(\frac{K-x_1}{x_1-x_2}\right)e^{-x_2t} - \left(\frac{K-x_2}{x_1-x_2}\right)e^{-x_1t}\right]\right) \qquad (2.5)$$

where H = thickness of the soil layer, $K = \frac{a}{a+b} K_1$, $K_1 = \frac{n^2 \pi^2 c_v}{4H^2}$,

$c_v = \frac{k}{a\gamma_w}$, $\begin{matrix} x_1 \\ x_2 \end{matrix} = \frac{(\alpha + K_1) \pm \sqrt{[(\alpha + K_1)^2 - 4\beta K_1]}}{2}$, $\alpha = (\frac{1}{a} + \frac{1}{b})\lambda$, and

$\beta = \frac{\lambda}{b}$. The pore pressure is given by the expression

$$u = \frac{4}{\pi}\,\frac{a+b}{a}\,q_o \sum_{n=odd}^{\infty} \frac{1}{n} \left(\frac{x_1\left(\frac{a}{a+b} - \frac{x_2}{K_2}\right)}{x_1 - x_2} e^{-x_1 t} - \frac{x_2\left(\frac{a}{a+b} - \frac{x_1}{K_2}\right)}{x_1 - x_2} e^{-x_2 t} \right) \sin \frac{n\pi Z}{2H} \tag{2.6}$$

For a soil which is infinitely viscous ($\lambda \rightarrow 0$) or exhibits no secondary compression ($b \rightarrow 0$) the above equations reduce to those of the classical solution of Terzaghi.

These equations have been programmed for solution by computer and the program is given in Appendix K. The program assumes that the soil layer is doubly drained and solves for the settlement and pore pressures (at the eighth points of the layer) for each specified time. The thickness of the layer is adjusted after each settlement computation to maintain the appropriate length of drainage path.

For large values of time the settlement becomes

$$S(t) = q_o H\ [a + b\ (1 - e^{\frac{\lambda}{b} t})] \quad t \geq t_a \tag{2.7}$$

and in the limit $t \rightarrow 0$, the ultimate settlement of the layer is given as

$$S_{ult} = (a + b) q_o H \tag{2.8}$$

To determine the parameters a, b, and λ it is necessary to plot a graph of $\log_{10}(\delta_2 - \delta_1)$ versus t_1, where δ_2 and δ_1 are the settlements at times t_2 and t_1, respectively, and $t_2 - t_1 = \Delta t$ = constant. Using equation 2.7 the following expression is derived,

$$\log(\delta_2 - \delta_1) = \log I - 0.434 \frac{\lambda}{b} t_1 \tag{2.9}$$

where $I = q_o H b (1 - e^{-\frac{\lambda}{b} \Delta t})$. The intercept of the graph represents log I, thus

$$b = \frac{I \times 10^{-4}}{q_o H (1 - e^{-\frac{\lambda}{b} \Delta t})} \tag{2.10}$$

The slope of the line is given by $0.434 \frac{\lambda}{b}$. The value of a can be found from

$$a = \frac{\epsilon(t_a)}{q_o} - b(1 - e^{-\frac{\lambda}{b} t_a}) \tag{2.11}$$

where $\epsilon(t_a)$ represents the strain at time $t = t_a$. Figure 6.4 in the First Annual Report shows a plot of log $(\delta_2 - \delta_1)$ versus t_1 for papermill sludge.

The rheological model proposed by Wahls (1962) for the analysis of primary and secondary consolidation is shown in Figure 2.1b. Here primary compression is represented by the Kelvin elements and secondary compression is represented by the secondary dashpots. The time dependent transfer of stress from the pore fluid to the soil skeleton is mathematically modeled by the transfer of stress from the viscous dashpot to the Hookean spring in the Kelvin element. Thus, for an increment of load, Δp, we can write for the nth element,

$$\Delta p = \frac{R_n}{A_n} + \frac{dR_n}{dt} \frac{1}{B_n} \tag{2.12}$$

where R_n is the compression of the nth Kelvin body, A_n is the spring constant for the nth elastic spring, and B_n is the dashpot constant for the nth viscous dashpot. By solving equation 2.12 for R_n and summing over all the elements to obtain the total primary compression, R_1, at time t, Wahls (1962) arrived at

$$R_1 = \sum_{n=0}^{\infty} R_n = \Delta p \sum_{n=0}^{\infty} A_n (1 - e^{-\frac{B_n}{A_n} t}) \tag{2.13}$$

Since the Terzaghi solution for primary compression provides a good representation of the hydrodynamic effect, Wahls (1962) chose his constants A_n and B_n to make equation 2.13 identical to the Terzaghi equation, arriving at the following deformation equation of the rheological model for primary compression,

$$R_1 = A_p \Delta p \, f(T_v) \tag{2. 14}$$

where $f(T_v) = 1 - \frac{8}{\pi^2} \sum_{n=0}^{\infty} \frac{1}{(2n+1)^2} \exp \{ - \frac{(2n+1)\pi}{2} \}^2 T_v$,

$A_p = \sum_{n=0}^{\infty} A_n$ = coefficient of compressibility, $T_v = \frac{c_v t}{H^2}$, and c_v = coefficient of consolidation.

Certain assumptions made by Wahls (1962) concerning secondary compression lead to its representation by the viscous dashpots linked in series with each Kelvin body as shown in Figure 2. 1b. The deformation equation of the nth secondary dashpot is assumed to be

$$\frac{dR_n}{dt} = \frac{C_n}{1 + \frac{B_n}{A_n} t} (p_o + \Delta p) \tag{2. 15}$$

where R_n is the compression of the nth secondary dashpot and C_n is the dashpot constant of the nth secondary dashpot. Solving this equation for R_n and summing to determine the total secondary deformation, Wahls (1962) arrived at the equation

$$R_2 = \sum_{n=0}^{\infty} R_n = C_\alpha \, h(T) \tag{2. 16}$$

where

$$h(T) = 1.08516 \, \frac{8}{\pi^2} \sum_{n=0}^{\infty} \frac{1}{(2n+1)^2} \log_{10} \left[1 + \left(\frac{2n+1}{2} \pi\right)^2 T_v \right] \quad \text{for } T_v \le 7$$

and $h(T) = 0.8353 + \log_{10} T_v$ for $T_v > 7$ and $C_\alpha = \Delta H/H_p \big/ \Delta \log t$ = strain per cycle log time. Thus the total compression, R_T, caused by a pressure increment, Δp, is

$$R_T = R_1 + R_2 = A_p \Delta p \, f(T_v) + C_\alpha H_p \, h(T_v) \tag{2. 17}$$

where $A_p \Delta p = \Delta H_p$ = total estimated primary compression, and H_p = thickness of the layer at the end of primary compression. Wahls (1962) has determined values of the functions $f(T_v)$ and $h(T_v)$ for different values of T_v and these have been used to determine theoretical time-settlement curves for the papermill sludge. It should be noted that ΔH_p represents primary compression only, and any estimate of primary compression based on field piezometer readings or laboratory C_c values must have the appropriate theoretical amount of secondary compression subtracted from it. This is discussed in Chapter VI. Wahls' (1962) theory provides no estimate of pore pressures.

A soil deposit is said to be normally consolidated if the present effective overburden pressure equals the maximum pressure to which the deposit has ever been consolidated at any time in its history. Leonards (1962) discussed in detail the void ratio-effective stress relationships for normally consolidated soil samples, and these concepts are used in the interpretation and analysis of consolidation tests performed on undisturbed samples of sludge taken from the landfill. Figure 2.2 illustrates typical void ratio-logarithm of pressure relationships for a normally consolidated clay subjected to various loading conditions and degrees of disturbance. It can be seen that the curve obtained using small load increments best defines the in situ void ratio-logarithm of effective stress relationship, and that this relationship can be substantially affected by sample disturbance. There is a sharp break in the void ratio-logarithm of pressure curve at a stress level equal to the effective overburden pressure for soils that have experienced little secondary compression. Bjerrum (1967) and Leonards and Ramiah (1959) discussed the increase in p_o (effective stress at which in situ consolidation begins) as a result of long term secondary compression. An increase in p_o can also occur from thixotropic and cementation effects. For soils that have been substantially disturbed during sampling, there is no well defined break in the void ratio-logarithm of pressure curve and it is difficult to accurately determine p_o. In the analysis of the consolidation tests on papermill sludge, the Casagrande (1936) construction was used to estimate p_o from the laboratory void ratio-logarithm of pressure curves.

Fill Movement and Stability

Dewatered high ash pulp and papermill sludges disposed of in landfills may have a solids content as high as 40 percent by weight (equivalent to 150 percent water content by dry weight). When pulp fibers are present in significant amounts (greater than 15 percent by weight) the sludge appears fibrous and will hold its shape in the dewatered condition. In the absence of fiber, the sludge is putty-like, and fluid at solids contents as high as 35 percent. The ash materials in these sludges are comprised mostly of kaolinite clay with small amounts of lime, titanium oxide and iron. The semi-liquid to liquid state of these dewatered sludges means that lateral confinement is needed in order to place the material to a depth suitable for a cell type of landfill construction.

The First Annual Report has shown that the use of drainage blankets together with a small earth surcharge permits drainage of water from the sludge resulting in a significant decrease in volume and an increase in the strength of the sludge. The weight of overlying sludge helps consolidate material at lower levels. Information on shear strength is given later in this report. The vertical movement or settlement of the experimental landfill surface was produced entirely by the decrease in water content associated with consolidation. Photomicrographs of fibers from papermill waste deposits that have been in place for up to 12 years have shown that virtually no decomposition of the fiber had occurred (Gillespie, Mazzola, and Gellman, 1970). The presence of lignin (Umbreit, 1962) and clay (Lynch, 1956) and the absence of sufficient available nitrogen (Imshenetsky, 1968) are known to inhibit the biological breakdown of cellulose. All three of these conditions probably exist in the experimental papermill sludge landfill. Prediction of the amount and rate of settlement observed in the experimental sludge landfill has been presented in the First Annual Report with additional information included in later chapters of this report.

Lateral movement may occur when an excavation is to be made in the sludge landfill or when the foundation for a structure is to be placed on the consolidated papermill sludge. Factors affecting the behavior of excavated slopes include slope height, slope angle, unit weights, pore pressures, initial stress conditions (prior to excavation), stress-strain and strength characteristics of the sludge, creep characteristics of the sludge, drainage conditions, time, and perhaps more. Information on initial stresses are available from the First Annual Report based on the total pressure cell data taken towards the end of the consolidation period. Data on other factors are given later in this report. During excavation the stresses on the slope surface are reduced to zero. This reduction in stresses will induce strains and displacements in the exposed sludge slope. Numerical techniques for predicting slope deformations require information on the stress-strain behavior of the consolidated sludge. Experimental data are given later in this report on sludge samples tested under conditions closely simulating field conditions.

Information on bearing capacity and slope stability of papermill sludges in landfills is not available. One must draw on methods available in the field of soil mechanics which require data on the shear strength of the sludge material in question. Experience has shown that the Mohr-Coulomb theory of failure has been very successful for defining failure in soil materials (Terzaghi and Peck, 1967). This theory, represented in the form

$$\tau_{ff} = c + \sigma_{ff} \tan \phi \qquad (2.18)$$

states that the shear stress τ_{ff} on a failure surface at failure is a function of the normal stress σ_{ff} on that plane at failure and the material properties cohesion c and angle of internal friction ϕ. In this form the soil skeleton must carry all the normal stress, that is the soil must be free draining.

For cohesive soils or papermill sludges that are not free draining, the pore fluid will carry part of the normal stress. This portion cannot contribute to the frictional resistance and shear strength. Hence for these materials the stress carried by the pore fluid must be subtracted from the total normal stress and the shear strength will be based only on that portion of the normal stress carried by the soil skeleton. This is done by measuring the pore water pressure during triaxial testing and presenting the results in terms of effective stresses. Equation 2.18 now becomes

$$\tau_{ff} = \overline{c} + (\sigma_{ff} - u) \tan \overline{\phi} \qquad (2.19)$$

where u is the pore water pressure, $\bar{c}$ is the cohesion intercept based on effective stresses, and $\bar{\phi}$ is the angle of internal friction based on effective stresses. Equation 2. 19 represents a straight line with intercept on the shear stress axis equal to $\bar{c}$ and slope angle equal to $\bar{\phi}$ as shown in Figure 2. 3. The shear strength, so defined, is the maximum shear stress that may be sustained on any plane in a given soil or sludge material. When information on the pore pressure u is not available or when total stresses are to be used in a stability analysis, the undrained shear strength τ_{ff}, defined as

$$\tau_{ff} = c_u + \sigma_{ff} \tan \phi_u \tag{2. 20}$$

may be used. The total stress strength parameters c_u and ϕ_u denote the apparent cohesion and the angle of shearing resistance, respectively. When ϕ_u equals zero, c_u equals $1/2\,(\sigma_1 - \sigma_3)_f$ where σ_1 and σ_3 are the major and minor total principal stresses at failure.

Experience has shown that the $\bar{c}$ and $\bar{\phi}$ values determined by consolidated-undrained triaxial tests on soils with pore pressure measurements (Bishop and Henkel, 1962) correlated well with field behavior. For these tests a soil sample, usually 1 1/2-in. in diameter by 3 in. high, is subjected to an all-around pressure σ_3 and allowed to consolidate under drained conditions. The vertical stress σ_1 is next increased under undrained conditions until the sample fails. Failure is taken to be the maximum deviator stress $(\sigma_1 - \sigma_3)$ or for some soils is taken at an arbitrary strain of 10 percent or 20 percent. During the loading period measurements are taken of pore water pressure, axial deformation, and axial load. Results from each test are represented by an effective stress circle at failure. If several triaxial tests are performed with different consolidation pressures and the measured stresses corresponding to failure plotted, the points representing failure are given by the envelope of stress circles. This envelope is known as the rupture line and, although it may not be perfectly straight, it can be represented by a straight line with sufficient accuracy so that the resulting material properties adequately reflect field behavior for soils. In normal laboratory evaluation three to five tests are made and the rupture line is drawn tangent to the observed failure circles. Since this method of evaluation depends on visual determination of the tangent points, it is desirable to adopt a method that uses the points of maximum shear stress at failure. Lambe and Whitman (1969) represented these points as

$$\bar{p}_f = \frac{\bar{\sigma}_1 + \bar{\sigma}_3}{2} \quad \text{and} \quad \bar{q}_f = \frac{\bar{\sigma}_1 - \bar{\sigma}_3}{2} = \frac{\sigma_1 - \sigma_3}{2} \qquad (2.21)$$

These points are unambiguous and precisely determined, allowing curve fitting methods to determine the line of best fit. This method gives the K_f failure line and results in a y intercept $\bar{a}$ and a slope angle $\bar{\alpha}$. The geometric transformations given in Figure 2.3 permit computation of the desired values of $\bar{c}$ and $\bar{\phi}$. Detailed information on triaxial tests used in this study are given in Chapter III.

Soil or sludge located beneath a sloping surface has a tendency to move downward and outward under the influence of gravity. Material beneath foundations moves downward and outward as loads approach the bearing capacity of the material. When this tendency is counteracted by the shearing resistance of the soil or sludge, the slope or foundation is stable. Otherwise a failure occurs. For a slope this failure may take the form of a flow, a rotational movement along a circular slip surface, or a movement along a composite slip surface. Slides in soil or sludge may be caused by external disturbances such as excavation near the base of the slope or additional loading on or behind the slope from more fill or the placement of some other load. Failure in soils may also be caused by a temporary increase in porewater pressure or by a progressive deterioration of the strength of the material. Methods for evaluating the stability of slopes are summarized in the next section.

Methods of Analyses

In principle an analysis of the distribution of displacements or stresses throughout a slope could be used to decide the question of its behavior. At present, however, there is generally insufficient knowledge of the in situ stresses and stress-deformation-time properties of soils to make this approach practicable. As a result it is general practice to use limit equilibrium methods to assess the stability of soil slopes (Lambe and Whitman, 1969). In all methods of limit equilibrium analysis, a condition of incipient failure is postulated along a continuous slip surface of known or assumed shape. A quantitative estimate of the factor of safety of the slope with respect to shear strength is then obtained by examining the equilibrium of the soil mass above this rupture surface. The problem is usually assumed to be one of plane strain. The two methods of analysis summarized include rotational movement along a circular slip surface and movement along a composite (non-circular) slip surface. A summary of a recent approach for investigating the development of failure zones around slopes during excavation completes this chapter.

Rotational Movement. The circular arc analysis which is sufficiently accurate for most purposes is that given by Bishop (1954) and generally termed the Bishop simplified method (Figure 2. 4a). This method is derived by equating the moments about point 0 of the weight of soil within ABCD with the moment of the shear forces acting on the slip surface. For convenience the soil within ABCD is divided into a number of slices, one of which is shown in Figure 2. 4a. The normal effective force ($P - u\ell$) on the base of the slice considered, denoted by $\overline{P}$, is found by resolving forces vertically. Thence, assuming that $(X_n - X_{n+1}) = 0$, the following expression for the factor of safety F is obtained:

$$F = \frac{1}{\Sigma W \sin \alpha} \cdot \sum \left[\{ \overline{c}\, b + (W - u\, b) \tan \overline{\phi} \} \frac{1}{m_\alpha} \right] \qquad (2.22)$$

where

$$m_\alpha = \cos \alpha \left(1 + \frac{1}{F} \tan \alpha \cdot \tan \overline{\phi}\right) \qquad (2.23)$$

Symbols are defined in Figure 2. 4a. The factor of safety F is defined as the ratio of the available shear strength of the soil to that required to maintain equilibrium. As the term F appears on both sides of equation 2. 22 the solution has to be obtained by a process of successive approximation. Convergence is very rapid and the method can be carried out easily by hand or by computer (Bailey and Christian, 1969). Values of m_α can be read off a chart for any assumed value of F. In general the error resulting from use of the Bishop simplified method is 7 percent or less and is usually under 2 percent (Whitman and Bailey, 1967).

For the total stress ($\phi_u = 0$) analysis the shear strength mobilized equals c_u/F. Since this shear strength is independent of the normal stress on the slip surface, a simplification results. Equating moments, as before, yields the expression for the factor of safety F. If the method of slices is used this expression has the form:

$$F = \frac{\Sigma c_u \ell}{\Sigma W \sin \alpha} \tag{2.24}$$

This expression is exact, and is easily adaptable to irregular slope profiles and non-uniform shear strength conditions.

Composite Sliding Surface. A rather accurate method of analyzing noncircular slip surfaces is given by Janbu (1954, 1957). In order to render the problem statically determinate Janbu assumed that the reaction forces dN (Figure 2.4b) acted at the center of the base $d\ell$ of the slice and that the position of the resulting earth pressures E and E + dE at the interface between adjacent slices are known. Using the notation of Figure 2.4b the equations of equilibrium for each slice are:

Vertical: $dW + dP + dT = dS \sin \alpha + dN \cos \alpha$ (2.25)

Horizontal: $dE - dQ = - dS \cos \alpha + dN \sin \alpha$ (2.26)

Moment about M: $TDx + E\, dy_t - dE\, h_t + dQ\, z = 0$ (2.27)

For a stability analysis in terms of effective stresses, introduction of the appropriate expression for shear strength leads to the following working formula for finite differences:

$$F = \frac{\Sigma\, \tau_f \cos^{-2} \alpha \cdot \Delta x}{Q - E_b + \Sigma(p + t) \tan \alpha \cdot \Delta x} \tag{2.28}$$

where

$$\tau_f = \frac{\overline{c} + (p + t - u) \tan \overline{\phi}}{1 + (\tan \alpha \cdot \tan \overline{\phi}) \frac{1}{F}} , \tag{2.29}$$

$$p = \frac{\Delta W}{\Delta x} + \frac{\Delta P}{\Delta x} = \gamma z + q , \quad \text{and} \quad t = \frac{\Delta T}{\Delta x} .$$

By assuming a reasonable position for the line of thrust, accurate values for the internal forces, E and T, are obtained by means of successive approximation procedures. Initial values of E and T can be calculated for the condition $t = 0$. When τ_f is introduced into the moment equation for slip circle analyses one obtains the formula derived by Bishop (1954). Total stress ($\phi_u = 0$) analysis for non-circular slip surfaces is provided by using the average undrained shear strength on the base of the slice in equation 2. 29.

Failure Zone Around Slopes During Excavation. Failure zones develop in excavated slopes when the maximum shear stress values approach the shear strength of the papermill sludge or when tensile stresses exceed the very low tensile strength of the sludge. When idealized elastic properties are assumed for soil slopes, local overstress will occur when the factor of safety (by the slip circle method) lies below a value of about 1. 8 (Bishop, 1954). Plans for the experimental papermill sludge landfill included slope failure (factor of safety close to unity), hence local overstress, such as tension cracks, was anticipated. It appeared desirable to determine in what portions of the experimental slope failure first occurred and how it progressed. In order to predict stresses within the slope, it was necessary to employ analytical procedures other than the equilibrium methods. The finite element method of analysis, as used by Dunlop, et al.(1968) in their analyses of slopes in soil, appeared suitable for investigating the development of failure zones in the sludge slope. The basic concepts of the finite element method are summarized in the following paragraphs and its application to the experimental papermill sludge slope is given in chapter VI.

The finite element method may be thought of as an application of the displacement or stiffness method of structural analysis. The basic concept of the method is that a continuous structure may be represented as an assemblage of elements interconnected at a finite number of nodal points. The elements may be triangles, groups of triangles, or rectangles for two-dimensional plane strain analyses. Within each element, displacements are assumed to vary in such a way that compatibility within the element and along its boundaries is maintained. For triangular elements with three nodal points this may be accomplished by specifying displacements which vary linearly in two mutually perpendicular directions within the element. For elements with more nodal points, higher order displacement variations are employed.

The finite element analysis of an elastic continuum consists of four basic steps:

(1) Structural idealization of the continuum so that the finite element assemblage simulates the continuum,

(2) Determination of the stiffness characteristics of each element to obtain a total structural stiffness matrix,

(3) Analysis of the structure by standard structural methods to determine the nodal point displacements, and

(4) Determination of the element stresses from the nodal point displacements.

Because each element in the assemblage may have a different modulus value from its neighbors, the method is well-suited to soil problems involving heterogeneity. Approximate analyses of nonlinear earth structures are possible by incremental loading or iterative procedures. The finite element method is also capable of handling virtually any boundary conditions specified in terms of forces, stresses (resolved into forces) and displacements. Mixed boundary value problems may be handled as easily as problems involving only force or displacement boundary conditions.

Dunlop, et al. (1968) performed a detailed finite element analysis of excavated soil slopes. In their analysis the basic finite element consisted of a quadrilateral composed of four constant strain triangles which was used in a plane strain idealization of the slope. The study provided computations of displacements, strains, and stress distributions, and it enabled the location of failure zones. The effect of such factors as in situ stresses, anisotropy, variation of strength within the soil deposit, pore pressure distributions, and sequential construction were studied. Various constitutive laws, such as linear, bilinear, and multilinear (piecewise linear) were compared. Requirements for boundary conditions, element sizes and element shapes, and a finite element computer program for excavated slopes are given by Dunlop, et al. (1968).

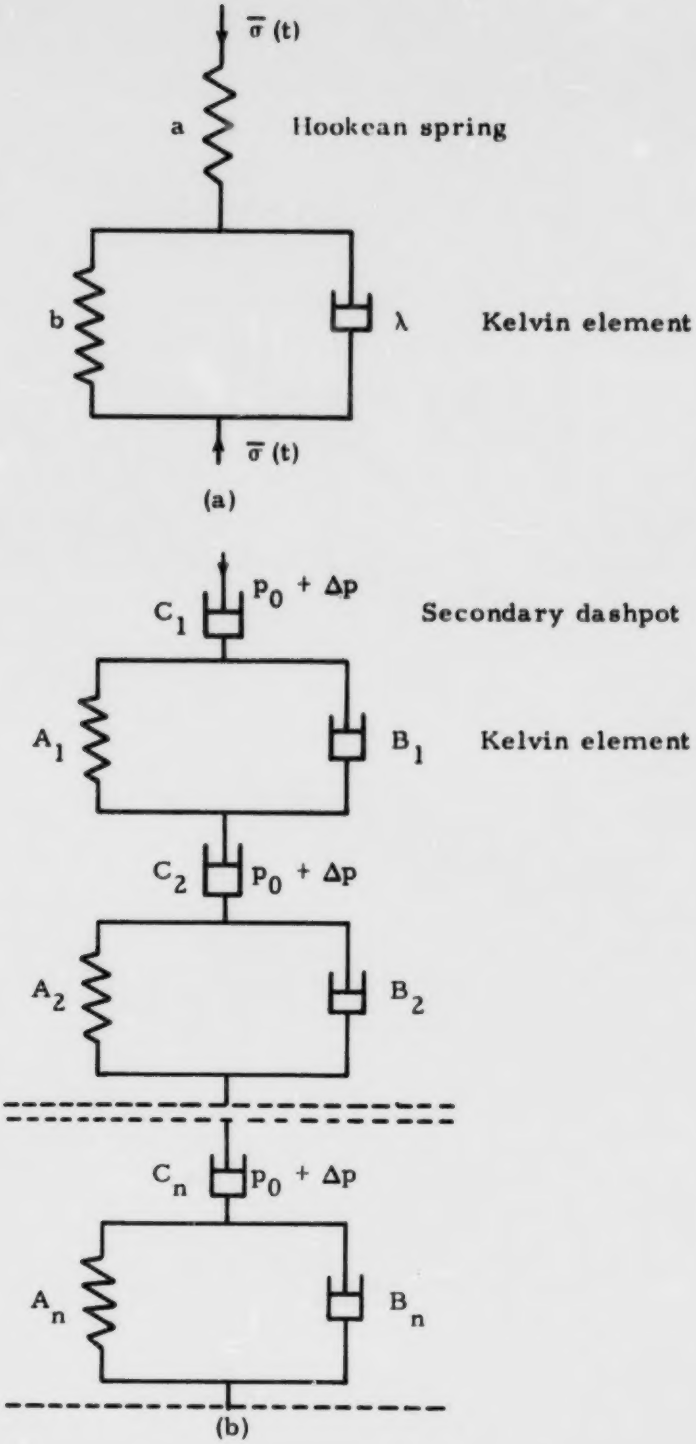
$\bar{\sigma}$ (t)
a
Hookean spring
b
λ
Kelvin element
$\bar{\sigma}$ (t)
(a)
C_1
$p_0 + \Delta p$
Secondary dashpot
A_1
B_1
Kelvin element
C_2
$p_0 + \Delta p$
A_2
B_2
C_n
$p_0 + \Delta p$
A_n
B_n
(b)

Figure 2.1. Models for the consolidation process. (a) Gibson and Lo (1961). (b) Wahls (1962).

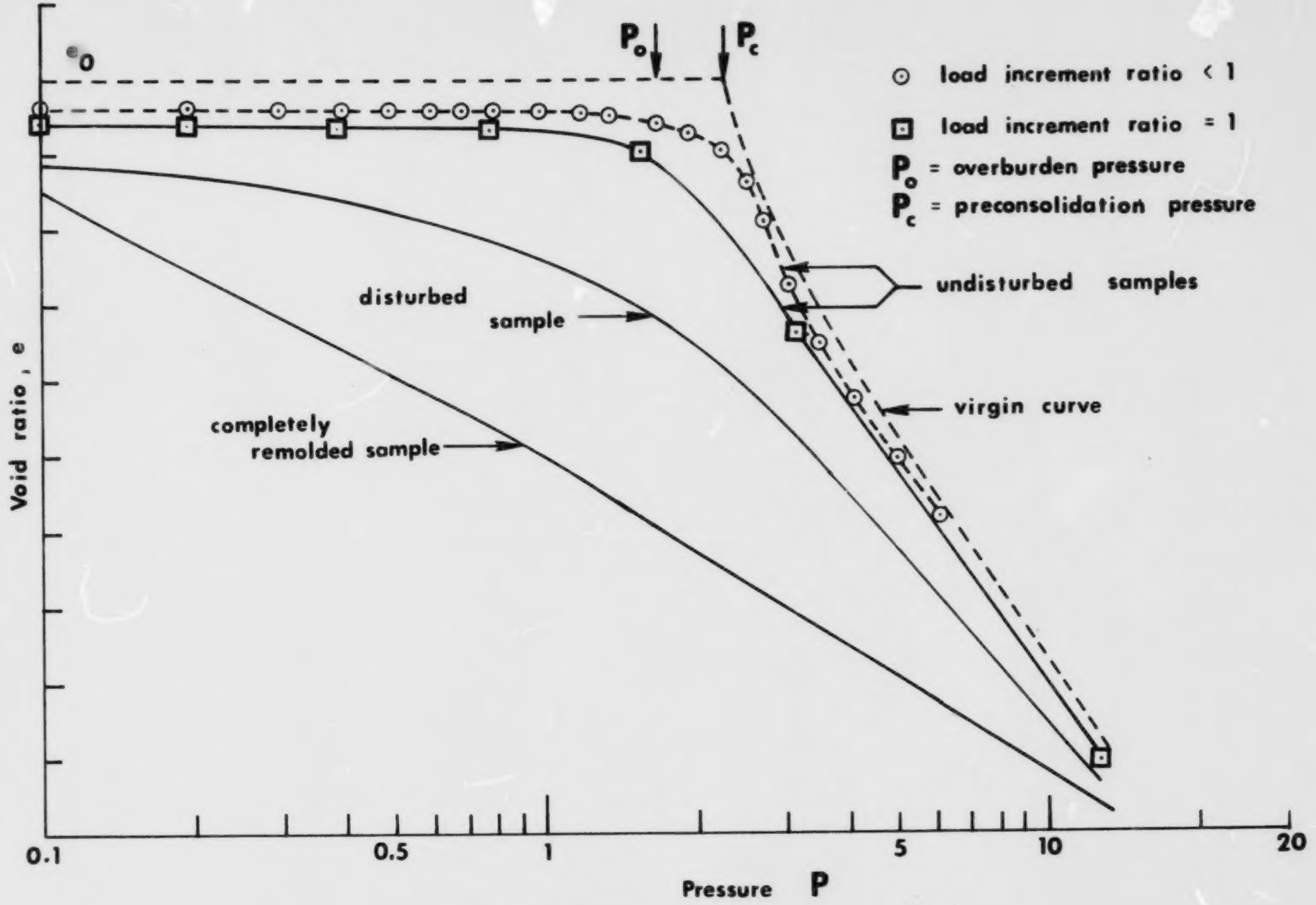

Figure 2.2 Void ratio--effective stress relationships for a normally consolidated clay (after Leonards, 1962).

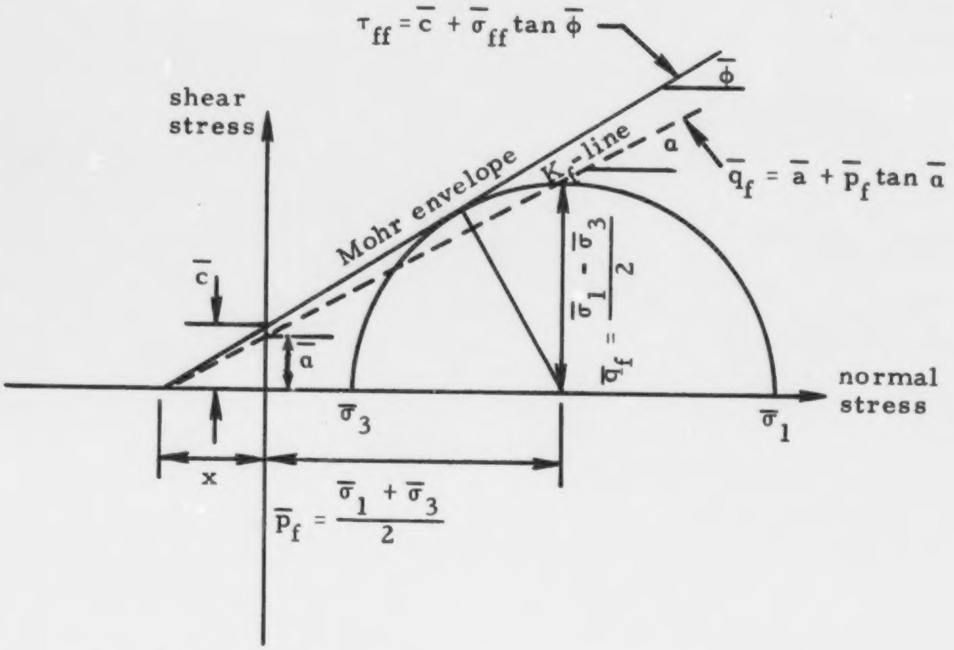
$\tau_{ff} = \bar{c} + \bar{\sigma}_{ff} \tan \bar{\phi}$
$\bar{\phi}$
shear stress
$\bar{K}_f$-line
$\bar{\alpha}$
$\bar{q}_f = \bar{a} + \bar{p}_f \tan \bar{\alpha}$
Mohr envelope
$\bar{c}$
$\bar{a}$
$\bar{q}_f = \frac{\bar{\sigma}_1 - \bar{\sigma}_3}{2}$
normal stress
$\bar{\sigma}_3$
$\bar{\sigma}_1$
x
$\bar{p}_f = \frac{\bar{\sigma}_1 + \bar{\sigma}_3}{2}$

$$\tan \bar{\alpha} = \frac{\dfrac{\bar{\sigma}_1 - \bar{\sigma}_3}{2}}{\dfrac{\bar{\sigma}_1 + \bar{\sigma}_3}{2} + x}$$

$$\sin \bar{\phi} = \frac{\dfrac{\bar{\sigma}_1 - \bar{\sigma}_3}{2}}{\dfrac{\bar{\sigma}_1 + \bar{\sigma}_3}{2} + x}$$

$$\therefore \tan \bar{\alpha} = \sin \bar{\phi}$$

$$\tan \bar{\alpha} = \frac{\bar{a}}{x} \quad \text{or} \quad x = \frac{\bar{a}}{\tan \bar{\alpha}}$$

$$\tan \bar{\phi} = \frac{\bar{c}}{x} \quad \text{or} \quad x = \frac{\bar{c}}{\tan \bar{\phi}}$$

$$\therefore \frac{\bar{a}}{\tan \bar{\alpha}} = \frac{\bar{c}}{\tan \bar{\phi}}$$

$$\text{but } \tan \bar{\alpha} = \sin \bar{\phi}$$

$$\therefore \frac{\bar{c}}{\tan \bar{\phi}} = \frac{\bar{a}}{\sin \bar{\phi}}$$

$$\bar{c} = \frac{\bar{a}}{\cos \bar{\phi}}$$

Figure 2. 3. Equations and definitions for shear strength theory, effective stress basis.

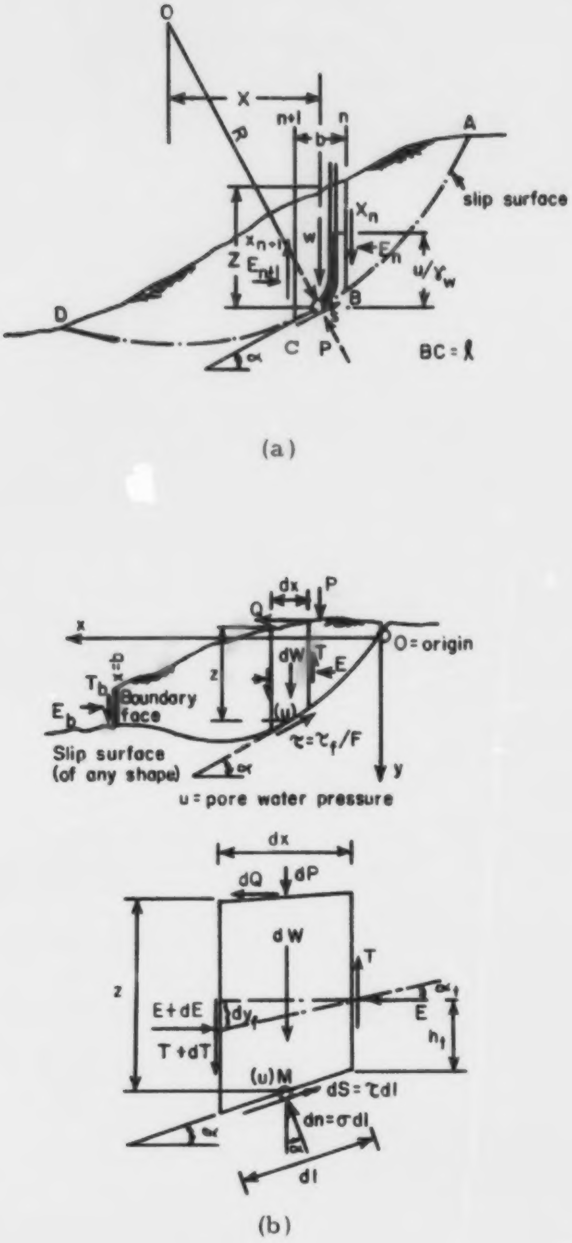
O
X
R
n+l
n
b
A
slip surface
X_n
X_{n+1}
W
E_n
u/γ_w
Z
E_{n+1}
B
D
C
P
α
BC = l
(a)
dx
P
Q
x
O = origin
dW
T
E
z
$\frac{dx}{x}$
T_b
E_b
Boundary face
(u)
$\tau = \tau_f / F$
Slip surface (of any shape)
α
y
u = pore water pressure
dx
dQ
dP
dW
T
z
E+dE
dy_t
E
α_t
h_t
T+dT
(u)M
dS = τdl
dn = σdl
α
dl
(b)

Figure 2.4. (a) Forces in the circular arc analysis (after Bishop, 1954). (b) Notation to Janbu's (1957) analytical procedure.

CHAPTER III. ENGINEERING PROPERTIES OF PAPERMILL SLUDGE

The physical properties and stress-deformation behavior of the papermill sludge are needed for making predictions, based on theory, of settlement and stability for comparison with observed field behavior of the experimental landfill. Methods and equipment for measurement of these engineering characteristics are described below. Reference is made to the First Annual Report and to standard test procedures where possible.

Physical Properties

Physical properties of papermill sludge characterize, to some extent, the quality of the sludge relative to engineering purposes. The First Annual Report includes information on measurement of water content, unit weight, specific gravity of the solids, ash (or organic) content, and consistency limits. The water content and unit weight have been used in describing changes in the sludge as a result of consolidation. Specific gravity was required for computations involving solids-water-air relationships. Additional ash contents from block samples provided more information on sludge uniformity. No additional consistency limits were run.

Stress Deformation Characteristics

The stress-deformation behavior of papermill sludge determines its volume change and settlement and will control stability of sludge landfills. The First Annual Report includes information on consolidation tests of fresh sludge samples. Methods used for evaluating the consolidation behavior of undisturbed sludge samples and the triaxial shear strength are given below.

Consolidation of Undisturbed Samples. Undisturbed block samples were obtained from the landfill when the north dike was removed for the stability study. Each block was cut from the exposed slope as shown in Figure 3.1a. The sides and top were wrapped in saran wrap and aluminum foil. Elevations were taken to properly describe the block location. Next a wooden box with the bottom removed was placed over the wrapped sludge. The block bottom was cut loose and the entire block turned over. After additional trimming, saran wrap and aluminum foil were folded over the bottom of the block. Warm paraffin was poured into the open spaces around the block and the box bottom was attached. These block samples of sludge were easily transported to the laboratory with a minimum of disturbance. Sludge blocks were protected against possible moisture loss during storage by placing each unopened box in a sealed plastic bag. Temperature during storage did not exceed about 24°C.

Two blocks were chosen to provide samples for laboratory consolidation tests. Block B was located at the mid-point of the upper sludge layer, 4.0 ft below the upper sand blanket, and block F was close to the mid-point of the lower sludge layer, 4.0 ft below the middle sand blanket. Because of the fibrous nature of the sludge, standard wire saws and other trimming devices could not be used to trim sludge from a block. A regular hand saw was first used to cut a 6 in. by 6 in. by 4 in. chunk of sludge from a block, then a small rotary hobby tool (Figure 3.1b) with a rapidly rotating (24,000 rpm) 3/4 in. diameter circular saw tooth blade was used to trim the sludge to the consolidation ring dimensions (3 in. diameter by 3/4 in. high). Once inside the ring, the sludge surface was wetted slightly and smoothed to conform to the ring height. Although this procedure resulted in some sample disturbance, both through handling and vibration from the saw, the low sensitivity of the sludge allowed good results to be obtained from the consolidation test.

A total of four consolidation tests were run on samples obtained from each block. Two of the tests used load increments of 15 minutes duration, and two with load increments of 12 hours duration. The rapid loading tests, using load increment ratios less than one, provided data for the void ratio versus logarithm of pressure curves. The 12 hour tests, using a load increment ratio of one, provided data on the time rate of consolidation. Details on consolidation equipment have been given in the First Annual Report.

Triaxial Shear Tests. The triaxial test requires that the cylindrical specimen (Figure 3.2a) be sealed in a water-tight membrane and be enclosed in a cell (Figure 3.2b) in which the specimen can be subjected to a fluid pressure. A load applied axially, through a ram acting on the top sample cap, was used to control the deviator stress. Under these conditions the axial stress was the major principal stress, σ_1, and the intermediate and minor principal stress (σ_2 and σ_3, respectively) were both equal to the cell pressure. Connections to the ends of the sample permitted either drainage of water and air from the voids in the sludge, or alternatively, the measurement of the pore pressure under conditions of no drainage. Generally the application of the all-around pressure and of the deviator stress form two separate stages of the test. Therefore triaxial tests are classified according to the conditions of drainage developed during each stage and any special conditions imposed on the sample to simulate field conditions. Sample preparation, undrained tests, and consolidated-undrained tests are described below. All triaxial tests were run at room temperature, close to 23°C.

Sample Preparation. For fresh sludge obtained during construction of the landfill, sample preparation involved placement into a cylindrical mold 7. 13 cm high by 3. 56 cm in diameter. Care was taken to work the sludge into the mold so as to minimize layering and the formation of any cavities. Fibers were not oriented in any preferred direction. With the mold filled, the ends were carefully trimmed until they were perpendicular to the sample axis. Next the mold was disassembled by pulling the sides directly away from the specimen. The sample was then weighed, placed in an air tight container, and stored in a high humidity compartment until just prior to mounting in the triaxial cell. Different organic content test specimens were obtained by the appropriate selection of sludge from the available field samples.

Undisturbed test specimens were obtained from block samples C and G. Specimen preparation involved cutting, by means of a hand saw, a 4 in. by 4 in. by 6 in. chunk from the block of sludge. For additional strength during handling, each end of the sample was wrapped with tape and encased in wax. This sample of sludge was then placed in a motorized soil lathe. Since wire trimming devices were not suitable, a hobby tool with a high speed rotating 3/4 in. diameter circular saw was used for trimming the sludge into cylindrical specimens 2 in. in diameter by 4 in. high (Figure 3. 2c). The low sensitivity of the consolidated sludge helped minimize sample disturbance. Specimens were prepared with the cylindrical axis vertical, horizontal, or at 45 degrees to the horizontal as needed for the test program. After trimming, sample dimensions and weight were recorded. Sample specimens were stored in a sealed plastic bag and placed in a high humidity compartment until just prior to test.

Undrained Test. The undrained strength of the sludge was determined by tests in which no overall water content change was permitted to occur during application of the deviator stress. When a saturated sludge is subjected to a change in magnitude of an all-around total pressure, without change in water content, the undrained strength in a given direction remains unaltered. Thus the sludge for these conditions behaves, in respect to changes in total stress, as a material with zero angle of shearing resistance, i. e., $\phi_u = 0$ and $c_u = 1/2(\sigma_1 - \sigma_3)$. This result is a consequence of the fact that a change in all-around pressure causes a precisely equal change in pore pressure, provided the sludge is fully saturated; and the effective stresses therefore remain unaltered. For partly saturated sludges there will be some increase in effective stresses as air in the voids is compressed and passes into solution. When stresses are large enough to cause full saturation the sludge again behaves as a material with zero angle of shearing resistance. Bishop and Henkel (1962) have shown that the increase in pore pressure Δu_{as} necessary to lead to full saturation is given by the expression

$$\Delta u_{as} = u_{ao} \cdot \frac{(1 - S_o)}{S_o H} \tag{3. 1}$$

where u_{ao} is the initial air pressure (abs.), S_o is the initial degree of saturation, and H is Henry's coefficient of solubility (approximately 0.02 at 20^{o}C). A backpressure of 20 psi (0.703 kg/cm^2) was used for fresh sludge samples and 40 psi (1.406 kg/cm^2) was used for undisturbed sludge samples to ensure full saturation. No back pressure or lateral pressure was used for the unconfined compression tests. The effect of sludge anisotropy on undrained strength was determined by testing samples with their axis oriented at zero, 45 degrees, and 90 degrees to the horizontal. More details for the undrained test are given by Bishop and Henkel (1962).

Consolidated-Undrained Test. Consolidation and application of the deviator stress form two separate stages of the test. For isotropic consolidation of the fresh sludge, samples were allowed to consolidate under a cell pressure of known magnitude, the three principal stresses thus being equal. Side drains consisting of filter paper strips (Bishop and Henkel, 1962) were used to accelerate consolidation. Then the sample was sheared under undrained conditions by increasing the deviator stress. A backpressure of 40 psi (1.406 kg/cm^2) was used for the undrained stage of the test to ensure full saturation of the undisturbed samples. The test result, in terms of total stresses, was expressed as the value of the undrained strength, c_u, plotted against consolidation pressure, p. As before, $c_u = 1/2(\sigma_1 - \sigma_3)_f$, since $\phi_u = 0$ with respect to changes in total stress during undrained shear. When pore pressures were measured during the undrained stage of the test, the results were expressed in terms of effective stress. This permitted evaluation of the strength parameters $\bar{c}$ and $\bar{\phi}$ as outlined in Chapter II. Side drains helped equalize pore pressures within the undrained specimen more rapidly when the deviator stress was increased.

The stress conditions under which consolidation occurs in most practical problems does not approximate equal all-around pressure. The consolidation of natural strata under their own weight occurs under conditions of no lateral yield, for which the stress ratio $\bar{\sigma}_3/\bar{\sigma}_1$ is equal to the coefficient of earth pressure at rest, K_o. Therefore, anisotropic consolidation with $K_o = 0.3$ was used on most of the undisturbed sludge samples. The K_o value selected was based on total pressure cell and piezometer data for the landfill. For selected specimens this test procedure was further modified by holding σ_1 constant and permitting σ_3 to decrease. This modified test procedure was intended to more closely reproduce field conditions existing during excavation. For example, excavation for the experimental sludge landfill slope involved primarily a decrease in lateral stresses while the vertical stresses remained constant. Both the method of consolidation and any special loading conditions are given with the experimental data reported in Chapter V. Details on test procedures are again referred to the Measurement of Soil Properties in the Triaxial Test by Bishop and Henkel (1962). Certain abbreviations describing most of the above test conditions which have come into general usage include:

- $\overline{\text{CIU}}$ -- consolidated undrained triaxial test with isotropic consolidation and pore pressure measurements,
- $\overline{\text{CAU}}$ -- consolidated undrained triaxial test with anisotropic consolidation and pore pressure measurements.

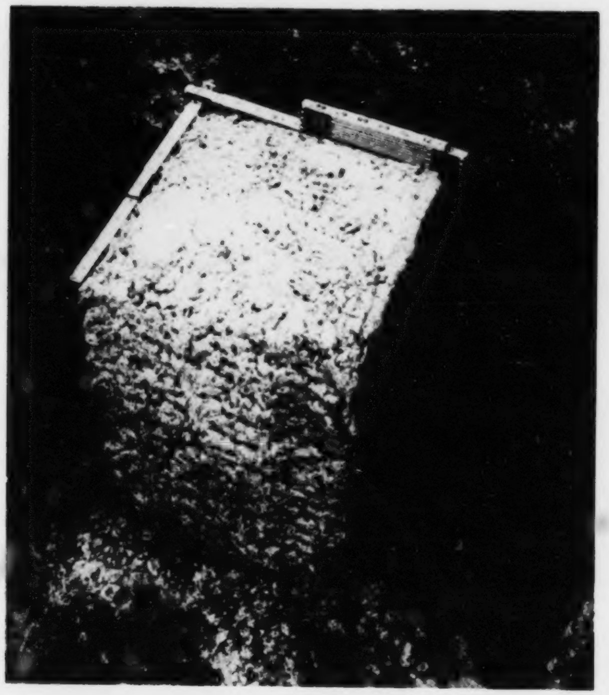

(a)

(b)

Figure 3. 1. (a) Undisturbed block sample of consolidated sludge.
(b) Sample preparation using a high speed rotary saw.

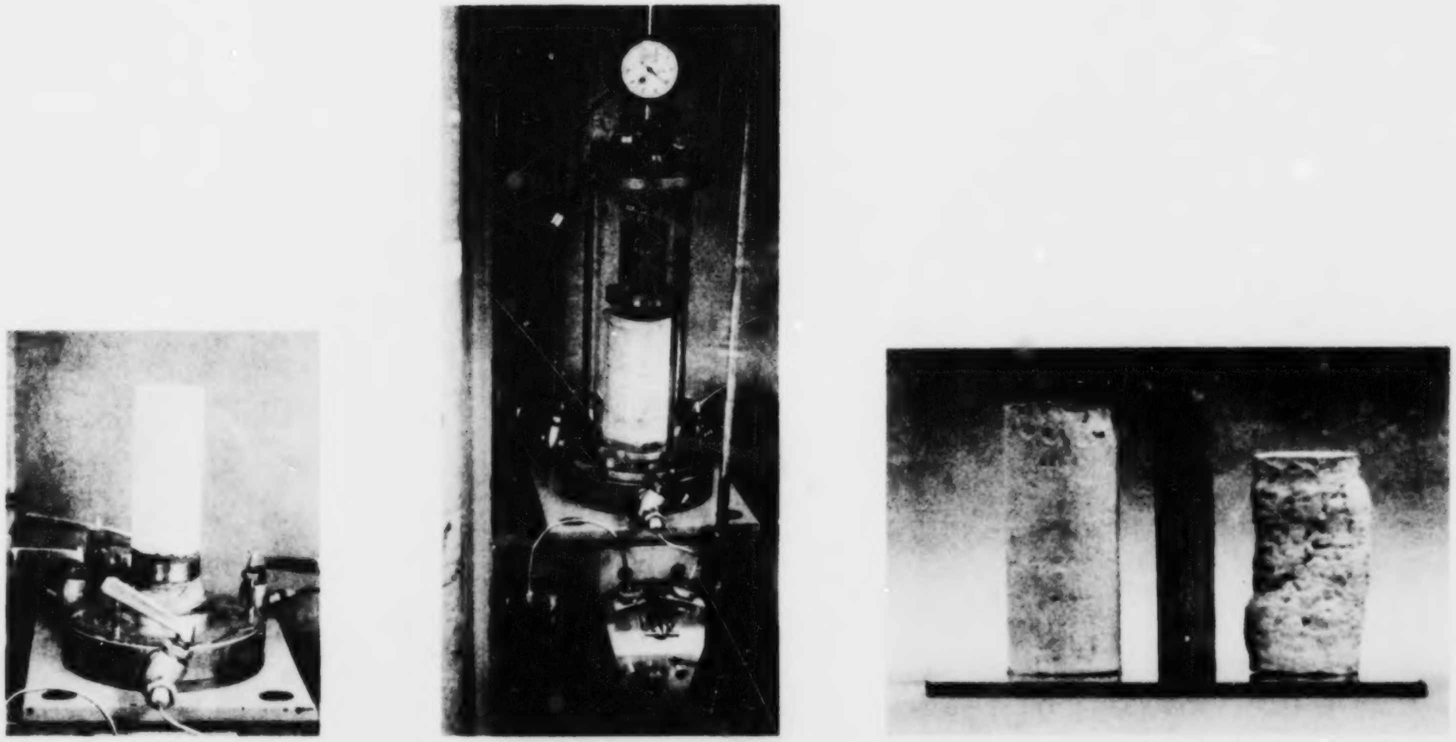

(a) (b) (c)

Figure 3. 2. Triaxial tests. (a) Mounting the cylindrical sample. (b) Anistropic consolidation in the triaxial cell. (c) Newly prepared sample left, failed and oven dry sample right.

CHAPTER IV. INSTRUMENTATION, MONITORING, AND EXCAVATION

Instrumentation and Monitoring

Instrumentation placed during construction of the experimental landfill continued to serve the monitoring needs during phase (2) of the project. Additional instrumentation placed September 7-11, 1972, included seven slope indicator casings, six more piezometers, and horizontal control stakes. These were located so as to provide information on the slope behavior. All instruments were monitored before, during excavation of the experimental slope, and as needed during the remainder of the second year of the project. Leachate sampling and analysis documented any changes in composition during the second year of the project. The following sections describe instrumentation for horizontal and vertical movement, piezometers, total pressure cells and temperature sensors, and the leachate sampling and analysis.

Horizontal Movement. Removal of the north dike and excavation of the experimental slope reduced lateral stresses on the exposed sludge surface to zero. Unloading the slope permits lateral deformations to occur which may be stress related and/or creep dependent. The magnitude of movement may vary with depth and with the location of any failure zones. Slope indicator casings and surface measurements provided information on these horizontal movements.

Slope Indicator Casings. Flexible vertical casings were installed through the earth surcharge, sand drainage blankets, and both sludge layers, to about one foot into the natural soil below the experimental landfill at locations A through G, shown on Figure 4. 1. Installation involved drilling a 6 inch hole using a hollow core auger, placement of the 3. 19 in. OD aluminum casing (0. 093 in. wall), and pumping a bentonite clay-water mixture into the opening outside the casing. Lateral movement in the sludge was transferred by the clay to the flexible casing. A precision instrument (Slope Indicator series 200B) was then lowered down the casing with orientation of the instrument predetermined by the grooves oriented either parallel to or normal to the experimental slope. Inclination readings taken at 2 foot intervals of depth were subsequently converted to lateral displacements. Instrument sensitivity permits displacement measurements in thin shear zones of less than 1/16 inch. Consecutive readings at the same depths, taken at periodic intervals of time, were used to determine the amount and rate of ground movement.

Surface Measurements. Wood control stakes, 2-in. by 2-in. by 1 1/2-ft long, were placed in the earth surcharge and dike opposite to the slope as shown in Figure 4. 2. Movements of the sludge embankment toward the slope were noted by an increase in measured distance from the three reference stakes placed in the dike. Consecutive readings taken at periodic intervals of time were used to determine rate of surface movement. Damage to the stakes from external sources was minimal.

Vertical Movement. Vertical movement results from consolidation of the sludge and downward movement at and near the face of the experimental slope during and following excavation. This movement was monitored using settlement plates placed during construction of the experimental landfill. Settlement plate locations are given by instrument group (Figure 4. 1) and plate number (Figure 4. 3). Each settlement plate consisted of a 2-ft by 2-ft by 1/8-in. thick aluminum plate with a 3/8-in. diameter steel rod of known length attached to the center. A 1 1/2-in. O. D. aluminum tube placed around the steel rod eliminated any adhesion between the sludge and the rod. The lower plate was located at the center of the group with each higher plate offset by 1 1/2-ft. Elevations taken with a surveyor's level (or transit) on the top of each steel rod were referenced to a bench mark outside the fill area. Duplicate plate locations also served as insurance in case of accidental loss and the additional data served as a check on adjacent groups.

Piezometers. Piezometers measure the static pressure or head (elevation to which water will rise in an open standpipe) of the fluid in the pore space between the solid sludge particles. Stress reduction to zero at the exposed experimental slope will reduce pore water pressures. Shear strains in the sludge mass serve to increase pore water pressures. Measurement of these pore pressure changes involved installation of six additional units as part of instrument group 4, near the experimental slope. Piezometer locations are given by instrument group (Figure 4. 1) and piezometer number (Figure 4. 3).

The pneumatic type piezometer (Slope Indicator Company Model 51401) used on the project did not require in-place calibration and was not subject to changes in sensitivity. The sensitivity of the unit approaches 0. 5-in. of water. The standard Norton Casagrande type filter with large pore size and low air entry pressure was used because the sludge has a high degree of saturation. All piezometers were separated from direct contact with the sludge by about 3-in. of sand so as to minimize any influence sludge decomposition might have on the piezometer operation. The transducer converts water pressure into pneumatic pressure which is relayed to the surface reading station by means of twin nylon tubing. Pore pressure readings were taken with the Model 51421 (Slope Indicator Company) portable pore pressure indicator from terminal boxes which were housed in two wooden boxes located on the landfill.

Total Pressure Cells and Temperature Sensors. Total pressure cells help in determining the state of stress in the sludge mass. Cell description and installation has been given in the First Annual Report. Locations of the two vertical cells and one horizontal cell, part of instrument group 7, are given on Figure 4. 3.

Temperature sensors, small YSI precision thermistors, provided temperature data at 2 ft depth intervals for a given location in the experimental landfill. Thermistors and the method of installation have been described in the First Annual Report. Thermistor elevations are given in Figure 4. 3.

Leachate Sampling and Analysis. A total of six leachate samples were periodically obtained from the landfill in accordance with the schedule shown in Table 4. 1. Samples identified as I through IV were obtained from the middle sand blanket at the point where it was exposed following excavation of the north side of the landfill to permit stability evaluation. As a consequence of the slope face being coated with snow and ice, sample V was collected from the bottom of a slope indicator pipe. Sample VI was extracted from a sludge sample removed from the upper sludge layer by pressing it in a laboratory press. Throughout the study, samples were collected and/or stored in transit in plastic containers.

Analyses performed upon samples I through V included (a) biochemical oxygen demand (BOD), (b) chemical oxygen demand (COD), (c) pH, (d) specific conductance, (e) turbidity, (f) color, (g) dissolved solids, (h) suspended solids, (i) total iron, (j) total hardness, (k) chloride, (l) alkalinity, and (m) sulfate. The same tests were performed upon sample VI, excluding total and suspended solids due to the manner in which the sample was obtained. Sample VI was also analyzed for total Kjeldahl nitrogen and total phosphorous. With the exception of color, all analyses were conducted in accordance with Standard Methods for the Examination of Water and Wastewater, 13th edition. Color determinations were made according to procedures given in NCASI technical bulletin No. 253.

Excavation for the Experimental Slope

Preparation of the experimental slope involved removal of the north dike and sludge excavation so as to give the slopes shown on Figure 4. 4. Preliminary information on the sludge stability was obtained September 21, 1972, by using a dragline bucket to excavate a trench about 40 ft long and 8 ft deep, down to the middle sand drainage layer. The trench face was about 20 ft forward from slope indicator casings B and C. The following day surface cracks had appeared about 2 ft back from the exposed sludge face. The trench excavation was continued to a depth close to 15 ft. The next day (September 23, 1972) the trench remained open but with new surface cracks about 4 ft back from the exposed face. Sand falling from the middle drainage blanket removed support for the upper sludge layer to about 1 1/2-ft back from the cut face. Dike removal was started on September 24, 1972. Heavy rain during the night softened the dike surface and adjacent area to an extent which prevented effective equipment operation. More rain delayed work until September 29, 1972. Dike material and sludge were removed, weather permitting, until completion of the 3:4 slope on October 13, 1972. Excavation work and the completed slope are shown in Figure 4. 5.

Movements in the 3:4 slope were small, hence excavation for the 1:8 slope was initiated at noon on October 24, 1972. The dozer removed sludge seven feet back from the toe of the 3:4 slope giving a vertical face to the lower sludge layer. Next the back-hoe removed sludge (Figure 4. 6a) so as to give the 1:8 slope. Sludge was removed from in front of the slope using the dozer (Figure 4.6b). Work was completed by noon on October 25, 1972.

TABLE 4.1. LEACHATE SAMPLES

Sample identification	Date sampled	Source
I	10/19/72	Middle sand blanket
II	11/21/72	Middle sand blanket
III	12/12/72	Middle sand blanket
IV	12/29/72	Middle sand blanket
V	2/10/72	*Bottom of a slope indicator pipe
VI	6/15/72	Pressed sludge sample

---

*Slope face covered with snow and ice, hence sample taken from a slope indicator pipe.

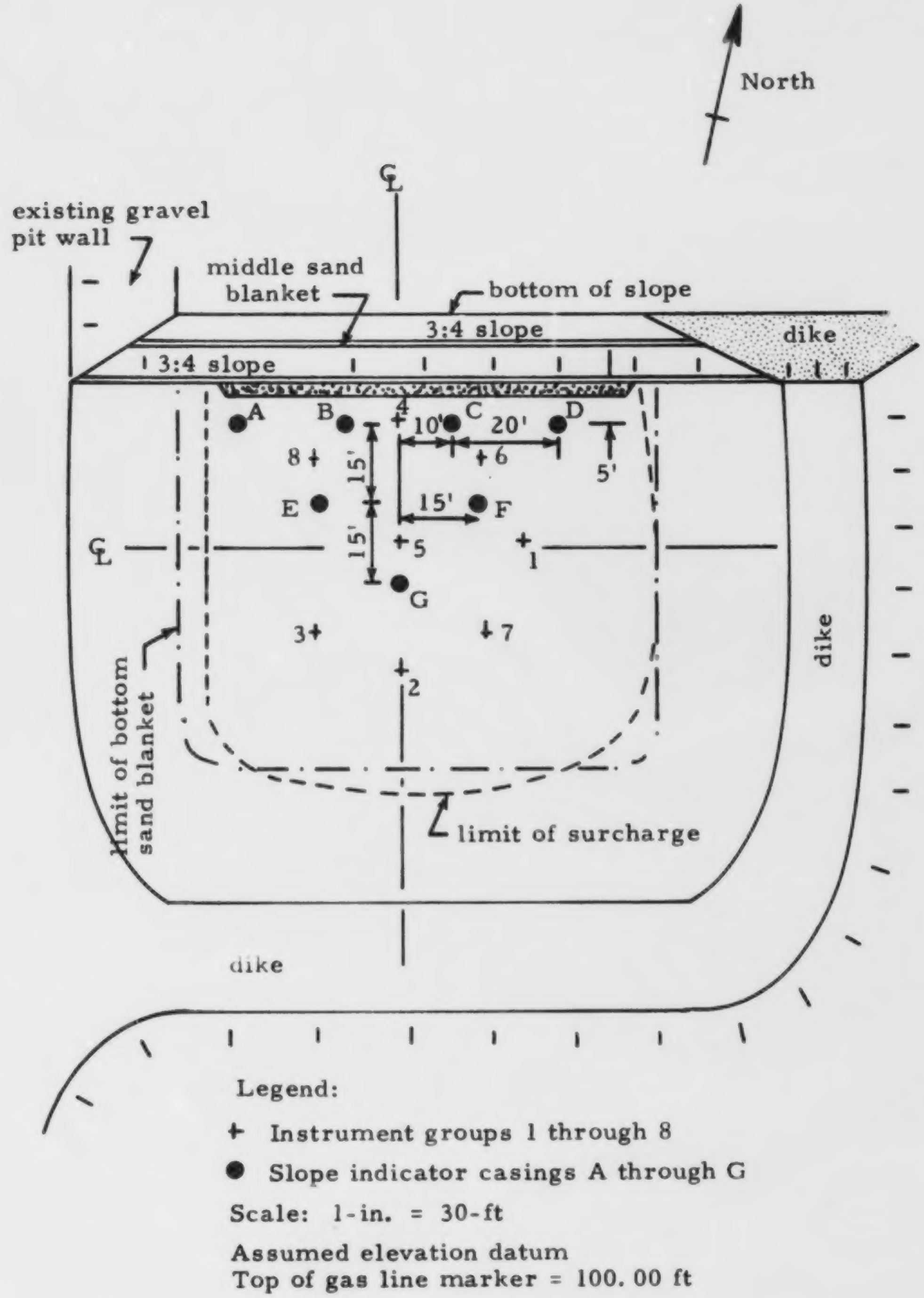

North
℄
existing gravel pit wall
middle sand blanket
bottom of slope
3:4 slope
3:4 slope
dike
A
B
4
C
D
10'
20'
8
6
5'
15'
E
15'
F
℄
5
1
15'
G
3
7
2
limit of bottom sand blanket
dike
limit of surcharge
dike
Legend:
+ Instrument groups 1 through 8
● Slope indicator casings A through G
Scale: 1-in. = 30-ft
Assumed elevation datum
Top of gas line marker = 100. 00 ft

Figure 4. 1. Slope indicator casing locations, A through G, and 3:4 slope, plan view.

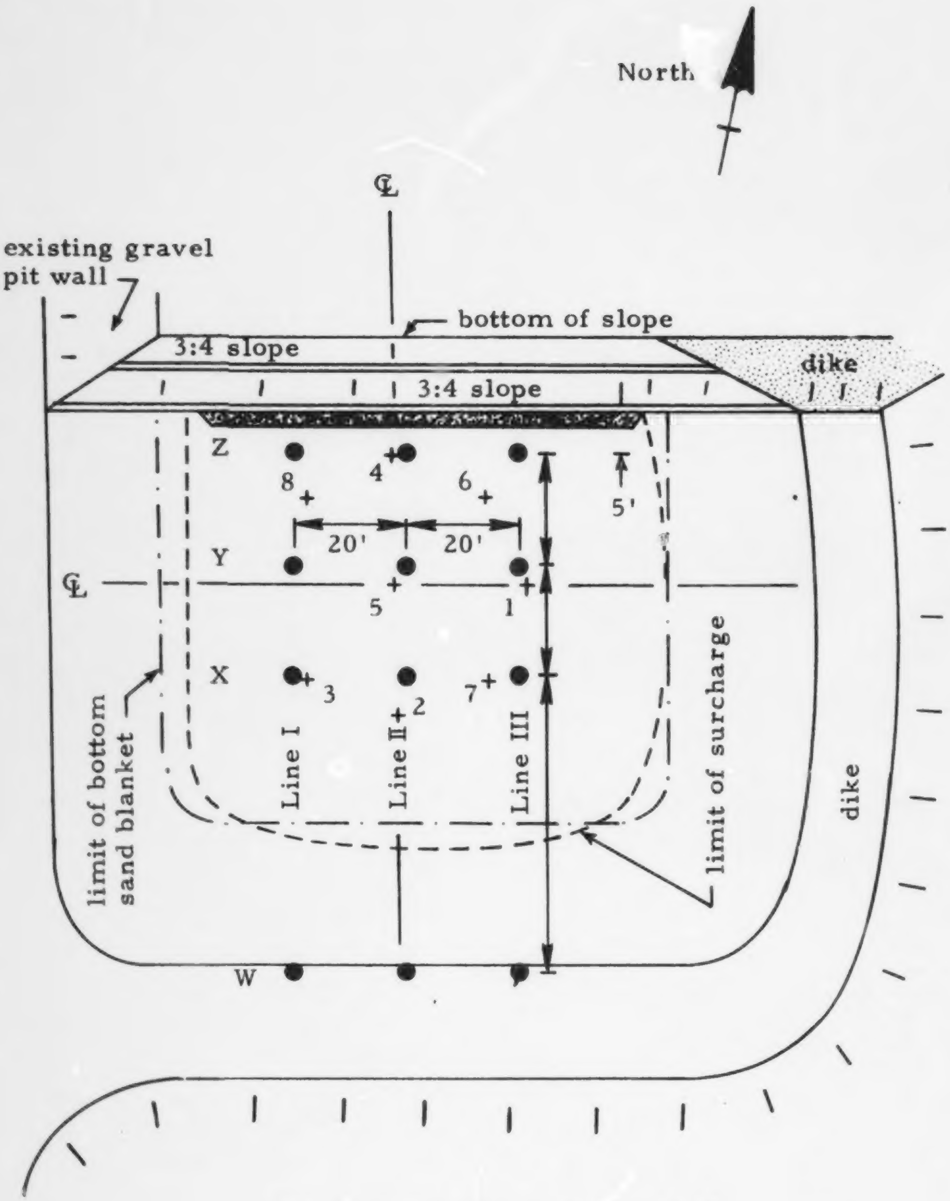
North
℄
existing gravel pit wall
bottom of slope
3:4 slope
3:4 slope
dike
Z
Y
X
W
8
4
6
5
1
3
2
7
20'
20'
5'
℄
Line I
Line II
Line III
limit of bottom sand blanket
limit of surcharge
dike

\+ Instrument groups 1 through 8

● Horizontal control stakes

Scale: 1-in. = 30-ft.

Assumed elevation datum
Top of gas line marker = 100.00 ft.

Figure 4.2. Horizontal control stake locations, plan view.

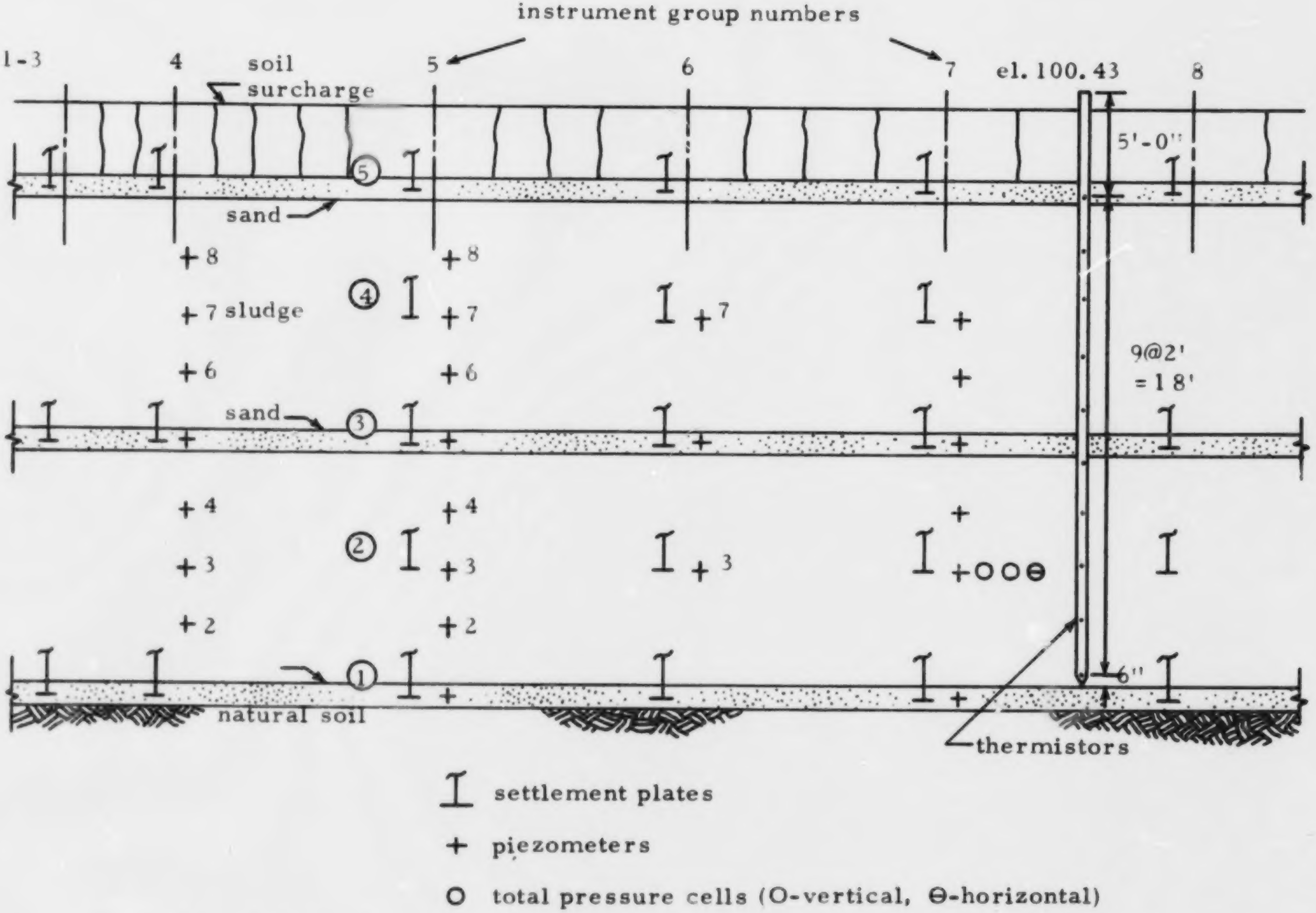
instrument group numbers
1-3
4
5
6
7
8
soil surcharge
sand
sludge
sand
natural soil
el. 100.43
5'-0"
9@2'
=18'
6"
thermistors
①
②
③
④
⑤
+8
+7
+6
+4
+3
+2
settlement plates
piezometers
total pressure cells (O-vertical, Θ-horizontal)

Figure 4.3. Distribution of settlement plates, piezometers, and total pressure cells in the instrument groups.

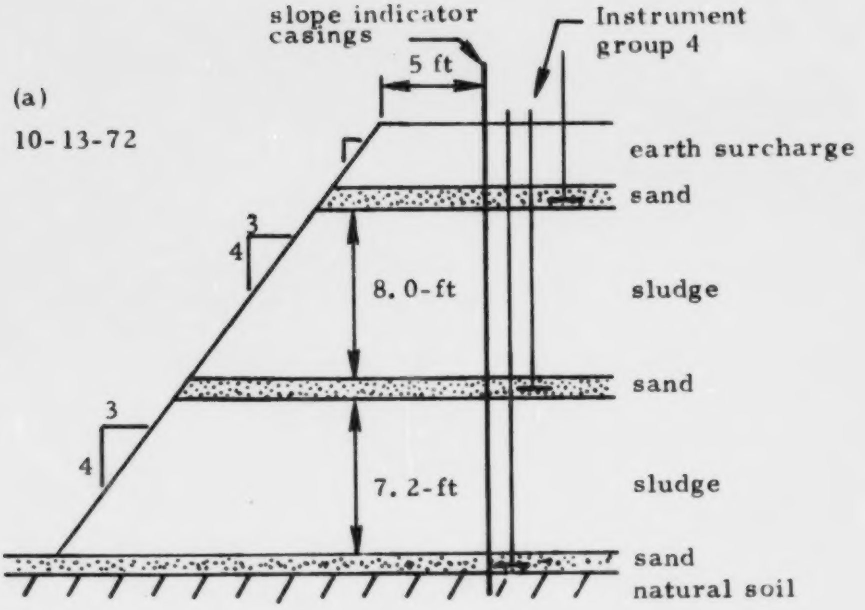
slope indicator casings
Instrument group 4
5 ft
(a)
10-13-72
earth surcharge
sand
3
4
8.0-ft
sludge
sand
3
4
7.2-ft
sludge
sand
natural soil

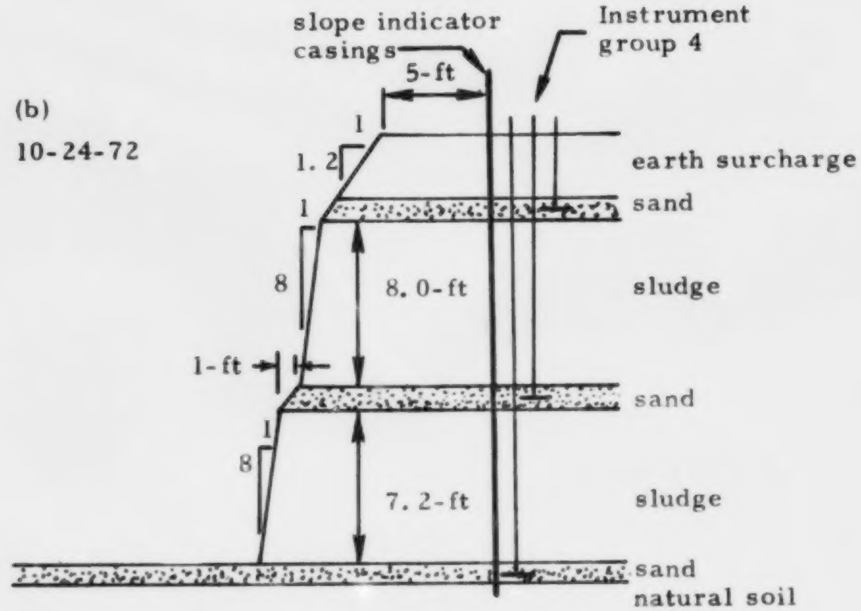
slope indicator casings
Instrument group 4
5-ft
(b)
10-24-72
1
1.2
earth surcharge
sand
1
8
8.0-ft
sludge
1-ft
sand
1
8
7.2-ft
sludge
sand
natural soil

Figure 4.4. Experimental slope cross-sections. (a) 3:4 slope. (b) 1:8 slope.

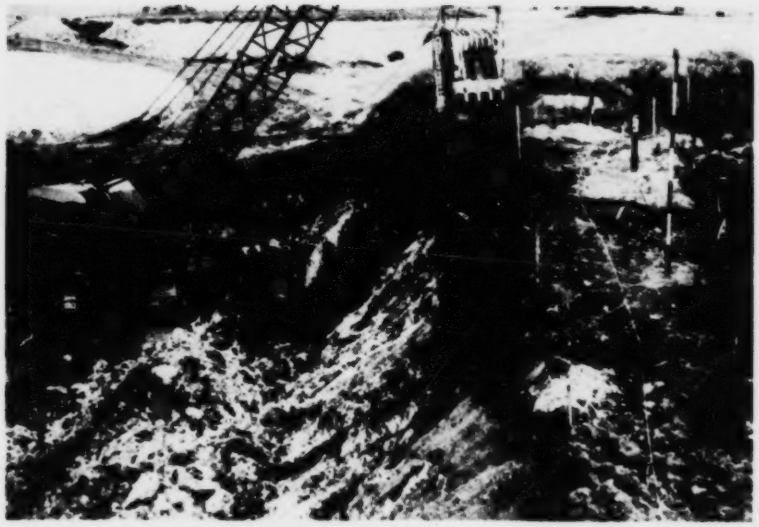

(a)

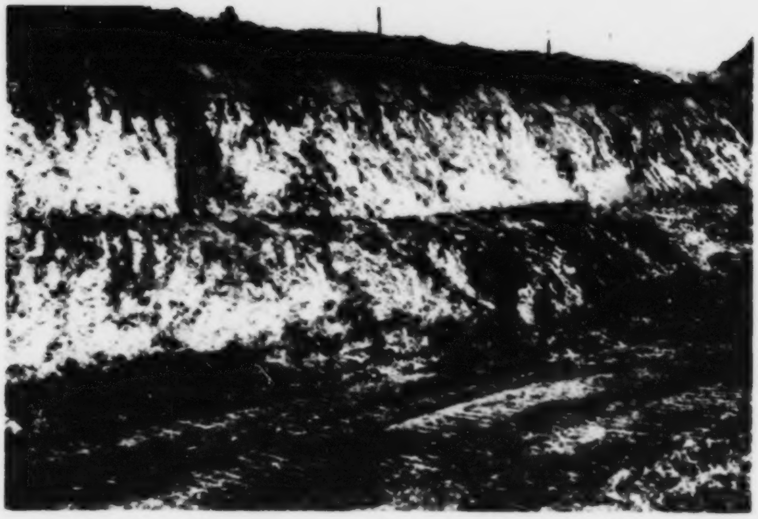

(b)

Figure 4.5. 3:4 slope preparation. (a) Sludge removal by dragline. (b) Slope cross-section, October 13, 1972.

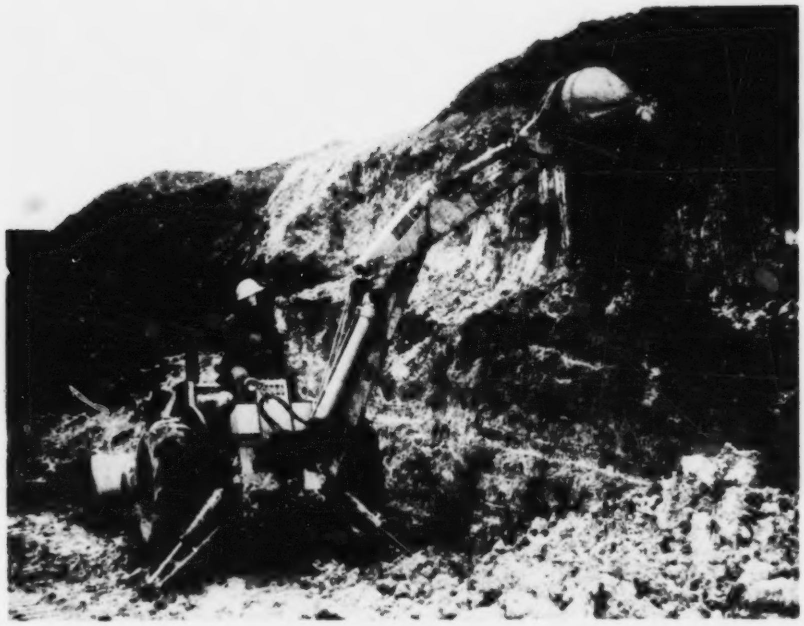

(a)

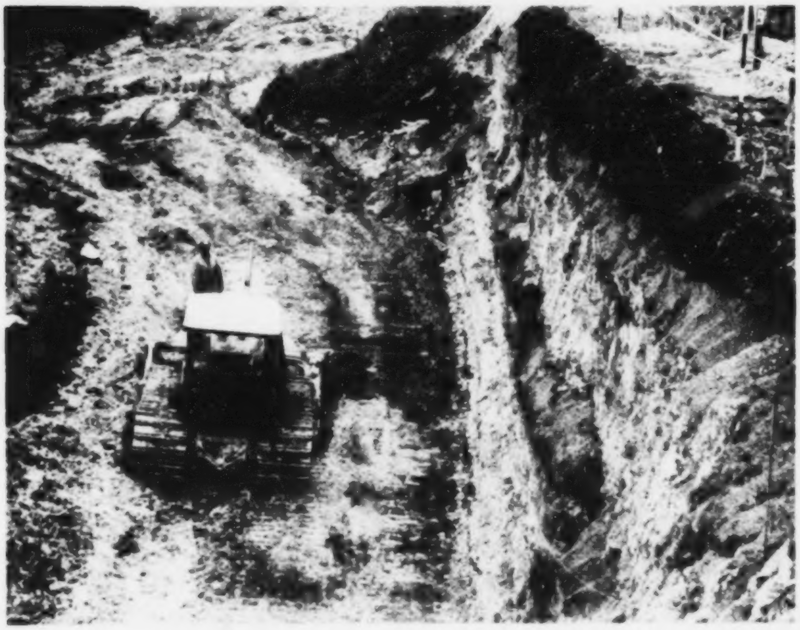

(b)

Figure 4.6. 1:8 slope preparation. (a) Trimming the upper sludge layer. (b) Sludge removal using a dozer, October 25, 1972.

CHAPTER V. EXPERIMENTAL RESULTS

The experimental results for phase II of the project are presented under four headings: physical properties of the papermill sludge, stress-deformation behavior of the sludge, slope behavior, and leachate analysis. Each section may include laboratory test data and/or field observations.

Physical Properties of the Papermill Sludge

Physical properties of the papermill sludge tabulated in Table 5. 1 include field water contents, ash contents, and unit weights. Water contents were taken at selected elevations immediately after excavation of the 3:4 slope (October 12, 1972) and 1:8 slope (October 30, 1972). A plot of this data in Figure 5. 1 shows a decrease in water content with a greater depth. The scatter of points on Figure 5. 1 is apparently due to the non-homogenous nature of the sludge. Small variations in ash (or organic) content appear to significantly alter the water content based on oven dry (105°C) weights. Water contents from 1 ft cube block samples B, C, F, and G tabulated in Table 5. 2, show the range in variability. Ash contents and unit weights given in Table 5. 1 refer to block samples B, C, F, and G on which extensive laboratory tests were conducted. Unit weights were determined from weight and volume measurements of carefully trimmed sludge samples. Greater consolidation of the lower sludge layer has significantly increased the unit weight.

Stress-Deformation Behavior of the Sludge

Stress-deformation behavior of the sludge is presented in terms of the consolidation of undisturbed samples and the triaxial shear strength. Both fresh and undisturbed samples have been used for the laboratory strength tests. In place vane shear tests provided data on the in situ undrained shear strength of the sludge after field consolidation.

Consolidation of Undisturbed Samples. Typical consolidation test results for the undisturbed sludge samples taken from the landfill are shown in Figures 5. 2 and 5. 3. Table 5. 3 summarizes the consolidation characteristics for each undisturbed sample test. In Figure 5. 2, two void ratio versus logarithm of pressure curves are shown for undisturbed block samples B and F along with a representative curve for a sample of fresh sludge. The curves obtained from the rapid increment tests are at higher equilibrium void ratios than those obtained from the slow tests because of the absence of secondary compression. The data indicate that the sample obtained from the lower layer has a lower compression index, lower initial void ratio, and a higher back-computed overburden pressure than the sample for the upper layer. The coefficient of consolidation, primary compression ratio, and coefficient of secondary compression have been plotted against the logarithm of effective pressure in Figure 5. 3. The coefficients of consolidation were obtained by the square root of time method and vary with pressure for both samples. Substantially higher values occur at pressures below the effective overburden stress. The primary compression ratio and coefficient of secondary compression both increase with an increase in the load increment and effective pressure.

Shear Strength. The shear strength of the papermill sludge has been measured using the triaxial test in the laboratory and the vane shear test in the field. Results from the triaxial tests are presented for fresh sludge samples obtained during construction of the landfill and undisturbed block samples taken after field consolidation. The vane shear strengths reported were obtained just prior to excavation of the slope for the stability study.

Fresh Sludge Samples. Samples taken during construction of the landfill have been identified and described in the First Annual Report. Portions of fresh sludge samples U-1, U-2, and U-3 were molded into triaxial test specimens with a summary of these test results given in Table 5. 4. Laboratory data are given in Appendix I, Tables I-1 through I-12. A back pressure of 20 psi was used on all the fresh sludge samples to ensure full saturation. Typical stress-strain behavior of the fresh sludge in undrained shear is given in Figure 5. 4. The obliquity $\overline{\sigma}_1/\overline{\sigma}_3$, deviator stress $(\sigma_1 - \sigma_3)$, pore pressure change Δu, and pore pressure parameter A are all plotted against axial strain. The obliquity becomes very large at larger axial strains because of the very small effective minor principal stress $\overline{\sigma}_3$. The A pore pressure parameter increases to about 0. 75 at failure, which appears to be typical for the fresh sludge. Triaxial strength data for sludge sample U-3 is summarized in Figure 5.5. The $\overline{p}_f$ - $\overline{q}_f$ plot has been used to obtain an angle of internal friction equal to 70.5 degrees. Next is shown the change in water content for several levels of all-around consolidation pressure. Part c of Figure 5.5 shows the increase in undrained strength versus consolidation pressure. Similar results are shown for sludge sample U-1 in Figure 5.6. The smaller angle of internal friction, 61.5 degrees, appears related to the lower organic content of sample U-1, 40.6 percent versus 63.5 percent for sample U-3.

Undisturbed Sludge Samples. Triaxial test specimens were cut from undisturbed block samples C and G which were obtained during excavation of the slope for the stability study. A summary of the triaxial test results is given in Table 5.4. Laboratory data are given in Appendix I, Tables I-13 through I-35. Except for the unconfined compression tests, a back pressure of 40 psi was used on all undisturbed sludge samples to ensure full saturation. Special test conditions used with specific tests include anisotropic consolidation and different orientations of the cylindrical axis with respect to horizontal. The stress-strain behavior of sample G-5, shown in Figure 5.7, corresponds to anisotropic consolidation. K_o equal to 0.3 was selected on the basis of field total pressure cell and piezometer data. The cylindrical axis for the test was vertical. Figure 5.7 includes the obliquity ratio, deviator stress, change in pore pressure, and the A pore pressure parameter all plotted against axial strain. The break in the obliquity curve corresponds to failure at about 19 percent axial strain. The deviator stress starts at a value greater than zero because of anisotropic consolidation. The A pore pressure parameter has decreased,in comparison to results for the fresh sludge, with the value at failure a little below 0.4. A summary of data from similar tests at other consolidation pressures is shown in Figure 5.8. The angle of internal friction obtained from the $\overline{p}_f$ - $\overline{q}_f$ plot is very large, close to 76.5 degrees. This suggests that some relationship exists between the angle of internal friction and the anisotropic nature of the sludge for this group of specimens. The water content and undrained strength plotted against consolidation pressure in Figure 5.8 show typical relationships.

The stress-strain behavior for sample G-10, shown in Figure 5.9, corresponds to all-around consolidation with the cylindrical axis horizontal. Lower obliquity ratios are noted and the A pore pressure parameter has increased in comparison to sample G-5 shown in Figure 5.7. The summary of data for specimens G-10 and G-11 is given in Figure 5.10. The angle of internal friction is much lower, about 45.5 degrees, and the undrained strengths are lower as compared to data given in Figure 5.8 for the vertical sample orientation.

Data shown in Figure 5.11 for sample C-11 represent an undrained test with σ_1 constant and σ_3 decreasing. This test procedure perhaps best approximates the loading conditions for a sludge element adjacent to the excavated slope. Negative pore pressure changes result for the unloading condition. The higher initial tangent modulus obtained from the deviator stress versus axial strain curve perhaps gives the best estimate of the field behavior. The A pore pressure parameter is again close to 0.53.

Unconfined Compression Tests. The unconfined compressive strength for undisturbed block samples of sludge are summarized in Figure 5.12 and Table 5.4 with the laboratory data given in Appendix I. Based on these strengths the sludge would be classified as soft to very soft (Terzaghi and Peck, 1967). The increase in strength with depth due to greater consolidation is apparent based on data for blocks C and G. The effect of sludge anisotropy on the unconfined compressive strength is shown in Figure 5.12 using data for sample orientations of zero, 45, and 90 degrees from the horizontal. Test specimens from the softer block C were more difficult to work with. The larger scatter in these test results indicates more sample disturbance for some specimens during sample preparation.

In-Place Vane Shear Tests. Information on the in-place vane shear strength of sludge has been given in the First Annual Report. Additional test details are included as footnotes to Tables F-1 and F-2, Appendix F of this report. The field data given in Table F-1 are summarized in Figure 5.13a. A gradual increase in undrained strength with depth is apparent for the normally consolidated sludge. The ratio c_u/p is large, close to 2.5, when compared to normally consolidated clays, which are generally less than 1. Unconfined compression data shown for two block samples in Figure 5. 13a are much less than the vane shear strength. This appears to be due to physical disturbance of the sludge during sampling and sample preparation for laboratory testing. Stress reduction during sampling permits small gas bubbles to expand which may cause additional disturbance. Shear strength data taken near the exposed slope shortly after excavation has been summarized in Table F-2, Appendix F. Comparisons for the same elevations show smaller undrained vane shear strengths, indicating that unloading of the slope appears to have had some influence. Also included in Table F-2 are data for the horizontal orientation of the vane. These values are larger as compared to the vertical vane orientation.

Dutch cone penetration data given in Table F-3, Appendix F, has been summarized in Figure 5. 13b. For the softer upper sludge layer no increase in cone resistance with depth was observed until the middle sand blanket was approached. Directly below the middle sand blanket the cone resistance increased with larger values observed for the more highly consolidated bottom half of the lower sludge layer.

Slope Behavior

Slope behavior was monitored in terms of lateral movement, vertical movement, change in pore water pressures, temperature, total pressure cell readings, and surface observations. Tables, figures and graphs are used to summarize the tabulated data which are given in the Appendix.

Lateral Movement. Lateral movement was monitored using both surface measurements on stakes (Appendix A) and slope indicator data (Appendix B) obtained using flexible vertical casings and a read out instrument. Surface movements along three lines labeled I, II, and III are given in Table A-1, Appendix A. Locations of the WX, WY, and WZ positions have been given in Figure 4. 2 with reference to instrument group locations and the plan view of the experimental slope. The stake for line II-WZ was lost after the 10-28-72 reading at which time a total surface movement of 3. 72 inches had been observed. Line III-WZ recorded a total of 7. 08 inches of movement as of 4-7-73. The slope moved back a small amount when the trench was filled with fresh sludge as shown by the final data in Table A-1. Limits of the slope failure in plan view for three different dates are shown in Figure A-1 for the 1:8 slope. These will be discussed in more detail under surface observations.

Lateral movement at various levels in the landfill is shown very clearly by the slope indicator data summarized in Figure 5.14a through 5.14f. Field data are given in Tables B-1 through B-13, Appendix B. Locations of the slope indicator casings A through G were given in Figure 4.1. All movements are referred to the base of each casing which was embedded about 1 ft into the natural soil beneath the landfill and to the initial readings taken on 9-19-72. Most of the movement toward the exposed slope occurred in the top sludge layer, reaching a maximum at the landfill surface. Each curve in Figure 5.14 is identified by the date on which readings were taken. Slope indicator casings A and D also moved significant amounts parallel to the slope as shown by the data summarized in Figure 5.14e. For convenient reference the elevations for each sludge layer and sand drainage blanket have been included in Figure 5.14.

Vertical Movement. Downward movement of the sludge near the exposed slope and any settlement are summarized by elevation readings for the settlement plates with data given in Tables C-1 through C-4, Appendix C. Location and identification of the settlement plates have been given in Figures 4.1 and 4.3. In Figure 5.15 the movement in the upper and lower sludge layers is shown by curves labeled ⑤ - ③ and ③ - ①, respectively. The quantity ⑤ - ③ equals the elevation of plate 5 minus the elevation of plate 3. The numbers ①, ③, and ⑤ refer to settlement plates located in the bottom, middle, and top sand drainage blankets, respectively. The largest movement occurred in the softer top sludge layer near the slope as shown by data for instrument group 5. Part of the settlement appears to have been initiated when the middle sand blanket became fully drained due to slope excavation about September 29, 1972.

Pore Water Pressures. Piezometers, identified as to location and number in Figures 4.1 and 4.3, gave the data summarized in Figure 5.16. Field data are given in Tables D-1 through D-4, Appendix D. Instrument group 4, closest to the slope, and instrument group 5, about 29 ft back from the slope, gave pore water pressures which appear to be directly related to the reduction of load at the excavated slope. The 3:4 slope was completed on October 13, 1972. This unloading of the slope is reflected by the decrease in pore pressures in both sludge layers in instrument group 4 and in the bottom sludge layer at instrument group 5. The reduction in pore pressure prior to this date was gradual as the excavation progressed. After October 13, 1972, lateral movements toward the slope (Figure 5. 14) appear to be the cause of the decrease in observed pore water pressure. The rate of pore water pressure decrease accelerated with excavation for the 1:8 slope and sharply increased after the initial slope failure.

Temperature. Thermistors used for temperature measurement gave the data tabulated in Table E-1 and are plotted against time in Figure 5. 17. Any change in temperature due to biological activity was not apparent for the second year. The observed temperatures show a pattern indicating that the sludge is responding to air and ground temperatures. Average daily air temperatures and precipitation during the entire project are given in Appendix J.

Total Pressure Cells. Total sludge pressures measured in the vertical and horizontal directions are tabulated in Table G-1 and plotted against time in Figure 5. 18. The two working cells and adjacent piezometer G7-3 were located in the middle of the lower sludge layer as part of instrument group 7. Original plans had intended that the cell be parallel to the excavated slope, however, the vertical cell was oriented normal to the excavated slope due to the contractor's change in plans. The data in Figure 5. 18 show a total horizontal stress of about 1. 4 psi during the period that the slope was being excavated. Over a period of time the stress again increased, perhaps due to internal stress adjustments related to creep. Pore pressures in the vicinity of the total pressure cells remained relatively constant during the period of slope excavation.

Surface Observations. Movements in the experimental slope became more evident as the actual slope failure was approached. Tension cracks appeared in the earth surcharge very shortly after completion of the 1:8 slope. Their appearance and location relative to the slope indicator casings are shown in Figure 5. 19. The initial slope failure (Figure 5. 20a) did not occur until four days later on October 29, 1972. Shortly thereafter additional failures occurred in the top sludge layer at other locations along the slope as shown in Figure 5. 20b. The surface extent of these slope failure areas for three different dates is given in Figure A-1, Appendix A. Close examination of these slope failures suggest that the typical cross-section would be as represented in Figure 5. 21. The tension cracks appeared to extend through the earth surcharge down to the upper sand drainage blanket. The failure surface in the sludge approximated a 1 on 1. 64 slope (about 58. 6 degrees from the horizontal). Failure surfaces in the drainage blankets were approximately as shown in Figure 5. 21.

Leachate Analysis

Six leachate samples, obtained periodically from the landfill as shown in Table 4. 1, were analyzed for those properties of importance to groundwater quality. The scope of the analyses, as well as the results are tabulated in Table 5. 6. A comparison of results among the various samples for (a) COD and BOD, (b) total iron, (c) specific conductance, (d) dissolved solids, (e) color, (f) turbidity, (g) hardness and alkalinity, and (h) chloride concentration are graphically illustrated by Figures 5. 22 through 5. 29.

A review of the data indicates that the concentrations of chemical constituents associated with sample VI are considerably greater than those observed with the remaining samples. However, it should be noted that the manner in which sample VI was obtained was unique and provides an assessment of the composition of the sludge layer interstitial water in situ.

Suspended solids concentration cited for sample V is a radical departure from the balance of the samples and can probably be attributed to the sample's origin in the bottom of a slope indicator pipe. However, concentration of identical constituents for samples I through V show wide variation. With the exception of pH, which is relatively consistent, maximum values are at least double the minimum. Nevertheless, that variation is not without some trend, as indicated in Figures 5. 22 through 5. 29 and examination of the data. Without exception, minimum values are associated with either sample II or III. Excluding suspended solids concentration for sample V, maximum values are observed with either sample I or IV. In a ranking from minimum value to maximum, concentrations reported for sample V are most commonly intermediate.

TABLE 5.1. PHYSICAL PROPERTIES OF THE PAPERMILL SLUDGE, OCTOBER 1972

Sludge sample		Water content	Ash[1] content	Sludge sample		Water content
No.	Elevation (ft)	(% dry wt)	(%)	No.	Elevation (ft)	(% dry wt)
Block A	91.8	196		moisture content samples	91.7	199
		202			91.6	177
		212			91.4	182*
Block B	88.8	214	38.6		91.2	200
		209			90.6	193
		200			90.5	187
Block C	87.5	183	49.1		90.4	188*
		165			89.9	194
		173			89.4	189
Block D	85.5	191*			89.4	201*
		187*			89.1	144
Block E	81.9	161*			88.7	149
		164*			88.4	161
		162*			88.4	172*
Block F	80.9	154*	39.3		88.0	177
		156*			87.7	173
		156*			87.4	164*
Block G	80.7	157*	39.0		85.4	207
		159*			84.4	175
		161*			84.4	211*
moisture content samples	92.8	199			83.4	204
	92.6	178*			83.4	175*
	92.4	179*			82.4	153*
	92.3	200			81.4	163*
	92.2	187			81.4	158*

Field water contents correspond to 3:4 slope, October 12, 1972, except * which correspond to 1:8 slope, October 30, 1972.

Unit weight: block B $\gamma = 72.6$ lb per cu ft.
block C $\gamma = 74.0$ lb per cu ft.
block F $\gamma = 76.5$ lb per cu ft.

[1] ASTM test method D586-63.

TABLE 5.2. VARIATION IN WATER CONTENTS FOR ONE CUBIC FOOT BLOCK SAMPLES

	Block B	Block C	Block F	Block G
	213 %	162 %	149 %	159.1 %
	206	157	162	157.7
	218	163	165	153.7
	222	169	154	157.2
	212	169	150	158.6
	209	170	164	158.6
	193	169		157.2
	212	178		157.0
	218			160.0
	211			158.6
	204			
	212			
	206			
	214			
	202			
	200			
Avg.	209.5%	167.1%	157.3%	157.8%
Block Elev.	88.8 ft	87.5 ft	80.9 ft	80.7 ft

TABLE 5.3. SUMMARY OF CONSOLIDATION CHARACTERISTICS, UNDISTURBED SLUDGE SAMPLES

Sludge Sample No.	Sludge Test No.	Load increment (kg/cm^2)	c_v (in^2/min.) log t	c_v (in^2/min.) $\sqrt{t}$	r (%)	C_α	C_c	Initial e_o	p_o kg/cm^2 Casagrande construction
B*	1[+]	rapid load increments (every 25 min.) See Fig. 5.2	$\frac{\Delta p}{p} < 1$	not computed	--	--	1.92	4.65	0.31
B*	2[+]	rapid load increments (every 15 min.)	$\frac{\Delta p}{p} < 1$	not computed	--	--	1.86	4.65	0.30
B*	3[+]	0-0.05	0.0956	0.0620	54.5	0.00216	1.84	4.48	0.28
		0.05-0.10	0.0525	0.0497	56.2	0.00427			
		0.1 -0.2	0.0386	0.0464	62.2	0.00687			
		0.2 -0.4	0.0273	0.0341	63.8	0.0130			
		0.4 -0.8	0.0150	0.0168	73.4	0.0184			
		0.8 -1.6	0.00930	0.0112	75.5	0.0218			
		1.6 -3.2	0.00542	0.00875	77.0	0.0187			
B*	4[+]	0-0.05	0.0378	0.0432	62.4	0.00264	1.61	3.81	--
		0.05-0.10	0.0224	0.0281	57.8	0.00427			
		0.10-0.20	0.0215	0.0400	79.2	0.00311			
		0.20-0.40	bad increment		--	--			
		0.40-0.80	0.00677	0.00990	80.5	0.0190			
		0.80-1.6	0.00400	0.00697	80.8	0.0215			
		1.6 -3.2	0.00279	0.00596	78.7	0.0243			

*Undisturbed sample 4.0 ft. below the upper sand blanket. [+]Bishop type consolidation machine.

c_v - coefficient of consolidation, t - time, r - primary compression ratio,

C_α - coefficient of secondary compression, C_c - compression index, e_o - initial void ratio,

p_o - back-computed in situ vertical effective stress.

TABLE 5.3. SUMMARY OF CONSOLIDATION CHARACTERISTICS, UNDISTURBED SLUDGE SAMPLES (CONTINUED)

Sludge		Load increment (kg/cm^2)	c_v $(in^2/min.)$		r (%)	C_α	C_c	Initial e_o	p_o kg/cm^2 Casagrande construction
Sample No.	Test No.		log t	$\sqrt{t}$					
F*	1^+	rapid load increments (every 15 min.) See Figure 5.2	$\frac{\Delta p}{p} < 1$	not computed	--	--	1.51	3.50	0.77
F*	2^+	rapid load increments (every 15 min.)	$\frac{\Delta p}{p} < 1$	not computed	--	--	1.51	3.52	0.77
F*	3^+	0-0.05	0.0537	0.0521	60.6	0.00121	1.55	3.50	0.64
		0.05-0.10	0.0447	0.0400	50.0	0.00218			
		0.10-0.20	0.0360	0.0364	50.6	0.00498			
		0.20-0.40	0.0282	0.0339	60.8	0.00674			
		0.40-0.80	0.0146	0.0233	73.2	0.00932			
		0.80-1.6	0.00712	0.00932	74.0	0.0174			
		1.6 -3.2	0.00417	0.00594	82.6	0.0159			
F*	4^+	0-0.05	0.0351	0.0395	61.0	0.00108	1.51	3.38	0.72
		0.05-0.10	0.0447	0.0308	46.7	0.00204			
		0.10-0.20	0.0291	0.0318	49.6	0.00344			
		0.20-0.40	0.0176	0.0229	61.5	0.00508			
		0.40-0.80	0.0113	0.0183	68.9	0.00944			
		0.80-1.6	0.00622	0.00898	71.6	0.0152			
		1.6 -3.2	0.00393	0.00524	77.6	0.0189			

*Undisturbed sample 4.0 ft. below the middle sand blanket. +Bishop type consolidation machine.

c_v - coefficient of consolidation, t - time, r - primary compression ratio,

C_α - coefficient of secondary compression, C_c - compression indes, e_o - initial void ratio,

p_o - back-computed in situ vertical effective stress.

TABLE 5.4. SUMMARY OF TRIAXIAL TEST RESULTS

Sludge sample	Consolidation pressure		Water content		Initial dry density	Undrained strength c_u	$\bar{\sigma}_{1_f}^{a}$	$\bar{\sigma}_{3_f}^{a}$	A_f
	p	K_o	Initial	Final					
	(kg/cm^2)		(%)	(%)	(pcf)	(kg/cm^2)	(kg/cm^2)	(kg/cm^2)	
U-1-10	0.703	1.0	182.9	116.2	25.86	0.52	1.02	0	0.69
U-1-11	1.41	1.0	200.0	101.2	26.60	0.83	1.76	0.10	0.78
U-1-12	2.11	1.0	194.4	94.3	25.78	1.17	2.44	0.09	0.85
U-1-13	3.52	1.0	180.2	84.2	27.50	1.90	4.08	0.28	0.85
U-2-21	3.52	1.0	215.0		23.88	2.07	4.36	0.23	0.79
U-3-1	0.703	1.0	310.0	150.9	18.96	0.45	0.91	0	0.77
U-3-2	0.703	1.0	306.0	147.4	18.41	0.62	1.20	0	0.60
U-3-3	1.40	1.0	276.2	118.8	19.25	1.48	3.05	0.056	0.45
U-3-4	2.11	1.0	258.0	111.2	20.39	sample tilted during test			
U-3-5	3.51	1.0	255.0		20.34	1.52	3.27	0.22	1.08
U-3-6	2.11	1.0	285.8	122.8	18.65	1.18	2.31	0	0.90
U-3-7	1.41	1.0	289.6	127	18.32	0.94	1.91	0.04	0.73
U-3-8	3.52	1.0	293.6	111	18.23	2.10	4.27	0.08	0.82
G-3	1.17	0.3	159.1	142	26.56	0.70	1.44	0.04	0.45
G-4	1.17	0.3	157.7	134	26.63	0.91	1.83	0.009	0.30
G-5	1.17	0.3	153.7	130	27.65	0.954	1.92	0.015	0.30
G-6	2.34	0.3	157.2	115	27.79	2.05	4.15	0.046	0.24
G-7	Unconfined compression		158.6	158.6	28.63	0.318	0.637	0	--
G-8	Unconfined compression		158.6	158.6	28.12	0.322	0.644	0	--
G-9	0.696	0.3	157.2	153	28.17	0.484	0.99	0.021	0.40
G-10[b]	0.703	1.0	157.0	145	29.00	0.449	1.08	0.18	0.57

TABLE 5.4. SUMMARY OF TRIAXIAL TEST RESULTS (CONTINUED)

Sludge sample	Consolidation pressure		Water content		Initial dry density	Undrained strength	$\overline{\sigma}_{1_f}$ [a]	$\overline{\sigma}_{3_f}$ [a]	A_f
	p (kg/cm^2)	K_o	Initial (%)	Final (%)	(pcf)	c_u (kg/cm^2)	(kg/cm^2)	(kg/cm^2)	
G-11[b]	2.11	1.0	160.0	114	28.71	1.12	2.66	0.43	0.75
G-12[b]	Unconfined compression		158.6	158.6	27.78	0.202	0.404	0	--
G-20[c]	2.34	0.3	159.0	122	27.78	--	--	--	--
G-21[c]	0.703	0.3		135	31.26	--	--	--	--
C-2	Unconfined compression		162	162	28.17	0.134	0.268	0	--
C-3	Unconfined compression		157	157	28.83	0.156	0.311	0	--
C-4	Unconfined compression		163	163	27.64	0.102	0.204	0	--
C-5[b]	Unconfined compression		169	169	27.73	0.094	0.189	0	--
C-6[b]	Unconfined compression		169	169	27.75	0.076	0.152	0	--
C-7[d]	Unconfined compression		170	170	28.35	0.104	0.208	0	--
C-8[d]	Unconfined compression		169	169	27.75	0.124	0.248	0	--
C-9	Unconfined compression		178	178	25.72	0.132	0.265	0	--
C-10[c]	0.703	0.3	177	150	26.94	--	--	--	--
C-11[c]	0.935	0.3	174.5	133.5	27.30	--	--	--	--
C-14[c]	2.343	0.3	174.3	104.3	27.26	--	--	--	--

[a] Total stress basis for unconfined compression. [b] Sample axis horizontal.

[c] Undrained shear with σ_1 constant and σ_3 decreasing. [d] Sample axis 45 degrees from the horizontal.

$\overline{\sigma}_{1_f}$ and $\overline{\sigma}_{3_f}$ equal the major and minor principal effective stresses at failure, respectively.

A_f equals the pore pressure parameter at failure.

TABLE 5. 5. SUMMARY OF $\overline{\phi}$ VALUES FOR THE TRIAXIAL TESTS

Sample No.	Organic content (100 - % ash)	Test procedure	$\overline{\phi}$ (degrees)	Remarks
U-1[a]	40.6	$\overline{\text{CIU}}$	61.5	Fresh sludge
U-2[a]	53.5	$\overline{\text{CIU}}$	66.2	Fresh sludge
U-3[a]	63.5	$\overline{\text{CIU}}$	70.5	Fresh sludge
Block G	61.0	$\overline{\text{CAU}}$	45.5	Field sample
Block G	61.0	$\overline{\text{CIU}}$[b]	45.5	Field sample
H-2[c]	28.6	$\overline{\text{CIU}}$	45.7	Fresh sludge
	34.7	$\overline{\text{CIU}}$	51.4	Fresh sludge
	43.6	$\overline{\text{CIU}}$	58.5	Fresh sludge
	50.1	$\overline{\text{CIU}}$	64.2	Fresh sludge

[a] Sample information given in the First Annual Report.

[b] Sample axis horizontal.

[c] Data after Andersland and Laza (1971).

$\overline{\text{CIU}}$ - Consolidated undrained triaxial test with istropic consolidated and pore pressure measurements.

$\overline{\text{CAU}}$ - Consolidated undrained triaxial test with anisotropic consolidated and pore pressure measurements.

$\overline{\phi}$ - angle of internal friction, effective stress basis.

TABLE 5.6. ANALYSIS OF LEACHATE QUALITY

Sample	I	II	III	IV	V	VI
Date sampled	10/19/72	11/21/72	12/12/72	12/29/72	2/10/73	6/15/73
COD (mg/l)	9,580	4,000	4,160	4,700	7,585	22,658
BOD (mg/l)	6,614	2,660	2,860	3,250	5,158	15,520
pH	7.6	7.7	7.7	7.8	7.5	7.4
Specific conductance (μmho/cm)	6,200	3,360	3,100	6,010	4,015	9,800
Turbidity (MTU)	56	13	9	17	15	80
Color (color units)	352	130	165	439	187	383
Total solids (mg/l)	11,786	4,960	5,130	9,730	8,885	--
Dissolved solids (mg/l)	11,710	4,840	5,100	9,570	7,651	19,062
Suspended solids (mg/l)	76	120	30	160	1,234	--
Total iron (mg/l)	2.5	1.6	1.5	4.3	3.6	0.7
Total hardness (mg/l as $CaCO_3$)	6,810	3,203	3,230	6,565	4,310	10,244
Chloride (mg/l)	201	75	70	206	111	181
Alkalinity (mg/l as $CaCO_3$)	8,670	4,130	4,130	8,770	5,810	11,780
Sulfate (mg/l)	< 1	< 1	< 1	< 1	< 1	< 1
Total Kjeldahl nitrogen (mg/l)						4
Total phosphorus (mg/l)						0.3

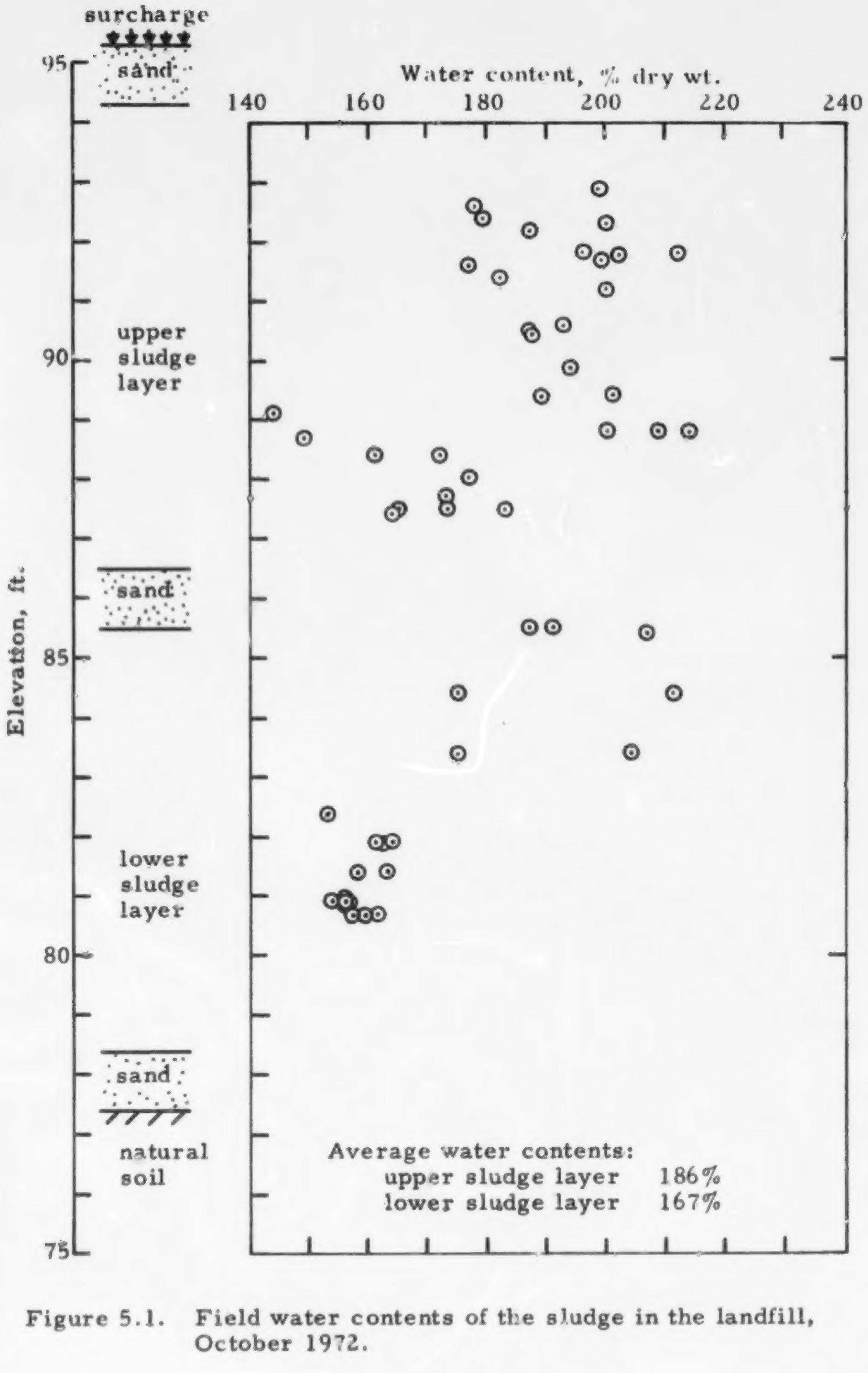

Figure 5.1. Field water contents of the sludge in the landfill, October 1972.

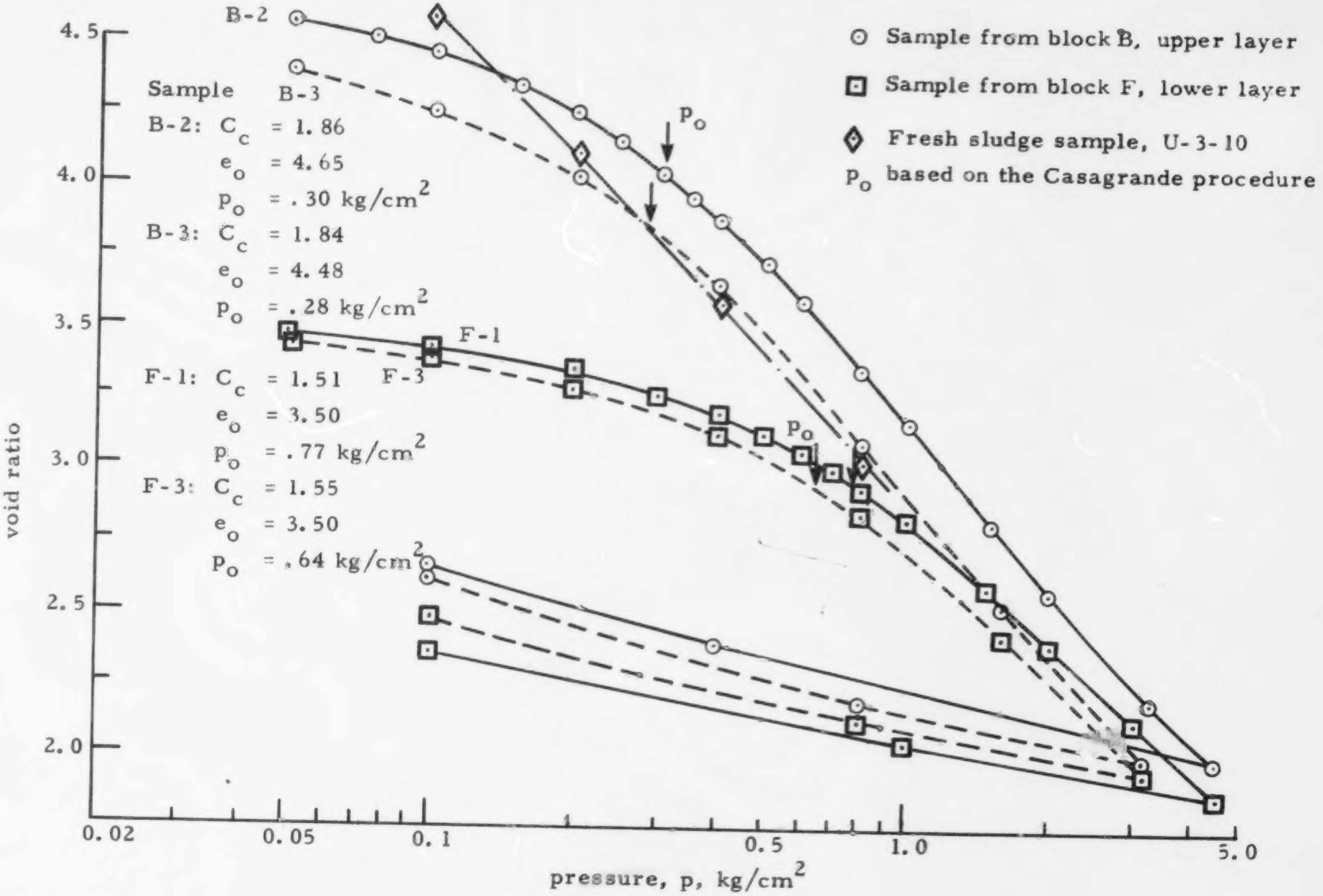

Figure 5.2. Void ratio--effective stress relationships, undisturbed sludge samples.

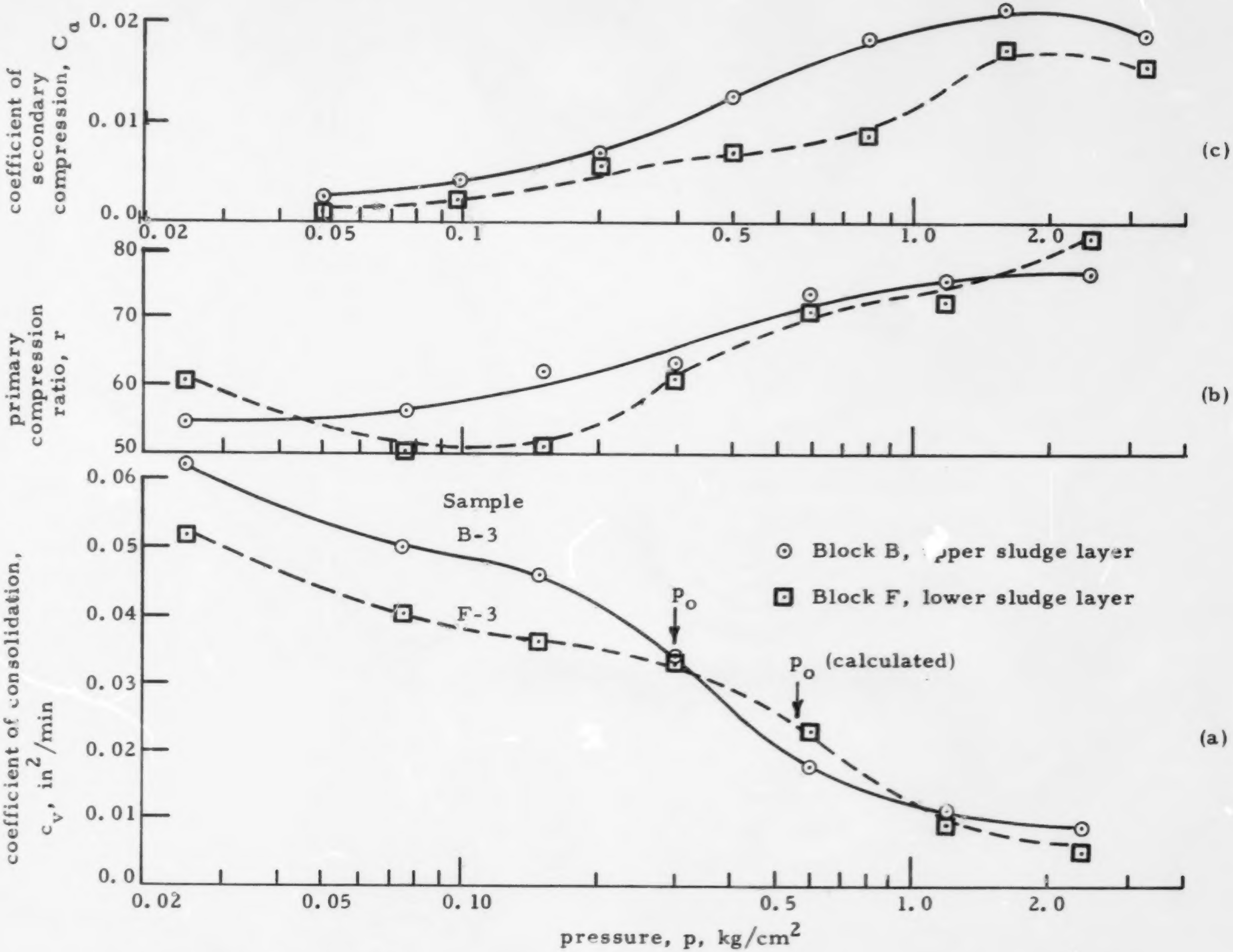

Figure 5.3. Consolidation characteristics for the undisturbed sludge samples. (a) Coefficient of consolidation, c_v. (b) Primary compression ratio, r. (c) Coefficient of secondary compression, C_α.

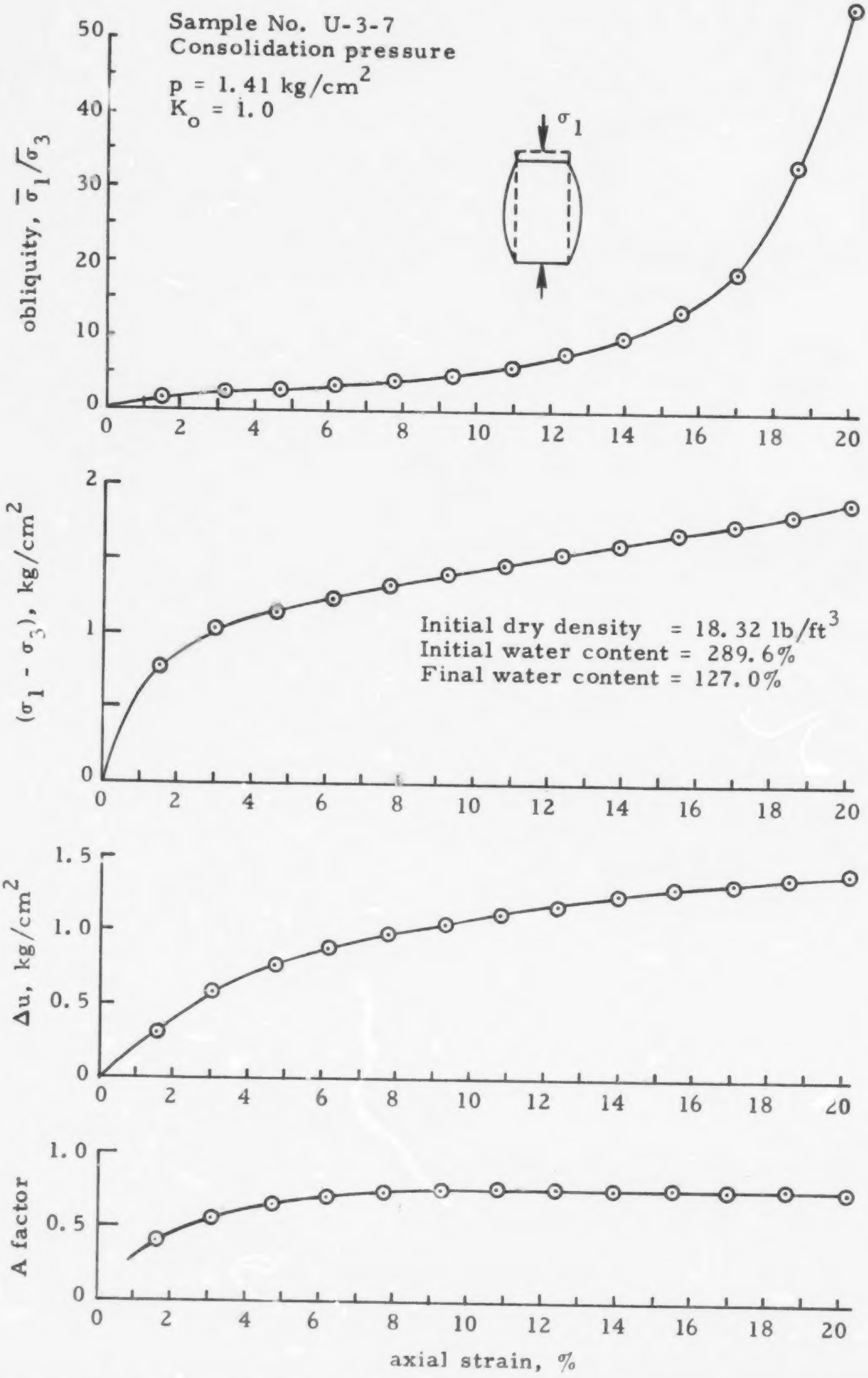

Figure 5.4. Stress-strain behavior of fresh sludge in undrained shear, sample U-3-7.

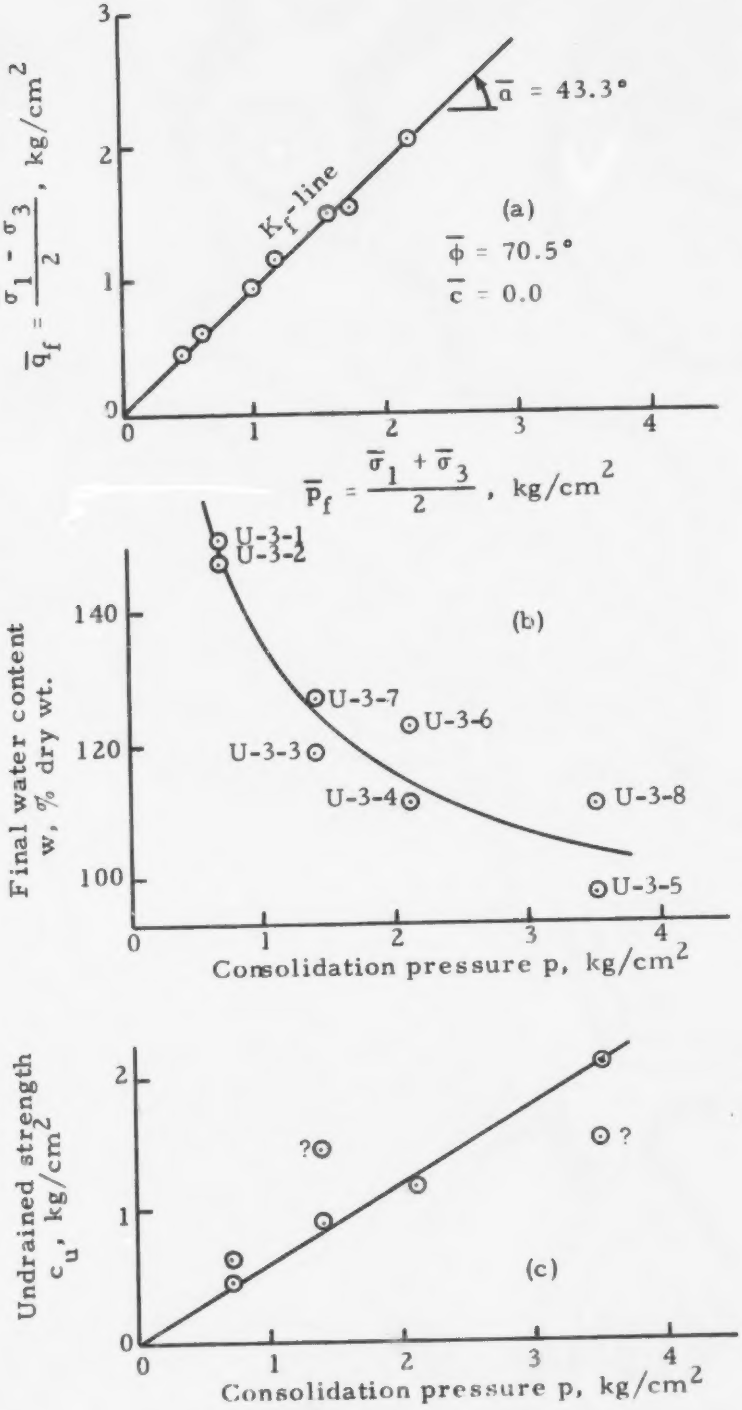

Figure 5.5. Consolidated undrained triaxial test results for sludge sample U-3. (a) K_f-line. (b) Water content. (c) Undrained strength.

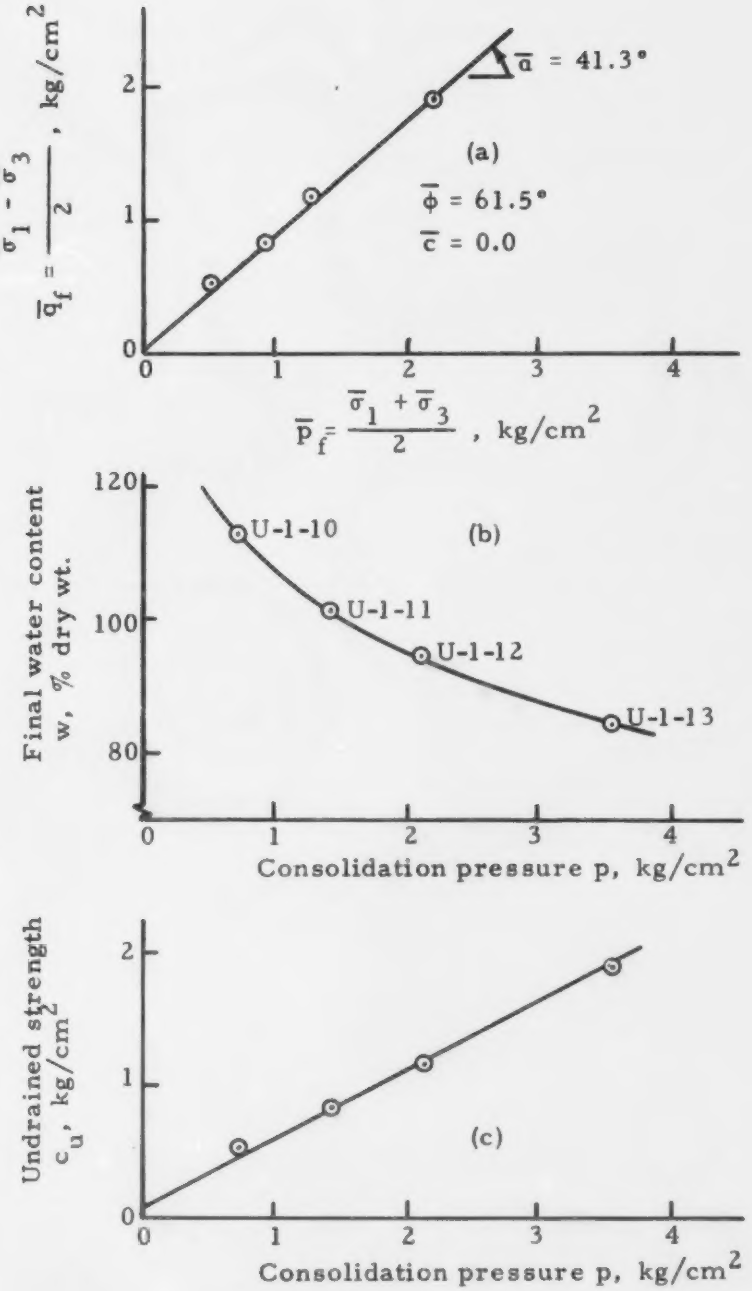

Figure 5.6. Consolidated undrained triaxial test results for sludge sample U-1. (a) K_f-line. (b) Water content. (c) Undrained strength.

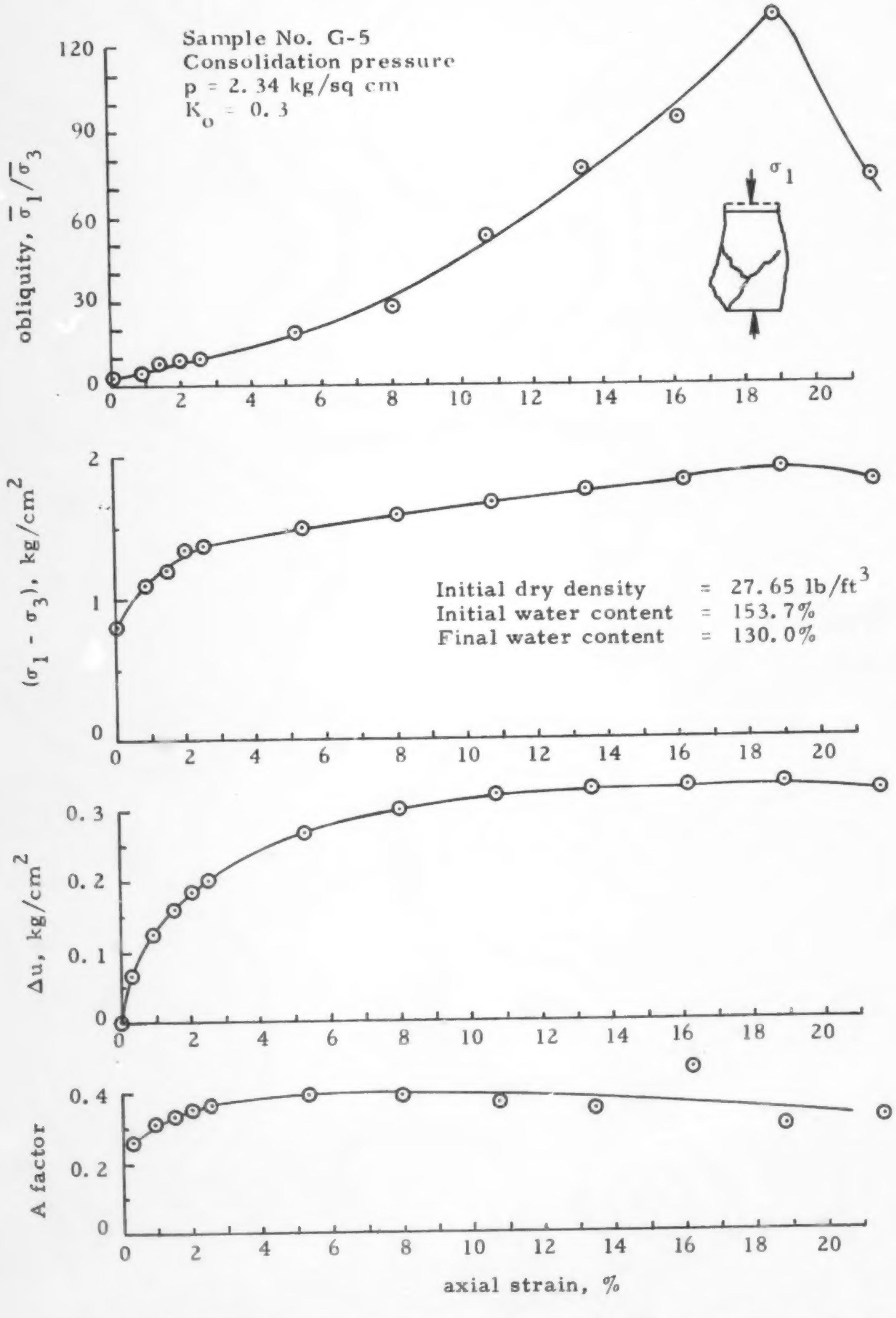

Figure 5.7. Stress-strain behavior of consolidated sludge in undrained shear, sample G-5.

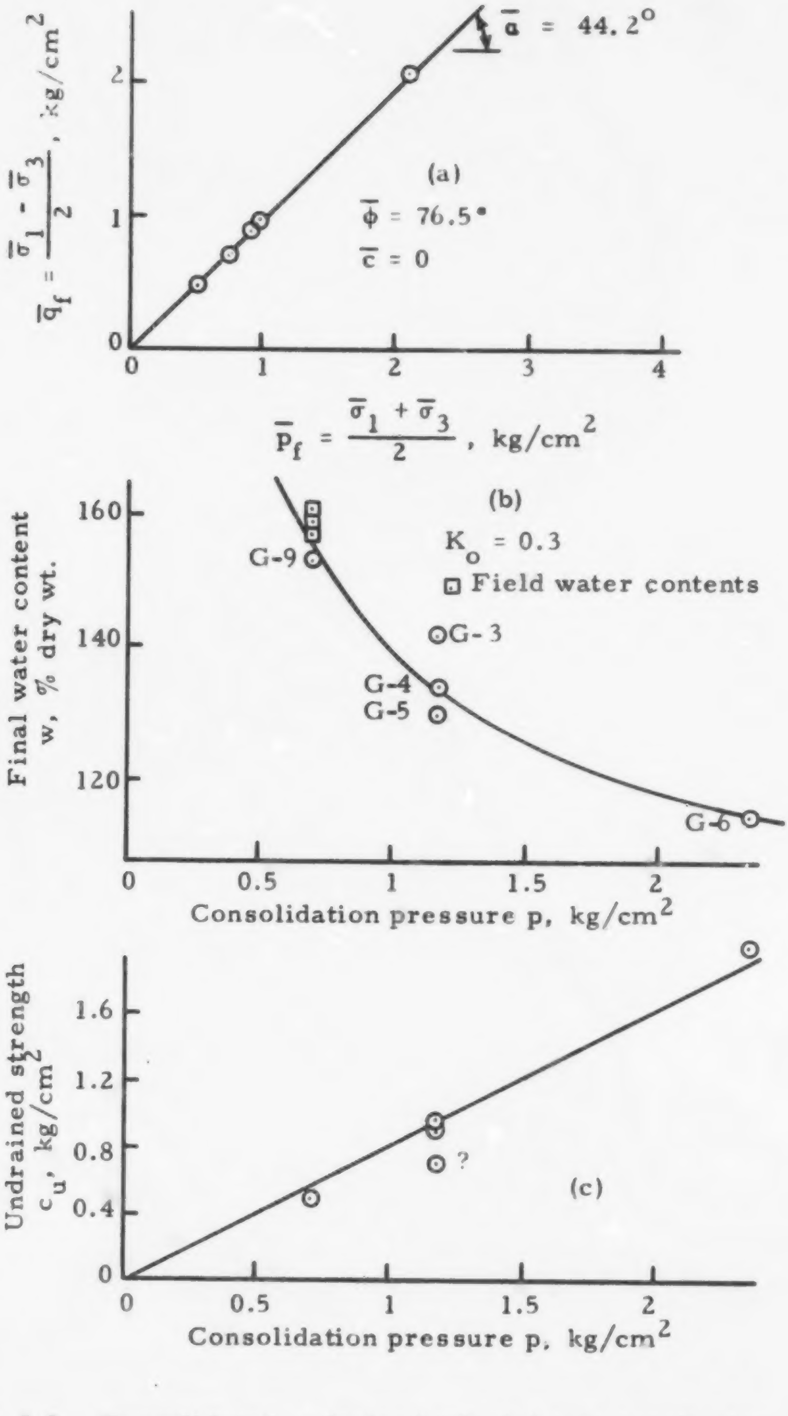

Figure 5.8. Consolidated undrained triaxial test results for block G, anisotropic consolidation and vertical axis. (a) K_f-line. (b) Water content. (c) Undrained strength.

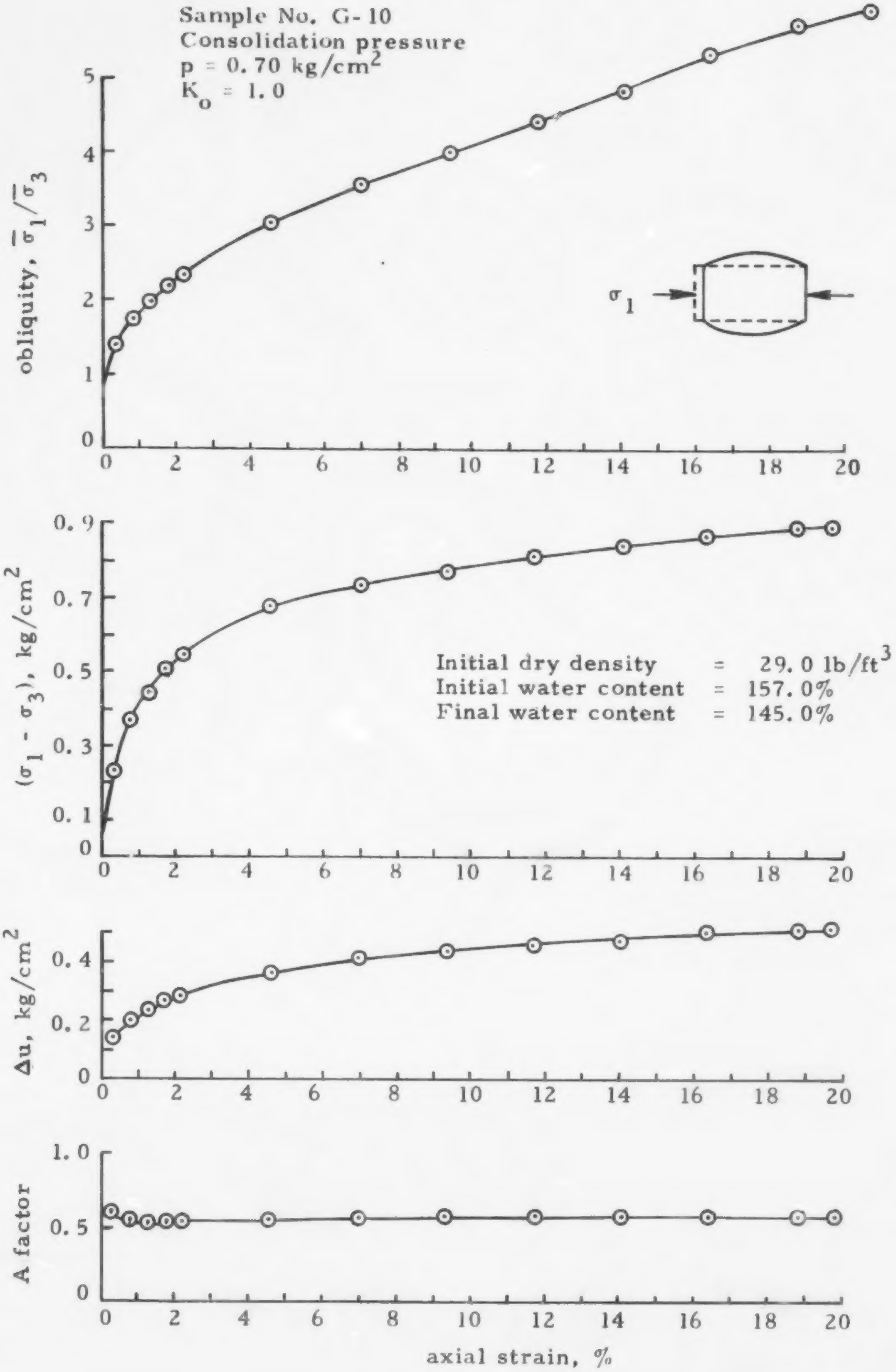

Figure 5.9. Stress-strain behavior of consolidated sludge in undrained shear, sample G-10 with the major principal axis horizontal.

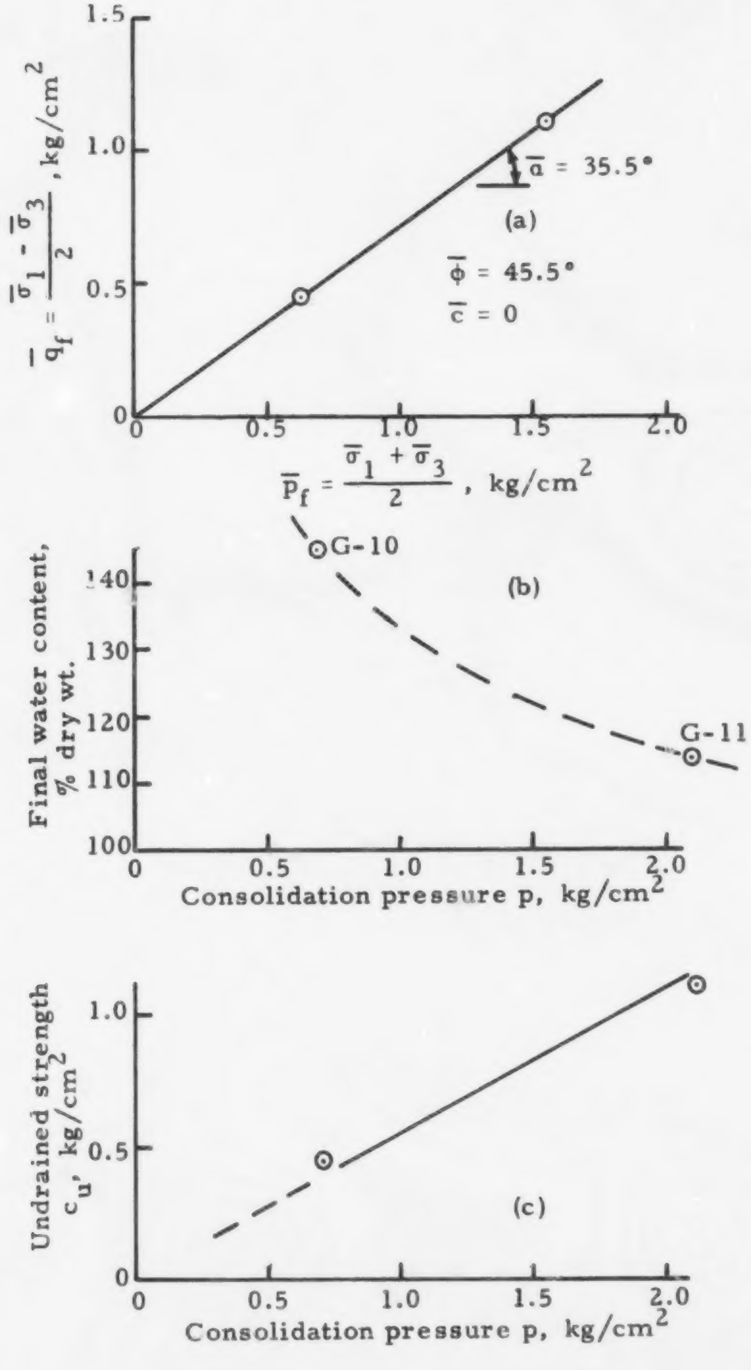

Figure 5.10. Consolidated undrained triaxial test results for block G, isotropic consolidation, and horizontal axis. (a) K_f-line. (b) Water content. (c) Undrained strength.

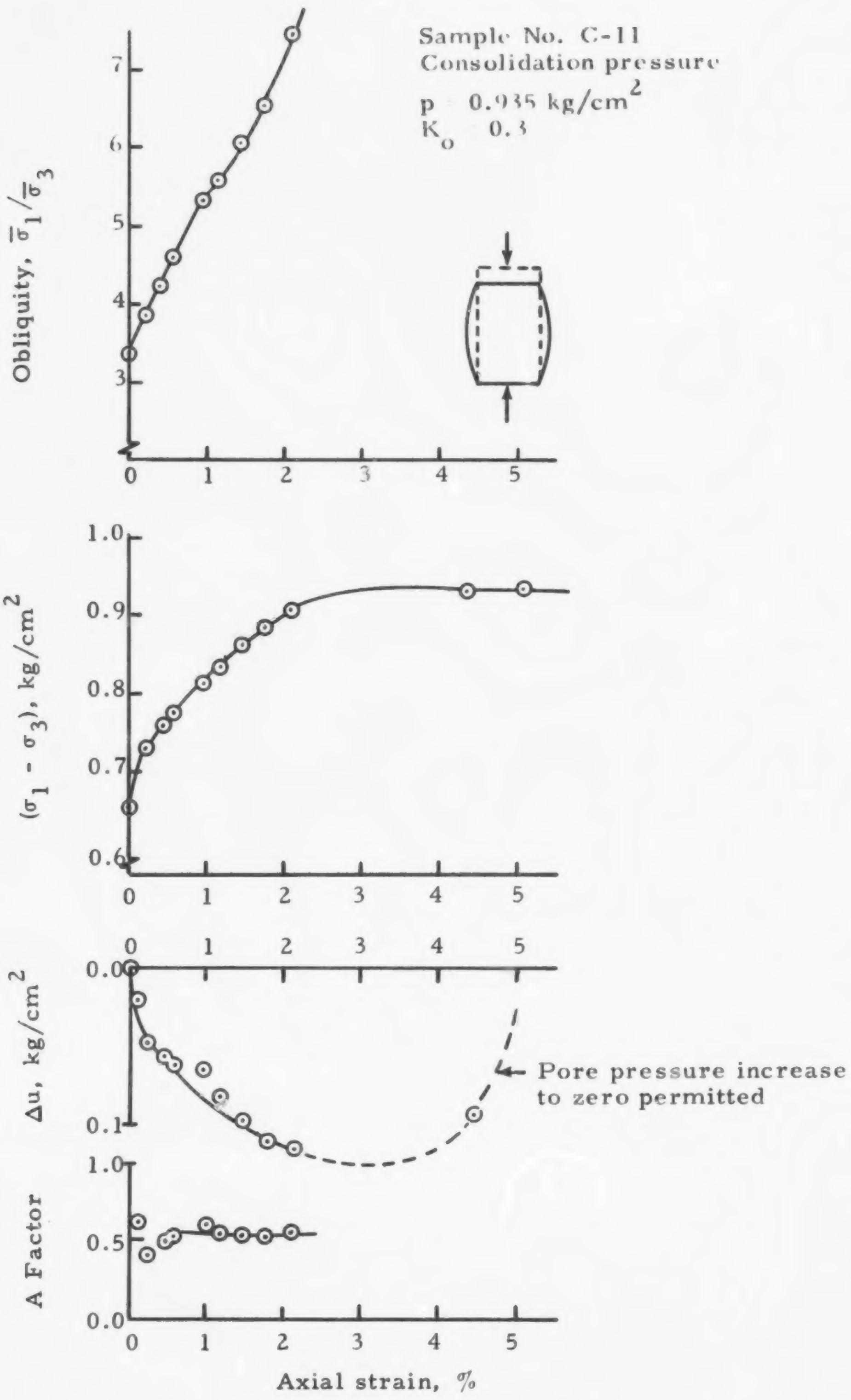

Figure 5.11. Stress-strain behavior of consolidated sludge in undrained shear, sample C-11 with σ_1 constant and σ_3 decreasing.

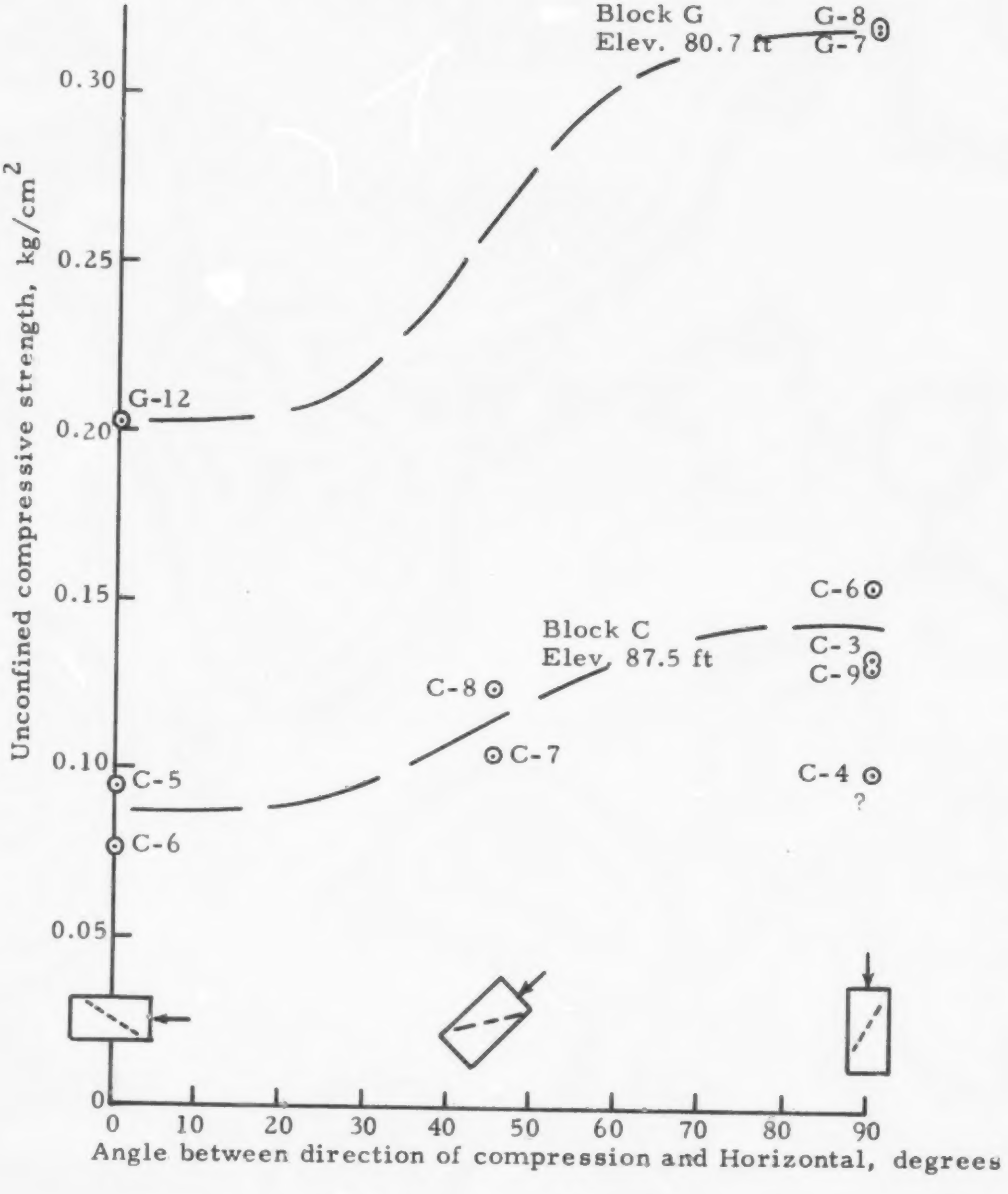

Figure 5.12. Variation of unconfined compressive strength with direction of compression.

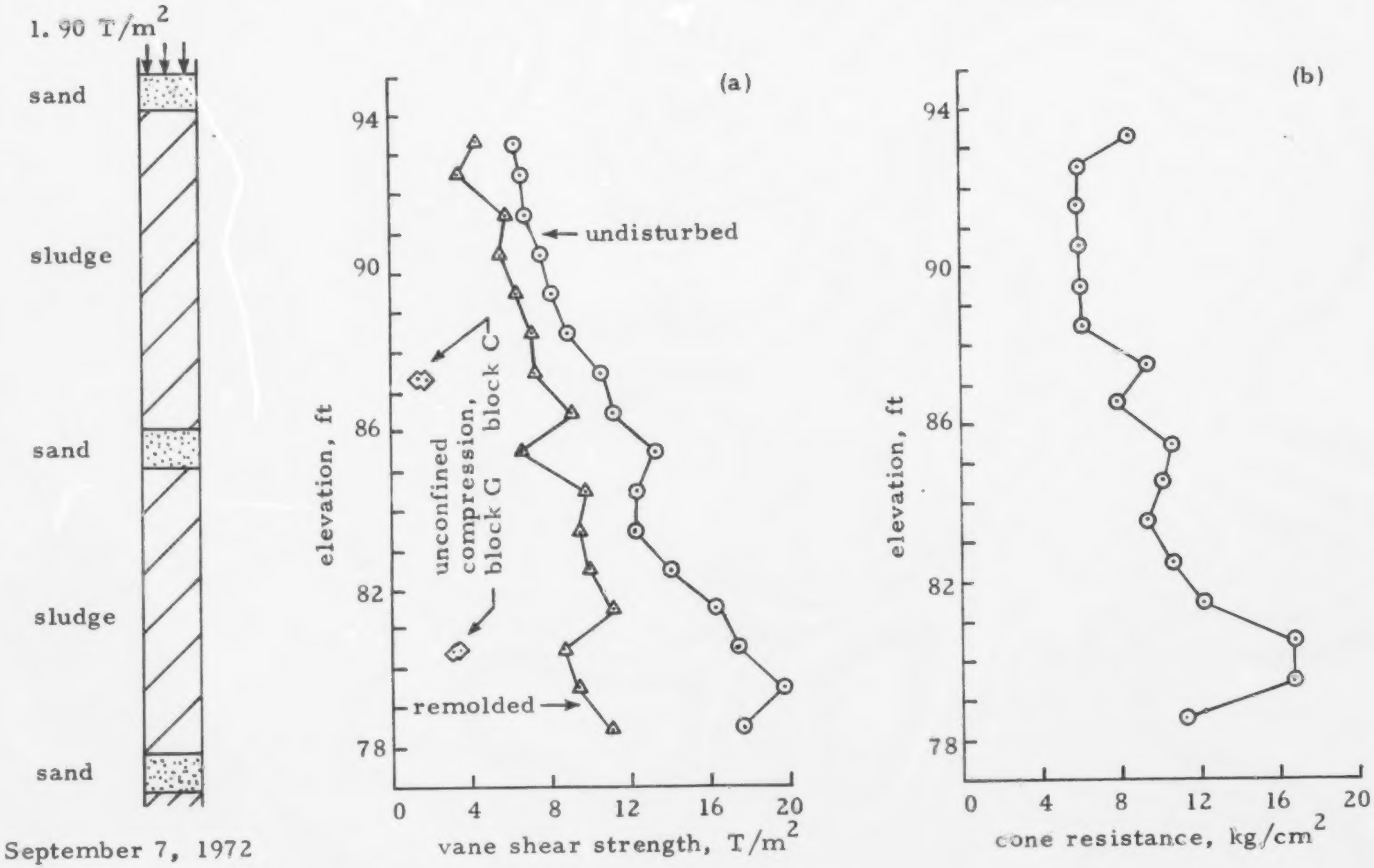

Figure 5. 13. Experimental landfill, immediately before slope excavation.
(a) Vane shear strength. (b) Dutch cone resistance.

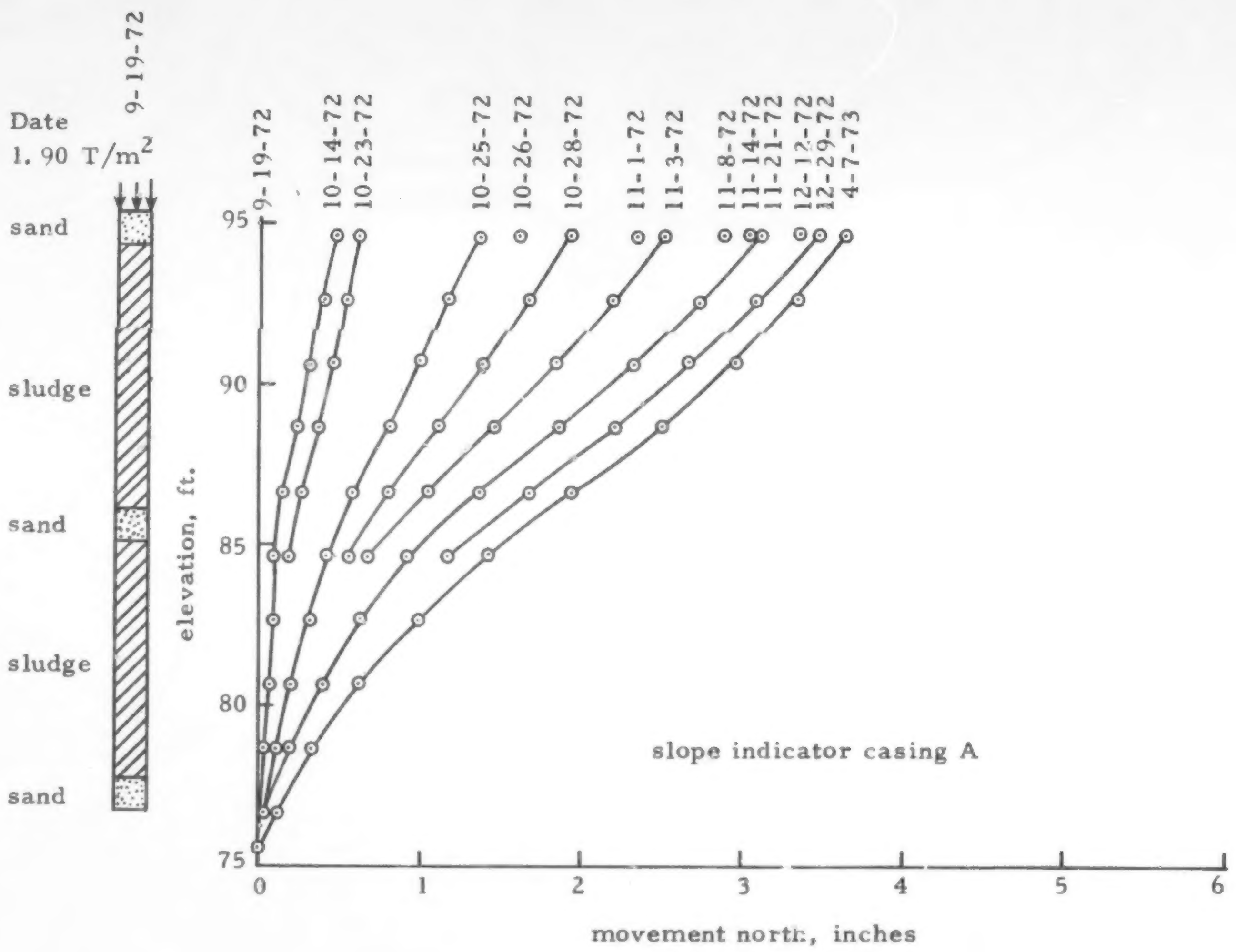

Figure 5. 14. Lateral movement. (a) Slope indicator casing A.

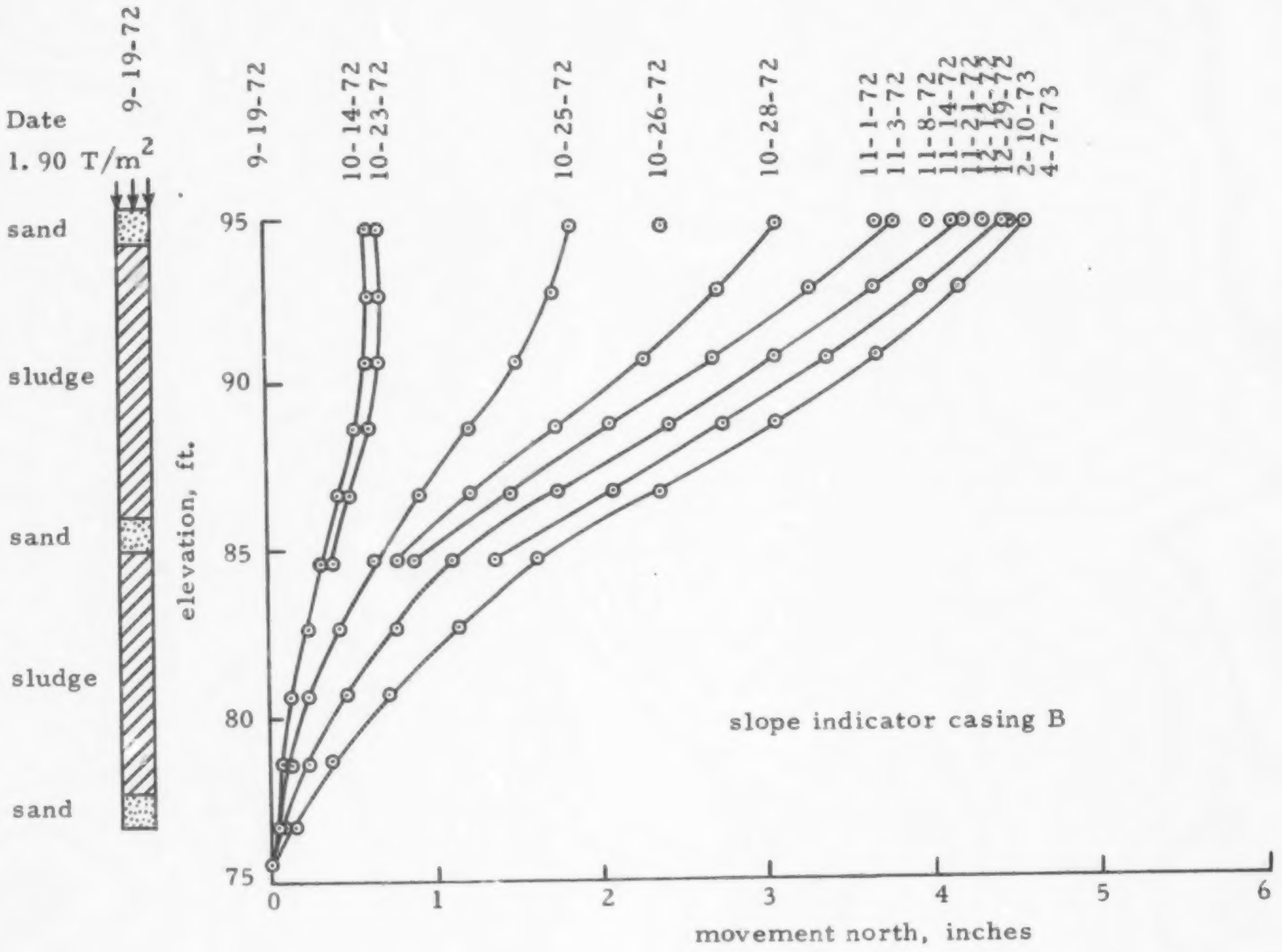

Figure 5. 14. Lateral movement. (b) Slope indicator casing B.

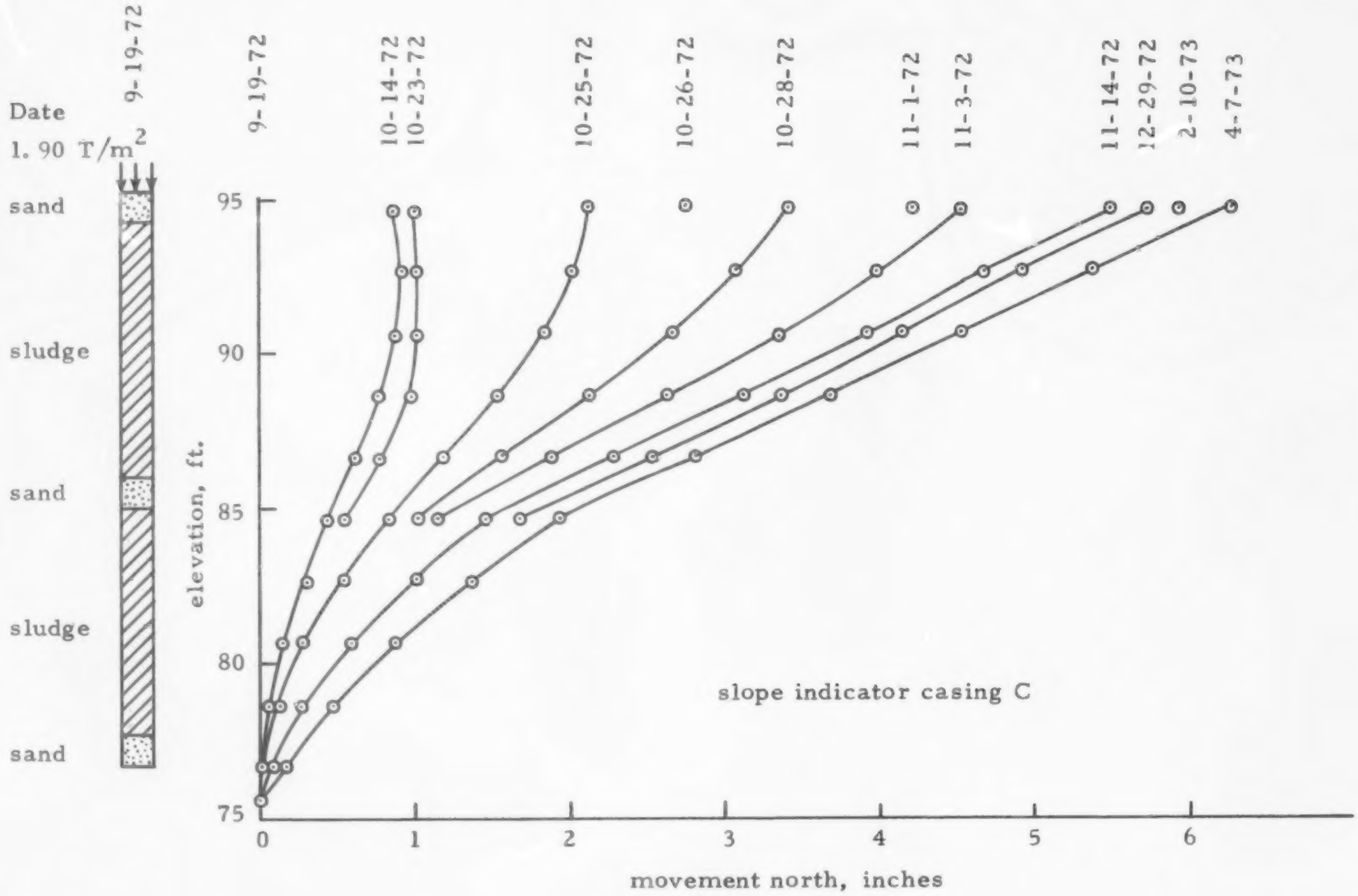

Figure 5. 14. Lateral movement. (c) Slope indicator casing C.

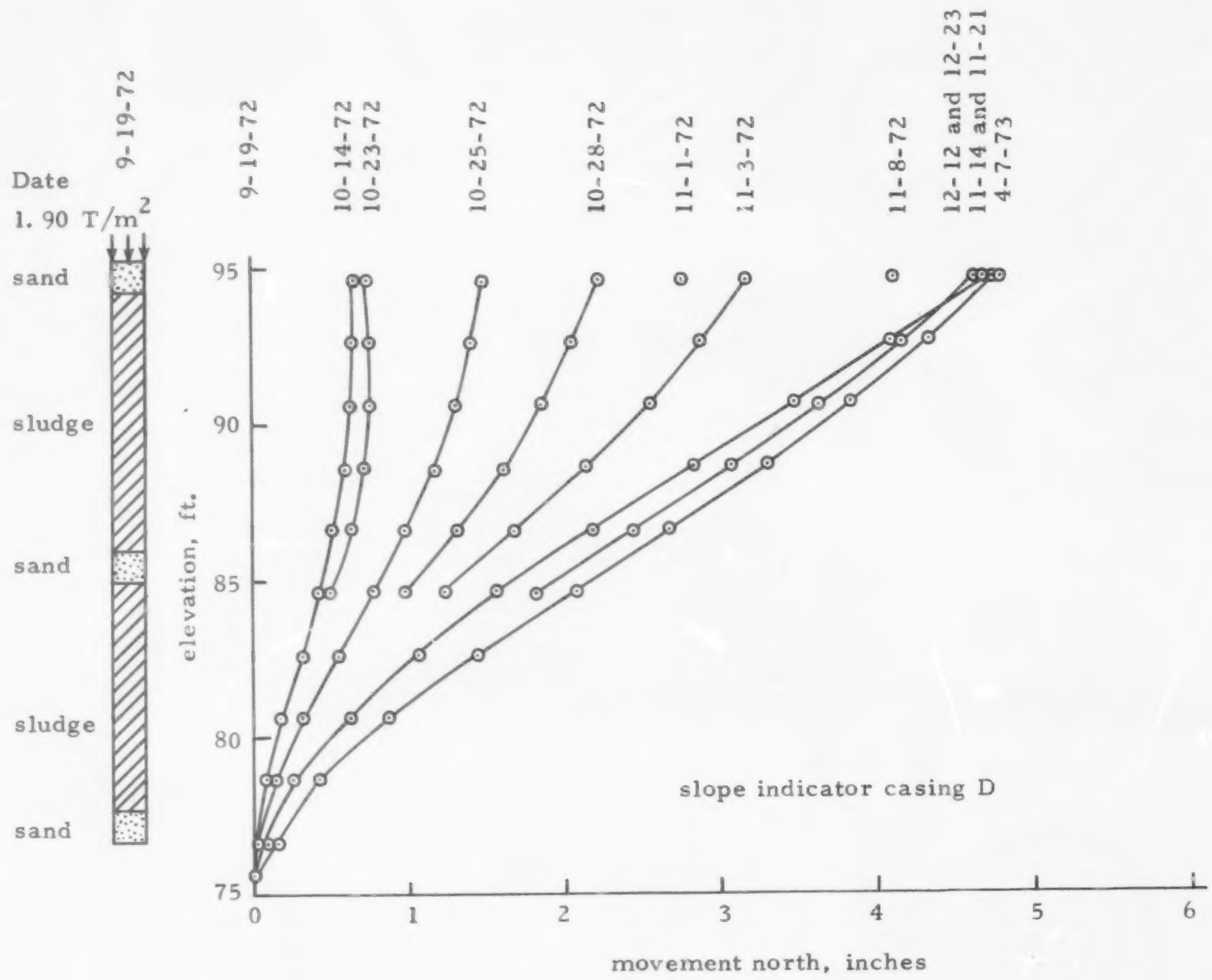

Figure 5. 14. Lateral movement. (d) Slope indicator casing D.

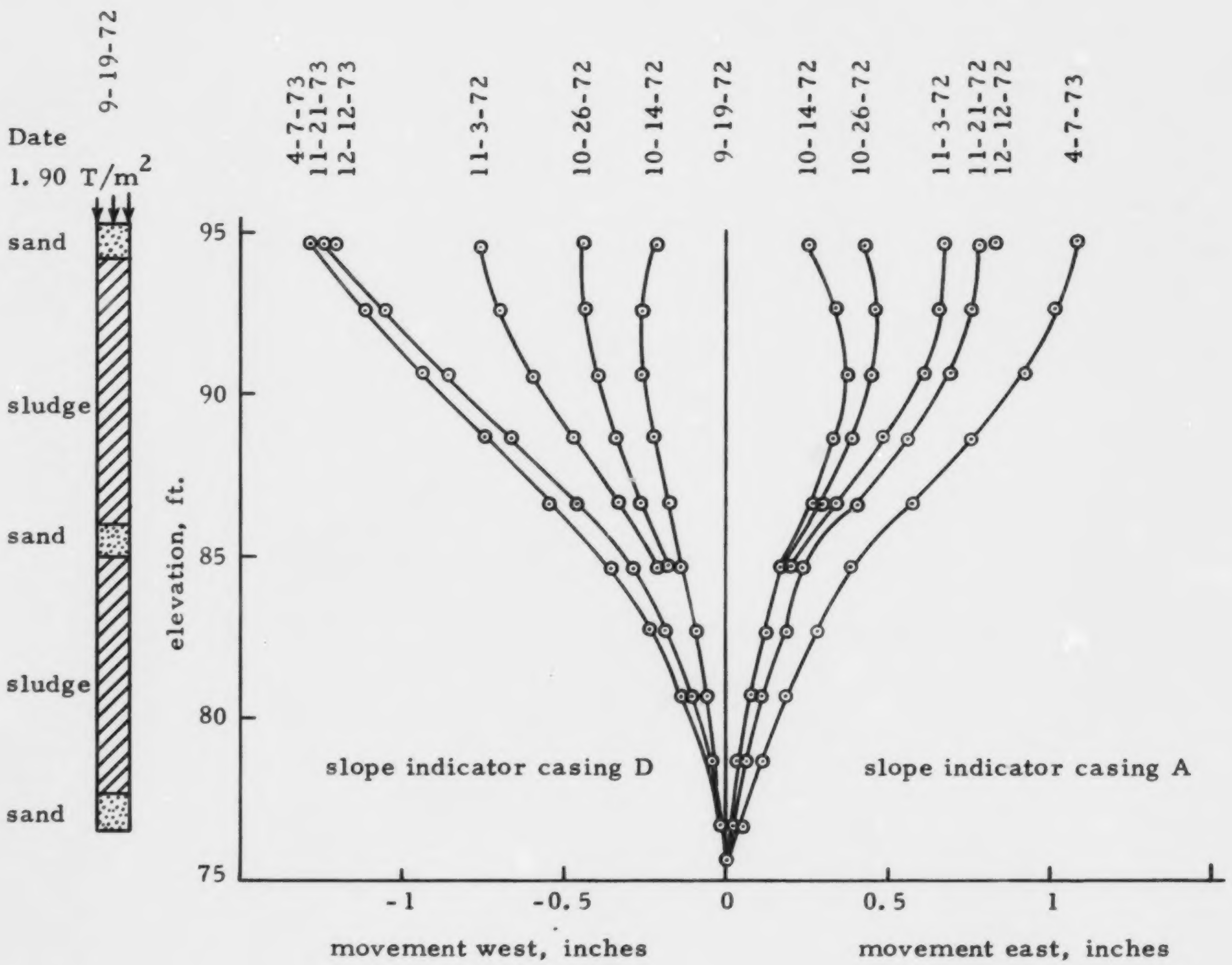

Figure 5. 14. Lateral movement. (e) Slope indicator casings A and D.

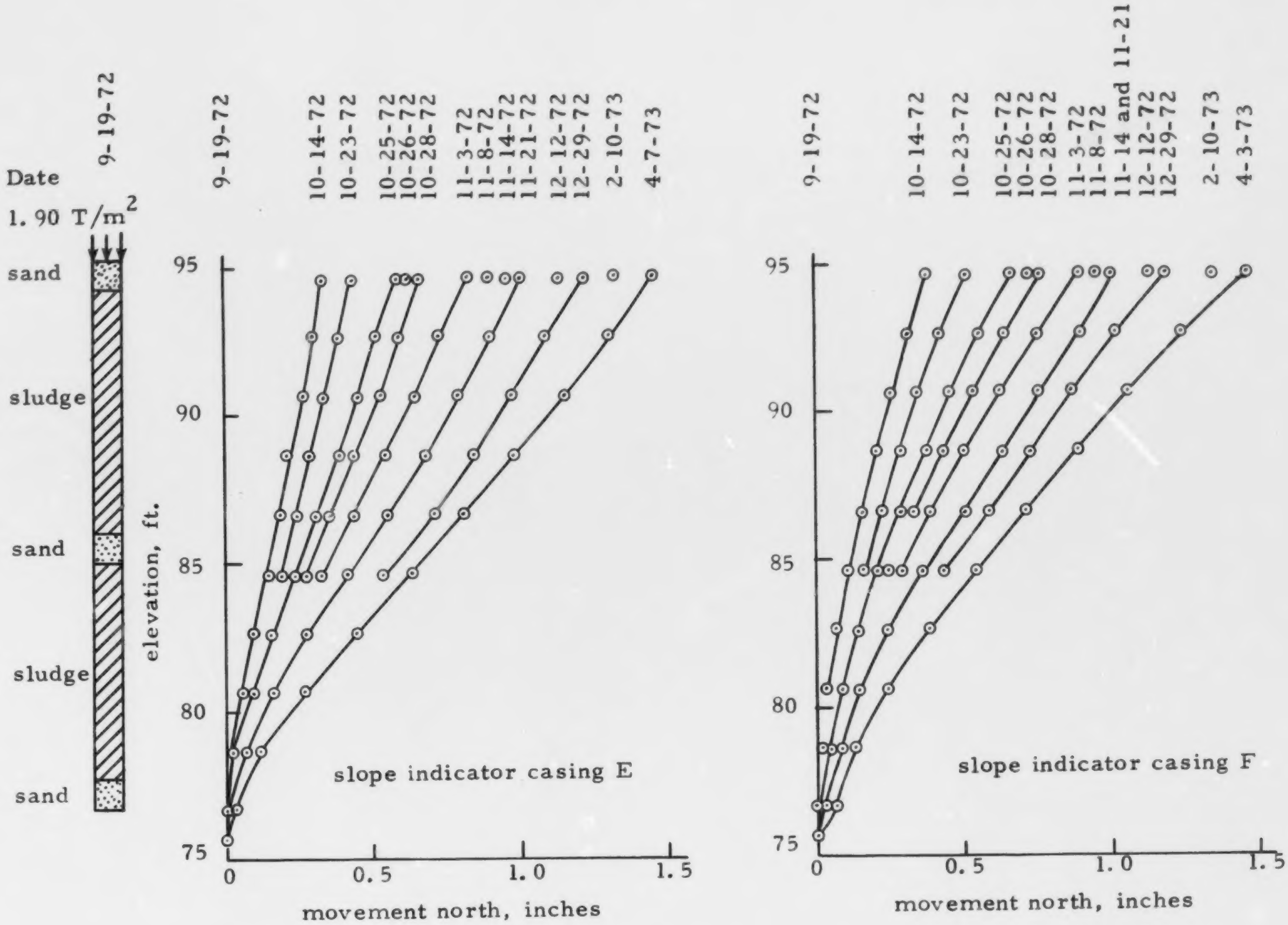

Figure 5. 14. Lateral movement. (f) Slope indicator casings E and F.

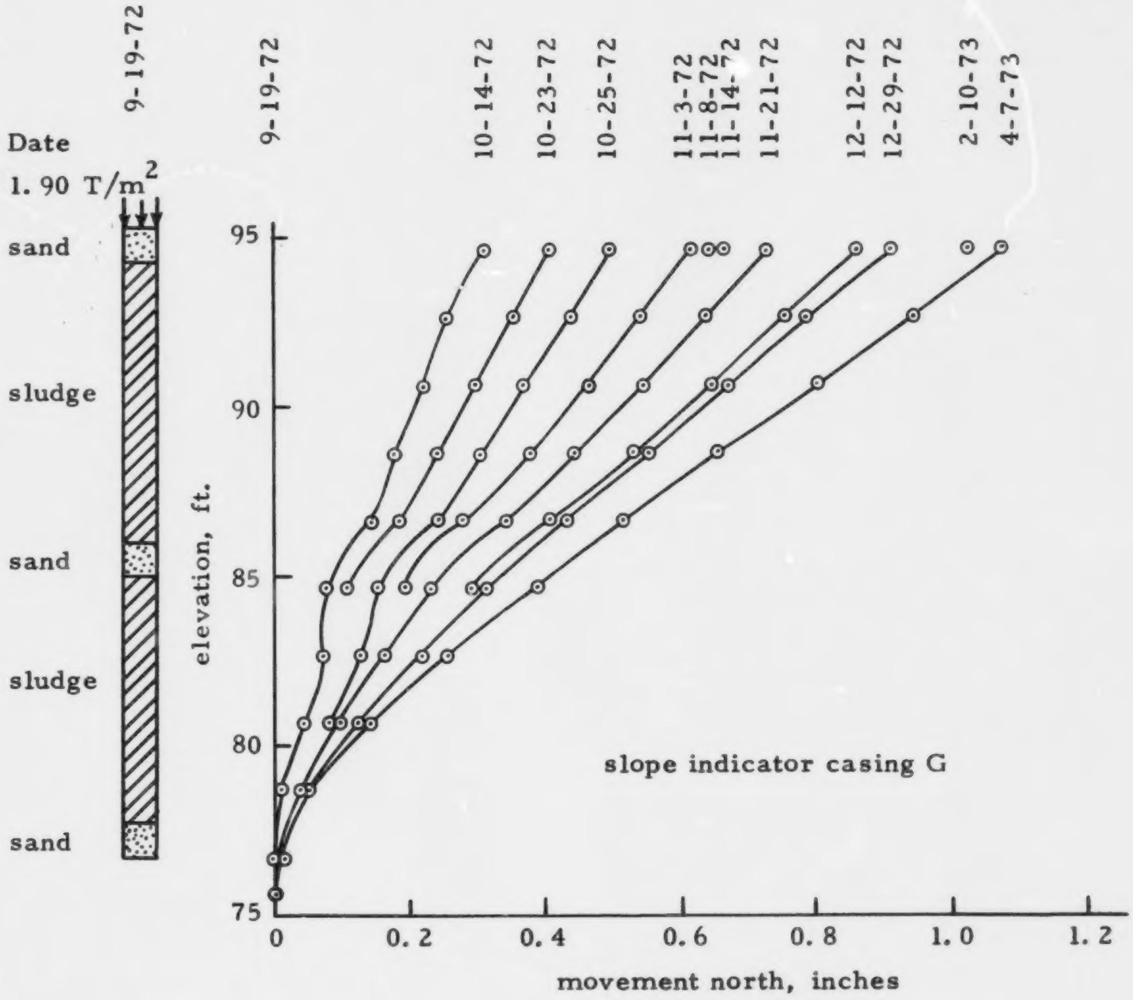

Figure 5. 14. Lateral movement. (g) Slope indicator casing G.

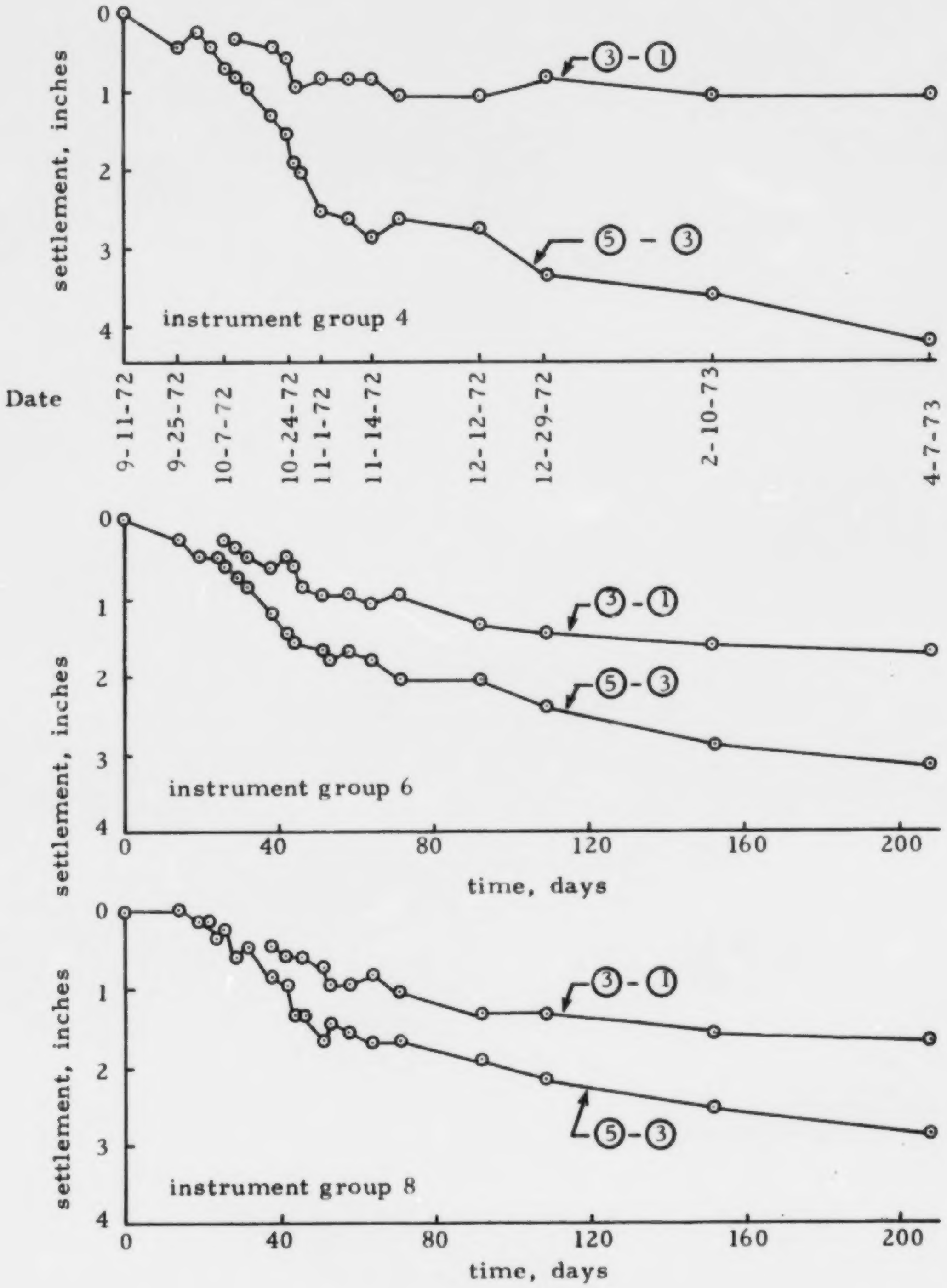

Figure 5. 15. Settlement in the top, ⑤-③, and bottom, ③-①, sludge layers. (a) Instrument groups 4, 6, and 8.

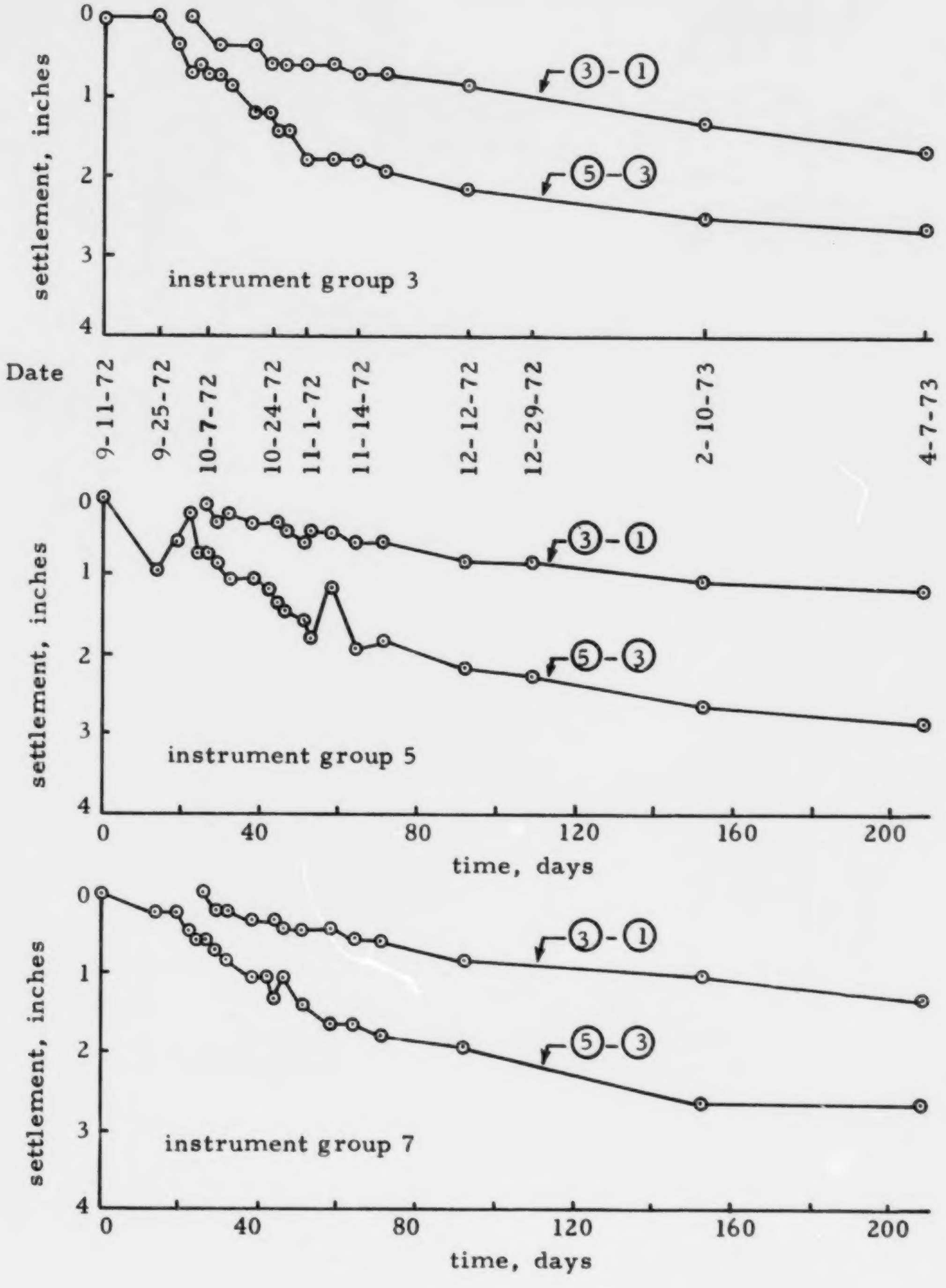

Figure 5. 15. Settlement in the top, ⑤ - ③, and bottom, ③ - ①, sludge layers. (b) Instrument groups 3, 5, and 7.

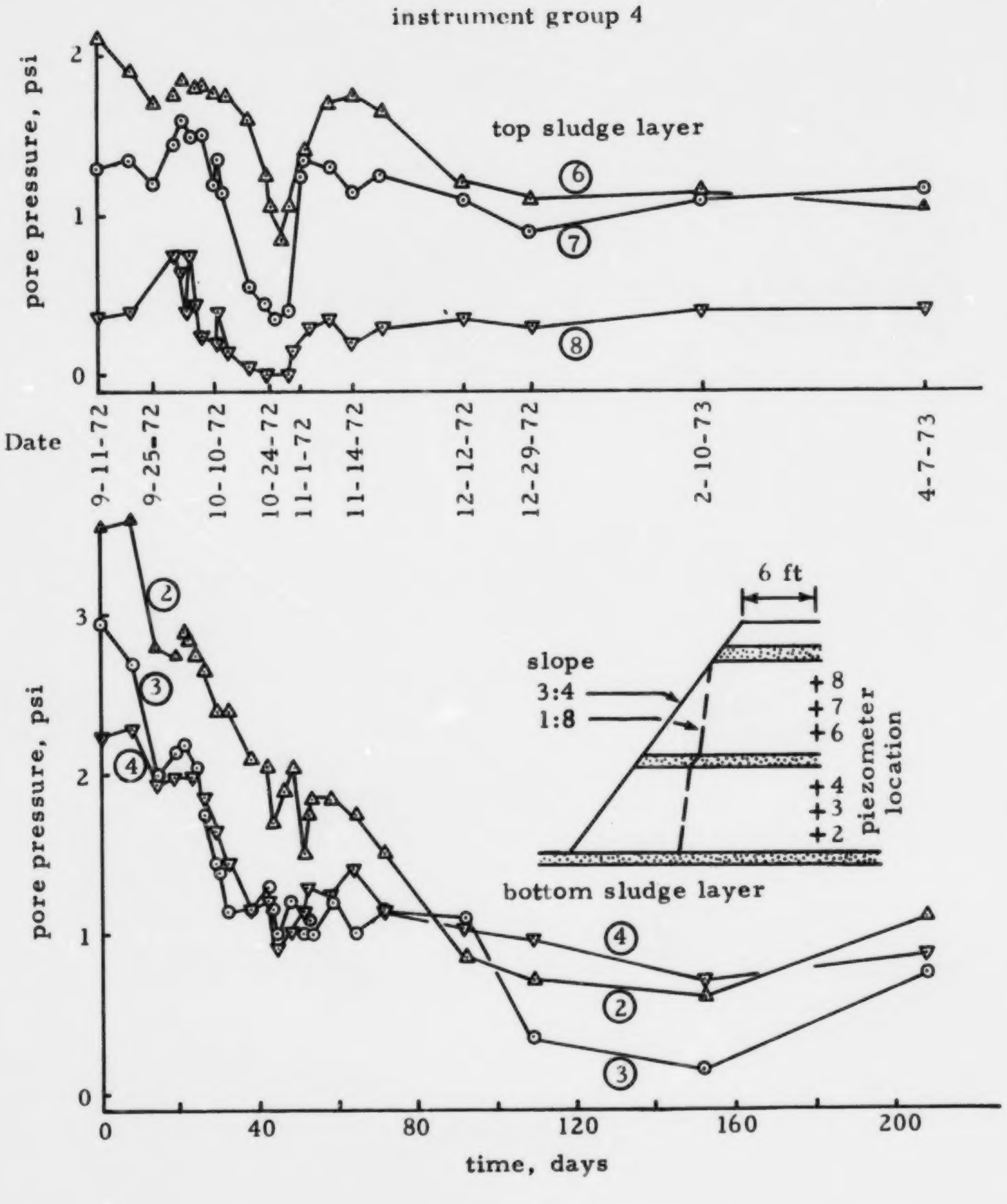

Figure 5. 16. Pore pressure versus time curves. (a) Instrument group 4.

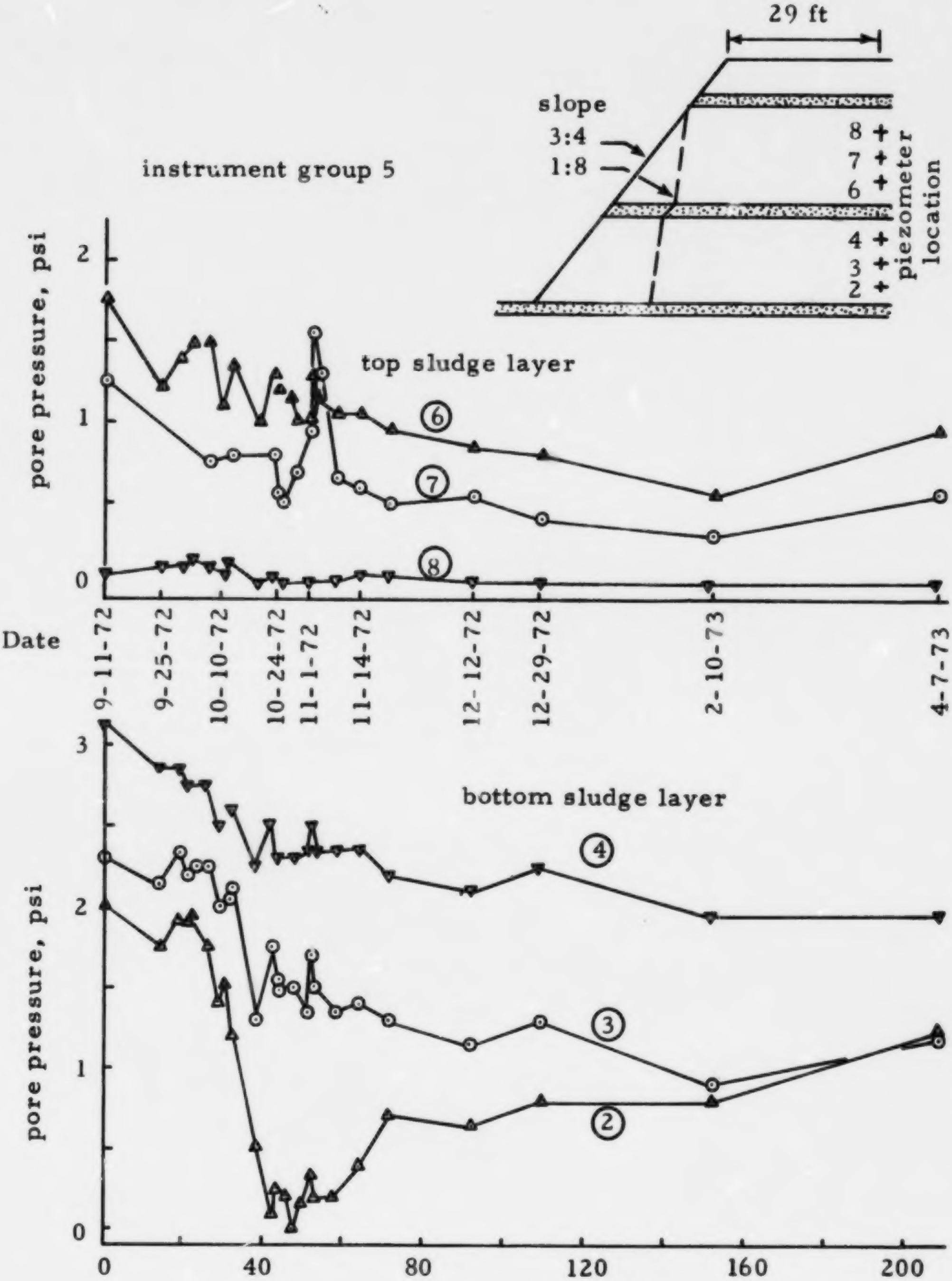

Figure 5. 16. Pore pressure versus time curves. (b) Instrument group 5.

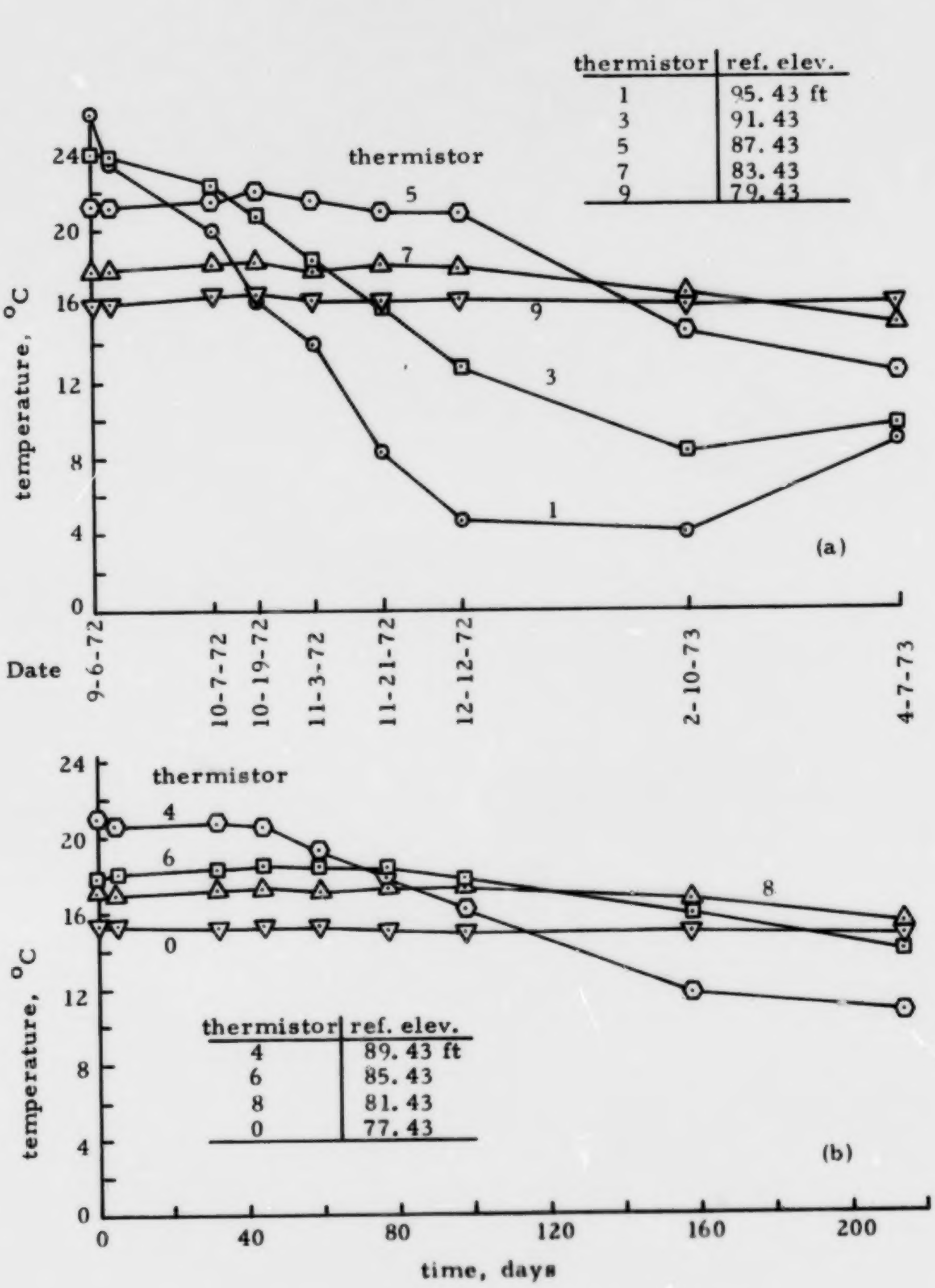

Figure 5. 17. Temperature versus time. (a) Thermistors 1, 3, 5, 7 and 9. (b) Thermistors 4, 6, 8, and 0.

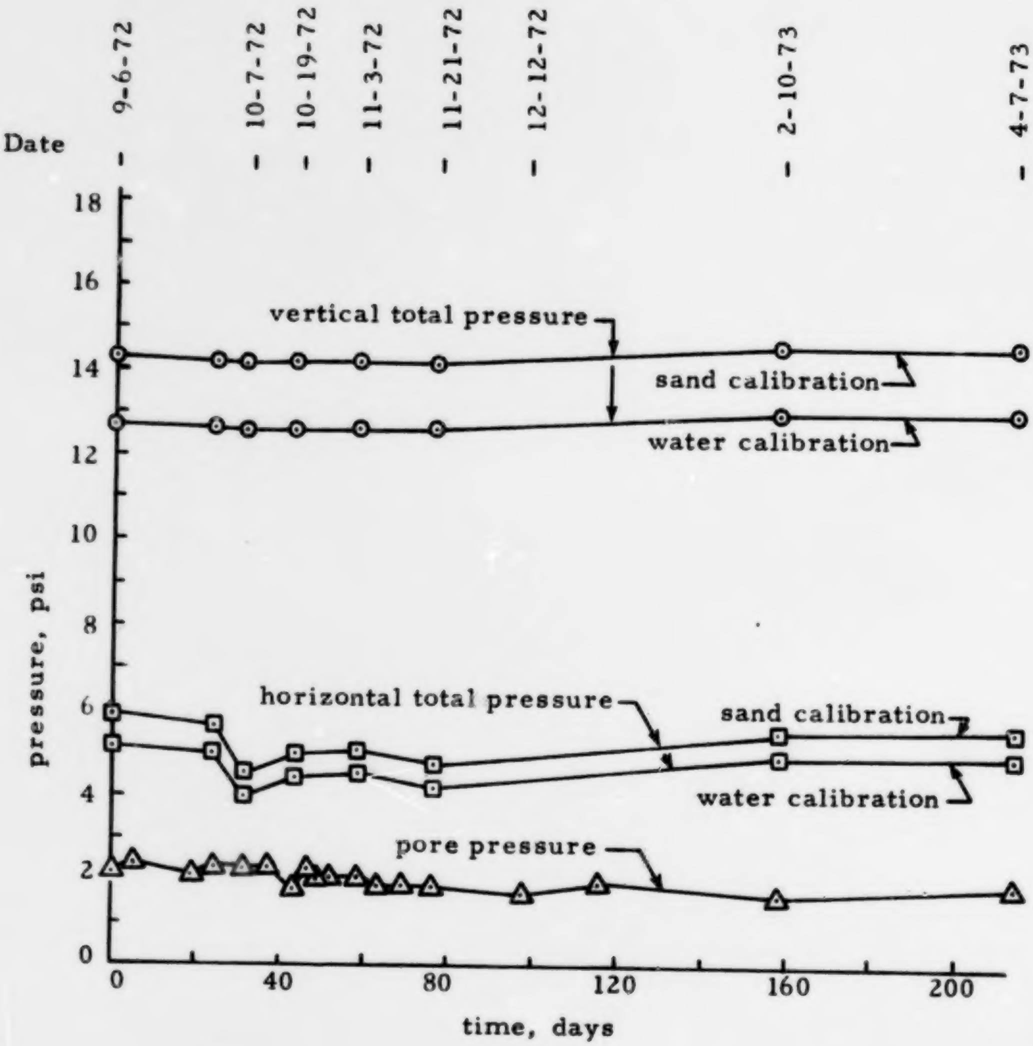

Figure 5. 18. Horizontal and vertical total stresses, bottom sludge layer.

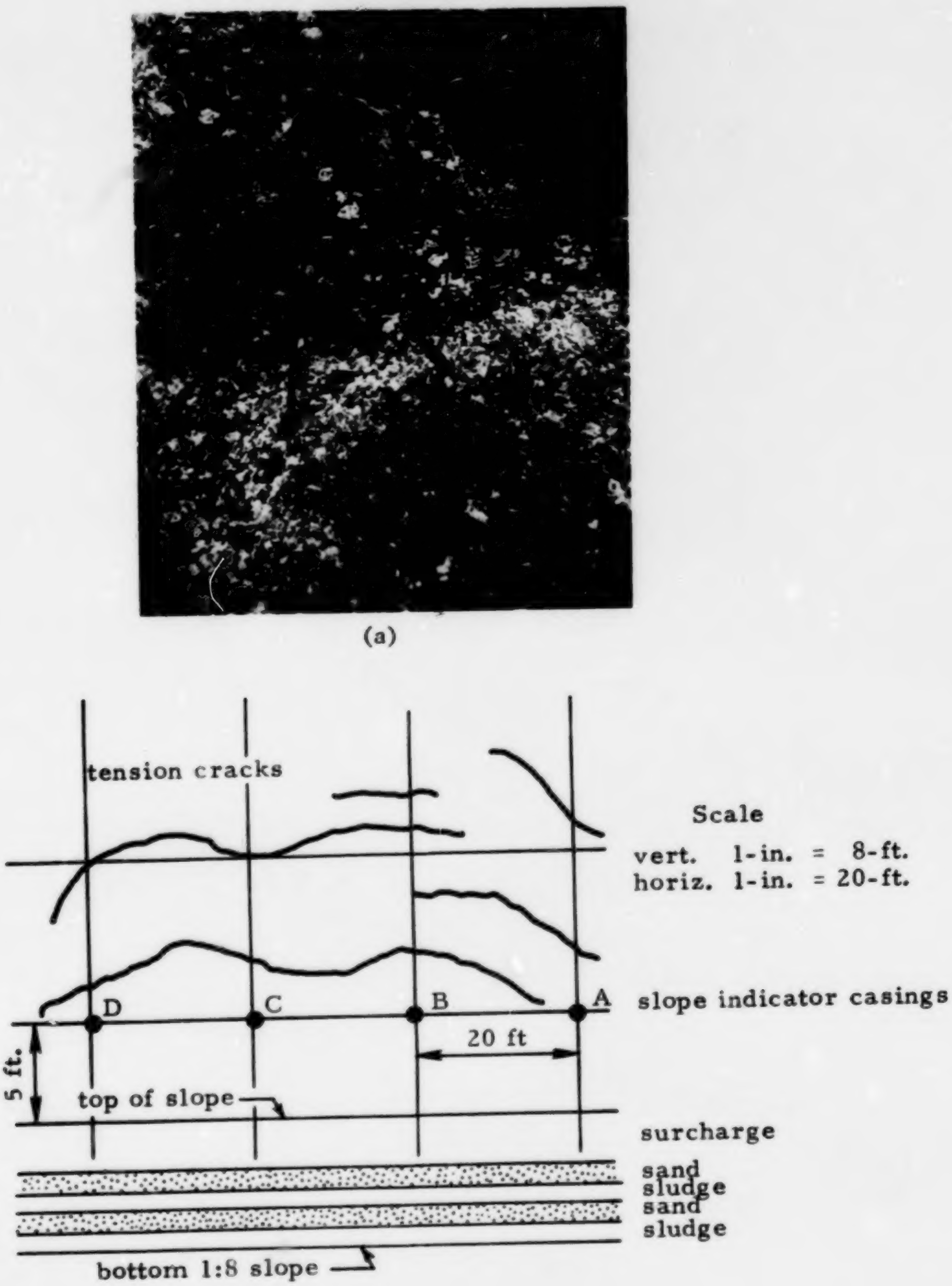

(a)

tension cracks
Scale
vert. 1-in. = 8-ft.
horiz. 1-in. = 20-ft.
D
C
B
A
slope indicator casings
20 ft
5 ft.
top of slope
surcharge
sand
sludge
sand
sludge
bottom 1:8 slope

(b)

Figure 5. 19. Tension cracks. (a) Photo. (b) Crack locations on October 25, 1972.

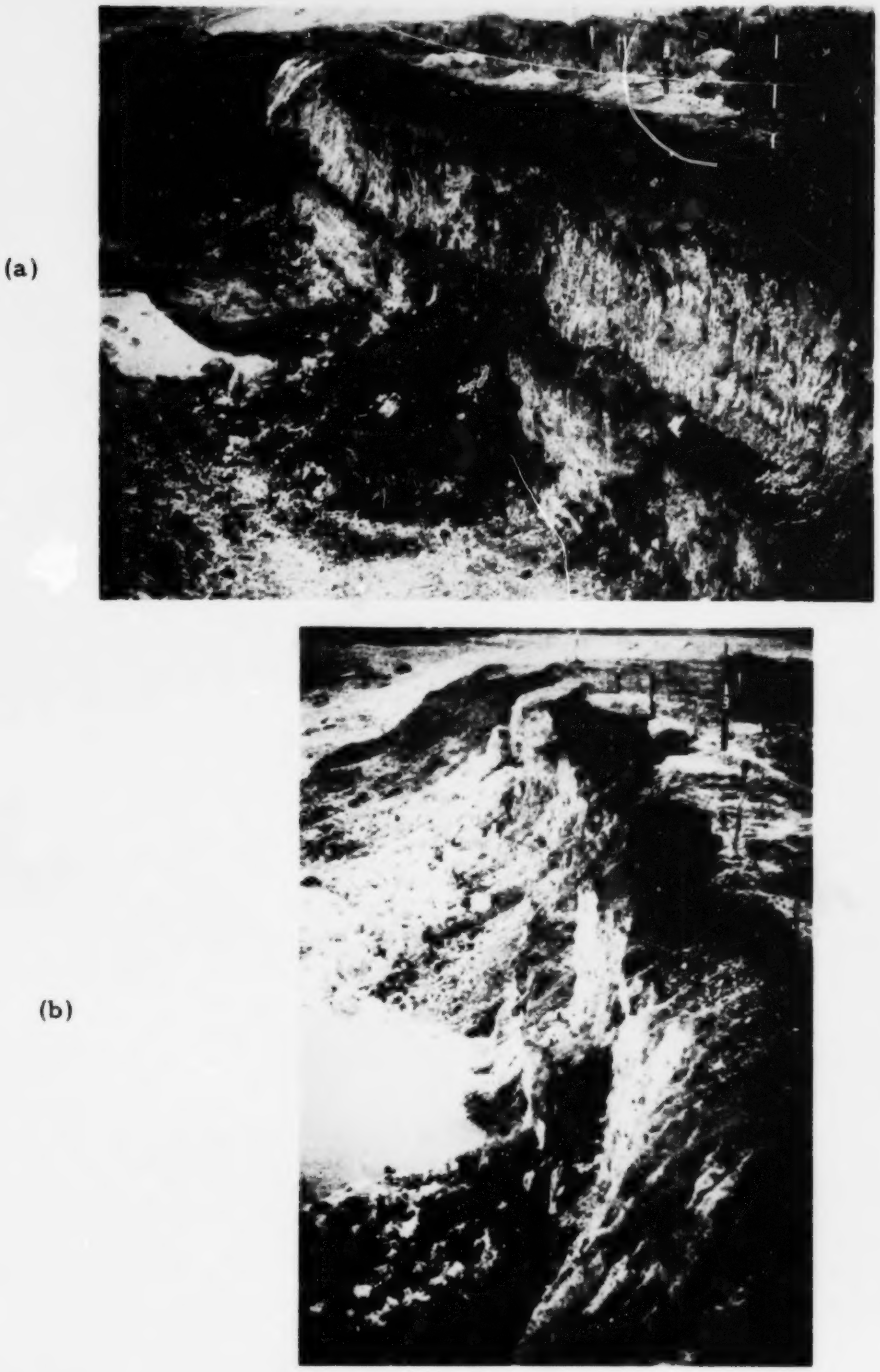

Figure 5. 20. (a) Initial slope failure, October 29, 1972.
(b) Slope condition on November 11, 1972.

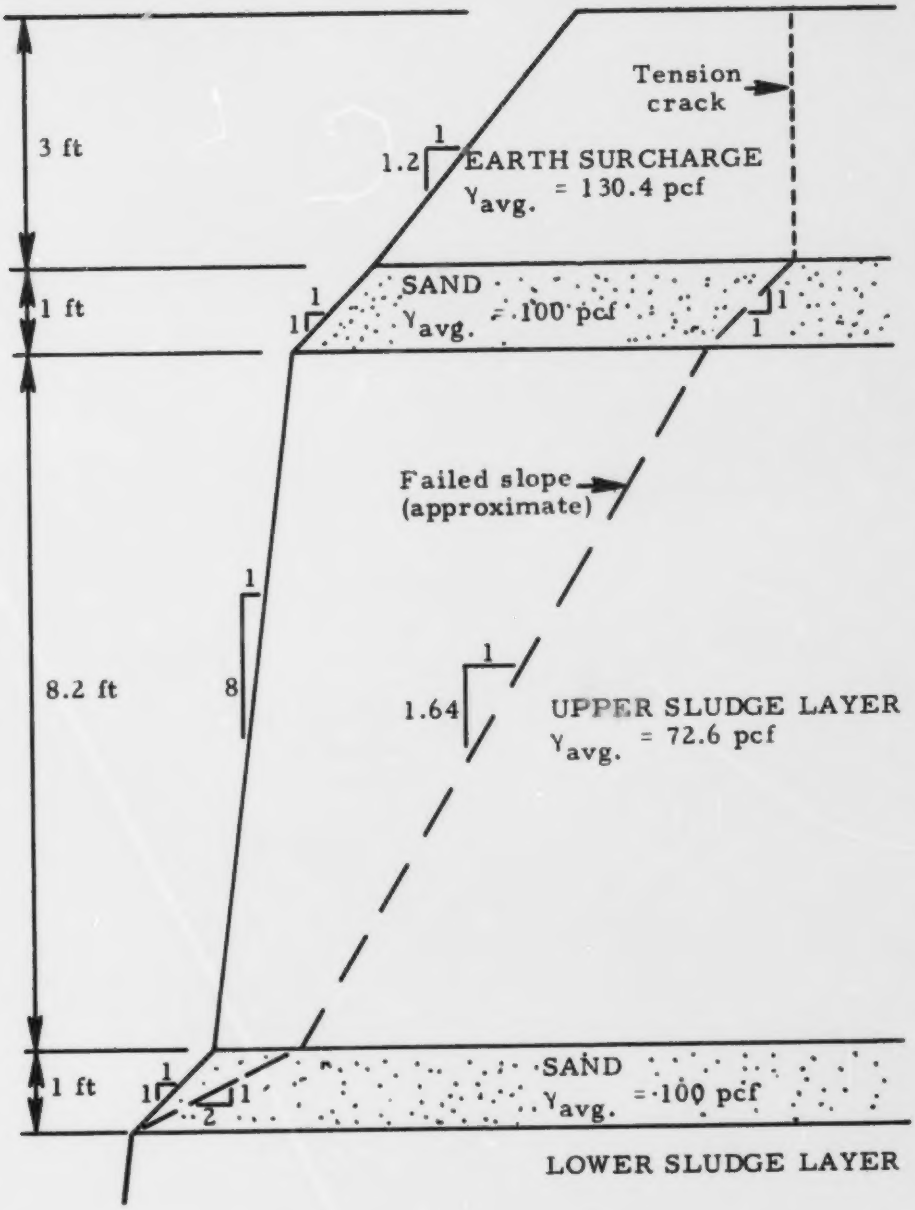

3 ft
1 ft
8.2 ft
1 ft
Tension crack
1.2
1
EARTH SURCHARGE
$\gamma_{avg.}$ = 130.4 pcf
SAND
$\gamma_{avg.}$ = 100 pcf
1
1
1
1
Failed slope (approximate)
1
8
1
1.64
UPPER SLUDGE LAYER
$\gamma_{avg.}$ = 72.6 pcf
SAND
$\gamma_{avg.}$ = 100 pcf
1
1
1
2
LOWER SLUDGE LAYER

Figure 5.21. Cross section of 1:8 slope, before and after failure.

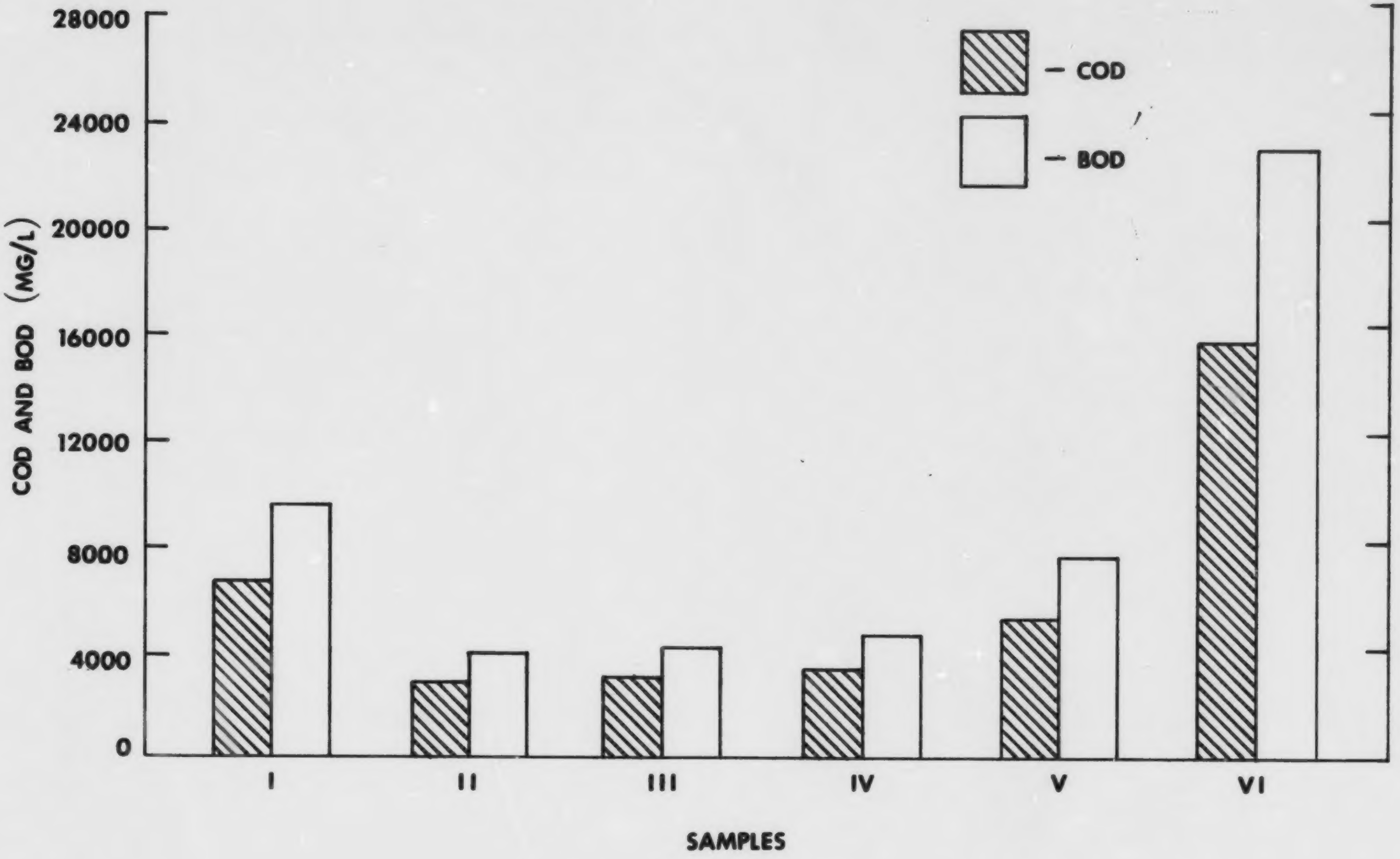

Figure 5.22. Biochemical oxygen demand (BOD) and chemical oxygen demand (COD) for leachate samples.

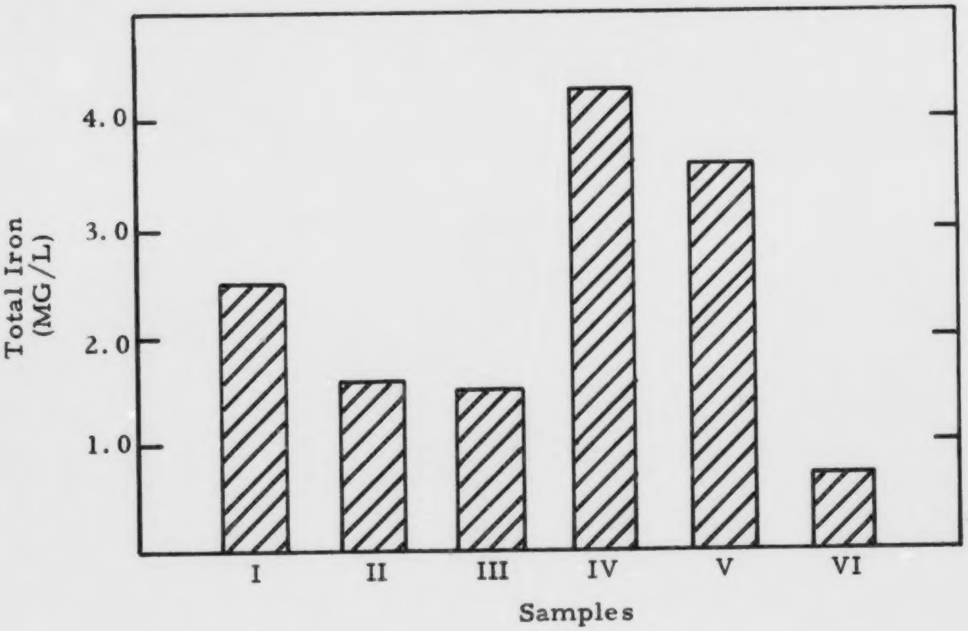

Figure 5.23. Total iron for leachate samples.

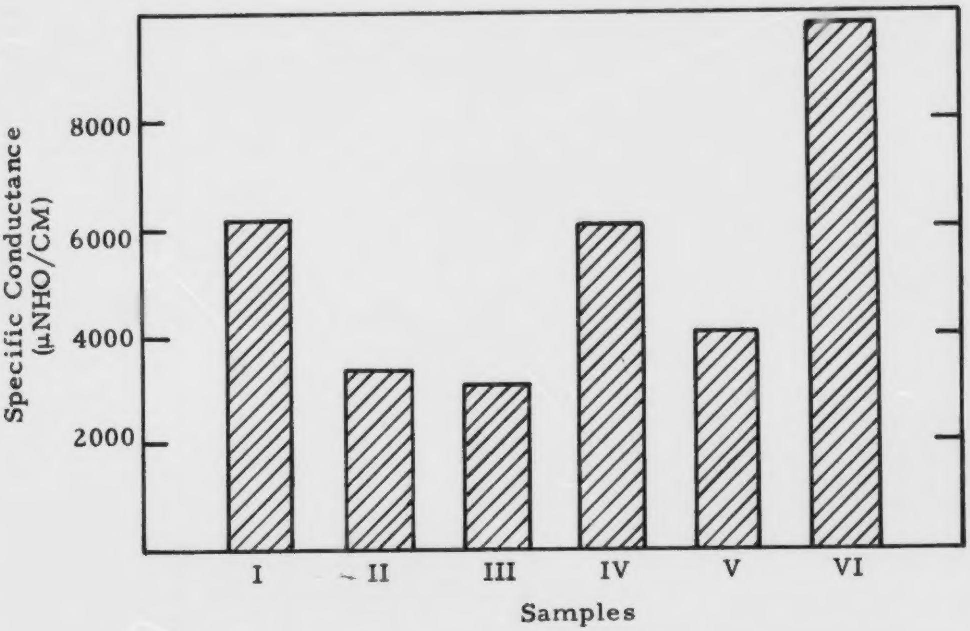

Figure 5.24. Specific conductance for leachate samples.

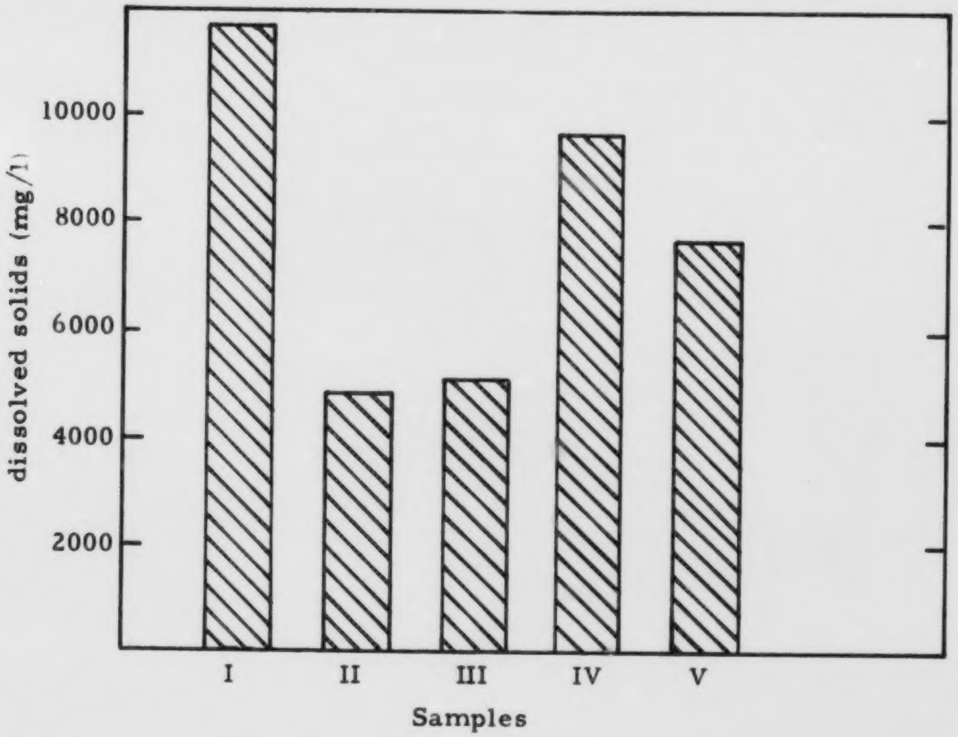

Figure 5. 25. Dissolved solids for leachate samples.

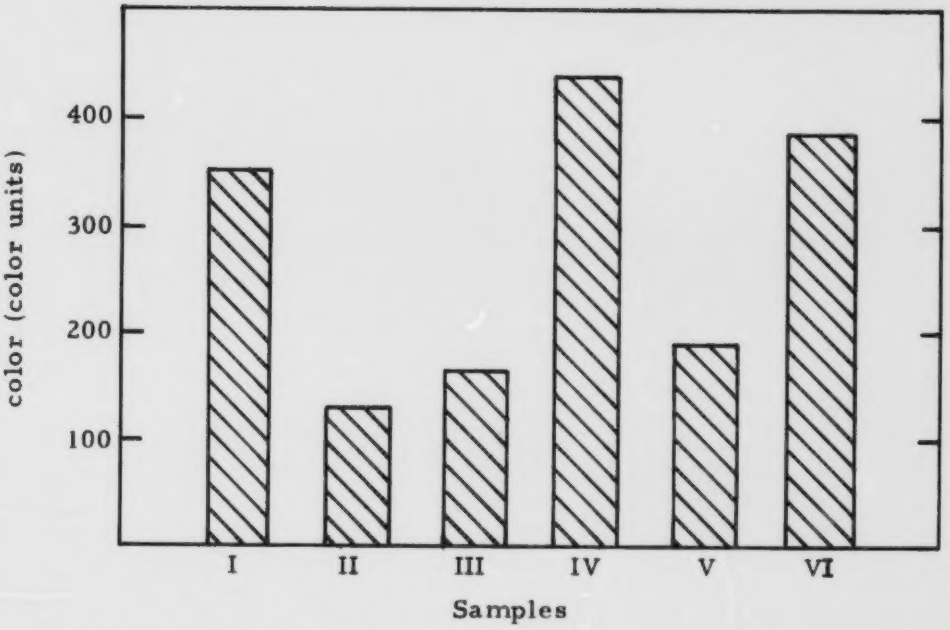

Figure 5. 26. Color for leachate samples.

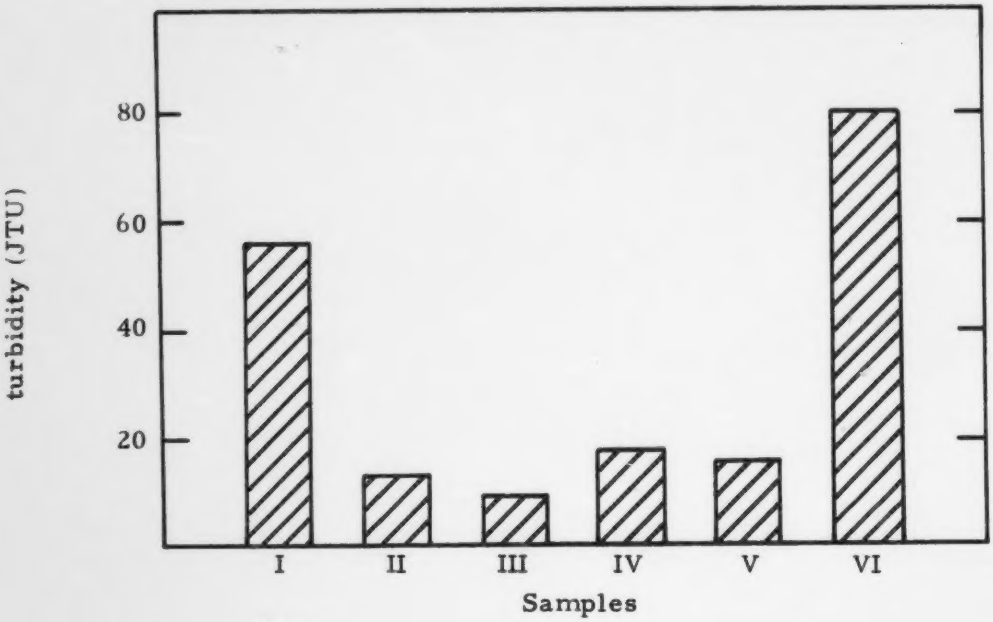

Figure 5. 27. Turbidity for leachate samples.

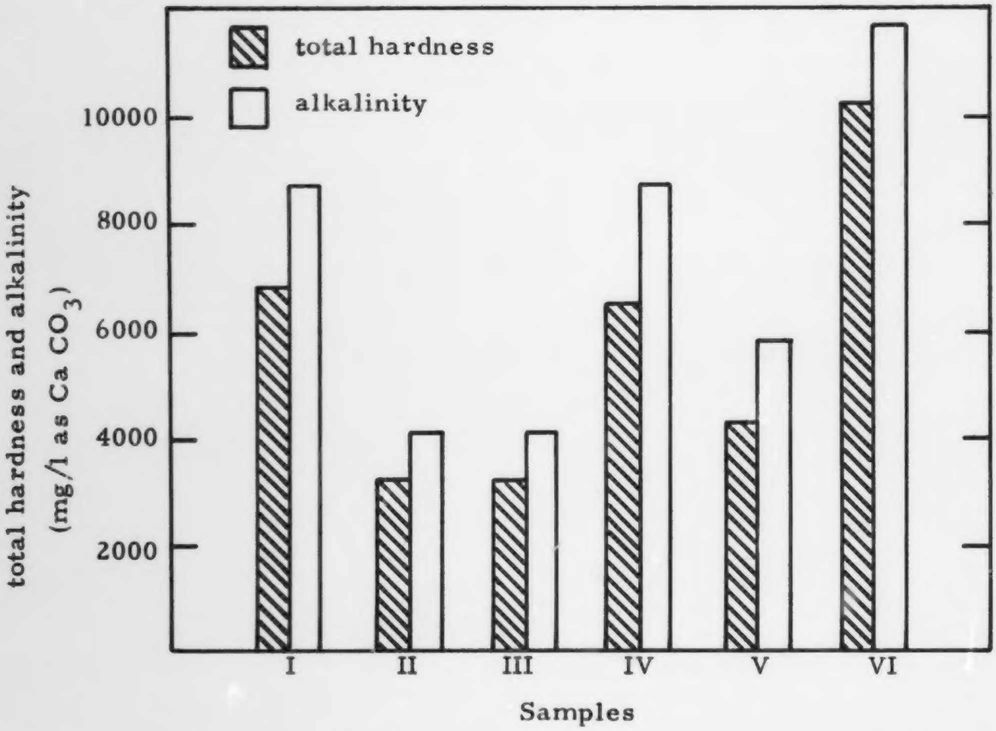

Figure 5. 28. Total hardness and alkalinity for leachate samples.

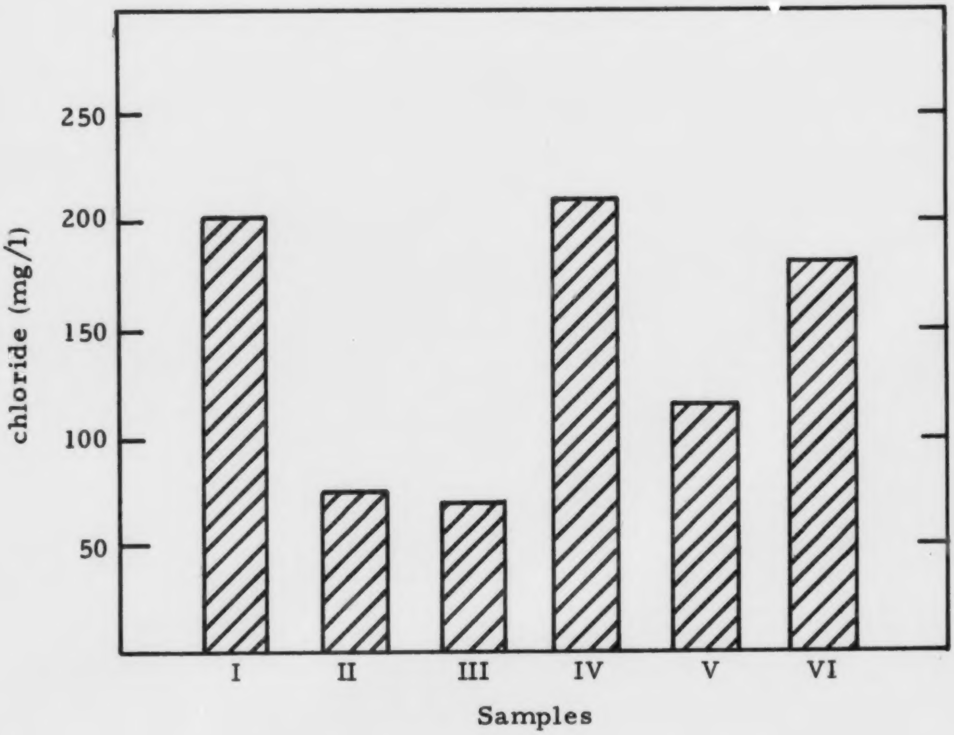

Figure 5.29. Chloride concentration for leachate samples.

CHAPTER VI. Discussion and Interpretation of Results

This discussion and interpretation covers laboratory and field results obtained after preparation of the First Annual Report. Both the landfill consolidation and the stability phases of the project are included. The material is presented in four sections: (1) physical properties, (2) consolidation and field settlement, (3) slope stability for the papermill sludge, and (4) leachate analysis.

Physical Properties

Water contents of the sludge in the landfill after consolidation are summarized in Figure 5. 1. The scatter in values appears to be related to variations in organic content of the sludge. Water retention of the sludge is greater for higher organic contents. Also, a small change in organic content will alter the dry weight because of large differences in specific gravity of the ash (clay) as compared to the organic material. Hence, two samples with the same volume of water may show significant differences in percent water content on an oven dry weight basis. Despite the somewhat wide range in observed water contents the average for the upper sludge layer dropped 71 percent to an average value close to 186 percent. For the lower sludge layer the average water content dropped 98 percent to an average value close to 167 percent. Conversion of these average changes in water content to one-dimensional volume changes gives reasonable agreement with observed ultimate field settlements. Sludge unit weights increased as water, with the lower specific gravity, drained from the material. The unit weight of the upper and lower sludge layers increased to 72. 6 lb per cu ft (block B) and 76. 5 lb per cu ft (block F), respectively as compared to the initial fresh sludge unit weight of 69. 7 lb per cu ft.

Representative ash contents for undisturbed block samples, given in Table 5. 1, are very close to the average for fresh sludge samples reported in the First Annual Report. These data show that ash contents for the sludge in the landfill range from about 32 percent to about 60 percent. Earlier work (Andersland and Laza, 1971) has shown that ash contents for papermill sludges based on ASTM test method D586-63 agree reasonably well with organic contents determined on the basis of the test method given in Agronomy No. 9, section 92-3.3 (Black, 1965). For information, weight loss for papermill sludge samples from blocks C and G, which were first dried to 105° C, have been plotted against temperature in Figure 6.1. The small samples, 6.7861 gm for block C and 5.0706 gm for block G, reached essentially a constant weight after one hour at each temperature. These data show no drastic weight loss for temperatures above 300°C, however, it appears that the higher temperatures are needed for complete burning of the organic material. Ash content has been plotted against liquid limit and plastic limit giving the relationships shown in Figure 6.2. The greater water retention of the organic material appears to be responsible for the higher limits at high organic contents (low ash content). The liquid limit data for the three sludges appear to give a consistent relationship with a continuous curve. Plastic limits are more difficult to measure at high organic contents since fibers interfere with crumbling of the thread at the appropriate water contents. It appears that the dashed curve shown in Figure 6.2 approximates the plastic limit data. The liquid limit and plasticity index have been plotted on the plasticity chart in Figure 6.3. All data points fall in the region designated organic clay with some of the sludge perhaps more closely related to peat (Casagrande, 1948, 1966).

Consolidation and Field Settlement

Laboratory consolidation behavior of fresh sludge samples and the settlement behavior of the landfill have been presented in the First Annual Report. This section discusses the laboratory consolidation behavior of undisturbed block samples and the determination of theoretical field settlement relations using the theories of Gibson and Lo (1961) and Wahls (1962).

Laboratory Consolidation. Consolidation tests on undisturbed sludge samples include the effects of stress history produced by the earth surcharge on the landfill. The void ratio versus logarithm of pressure curves are similar to those which might be obtained for a moderately disturbed normally consolidated clay sample. Values of the effective overburden pressure, p_o, have been estimated from the curves using the Casagrande construction (Leonards, 1962) and are shown in Figure 5.2. Using a sludge unit weight of 72.0 lb/cu ft and an average residual pore pressure of 1.2 psi, the calculated in situ vertical effective pressure for the upper sludge layer is 0.301 kg/sq cm, which agrees closely with the values obtained from the void ratio-logarithm of pressure curves. The lower layer calculated effective overburden pressure equals 0.55 kg/sq cm, which is less than the laboratory values shown for the lower layer in Figure 5.2 (0.65 to 0.77 kg/sq cm). This discrepancy may be due to limitations of the Casagrande construction for estimating p_o.

The vertical effective pressure in the lower layer obtained from the total pressure cell and piezometer data of Figure 5.18 equals 0.77 kg/sq cm (water calibration), which agrees closely with the estimated p_o value from the void ratio versus logarithm of pressure curve. However it is the author's opinion that this pressure is too high, primarily because of the increase in measured total pressure exhibited by the pressure cell after surcharge application. If the value of total pressure measured at the completion of surcharge application (Figure 5.11, First Annual Report) is used to compute the in situ pressure, a value of 0.65 kg/sq cm is obtained.

Since the block sample from the lower layer was under a greater in situ effective stress than the upper layer, it would be expected that the lower layer would have a lower initial void ratio and higher effective overburden pressure, p_o, as shown in Figure 5.2. The difference in the compression index, C_c, between the two block samples may be a result of small differences in organic content. Slightly higher ash contents were present in block sample F as compared to block sample B, which would help to account for this difference.

The higher values of the coefficient of consolidation, c_v, at stresses below the effective overburden pressure, shown in Figure 5.3a, are typical for clay soils (Lambe and Whitman, 1969). The low primary compression ratios below the existing overburden pressure, p_o, in Figure 5.3b indicate that creep of the soil skeleton was a significant portion of the measured deformation in this stress region. The values of the coefficient of secondary compression, C_α, shown in Figure 5.3c, are also smaller at low stresses, indicating that field consolidation has increased the resistance of the soil skeleton to creep deformation. The magnitude of C_α increases steadily over the entire stress range and approaches that of fresh sludge at the higher pressures. The sample from the lower layer has C_α values which are somewhat less than the upper layer, again indicating reduced compressibility of the soil skeleton due to the higher consolidation pressure.

Field Settlement. Gibson and Lo's (1961) theory has been used to obtain the theoretical time-settlement curves shown in Figure 6. 4a. Curves for three different values of c_v have been plotted, none of which closely follow the actual field settlement curve over the entire range of time. Part of the difference results from the predicted ultimate settlement being slightly larger than the actual settlement. At times up to approximately 300 hours, the theoretical curves for the two higher values of c_v are closely parallel to the field curve, but between 300 and 1000 hours the settlement predicted from theory increases at a faster rate than the actual settlement. For the given parameters, Gibson and Lo's (1961) theory predicts that the ultimate settlement is reached very rapidly without developing a linear (with log time) secondary compression curve. The theoretical type of secondary compression that develops from this theory is dependent on the value of a parameter, N, equal to $H^2/\frac{1}{\lambda}\, bc_v 4$. Values of this parameter for the sludge landfill are large (175 for $c_v = 0.063$ in^2/min) and result in the theoretical curves shown in Figure 6. 4a. For N values of approximately 0. 04, secondary compression occurs for a much longer period of time. The low value of the viscosity measured in the laboratory (6.95×10^4 lb/in^2/min) appears to be the soil property largely responsible for the theoretical results obtained, being on the order of 10^2 to 10^3 times smaller than values obtained from clays tested by Gibson and Lo (1961). These results appear to be consistent with the field observations, which indicate a decreasing secondary compression rate with log time.

Wahls' (1962) theory has been used to obtain the two theoretical curves shown in Figure 6. 4b. As discussed in Chapter II, ΔH_p in equation 2. 17 represents primary settlement only, and since Wahls' theory assumes that secondary compression can occur simultaneously with primary compression, it is necessary to establish a value of ΔH_p

from the parameters given. This was done by assuming an initial value of primary settlement equal to 16.7 in., obtained from field settlement and pore pressure data, and subtracting from this the theoretical amount of secondary compression that occurred during the time necessary to reach this amount of settlement (assuming $T_v = 1.0$ for the end of primary compression). This can be computed as $\Delta H_p = 16.7 - (0.0147) \cdot (103) \cdot (0.8684) = 15.4$ in. Here 0.0147 equals the assumed C_α, 103 equals H_p, and 0.8684 equals $h(T_v)$. Thus the time settlement relation is given by

$$\Delta H(t) = 15.4\, f(T_v) + (103)(0.0147)\, h(T_v) \tag{6.1}$$

The results obtained from Wahls' theory are similar to those that were obtained using Terzaghi's theory in the First Annual Report. The back computed field value of c_v (0.0626 in^2/min) accurately models the settlement up to the end of primary compression, and the laboratory determined value of C_α (0.0147 in^2/min) appears to be too low. A larger value of C_α would accurately model the settlement for only a limited time because Wahls' theory assumes a secondary compression rate that is linear with log time while the field secondary compression rate is decreasing with log time. Since Wahls' (1962) theory includes secondary compression in its mathematical formulation, it results in a smoother curve in the transition region than the method that was used to model secondary compression with Terzaghi's theory in the First Annual Report.

Leonards (1962) describes a simple procedure, suggested by Terzaghi, for obtaining the time-settlement relation of a clay layer subjected to a constant rate of loading. Using this procedure, the theoretical curve shown in Figure 6.5 has been drawn for the lower sludge layer and is seen to agree very well with the field curve and the previous theoretical solution given in the First Annual Report. The solution was obtained by using the simplified Terzaghi procedure in the linear loading range and then combining it with the Terzaghi solution for an instantaneous loading after the application of the surcharge.

Slope Stability for the Papermill Sludge

Slope stability for the papermill sludge is discussed under five headings: (1) laboratory and field shear strengths, (2) observed slope movements, (3) development of failure zones, (4) slope failure, and (5) analysis for the composite failure surface.

Laboratory and Field Shear Strengths. Laboratory tests on both fresh and undisturbed papermill sludge samples demonstrated that the shear strength behavior is similar to that for highly organic soils. Consider first the triaxial test results on fresh sludge samples U-1, U-2, and U-3 summarized in Table 5. 4. These samples were consolidated with an all-around pressure and failed by increasing the deviator stress for conditions of no drainage. The data plotted in Figures 5. 5a and 5. 6a give the K_f lines from which the angle of internal friction and the cohesion were obtained on an effective stress basis. These $\bar{\phi}$ values along with sample organic contents are summarized in Table 5. 5. Additional data from Andersland and Laza (1971) for fresh sludge sample H-2 has been included. A plot of $\bar{\phi}$ versus organic content, Figure 5. 6, suggests a linear relationship when comparisons are made using data obtained by a given test procedure. This agreement is quite good considering the accuracy of the organic content determinations. At lower organic contents the angle of internal friction should approach a value representative of the non-organic constituents in the papermill sludge. Extrapolation to zero organic content gives an angle of internal friction equal to about 24 degrees, close to a value of 25 degrees reported for kaolin clay by Gibbs, et al. (1960). If sludge decomposition is represented by a decrease in organic content, then for the same effective normal stress there will be a reduction in shear strength.

Water content has been plotted against all-around consolidation pressure in Figures 5. 5b and 5. 6b. With the higher organic content, sample U-3, a greater reduction in water content is observed for the same consolidation pressure. At the same time the higher organic content is responsible for a greater water retention at a given consolidation pressure. The tests results, in terms of total stresses, are expressed as the value of undrained strength c_u plotted against consolidation pressure p in Figures 5. 5c and 5. 6c. For the normally consolidated samples the ratio c_u/p appears to be a constant, its value dependent to some extent on the sludge organic content.

For the undisturbed sludge samples, anisotropic consolidation was used so as to approximate the field settlement condition of no lateral yield. Data from the total pressure cells buried in the landfill (Figure 5. 18) gave a ratio of horizontal to vertical effective stress ($\bar{\sigma}_h/\bar{\sigma}_v = K_o$) close to 0. 3. Consolidation under this stress ratio followed by increasing the deviator stress to failure gave the data summarized in Figure 5. 8. For the same organic content, an apparent increase in the angle of internal friction is noted for the anisotropically consolidated sludge. A reduced angle of internal friction (Figure 5. 10) was obtained when the sample axis was changed to the horizontal. For the same consolidation pressure, larger undrained strengths were obtained for the anisotropically consolidated sludge in comparison to samples consolidated with an all-around pressure. The ratio c_u/p has increased over the values obtained for the fresh sludge with isotropic consolidation. These differences appear to be related to structural anisotropy of the sludge. A form of structural anisotropy tends to develop in sludge when fibers align themselves at right angles to the direction of the major principal stress during field consolidation.

The stress change prior to failure of the experimental slope involved primarily a decrease in lateral pressure as sludge material was excavated. To reproduce this field stress condition in the laboratory a series of tests were run in which the axial stress was held constant and deformation was brought about by reducing cell pressure. The sludge response to this loading, illustrated in Figure 5. 11 for sample C-11, shows little sample deformation until the negative change in pore pressure was permitted to dissipate. Since the minor principal effective stress decreased to zero in tests C-10, C-11, and C-14, one obtains an angle of internal friction equal to 90 degrees. Tensile stresses carried by fibers must be responsible for this unorthodox material behavior. Taking c_u equal to $1/2(\sigma_1 - \sigma_3)]_{\epsilon=5\%}$, the ratio of c_u/p has increased to greater than 3 in contrast to values less than one for the other tests. Different levels of anisotropic consolidation, representing different elevations in the sludge landfill, give the stress-strain curves shown in Figure 6. 7. The data show an increase in modulus for higher consolidation pressures (greater depth). For the two levels of consolidation pressure which are representative of the upper sludge layer (samples C-10 and C-11) normalization gives essentially one curve. Here the ordinate is the stress difference, $(\sigma_1 - \sigma_3)$, divided by the consolidation pressure, p. For comparison, data from sample G-4 has been included to show the different behavior for failure with σ_1 increasing. The nonlinear behavior shown for samples C-10 and C-11 has been approximated with a bilinear relationship with elastic modulus values of 48.00p and 0.01. For computational purposes the smaller value is assigned to elements after failure.

Unconfined compression tests on undisturbed samples generally provide shear strengths for use in the total stress analysis for slope stability and provide information on the anisotropy of the consolidated sludge. Data summarized in Table 5.4 and plotted in Figure 5.12 show that the sludge was significantly weaker when failed in the horizontal direction as compared to the vertical. The natural alignment of fibers in the horizontal direction form a plane of weakness which may be the reason for the lower strength. The two curves in Figure 5.12 can be normalized when the respective unconfined compression strengths are divided by the effective overburden pressure p_o. For example, taking the vertical unconfined compression strengths, c_u/p equals 0.49 for sample blocks G and C. The unconfined compressive strengths are significantly lower than the undrained vane shear strengths shown by data plotted in Figure 5.13a. This lower strength is due partly to physical disturbance in sampling and sample preparation for laboratory testing. For soft clays with low to medium sensitivity Parry (1971) states that the physical disturbance and stress change are sufficient to reduce the laboratory shear strength below field values. Sensitivity of the sludge, equal to the undisturbed vane strength divided by the remolded vane strength, was very low (about 1.40) as shown by the data in Figure 5.13a. The vane shear strength to overburden pressure is reasonably constant. Some variation would be expected since ash contents, given in Table 5.1 for blocks B, C, F, and G were not completely uniform. Blocks B and C at close to the same elevation and different ash contents contain significantly different water contents due primarily to different organic contents. The Dutch cone penetration test was less sensitive to increase in shear strength with depth than the vane shear test (Figure 5.13b).

Observed Slope Movements. Field monitoring provided data on both lateral and vertical movements at a number of locations adjacent to the excavated slope. Consider first the lateral movements given by the surface stakes (Table A-1) and the slope indicator casings (Figure 5.14). The surface measurements provided data which were in agreement with the upper level of the slope indicator casings. In addition to movement towards the slope all casings showed some movement away from the east or west dikes (Figure 5.14e). The resultant movements close to the landfill surface (elevation 94.6 ft) for casings A through D are shown in Figure 6.8. The rate of movement is very much dependent on the stress release or excavation for the slope. The rate of movement for each casing is shown in Figure 6.9 by plotting lateral movement versus time. The low movement rate after completion of the 3:4 slope suggests that the sludge was relatively stable for this slope configuration. The highest movement rate occurred immediately after excavating the 1:8 slope. Rates decreased when partial slope failures occurred and reversed direction when fresh sludge was placed adjacent to the slope at the end of the field portion of the study.

Vertical movement (Figure 5.15) monitored by settlement plates was largest in the upper sludge layer adjacent to the excavated slope. A large part of this settlement appears to have been caused by consolidation related to complete drainage of the middle sand blanket when the slope was excavated on September 29, 1972. Increased settlement rates are observed for the top sludge layer at all instrument groups after this date. Secondary consolidation was small, approximately 1 1/4-inches for each layer, using a field value for the coefficient of secondary compression C_{α} equal to 0.0557 and H_o equal to 9.5 ft. This value was close to the observed settlement for the lower sludge layer during this period.

Development of Failure Zones. Sludge movement occurred as the slope was excavated and as stresses were reduced to zero on this slope. Stress conditions within the slope change during excavation. Failure zones develop in those regions where the maximum shear stress values exceed the undrained shear strength of the sludge. It is helpful to show these zones in a graphic manner. These zones can be determined by use of the finite element method of analysis (Dunlop, Duncan, and Seed, 1968).

For a slope excavated in the dry, both the earth and water pressures would be reduced to zero on the excavated slope. For analysis of these slopes, it was necessary to consider both the changes in earth and water pressures during excavation. This may be done by working with total stresses. At a depth y below the surface of a horizontal deposit with unit weight γ, the initial total stresses may be expressed as

$$\sigma_y = \gamma \cdot y \tag{6.2}$$

$$\sigma_x = K \cdot \sigma_y \tag{6.3}$$

where σ_y and σ_x are the total vertical and horizontal stresses and K is a total stress earth pressure coefficient. Field data (Figure 5. 18) has shown that K was close to 0. 4 just prior to excavation. It was convenient to consider the initial strains and displacements, before excavation, as being zero but with non-zero stresses. The stress-strain relationships for the sludge (Figures 5. 11 and 6. 7) were obtained from triaxial tests using test procedures which simulated field conditions existing before and during excavation of the slope.

Plane strain deformation has been assumed for the excavated slope since the distance normal to the section analyzed (Figure 6. 10a) was about five times the thickness of the sludge plus sand blankets. Field measurements of slope movement indicated that the assumption of plane strain deformation was reasonable. A finite element idealization of the slope cross-section in Figure 6. 10b includes boundaries representative of field conditions. The top and slope surfaces are free surfaces. Loads applied to the top surface nodes simulate the earth surcharge. Points along these boundaries are free to move in the vertical and horizontal directions. Since the sludge was very soft in comparison with the dike material and the natural soil below the landfill, it was assumed that these boundaries were fixed as shown in Figure 6. 10b. The dike was far enough from the slope so that shear stresses could be assumed equal to zero. Field data showed that there was no vertical movement of the bottom surface and that there was no reason to suspect any horizontal movement of the firm base of the landfill.

The finite element configuration of the slope with simulation of the excavation by removal of elements has been illustrated in Figure 6. 10c. The slope cross-section was represented by 252 rectangular elements with a total of 279 nodes. The basic element used was a quadrilateral composed of four constant strain triangles. Rectangles were used throughout with the exception of the region immediately adjacent to the sloping face, where triangles and trapezoids (Figure 6. 10b) were employed alternately. This scheme of elements was well-suited to simulation of slope excavation by the removal of elements outside the slope and it was convenient for automatic mesh generation within the computer. The analyses were conducted in a series of steps in the analysis. Eight steps were used to represent slope excavation. The stress-strain curve for any particular element was approximated by a bilinear curve (Figure 6. 7), consisting of two straight line portions corresponding to the two values of modulus. Material numbers and properties for each row of elements are given in Table 6. 1. Material 9 is the number assigned to elements after failure, and material 10 is the number assigned to elements which are being or have been removed.

The computer program given by Dunlop et al. (1968) was used to obtain the results summarized in Figure 6. 11 showing the development of failure zones in the experimental sludge slope for excavation depths of 6, 10, and 14 feet. Failure has been defined by the bilinear curve in Figure 6. 7 and a total horizontal strain of 10 percent. A simulated excavation depth to 6 ft, Figure 6. 11, shows that a small failure zone has developed behind the slope. A small tension zone now exists behind the crest of the slope. Additional excavation to 10 ft alters stress conditions sufficiently so that the failure zone now extends farther behind the slope and to a greater depth. The tension zone has increased in size. At this stage the overall factor of safety against slope failure would be approaching unity. Excavation to 14 ft shows the failure zone extending to the slope surface and behind the crest. Failure along the unsupported slope would be predicted and did occur. Line A-A in Figure 6. 11 shows the location of the observed field failure (Figure 5. 20a) which occurred four days after completing the excavation. Temporary tensile stresses related to fibers in the sludge may have contributed to the delay in failure. Increase in pore pressures, shown by piezometers in the upper sludge layer (Figure 5. 16), would explain a lower shear strength several days after completing the excavation. Failure zones shown in Figure 6.11 may be over estimated because a bilinear stress-strain representation of the sludge was used in the finite element analyses. Dunlop et al. (1968) have shown this to be the case for slopes in soil.

Slope Failure. The appearance of tension cracks in the earth surcharge (Figure 5.19) after completing excavation for the 1:8 slope indicated that the factor of safety with regard to slope stability was approaching unity. The rate of lateral movement shown by the slope indicator casings(Figure 6.9) was initially very high but did decrease somewhat before the initial slope failure occurred on October 29, 1972 (Figure 5.20). Slope indicator casings were located several feet behind the zone of failure. At this time other portions of the slope were very close to equilibrium with respect to sliding. Within the next three weeks additional failures occurred along the entire slope length as shown in Figure 5.20b. Surface measurements of the slope failure areas on three different dates (Figure A-1) show areal limits of failure. Based on field measurements a typical failed cross-section has been prepared in Figure 5.21. Failure in the sludge occurred on essentially a plane surface at a slope close to 1:1.64. The tension cracks appeared to extend down through the earth surcharge to the upper sand blanket. Slopes in the two sand blankets were close to those shown in Figure 5.21. Some variation to this average failed cross-section can be seen in Figure 5.20.

It is interesting to note that the angle of slope failure was very close to the failure surface observed for a number of undisturbed triaxial test specimens. Test specimen G-9, consolidated anisotropically with K_o equal to 0.3, is shown in Figure 3.2c after failure in compression and oven drying. The critical plane in both cases rises at an angle close to 58.6 degrees from the horizontal. If the Mohr-Coulomb failure theory were applicable, the failure plane should rise at an angle of $(45 + \frac{\bar{\phi}}{2})$ degrees and $\bar{\phi}$ would equal 27.2 degrees. This field behavior suggests that a frictional mechanism determines the shear strength of the sludge. A cohesive mechanism would have required that the angle be 45 degrees.

Analysis for the Composite Failure Surface. The failure surface shown in Figure 5.21 involves a composite sliding surface which can best be analyzed using Janbu's (1954, 1957) method. At failure the factor of safety against sliding equals one. A computed factor of safety should also equal one when the method of analysis is appropriate to the field problem. Shear strengths used in the analysis must be representative of the consolidated sludge in the landfill. Difficulty in determining the actual pore pressures in the sludge at the sliding surface require that a total stress basis be used in the analysis. Piezometers in instrument group 4 were located several feet behind the failure surface. The top and middle sand blankets were fully drained so that total stresses equal effective stresses in the sand. Undisturbed vane shear strengths (Figure 5.13a) cannot be used directly in Janbu's (1954, 1957) method. Bjerrum (1972) has suggested that the discrepancy between the vane shear strength and the field shear strength can be attributed to differences in rate of loading and to the anisotropic nature of shear strength. He has recommended a correction factor μ (Figure 6.12) which is correlated to the plasticity index of soft clays. The average plasticity index for the sludge (Table 5.1, First Annual Report) was close to 148 giving a correction factor for the vane shear strengths equal to about 0.6. Therefore

$$(s_u)_{field} = (s_u)_{vane} \times 0.6 \qquad (6.4)$$

Application of Janbu's (1954, 1957) method requires that the sliding mass of sludge be divided into an appropriate number of slices. This has been done in Figure 6.13 where slice boundaries, for convenience, have been taken at points separating zones with different material properties or at points where a break occurs in the upper or lower boundary of the sliding mass. Janbu's (1954, 1957) method involves the use of successive approximations, hence a tabular computation form is convenient. Part of this tabular computation is given in Figure 6.13. Values from the cross-section including slice number, tan α, Δx, and p are given in the first four columns. For the sludge A'_o equals $s_u \cdot \Delta x$ and for the sand A'_o equals $p \cdot (\tan \bar{\phi}) \cdot \Delta x$. The table is complete only for the initial calculation ($t = {}^{\Delta T}/_{\Delta x} = 0$) for which F_o equals 1.006. Two additional approximations give a more accurate value of F_2 equal to 1.004. The line of thrust for side forces on each slice was taken at the 1/3 points. Janbu (1954, 1957) states that the inclusion of the second step in calculation leads to an F-value that is usually within 1 to 1.5 percent of a rigorous F-value. In this case the agreement between the actual and computed factor of safety was excellent, the difference equal to about 0.4 percent. Larger variations in F are likely if inaccuracies exist in the measured sludge shear strength.

Use of the vane shear strength corrected to the field value (Bjerrum, 1972) in the stability analysis has avoided uncertainties with regard to probable sludge disturbance during sampling and sample preparation for laboratory testing. These disturbances may be caused by physical disruption and also by stress change associated with unloading. Small gas pockets, observed in block samples which had been stored for some time, would reduce unit weights and contribute to lower unconfined compressive strengths. Comparisons between vane shear strengths corrected to $(s_u)_{field}$ values and unconfined compressive strengths in the vertical direction (Figure 5.12) show that the latter values are much smaller. For these reasons use of unconfined compressive strengths in place of the corrected vane strengths in the stability analysis would have given an erroneously low factor of safety.

Leachate Analysis

The concentration of chemical constituents contained in the various samples of landfill leachate does require elaboration with regard to (a) the significant variation among those samples of common origin (I-V), and (b) the considerable deviation of the properties of those same samples from those associated with the interstitial water in the sludge blanket represented by sample VI. Experience with landfills of municipal refuse would suggest that the generation of leachate and the magnitude of its chemical constituents does show a seasonal variation in response to climatic conditions. However, the relative impermeability of the sludge, and an inherent origin of leachate within the sludge layer itself would minimize, in this case, the effect of such a variation except for the manner in which the fill was constructed. The direct seepage of rainfall into the sand drainage blankets, previously cited, would provide a source of dilution for leachate emanating from the overlying sludge layer, as opposed to a displacement of interstitial water associated with infiltration of the fill material itself. Thus, in this instance, a leachate of weaker strength would be associated with periods of greater rainfall. In reviewing the meteorological data (Table J-1) originating at the municipal airport in Dayton, Ohio, approximately 23 miles from the landfill site, it was observed that the greatest accumulated rainfall (0.3 in. to 0.4 in.) inclusive of and two days prior to the sampling date was associated with samples II and III, those of least concentration. Similarly, the least accumulated rainfall (0.0 in. to 0.08 in.) was associated with those samples of greatest concentration, I and IV. Accordingly, the latter would be most representative of leachate discharged from the fill through the drainage beds during consolidation. Nevertheless, leachate strength of samples I and IV remains significantly less than that of the sample considered most indicative of interstitial water within the landfill, sample VI. The capacity of soil percolation to rapidly decrease the concentration of potential chemical pollutants has been documented in the literature, as well as the lysimeter work associated with this study. While chlorides and hardness constitute partial exceptions (Salvato et al., 1971), reductions in such a manner can be significant. With percolation through little more than the drainage blanket, the superior leachate quality of samples I and IV in comparison with sample VI would further substantiate the benefits of soil percolation.

Leachate constituents present in the greatest quantities include dissolved organic matter and mineral salts, which contribute to specific conductance and alkalinity. Alkalinity was consistently greater than total hardness, indicating that hardness was entirely of carbonate origin. Consistent with the buffering capacity associated with leachate alkalinity, pH varied over the narrow range of 7.4 to 7.8. Such a pH is uncharacteristic of domestic landfill leachates whose acidic nature and lower pH values tend to reduce exchange capacities of renovating soils (Fungaroli, 1971). Specific conductance values observed in this study do exceed the single value of 3000 µmho/cm cited by Emrich (1970) in illustrating that parameter as an example of persistence for as long as 20 years of the pollutional potential of leachate emanating from landfills of municipal refuse. Concentrations of BOD, hardness, and dissolved solids reported for leachates originating from landfills of domestic refuse span a wide range and encompass the values observed in this study (Salvato et al., 1971; Fungaroli, 1971; California State Water Quality Control Board, 1967; and Emrich, 1970). A ratio for BOD to COD of 0.68 was also observed over the entire range of values, as shown by Figure 6.14. With the exception cited above, suspended solids did not exceed 160 mg/l, nor was turbudity in excess of 56 JTU. Considering the origin of the fill material utilized for this evaluation, it is not surprising that leachates would be nearly void of organic nitrogen and phosphorous. In a number of instances concentrations of iron and chloride in samples I through V nominally exceeded the 0.7 mg/l and 181 mg/l concentrations for those respective constituents in the in situ sample, suggesting the possibility of some leaching from the drainage beds or, perhaps, a decrease in those residuals by the conclusion of the study. Concentrations of nitrogen and phosphorous as well as chloride and sulfate concentrations, are significantly less than reportedly present in domestic landfill leachates.

Whatever similarities might be suggested between leachate concentrations typical of this study and domestic landfills, the significant differences in the mass of constituents discharged is made apparent in Figure 6.15. The high ash sludge landfill constituent mass was estimated assuming a hypothetical leachate strength as great as that represented by the dry weather concentrations previously described for the entire volume displaced. Representative domestic refuse landfill masses were estimated based upon data reported by the California State Water Pollution Control Board (1961). Based upon these estimates, the mass of BOD per unit weight of dry solids associated with the high ash sludge was but 7 percent of that reported for domestic refuse; alkalinity approximated 40 percent.

For a given site, factors affecting the impact of a landfill upon groundwater resources would include (a) composition of the fill material with regard to the nature and rate of solids degradation, (b) capacity for rainfall infiltration, and (c) the rate in which interstitial water exceeding field capacity is discharged during fill consolidation.

The alteration of the composition and properties of a fill's organic components by microbial attack could result in the loss to the leachate of intermediate metabolic products which may otherwise be retained in the fill. The landfill environment as well as the absences of such supplemental nutrients as nitrogen and phosphorous, significantly retards the degradation of the fibrous sludge constituents. Paper products have been found unchanged in landfills that had been completed for 15 to 25 years (Sorg and Hickman, 1968). Previous NCASI field studies of high ash landfills would further substantiate the slow rate of decomposition. On the basis of photomicrographs of core samples, fiber contained in samples estimated to be 10 to 12 years old was nearly indistinguishable from that contained in a fresh sample. Consequently, further leachate contamination resulting from fill decomposition would be moderated by the retarded degradation rate over a protracted length of time.

The quantity of leachate in excess of field capacity available to the groundwater is dependent upon the magnitude of rainfall infiltration as well as the moisture originating within the fill material. The inherent low permeability of high ash sludges would minimize rainfall infiltration of the landfill as a potential leachate source. However, in such a case, caution would have to be exercised to prevent runoff and subsequent drainage into surface waters.

Where infiltration is small, the primary leachate source will originate within the fill material and be discharged in conjunction with fill consolidation. The nature of fill consolidation and associated leachate discharge is such that beyond primary consolidation, discharge occurs at a decreasing rate, allowing greater residence times in the intermediate soil strata and greater dilution upon percolation into the groundwater. In excess of 50 percent of the total quantity of leachate discharge occurred during the initial 35 days following surcharge placement. During that period, the discharge rate dramatically declined to less than 3000 gallons per day and over the balance of the study approached a value of 161 gpd. Any leachate intrusion into the groundwater would be greatest during the time that leachate strength is a minimum. Previously reported lysimeter work at hydraulic application rates simulating the average discharge during primary consolidation and the maximum discharge during secondary consolidation showed that certain soils have the capacity to render the percolate innocuous.

TABLE 6.1. MATERIAL NUMBERS AND PROPERTIES FOR THE FINITE ELEMENT ANALYSIS

Material	Unit weight (pcf)	Elastic* modulus (psf)	Poisson's ratio	Undrained strength (psf)	Coeff. of total pressure
1	69.75	26900.	0.475	280	0.4
2	70.75	33600.	0.475	350.5	0.4
3	71.75	40500.	0.475	422	0.4
4	72.75	47500.	0.475	494.5	0.4
5	87.00	55200.	0.475	574.5	0.4
6	74.75	62900.	0.475	655.5	0.4
7	75.75	70200.	0.475	731	0.4
8	76.75	77500.	0.475	807.5	0.4
9	71.91	0.01	0.475	--	--
10	0	0.01	0.475	--	--

*Bilinear approximation to the stress-strain behavior shown in Figure 6.7.

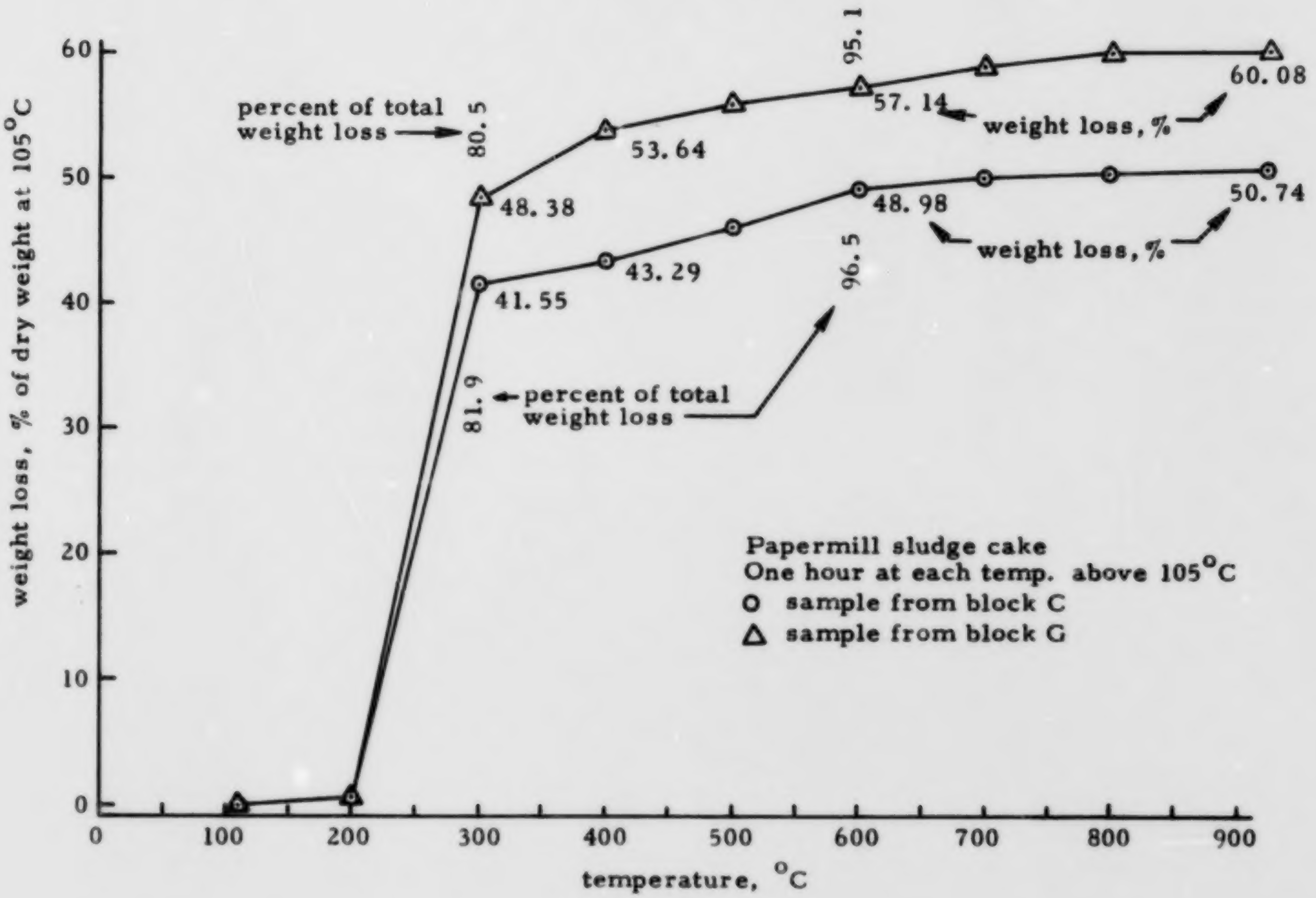

Figure 6. 1. Weight loss versus temperature for papermill sludge samples from blocks C and G.

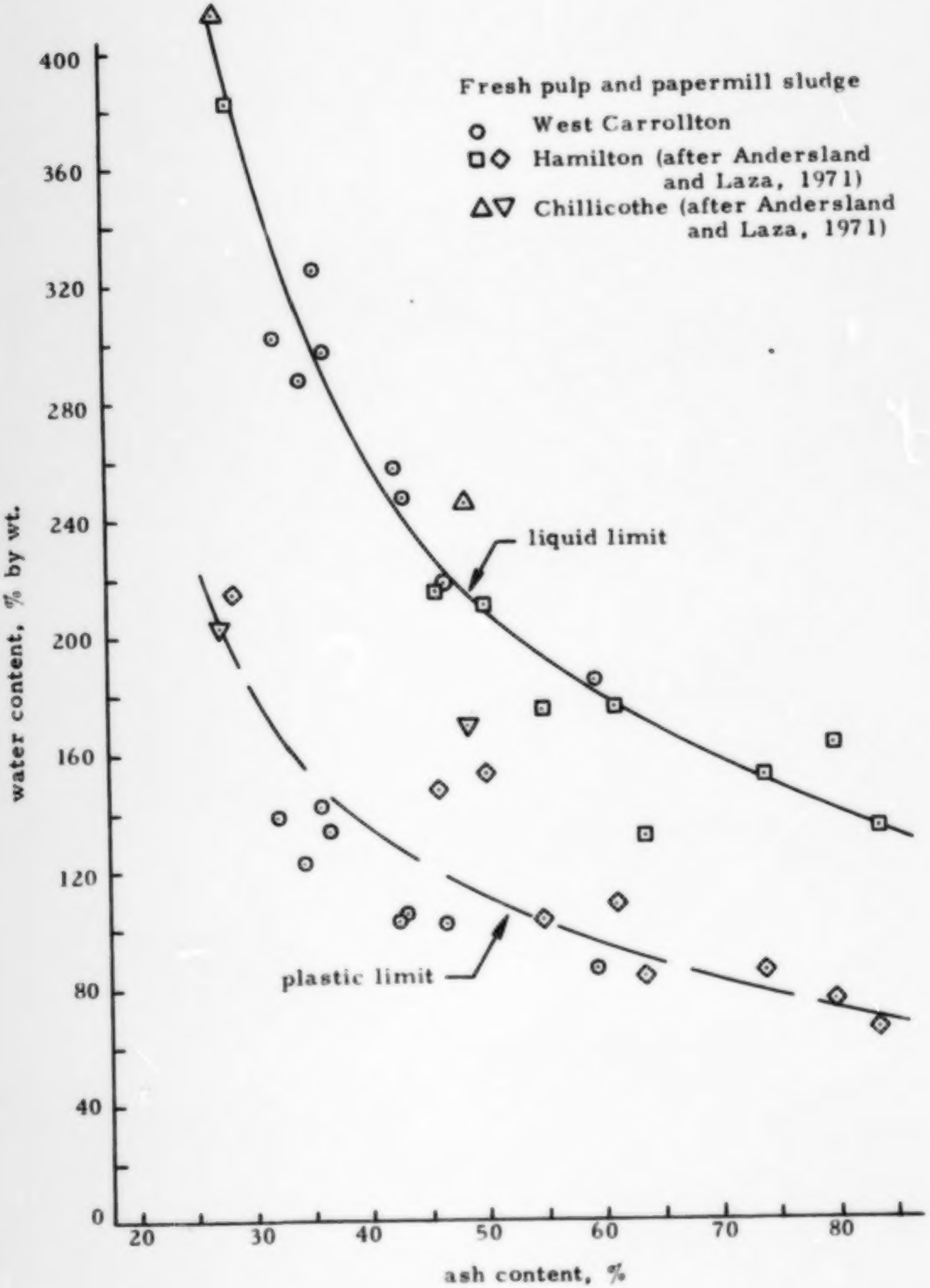

Figure 6. 2. Relationships between ash content and consistency limits.

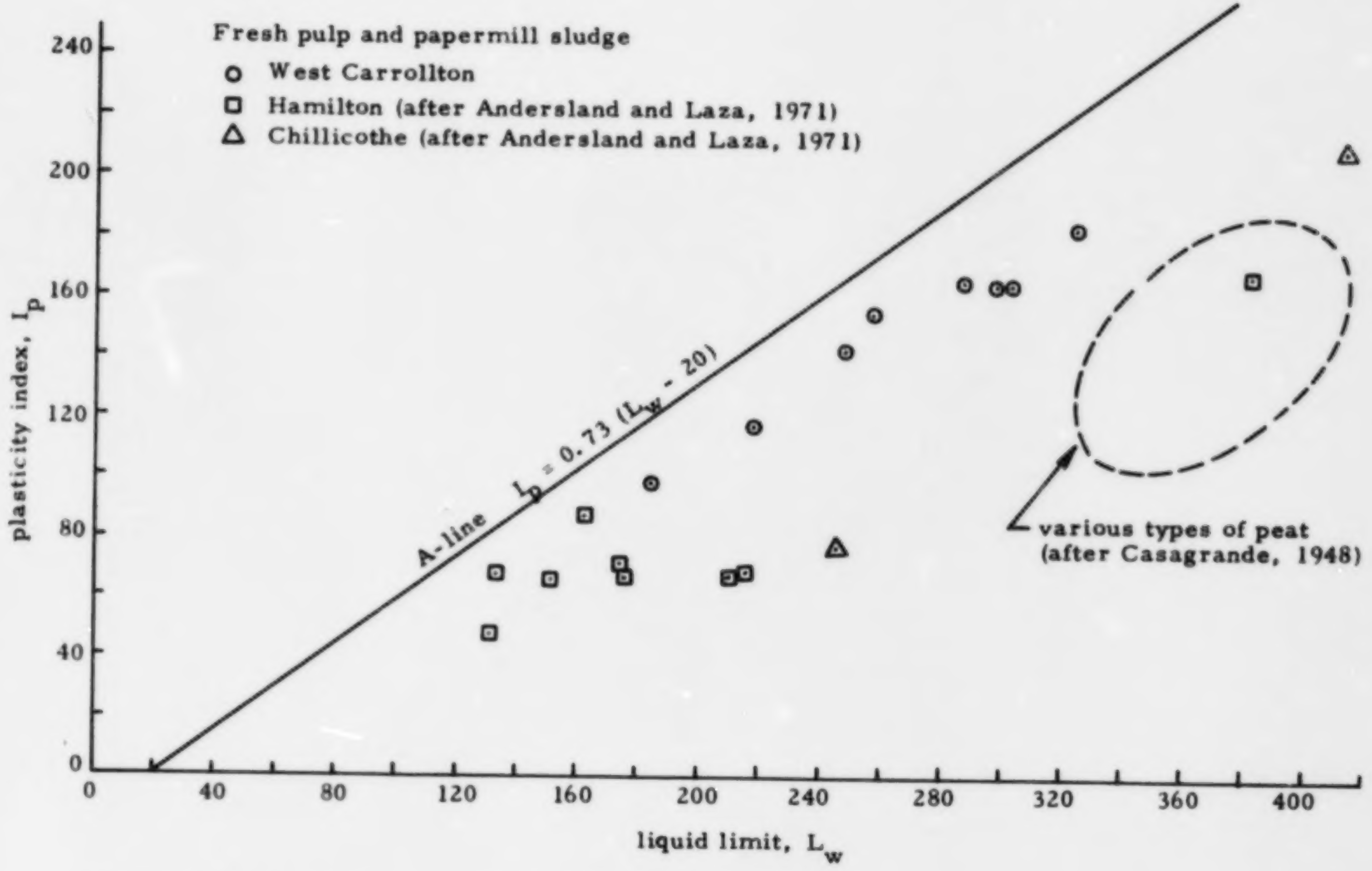

Figure 6. 3. Plasticity chart (Unified Soil Classification System) with data points for several fresh pulp and papermill sludges.

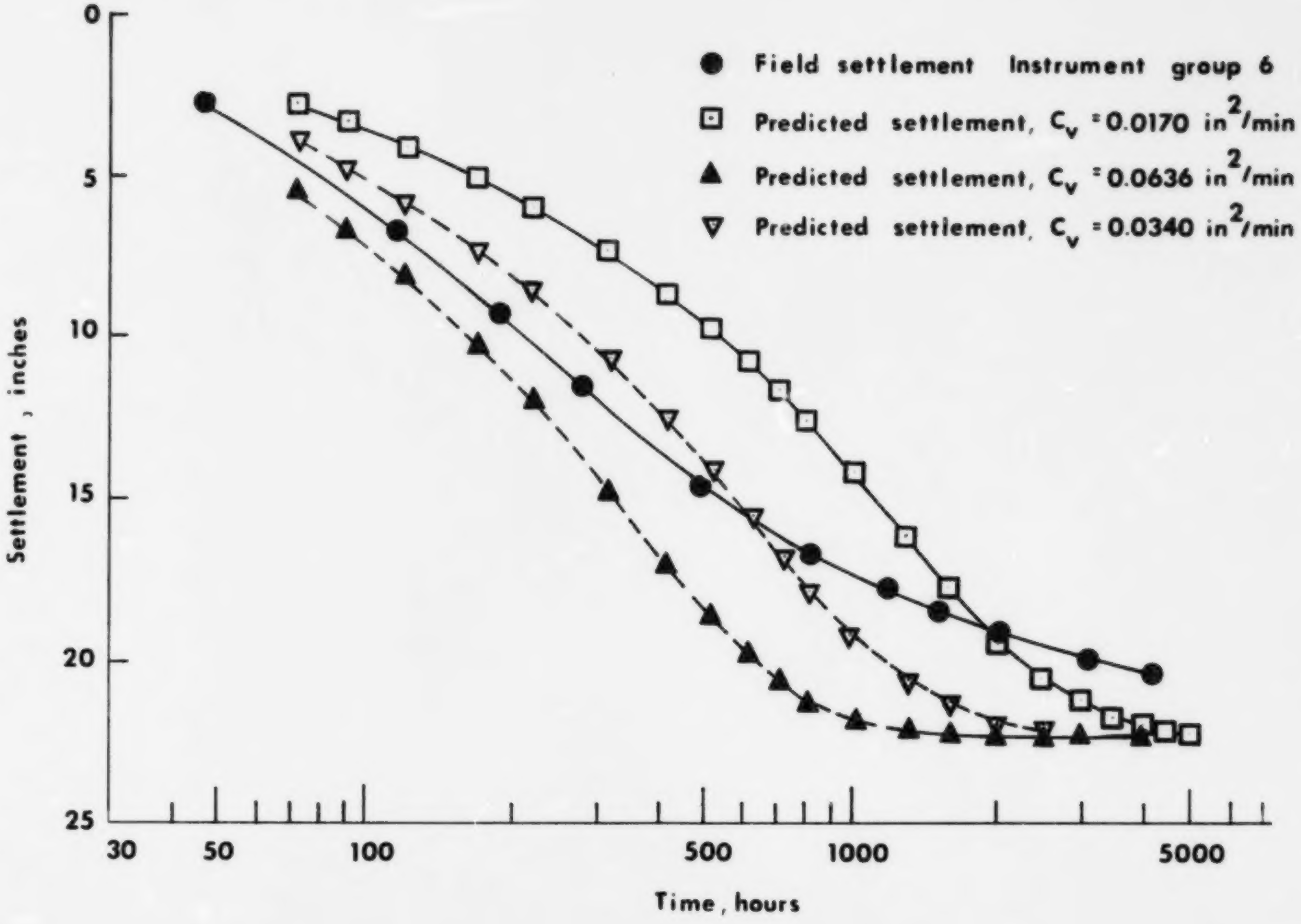

Figure 6.4 Comparison of actual and predicted time-settlement curves, upper sludge layer. (a) Theory of Gibson and Lo (1961)

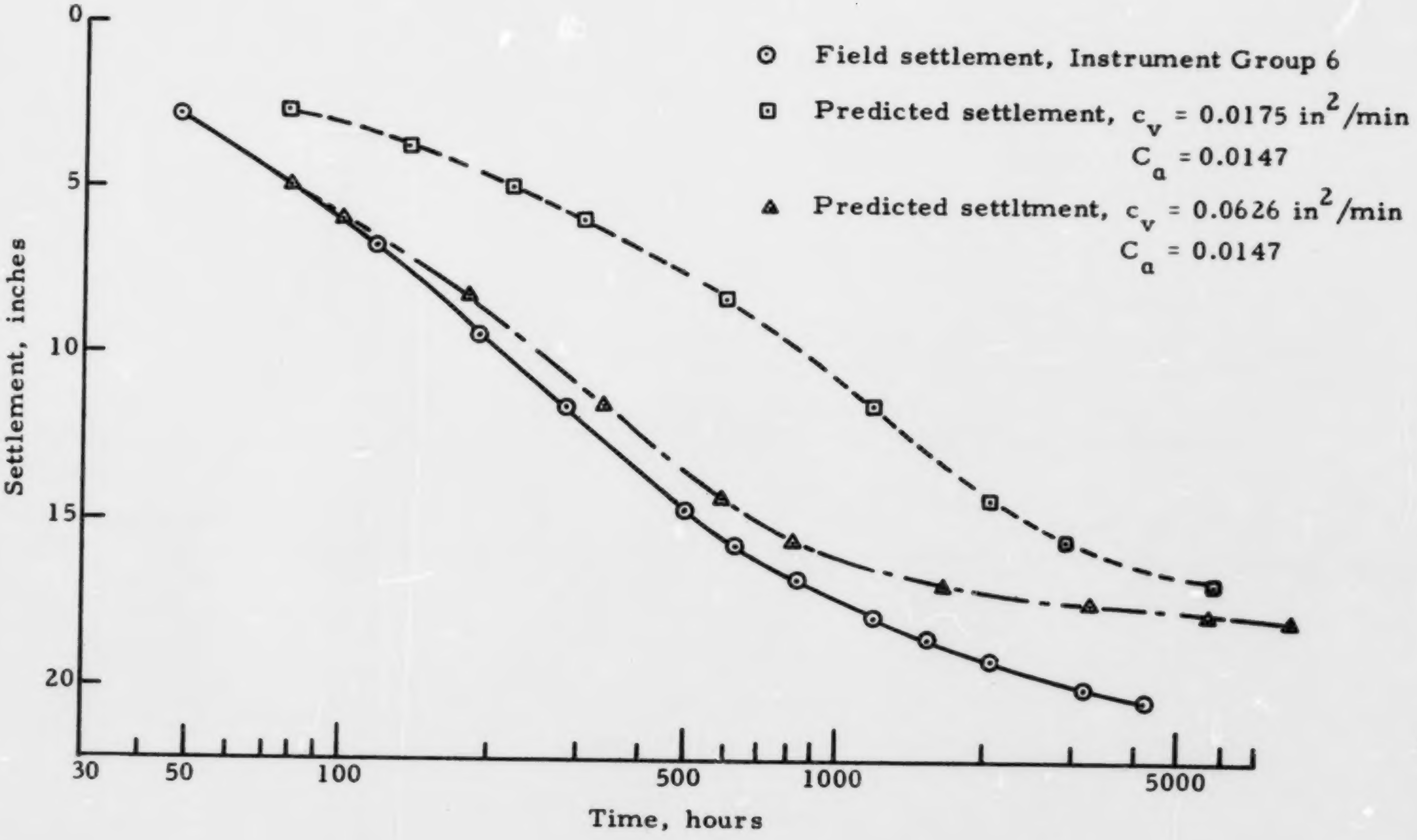

Figure 6.4. Comparison of actual and predicted time--settlement curves, upper sludge layer. (b) Wahls' theory (1962).

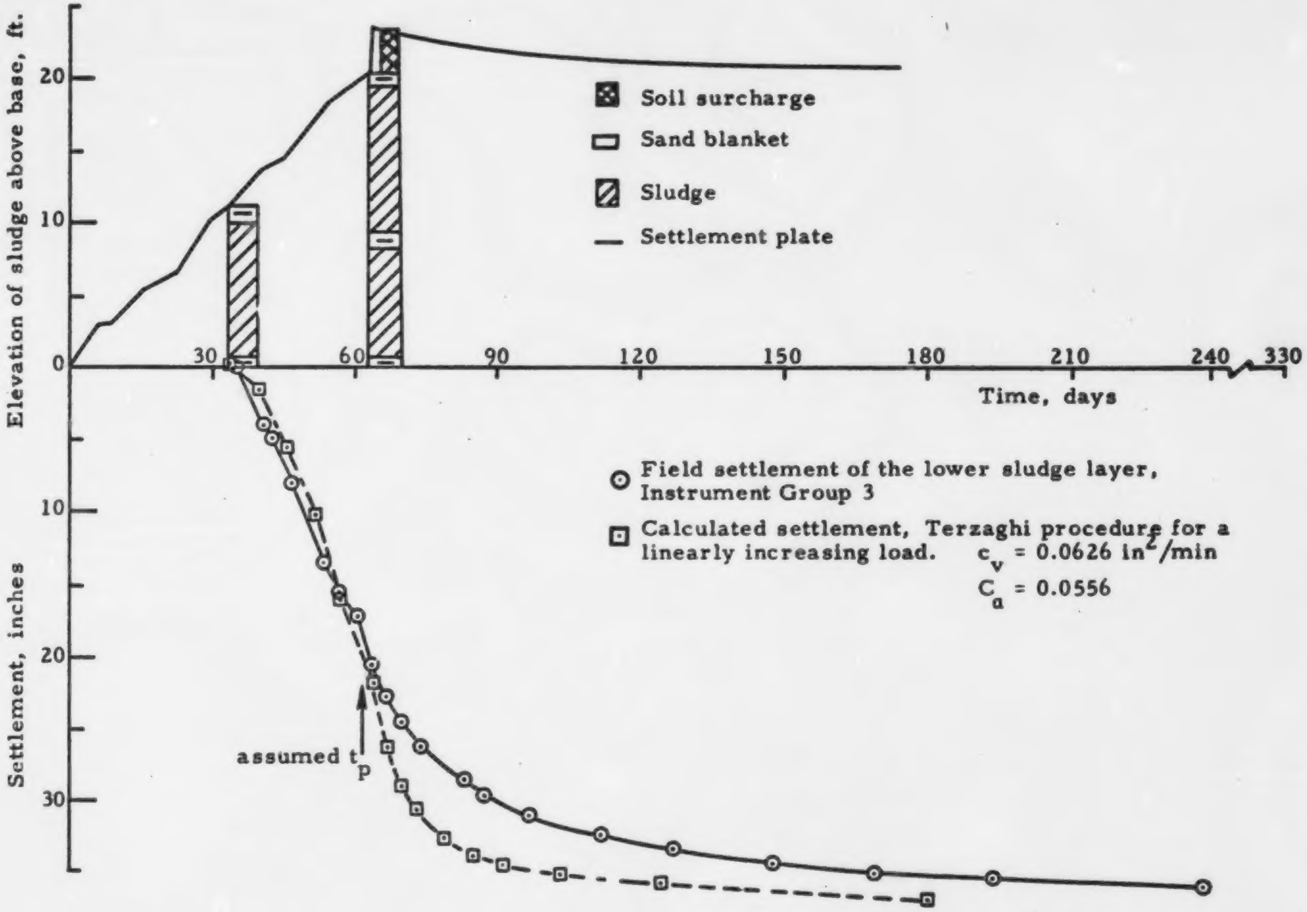

Figure 6.5. Comparison between the predicted and measured time--settlement curves, lower sludge layer, Terzaghi procedure for a linearly increasing load.

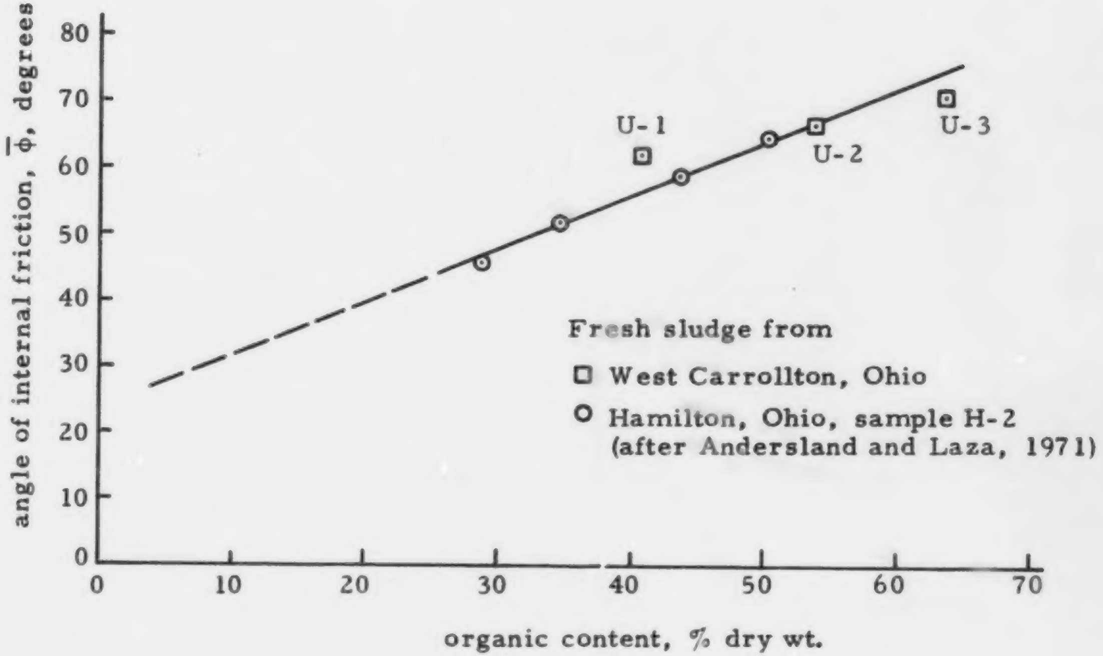

Figure 6.6. Influence of organic content on the angle of internal friction, effective stress basis.

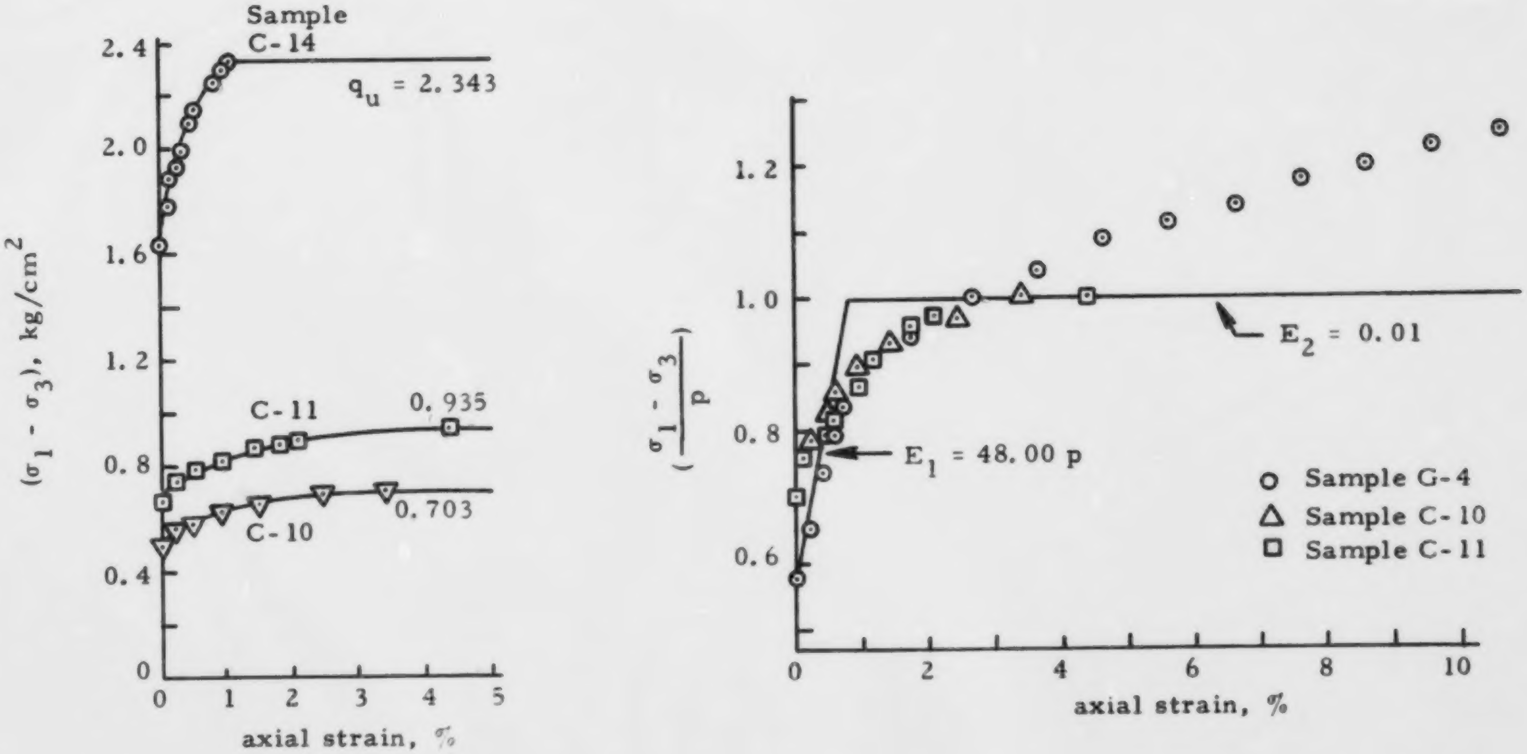

Figure 6.7. Undrained stress-strain behavior of normally consolidated papermill sludge; samples C-10, 11, and 14, failure with σ_3 decreasing; sample G-4, failure with σ_1 increasing.

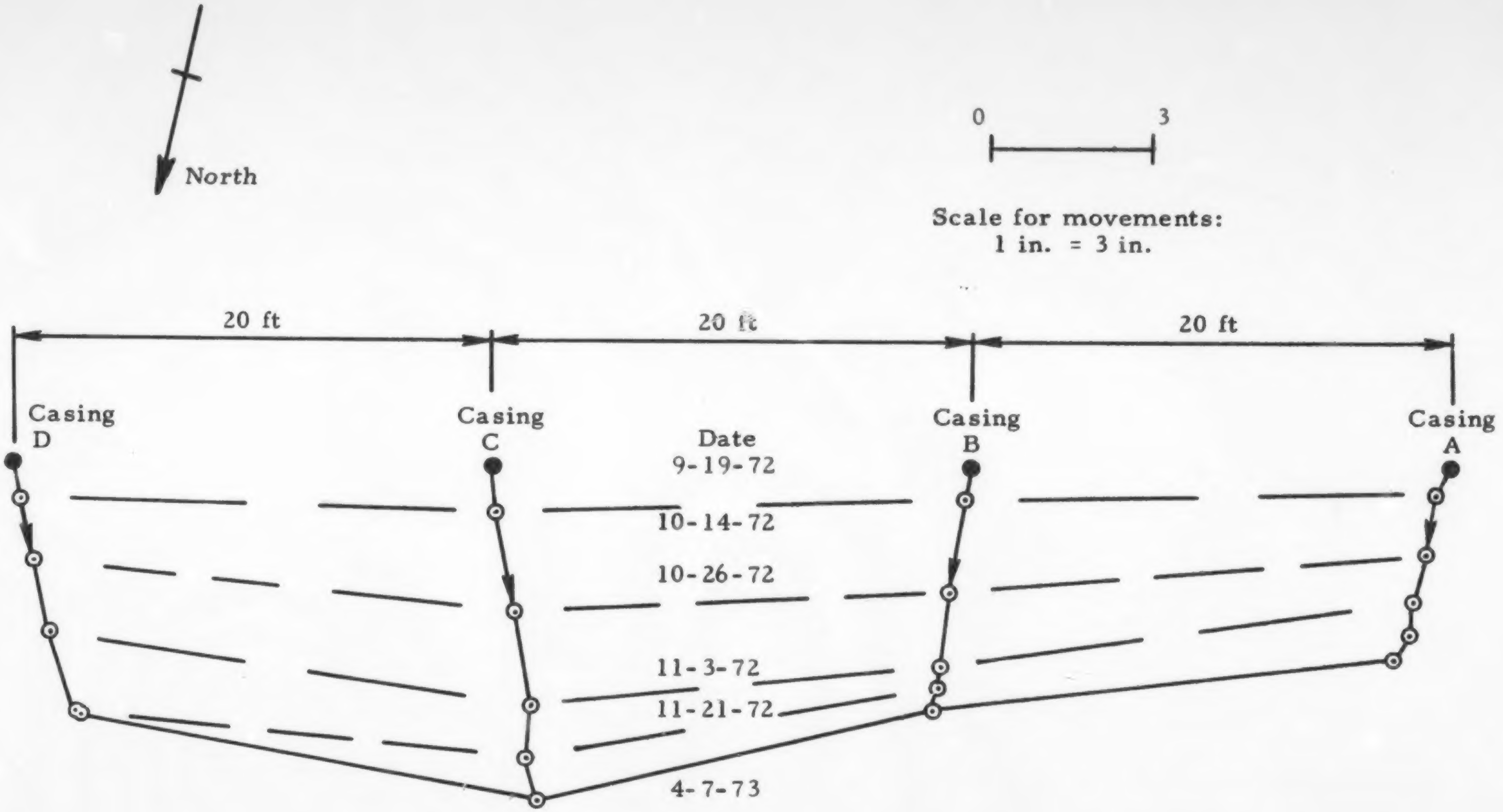
North
0
3
Scale for movements:
1 in. = 3 in.
20 ft
20 ft
20 ft
Casing D
Casing C
Casing B
Casing A
Date
9-19-72
10-14-72
10-26-72
11-3-72
11-21-72
4-7-73

Figure 6.8. Casing movements at elevation 94.6 ft. during and after excavation for the experimental slope.

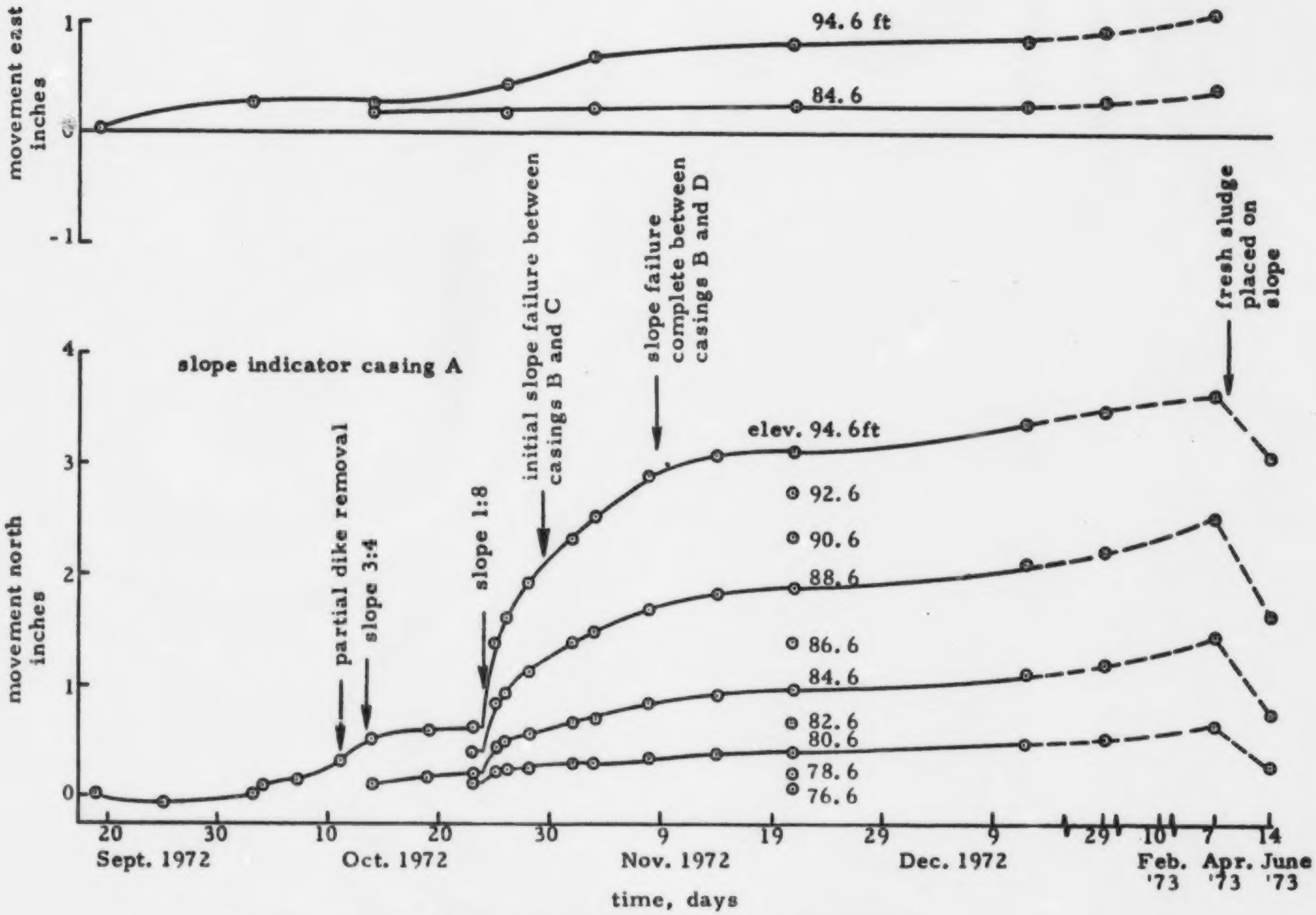

Figure 6.9. Time-rate of lateral movement. (a) Slope indicator A.

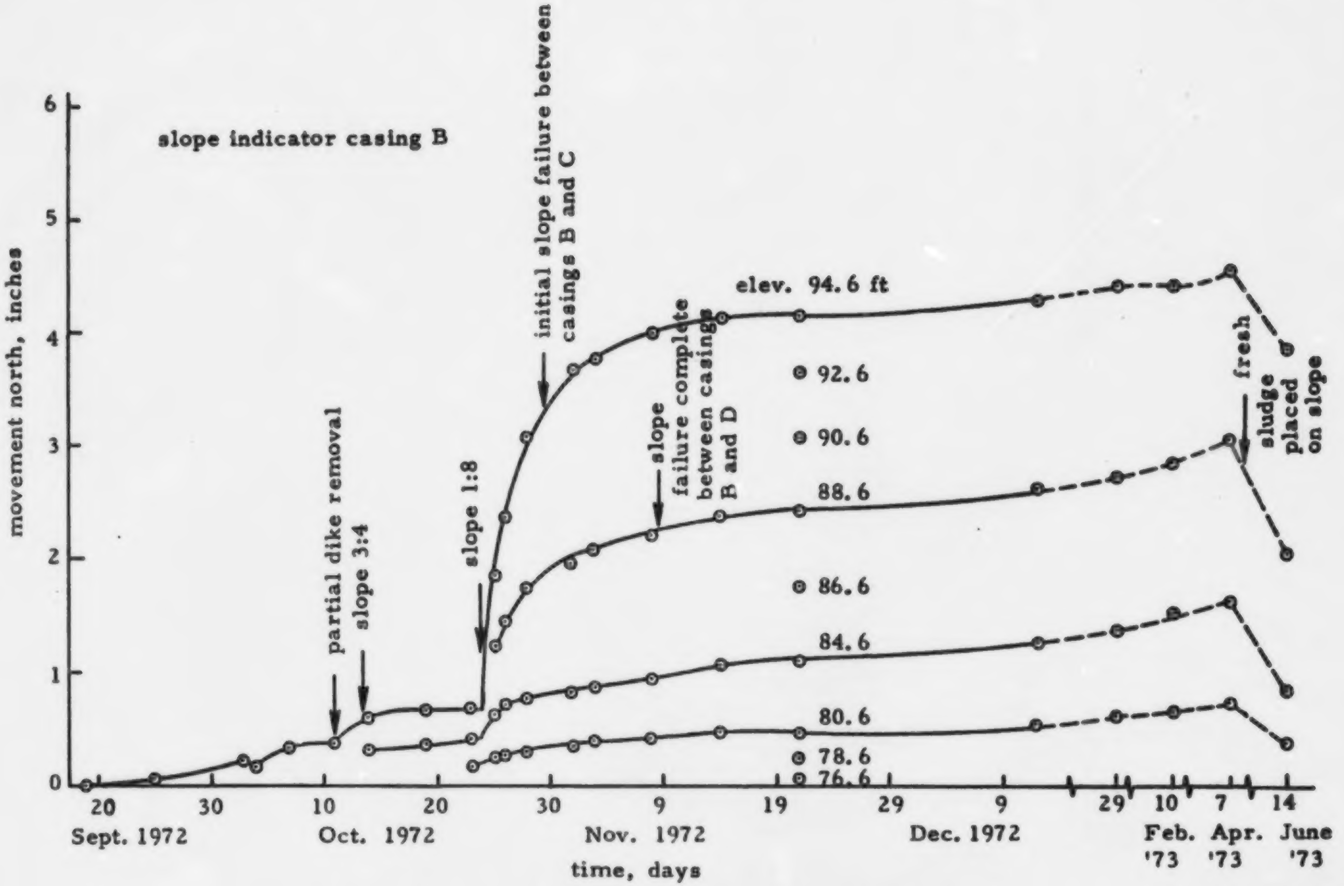

Figure 6. 9. Time-rate of lateral movement. (b) Slope indicator B.

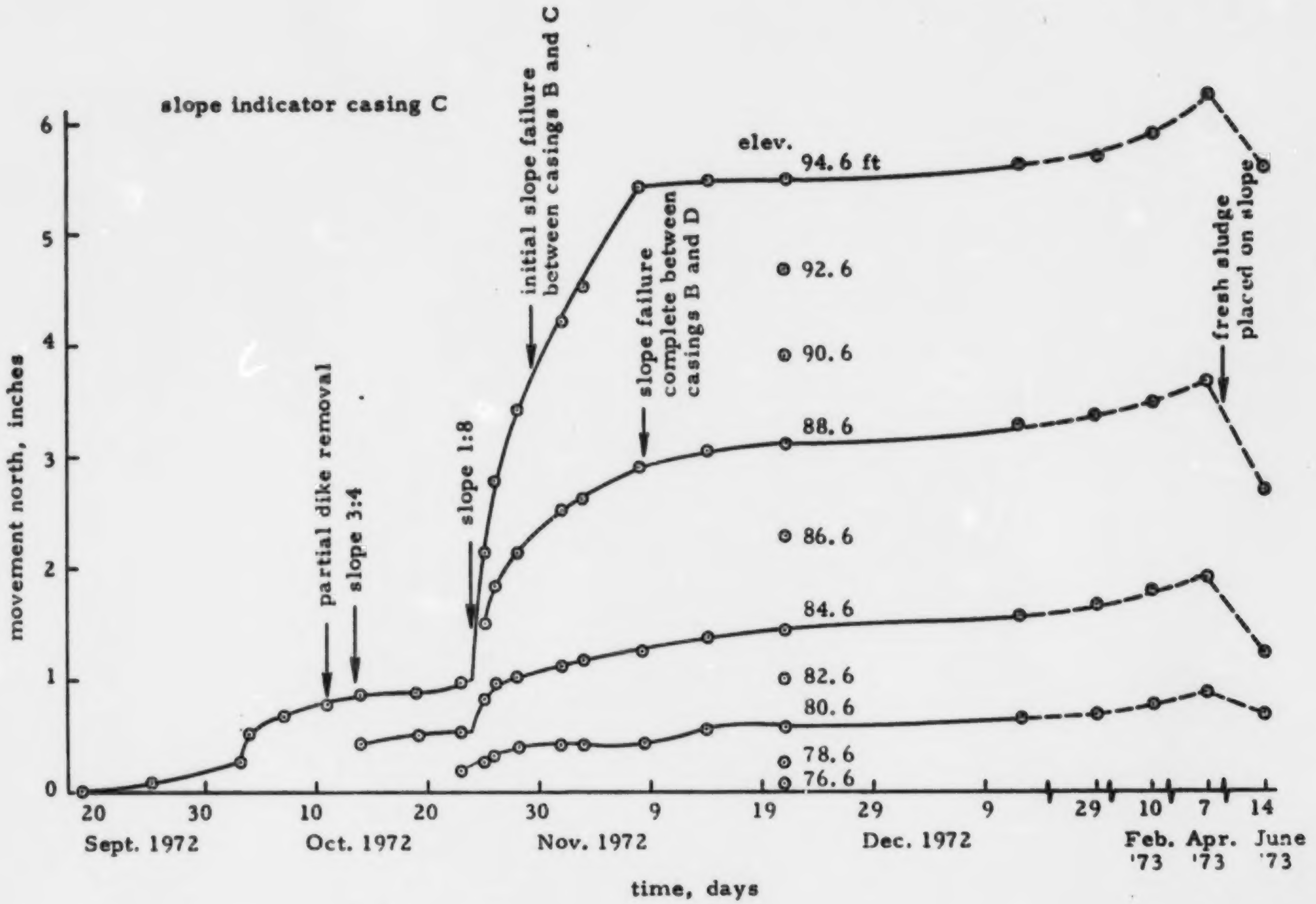

Figure 6.9. Time-rate of lateral movement. (c) Slope indicator C.

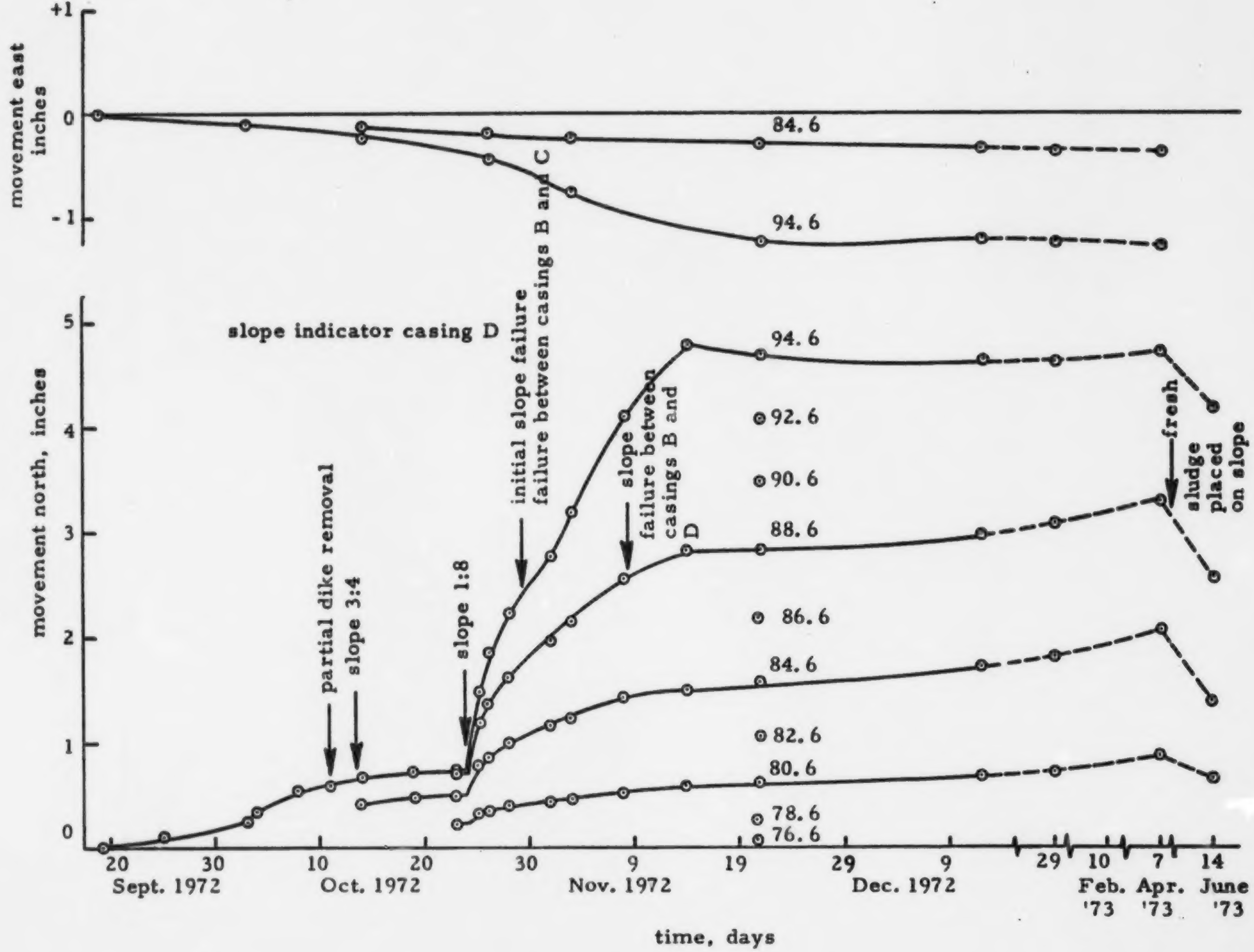

Figure 6. 9. Time-rate of lateral movement. (d) Slope indicator D.

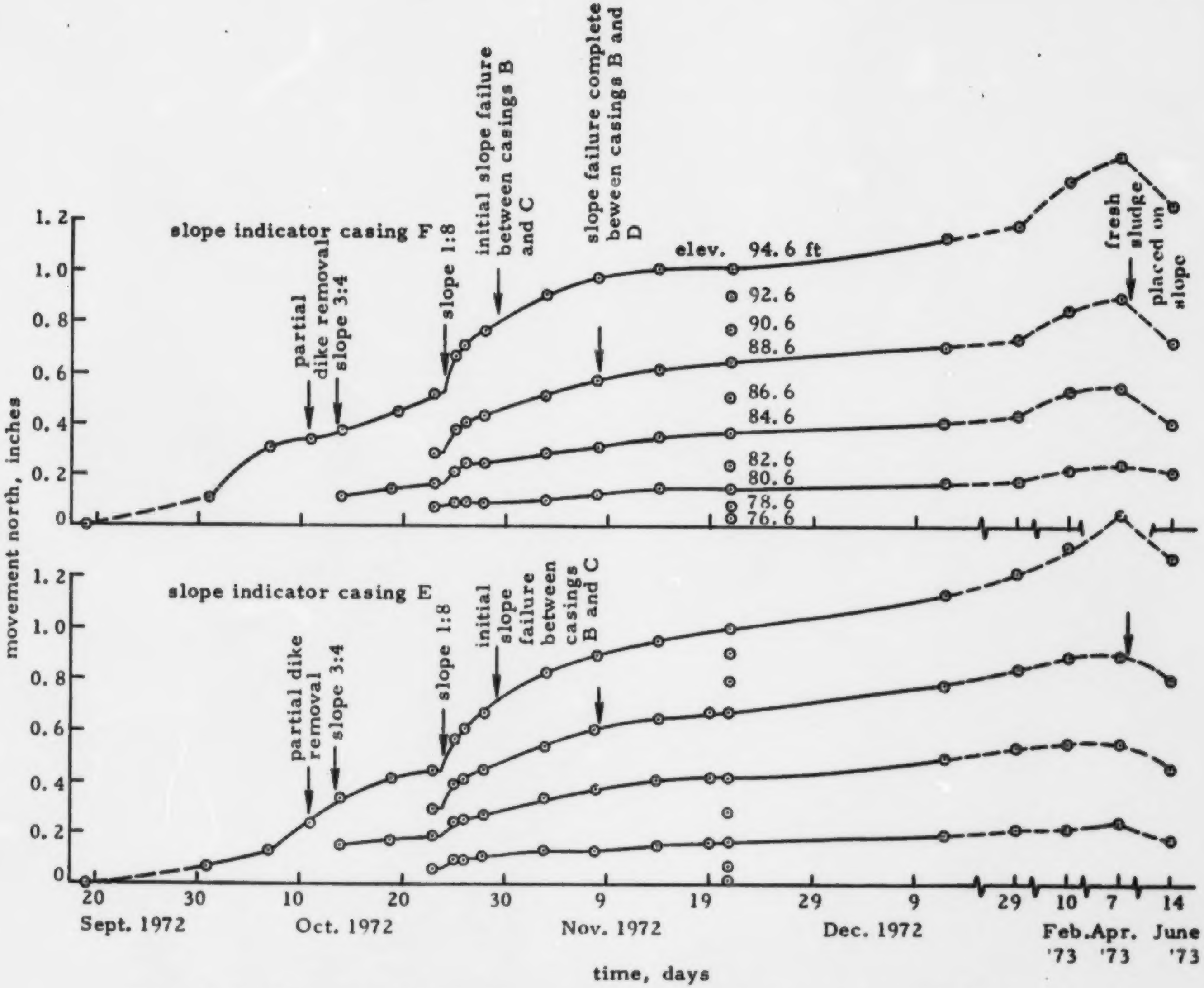

Figure 6. 9. Time rate of lateral movement. (e) Slope indicator casings E and F.

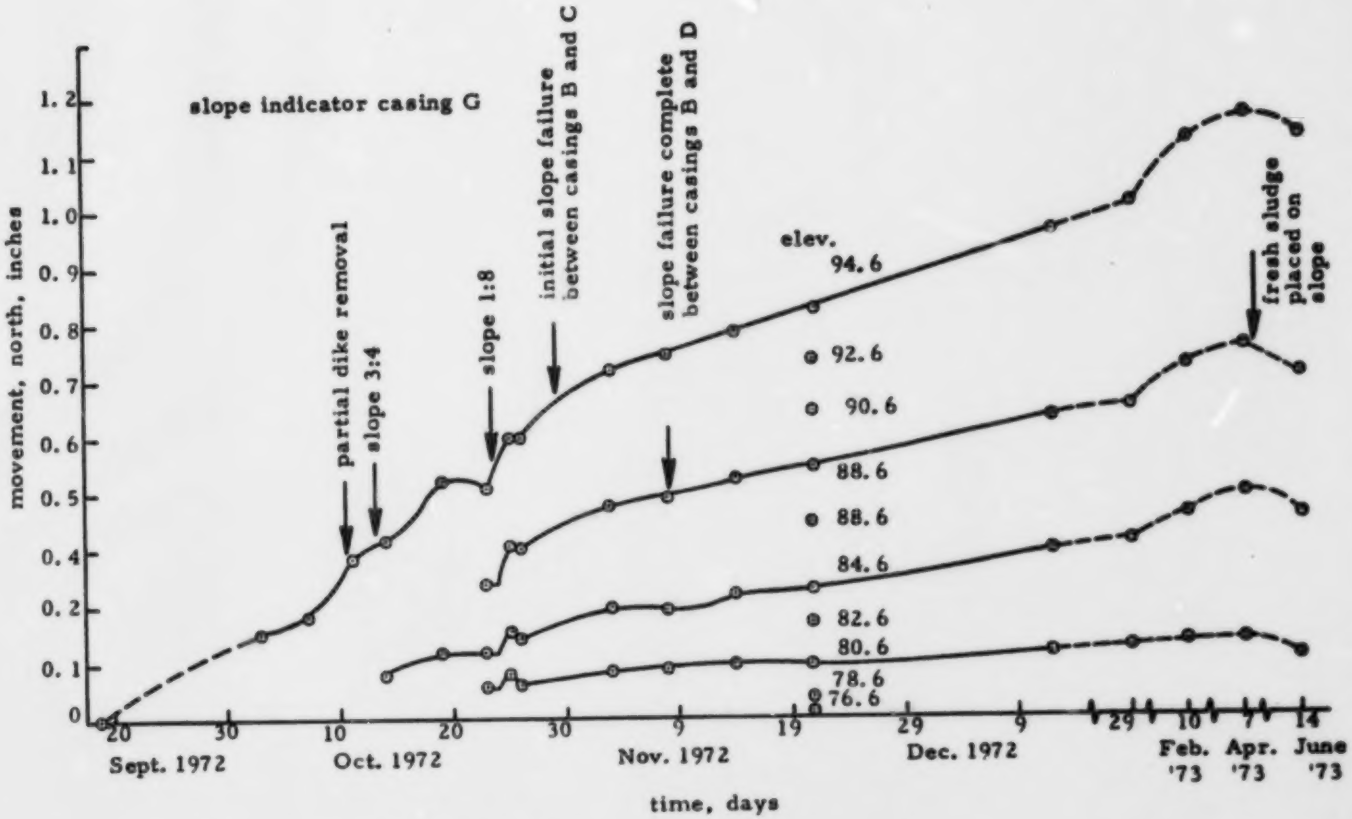

Figure 6.9. Time-rate of lateral movement. (f) Slope indicator G.

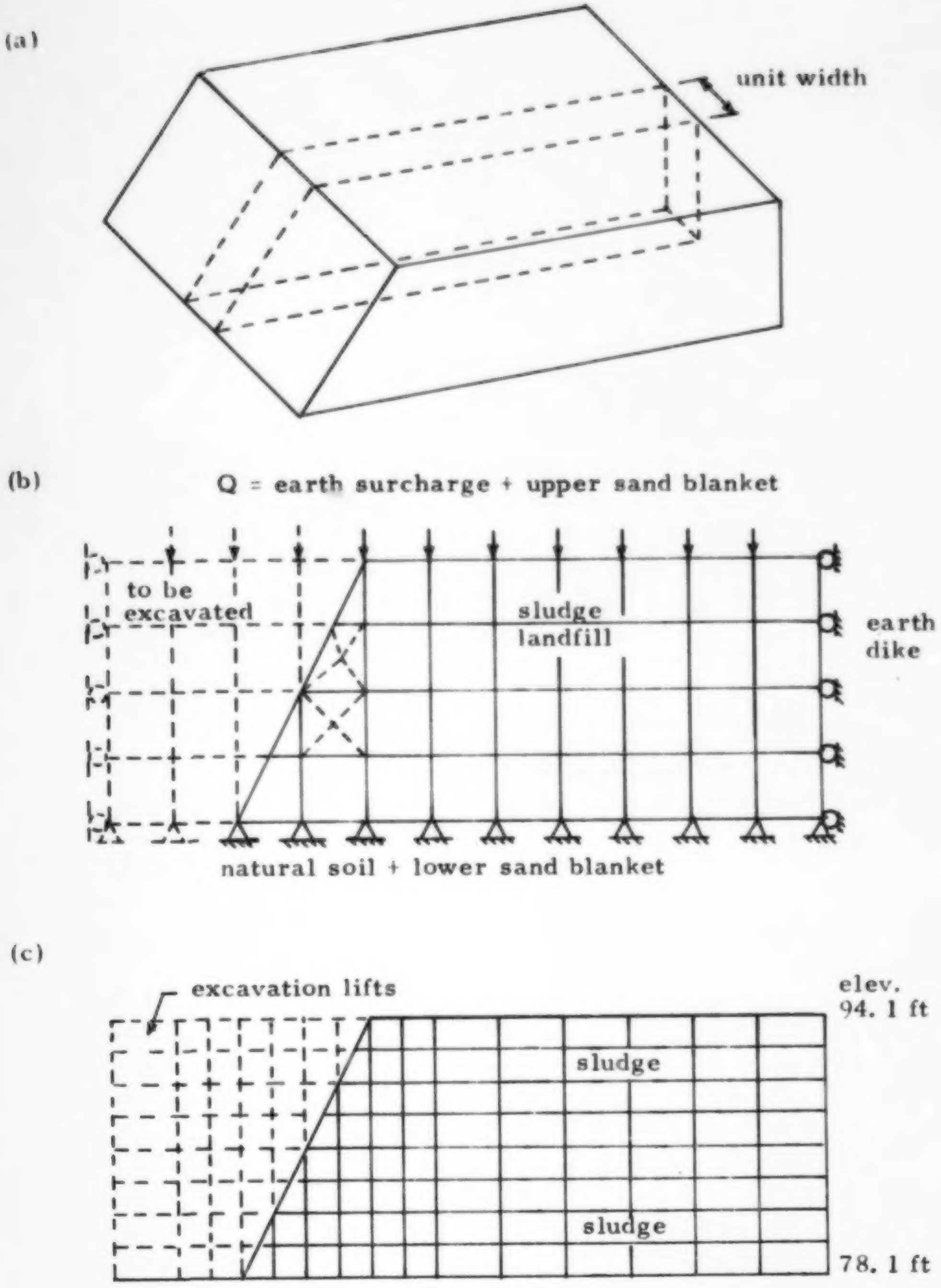
(a)
unit width
(b)
Q = earth surcharge + upper sand blanket
to be excavated
sludge landfill
earth dike
natural soil + lower sand blanket
(c)
excavation lifts
elev. 94.1 ft
sludge
sludge
78.1 ft

Figure 6.10. (a) Excavated slope showing the section to be analyzed.
(b) Finite element idealization of slope cross-section.
(c) Typical finite element configuration of the slope showing the excavation sequence.

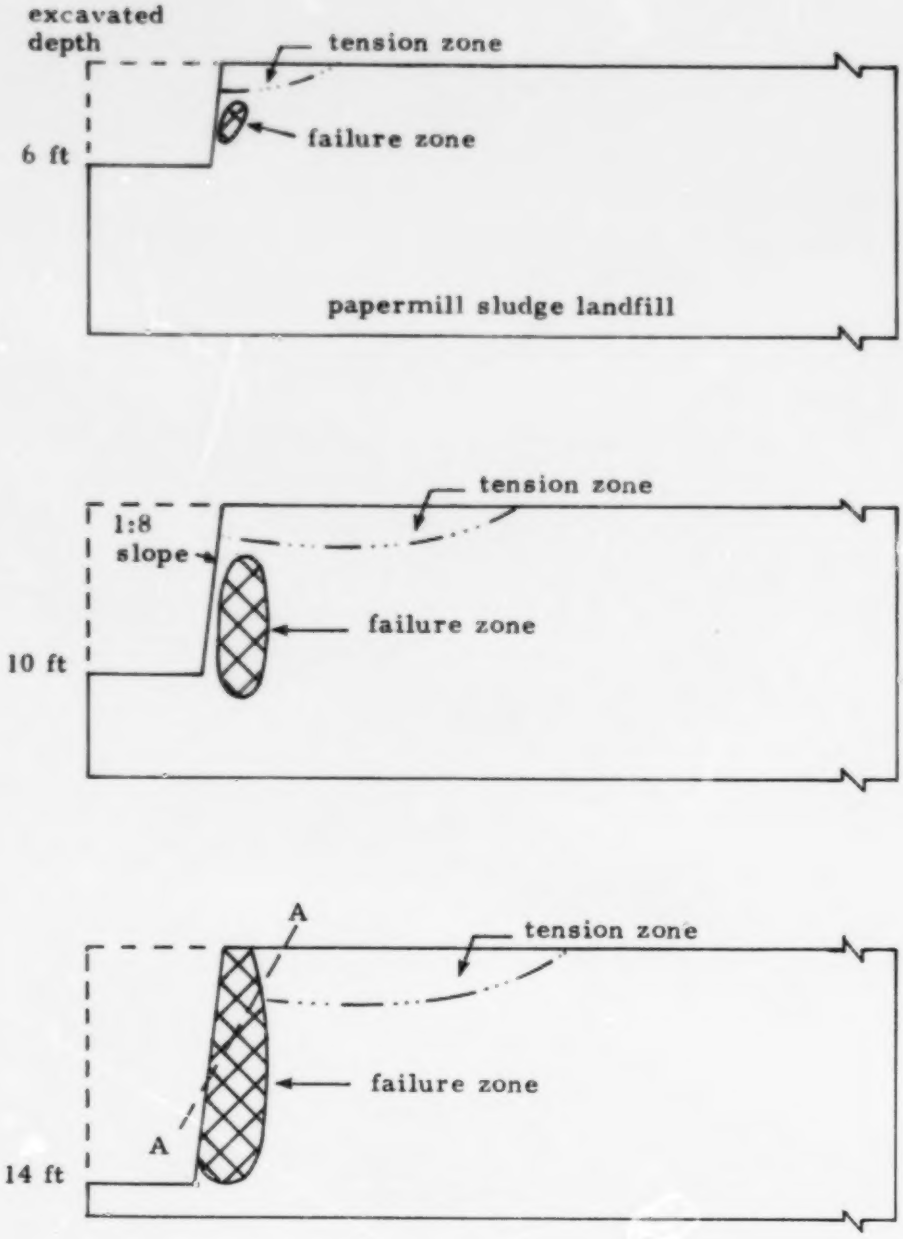
excavated depth
tension zone
failure zone
6 ft
papermill sludge landfill
tension zone
1:8 slope
failure zone
10 ft
A
tension zone
failure zone
A
14 ft

Figure 6. 11. Development of failure zones for the 1:8 slope, $s_u/p = 1.00$ and $K = 0.4$.

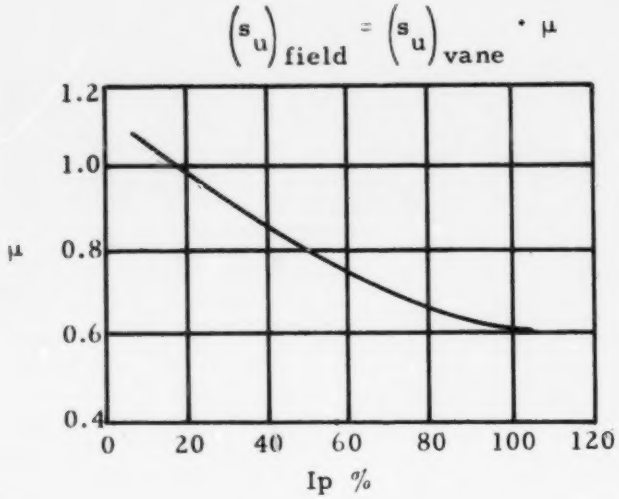

Figure 6.12. Correction factor for converting vane shear strengths to field shear strengths (after Bjerrum, 1972).

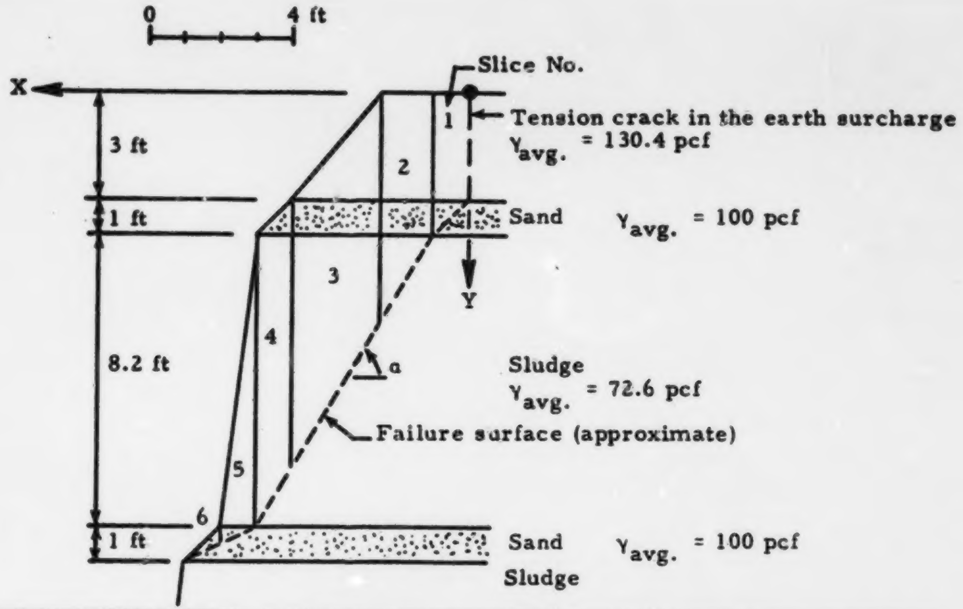
0
4 ft
Slice No.
X
1
Tension crack in the earth surcharge
γavg. = 130.4 pcf
3 ft
2
1 ft
Sand γavg. = 100 pcf
3
Y
8.2 ft
4
α
Sludge
γavg. = 72.6 pcf
Failure surface (approximate)
5
6
1 ft
Sand γavg. = 100 pcf
Sludge

	Values from the cross-section					Computations			
Slice No.	$\tan\alpha$	Δx (ft)	p (psf)	s_u (psf)	$\bar{\phi}$ (deg.)	B_o	A_o'	n_α	A_o
1	1.00	1.0	441.2	--	39.0	441.2	357.3	0.9029	395.7
2	1.64	1.5	580.5	768.1	0	1428.0	1152.2	1.0	1152.2
3	1.64	2.5	623.0	983.2	0	2554.3	2458.0	1.0	2458.0
4	1.64	1.0	585.8	1339.6	0	960.7	1339.6	1.0	1339.6
5	0.50	1.0	322.7	--	39.0	161.4	261.3	1.1416	228.9
6	0.50	1.0	25.0	--	39.0	12.5	20.2	1.1416	17.7
					Σ =	5558.1	5588.6		5592.1

Δx = slice width,

p = average stress on slice base,

$s_u = (s_u)_{vane} \cdot \mu$ = undrained shear strength, $\bar{\phi}$ = angle of internal friction,

$B_o = p \tan\alpha \cdot \Delta x$, $A_o' = s_u \cdot \Delta x$ or $p \tan\bar{\phi} \cdot \Delta x$, $A_o = A_o'/n_\alpha$,

$n_\alpha = \cos^2\alpha \left(1 + \frac{\tan\alpha \tan\bar{\phi}}{F}\right)$

Table complete only for $F_o = \frac{\Sigma A_o}{\Sigma B_o} = \frac{5592.1}{5558.1} = 1.006$

Additional calculations give $F_2 = \frac{\Sigma A_2}{\Sigma B_2} = 1.004$ for a line of thrust for side forces on each slice thru the lower 1/3 points.

Figure 6.13. Stability calculations using Janbu's method (1954, 1957), total stress basis.

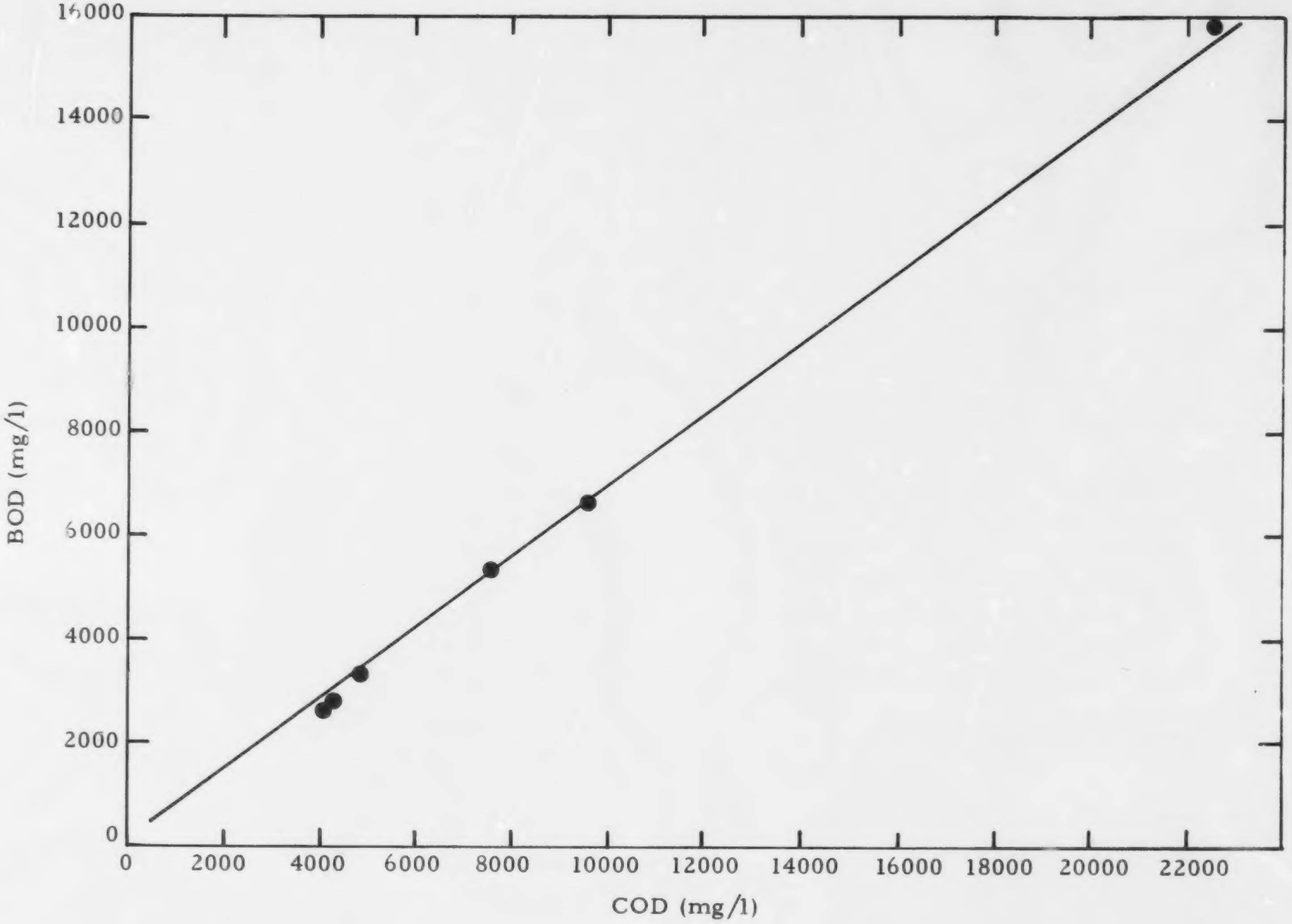

Figure 6. 14. Biochemical oxygen demand (BOD) versus chemical oxygen demand (COD).

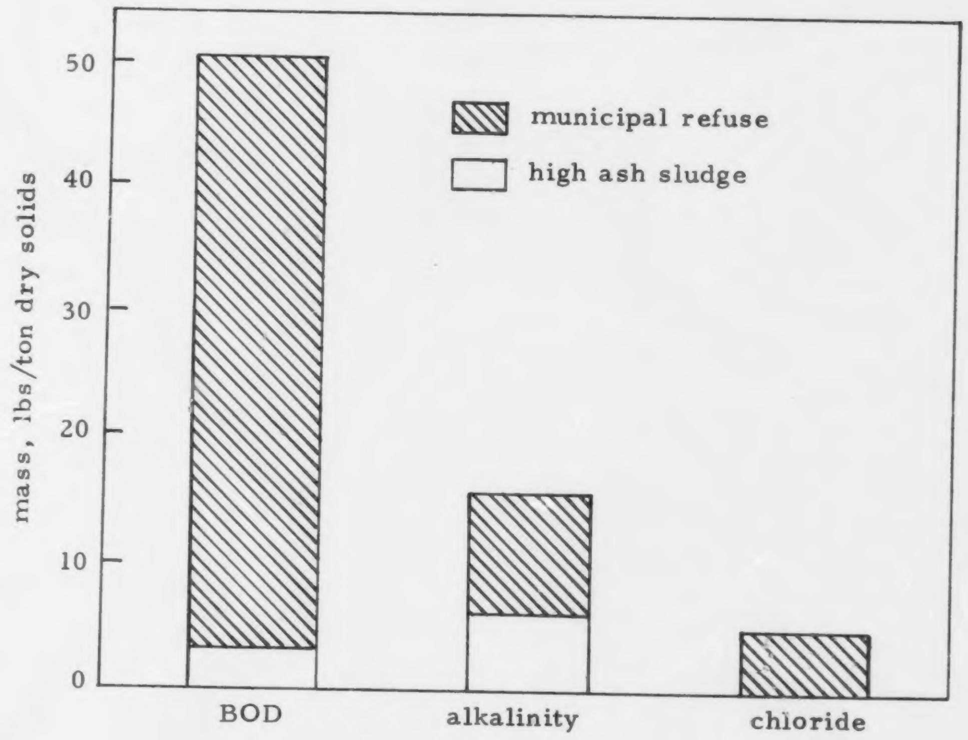

Figure 6. 15. Mass of leachate constituents.

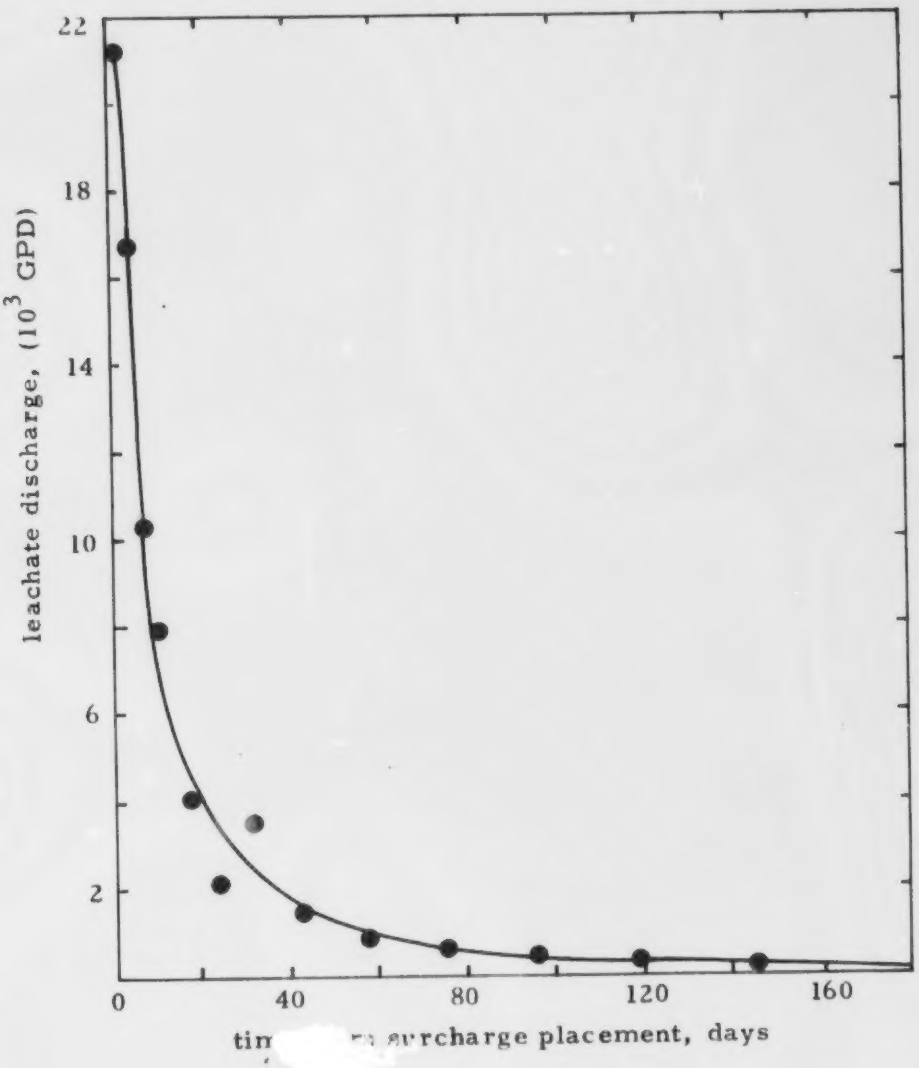

Figure 6. 16. Magnitude of leachate flow.

CHAPTER VII. SUMMARY AND CONCLUSIONS

The summary and conclusions are presented under five headings: (1) engineering properties of the sludge, (2) sludge landfill settlement, (3) slope stability of the consolidated sludge, (4) leachate analysis, and (5) practical implications of the investigation. Conclusions given in the First Annual Report are not repeated.

Engineering Properties of the Sludge

Both physical properties and stress-deformation characteristics of the papermill sludge were determined relative to evaluating the consolidation behavior and slope stability of the experimental sludge landfill. Physical properties included water content, unit weight, specific gravity of the sludge solids, ash (or organic) content, and consistency limits. Stress-deformation characteristics refer to consolidation behavior and shear strength parameters of both fresh sludge and undisturbed samples from the consolidated landfill. The following conclusions refer to the engineering properties of the papermill sludge.

1. Physical properties of the papermill sludge are dependent on composition which may vary with production changes at the mill. An increase in organic content gives the sludge a higher water retention and lower unit weights for the same consolidation pressure. Liquid limits and plastic limits both increase with higher organic contents.

2. Relatively small consolidation loads produce a significant decrease in water content and increase in shearing strength of the papermill sludge. Vane strengths increased from less than 1 T/m^2 for the fresh sludge to almost 20 T/m^2 at the bottom of the consolidated lower sludge layer.

3. Consolidation tests on undisturbed sludge samples from the landfill gave void ratio-logarithm of pressure curves similar to inorganic clays. These tests provided data on the coefficient of consolidation c_v, primary compression ratio r, coefficient of secondary compression C_α, and the compression index C_c. Using the Casagrande construction, reasonable estimates were obtained for the preconsolidation pressures which were in agreement with existing overburden pressures.

4. Triaxial test data show that the strength of papermill sludge is essentially frictional and in accordance with the principle of effective stress. The angle of internal friction appears to vary linearly with organic content when comparisons are made using data obtained by a given test procedure. Extrapolation to zero organic content gave a value for the angle of internal friction very close to that of kaolin clay, the major inert component of the sludge.

5. For a given organic content, anisotropic consolidation increased the angle of internal friction when the direction of compression was normal to the plane in which fibers would tend to be aligned. Unconfined compressive strengths were also greatest for sample compression in the vertical direction. Lower values for the angle of internal friction and the unconfined compressive strength were observed when the direction of compression was in the plane of maximum fiber alignment (horizontal).

6. The undrained strength was directly related to consolidation pressure for papermill sludges having essentially the same composition. Hence the undrained strength of a fairly uniform normally consolidated sludge may be characterized by the ratio of undrained strength to effective overburden pressure, c_u/p.

Sludge Landfill Settlement

The experimental papermill sludge landfill consisted of 2 sludge layers, initially 10 ft thick, with sand drainage blankets at the top, middle, and bottom. An earth dike provided lateral confinement for the soft sludge during and after construction, and the surface load consisted of 3 ft of earth fill material. Instrumentation included settlement plates and piezometers placed at a number of locations in the landfill. Field and laboratory data, not available during preparation of the First Annual Report, and additional theoretical analyses are presented in this report. The following conclusions are in addition to those on settlement and pore pressures in the First Annual Report.

1. Gibson and Lo's (1961) theory provides an accurate estimate of total settlement and time-rate of settlement under instantaneous loading conditions. The time-settlement relation was dependent on the value of c_v and predicts that the ultimate settlement should be reached without the development of a linear (with log time) secondary compression curve.

Careful laboratory tests were required to determine the parameters a, b, and λ used in this theory.

2. Wahls' (1962) theory appears to adequately predict the hydrodynamic portion of the time-settlement relation for the sludge, provided that an appropriate value for the coefficient of consolidation, c_v, has been used in the theory. Estimates of secondary compression, based on Wahls' (1962) theory, are too low when based on laboratory values for the coefficient of secondary compression, C_α.

3. Consolidation theory may be used to estimate volume requirements for a papermill sludge landfill when consolidation parameters are known and when consolidation loads in the proposed landfill can be reasonably predicted.

Slope Stability of the Consolidated Sludge

After consolidation of the sludge under the 3 ft earth surcharge, seven slope indicator casings and additional piezometers were installed in preparation for the slope stability study. Earlier instrumentation remained operative and monitoring was continued. At this stage the north dike was removed and the sludge was excavated to a 3:4 slope. After about 10 days it was apparent that the slope was stable since little lateral movement had occurred. Next the 1:8 slope was excavated with subsequent events leading to an initial slope failure in the top sludge layer about four days later. Relatively large lateral movements were recorded prior to failure causing tension cracks to form in the earth surcharge. The following conclusions refer to lateral movements, slope stability, and methods of analysis.

1. The significant increase in shear strength of the papermill sludge as a direct consequence of consolidation resulted in a stable 3:4 slope with small observed lateral movements, less than one inch at the surface. This behavior was in contrast to the very soft, almost fluid behavior of the fresh sludge placed in the landfill during construction.

2. Lateral movements in the sludge landfill increased rapidly after excavation of the 1:8 slope. Rate of movement decreased with time suggesting that creep behavior of the sludge was re[illegible] a large portion of the final 6 inches of movement at the surfac[illegible] amount of movement decreased with depth.

3. Computed stresses, based on measured sludge properties and a simulated excavation to 6, 10, and 14 ft, show a failure zone developing behind the 1:8 slope. A tension zone behind the slope crest increased in size with more excavation. Failure along the unsupported slope would have been predicted and did occur.

4. The vane shear test appears to be appropriate for in situ measurements of the undrained shear strength of the soft papermill sludge. Uncertainties with regard to sludge disturbance during sampling and preparation for laboratory testing were avoided. This vane strength must be corrected for deformation rate and sludge anisotropy effects before use in a stability analysis.

5. Stability analysis of the 1:8 slope, using Janbu's method for a composite failure surface, gave excellent agreement between the actual factor of safety and the computed factor of safety when vane shear strengths were corrected to field strengths. The correction factor (Bjerrum, 1972) was selected on the basis of experience with soft clays and the measured plasticity index of the papermill sludge.

6. Some lateral movement, less than 0.9 inch at the upper sludge surface, was measured during the five months of observation after the planned slope failure. The slope remained intact with only local surface changes due to snow or ice development.

Leachate Analysis

Leachate samples obtained periodically from the landfill were analyzed for those parameters considered to be of significance to groundwater quality and consistent with the nature of the landfill material. Variation among samples appears to be related primarily to rainfall entering the drainage blanket and diluting the leachate. Fluid from the pressed sludge sample gives an indication of leachate which could leave the sludge if additional consolidation were induced by greater surface loads. The following conclusions are in addition to those presented in the First Annual Report.

1. Concentrations of dissolved organic matter, mineral salts, and hardness were within the broad range of those reported for leachates originating in landfills of municipal refuse. However, on a mass basis,

the leachate constituents associated with high ash papermill sludge were significantly less. These substances are those most likely to prove objectionable should the landfill leachate become a part of the groundwater.

2. Sulfate, Kjeldahl nitrogen, and phosphorous were present in only negligible quantities. Leachate concentrations of those constituents, as well as iron and chloride were well below values cited for municipal refuse.

3. The low permeability of high ash papermill sludge together with a decreasing rate of leachate flow, associated with fill consolidation, exerted a moderating effect upon the quantity of leachate leaving the landfill.

Practical Implications of the Investigation

Soil mechanics theory was effective in predicting the settlement of the papermill sludge on the basis of laboratory data. This settlement or reduction in volume of the sludge, when properly accounted for, will permit significantly larger volumes of sludge to be placed in a landfill designed for a particular use, whether it be a green area, or for recreational, agricultural, or for light construction purposes.

The field rate of primary compression of the sludge was very rapid (high coefficient of consolidation, c_v) suggesting that preloading may be an effective way for stabilization and minimizing long-term compression. About 30 days was required for primary consolidation of a 10 ft sludge layer drained at the top and bottom surfaces. The preload, consisting of an earth surcharge, must be of sufficient magnitude and duration to cause compression of the sludge which would normally occur under the proposed design load over the expected life of the structure. The magnitude of the preload may be limited by stability considerations which are largely governed by the rate of porewater pressure dissipation. A method for estimating the magnitude and duration of a preload on highly organic soils has been given by MacFarlane (1969).

Sludge unit weights increased from 69.7 pcf for the fresh dewatered sludge to about 88 pcf at the bottom of the lower sludge layer. This fact combined with the relatively high stability of the consolidated sludge landfill suggests its use as a lightweight fill material for earth embankments and other special needs such as sound deflecting barriers. The fresh dewatered sludge from a mill could be deposited in a landfill which includes drainage blankets and a surcharge load. After sufficient time for primary consolidation the surcharge could be removed and the consolidated sludge removed for use as a lightweight fill material in another location.

The considerable increase in shear strength of the papermill sludge resulting from consolidation combined with the observed stability of the experimental 3:4 slope suggests that a landfill could be contoured so as to provide a golf course or coasting ramp during the summer and a toboggan run or ski hill during the winter. A soil cover capable of growing vegetation would serve to make the area suitable both as a recreational area as well as a green area.

Sand or gravel blankets and/or tile drains used in connection with a papermill sludge landfill can serve a dual purpose. With proper placement they will shorten the drainage path within the sludge thereby reducing the time needed for primary consolidation and drainage. Hence, much of the settlement under an earth surcharge could be accelerated permitting more options for operation and final use of a papermill sludge landfill. These drains could also be utilized to collect leachate for subsequent treatment by conventional means, should that alternative represent the optimum or most suitable method for protection of groundwater quality. The demonstrated capacity of soil percolation to effect a degree of renovation equivalent or superior to conventional treatment requires that it be considered as an alternate to collection and treatment. The success of percolation is contingent upon the existence or provision of a suitable soil of sufficient depth and distribution to provide the necessary changes in quality of the leachate prior to groundwater utilization. Further sludge dewatering, consistent with technological capability, remains as an additional option for minimizing the quantity of leachate to be renovated. The options available suggest that any selection be made on a case by case basis as opposed to a single universal approach to groundwater protection from landfill leachate intrusion.

REFERENCES

1. American Society for Testing and Materials, Book of ASTM Standards, Part 15, Philadelphia, Pennsylvania.

2. Andersland, O. B., and Laza, Robert W., "Shear strength and permeability of high ash pulp and papermill sludges," Tech. Rpt. 1 for the National Council of the Paper Industry for Air and Stream Improvement, Inc., Div. of Engineering Research, Mich. State Univ., E. Lansing, Mich., 1971.

3. Bailey, W. A., and Christian, John T., "ICES LEASE-1, A Problem Oriented Language for Slope Stability Analysis," Soil Mechanics Publ. No. 235, Mass. Inst. of Technology, Cambridge, Mass., April, 1969.

4. Black, C. A., ed., Methods of Soil Analysis, No. 9 in the series Agronomy, Am. Soc. of Agronomy, Inc., Part 2, 1965.

5. Bishop, A. W., "The use of the slip circle in the stability analysis of slopes," Geotechnique, London, 5:7-17, 1954.

6. Bishop, Alan W., and Henkel, D. J., The Measurement of Soil Properties in the Triaxial Test, Edward Arnold (Publishers) Ltd., London, 1962.

7. Bjerrum, Laurits, "Engineering geology of Norwegian normally-consolidated marine clays as related to settlements of buildings," Geotechnique, London, 17:81-118, 1967.

8. Bjerrum, Laurits, "Embankments on soft ground," Proc. of the Specialty Conf. on Performance of Earth and Earth-Supported Structures, American Society of Civil Engineers, II:1-54, June 11-14, 1972.

9. Casagrande, A., "The determination of the preconsolidation load and its practical significance," Proc. 1st Internat. Conf. on Soil Mech. and Found. Engr., Cambridge, 3:60, 1936.

10. Casagrande, A., "Classification and identification of soils," Trans. Am. Soc. of Civil Engineers, 113:901-930, 1948.

11. Casagrande, A., "Construction of embankments across peaty soils," Journ. of the Boston Soc. of Civil Engineers, 53:3:272-317, 1966.

12. California State Water Pollution Control Board, "Report on the investigation of leaching of a sanitary landfill," Publ. No. 10, Sacramento, California, 1954.

13. California State Water Pollution Control Board, "Effects of refuse dumps on ground water quality," Publ. No. 24, Sacramento, California, 1961.

14. California State Water Quality Control Board, "In situ investigation of movements of gases produced from decomposing refuse," Publ. No. 35, Sacramento, California, 1967.

15. Dunlop, Peter, Duncan, J. M., and Seed, H. Bolton, "Finite element analyses of slopes in soil," Rpt. No. TE-68-3, Soil Mech. and Bituminous Materials Research Lab., Dept. of Civil Engineering, Univ. of Calif., Berkeley, 1968.

16. Emrich, G. H., "Guidelines for sanitary landfills- ground water and percolation," Environmental Foundation Conf. on the Application of Environmental Research and Development on Landfill Disposal of Solid Wastes, Deerfield, Mass., August 24-28, 1970.

17. Fungaroli, A. A., "Pollution of subsurface water by sanitary landfills," Vol. I, Drexel Institute of Technology, Solid Waste Management Research Grant 000162, U. S. Environmental Protection Agency, 1971.

18. Gibbs, H. J., Hilf, J. W., Holtz, W. G., and Walker, F. C., "Shear strength of cohesive soils," Proc. Research Con. on Shear Strength of Cohesive Soils, American Society of Civil Engineers, 1960.

19. Gibson, R. E., and Lo, K. Y., "A theory of consolidation for soils exhibiting secondary compression," Norwegian Geotechnical Institute, Publ. No. 41, Oslo, Norway, 1961.

20. Gillespie, W. J., Mazzola, C. A., and Gellman, I., "Landfill disposal of papermill waste solids," presented at the 7th Technical Association of the Pulp and Paper Industry Air and Water Conference, Minneapolis, Minn., June 7-10, 1970.

21. Imshenetsky, A. A., "Decomposition of cellulose in the soil," The Ecology of Soil Bacteria, University of Toronto Press, Canada, 1968.

22. Janbu, N., Discussion on "Application of composite slip surfaces for stability analyses," European Conf. on Stability of Slopes, Stockholm, III:43-49, 1954.

23. Janbu, N., "Earth pressures and bearing capacity calculations by generalized procedure of slices," Proc. 4th Internat. Conf. on Soil Mech. and Found. Engr., II:207-212, 1957.

24. Lambe, T. William, Soil Testing for Engineers, John Wiley and Sons, Inc., New York, 1951.

25. Lambe, T. William, and Whitman, Robert V., Soil Mechanics, John Wiley and Sons, Inc., New York, 1969.

26. Leonards, G. A., Foundation Engineering, McGraw-Hill Book Co., Inc., New York, 1962.

27. Leonards, G. A., and Ramiah, R. K., "Time effects in the consolidation of clay," Am. Soc. for Testing and Materials, Spec. Tech. Publ. No. 254, pp. 116-130, 1959.

28. Lynch, D. L., and Cotnoir, L. J., Jr., "The influence of clay minerals on the breakdown of certain organic substrates," Soil Science Soc. Am., Vol. 20, pp. 367-370, 1956.

29. MacFarlane, Ivan C., ed., *Muskeg Engineering Handbook*, Univ. of Toronto Press, 1969.

30. National Council of the Paper Industry for Air and Stream Improvement, Inc., "An investigation of improved procedures for measurement of mill effluent and receiving water color," Tech. Bull. No. 253, 1971.

31. Parry, R. H. G., "Stability analysis for low embankments on soft clays," *Stress-Strain Behaviour of Soils*, Proc. of the Roscoe Memorial Symposium, Cambridge University, England, 29-31 March 1971.

32. Salvato, J. A., Wilkie, W. G., and Mead, B. E., "Sanitary landfill leaching prevention and control," Journ. Water Pollution Control Federation, 43:10:2084, 1971.

33. Sorg, T. S., and Hickman, H. L., "Sanitary landfill facts," U. S. Dept. of Health, Education, and Welfare, Publ. SW-4ts, 1968.

34. *Standard Methods for the Examination of Water and Wastewater*, 13th ed., Am. Public Health Assoc., New York, N. Y., 1971.

35. Terzaghi, Karl, *Theoretical Soil Mechanics*, John Wiley and Sons, Inc., New York, 1943.

36. Terzaghi, Karl, and Peck, Ralph B., *Soil Mechanics in Engineering Practice*, 2nd ed., John Wiley and Sons, Inc., New York, 1967.

37. Wahls, Harvey E., "Analysis of primary and secondary consolidation," Journ. of the Soil Mech. and Found. Div., Am. Soc. of Civil Engineers, 88:SM6:207-231, 1962.

38. Whitman, R. V., and Bailey, W. A., "Use of computers for slope stability analysis," Journ. of the Soil Mech. and Found. Div., Am. Soc. of Civil Engineers, 93:SM4:475-498, 1967.

39. Umbreit, W. W., "Soil Microbiology," *Modern Microbiology*, W. H. Freeman and Company, San Francisco, 1962.

APPENDIX A

TABLE A-1. SURFACE MOVEMENTS

Date	Horizontal distance, ft									Remarks
mo-da-yr	I-WX	I-WY	I-WZ	II-WX	II-WY	II-WZ	III-WX	III-XY	III-WZ	
9-19-72	51.47	71.61	91.39	51.85	70.80	91.17	51.60	71.38	91.29	— initial distance
9-25-72	51.46	71.62	91.37	51.88	70.82	91.18	51.63	71.40	91.29	
9-30-72	-	-	-	51.89	70.83	91.21	-	-	-	
10- 2-72	51.45	71.61	91.36	51.87	70.80	91.18	51.63	71.40	91.29	
10- 3-72	-	-	91.36	-	-	91.18	-	-	91.29	
10- 4-72	51.46	71.62	91.37	-	-	91.19	-	71.40	91.31	
10- 7-72	51.46	71.62	91.37	51.87	70.82	91.19	51.63	71.42	91.33	
10-10-72	51.47	71.63	91.38	51.87	70.82	91.21	51.63	71.42	91.34	
10-13-72	51.48	71.65	91.41	51.90	70.85	91.23	51.66	71.44	91.36	
10-19-72	51.49	71.66	91.42	51.90	70.86	91.24	51.66	71.44	91.36	— 3:4 slope completed
10-23-72	-	-	91.41	-	-	91.23	-	-	91.35	
10-25-72	-	71.67	91.52	-	70.87	91.37	-	71.46	91.47	— 1:8 slope completed
10-26-72	-	71.67	91.56	-	70.88	91.40	-	71.46	91.50	
10-28-72	51.50	71.67	91.62	51.91	70.88	91.48	51.69	71.48	91.55	
11- 1-72	-	71.67	91.67	-	70.88	lost	-	71.47	91.58	
11- 8-72	-	71.69	91.73	-	-	-	-	71.49	91.73	
11-14-72	-	71.69	91.76	-	-	-	-	71.49	91.80	
11-21-72	-	71.70	91.76	-	-	-	-	71.49	91.80	
4- 7-72	51.55	71.73	91.75	51.95	70.91	-	51.71	71.50	91.88	
6-14-72	51.52	71.70	91.68	51.93	70.90	-	51.72	71.50	91.83	— trench filled with sludge

Line -- I West 20 ft
II Centerline of fill
III East 20 ft
} see Figure 4.2

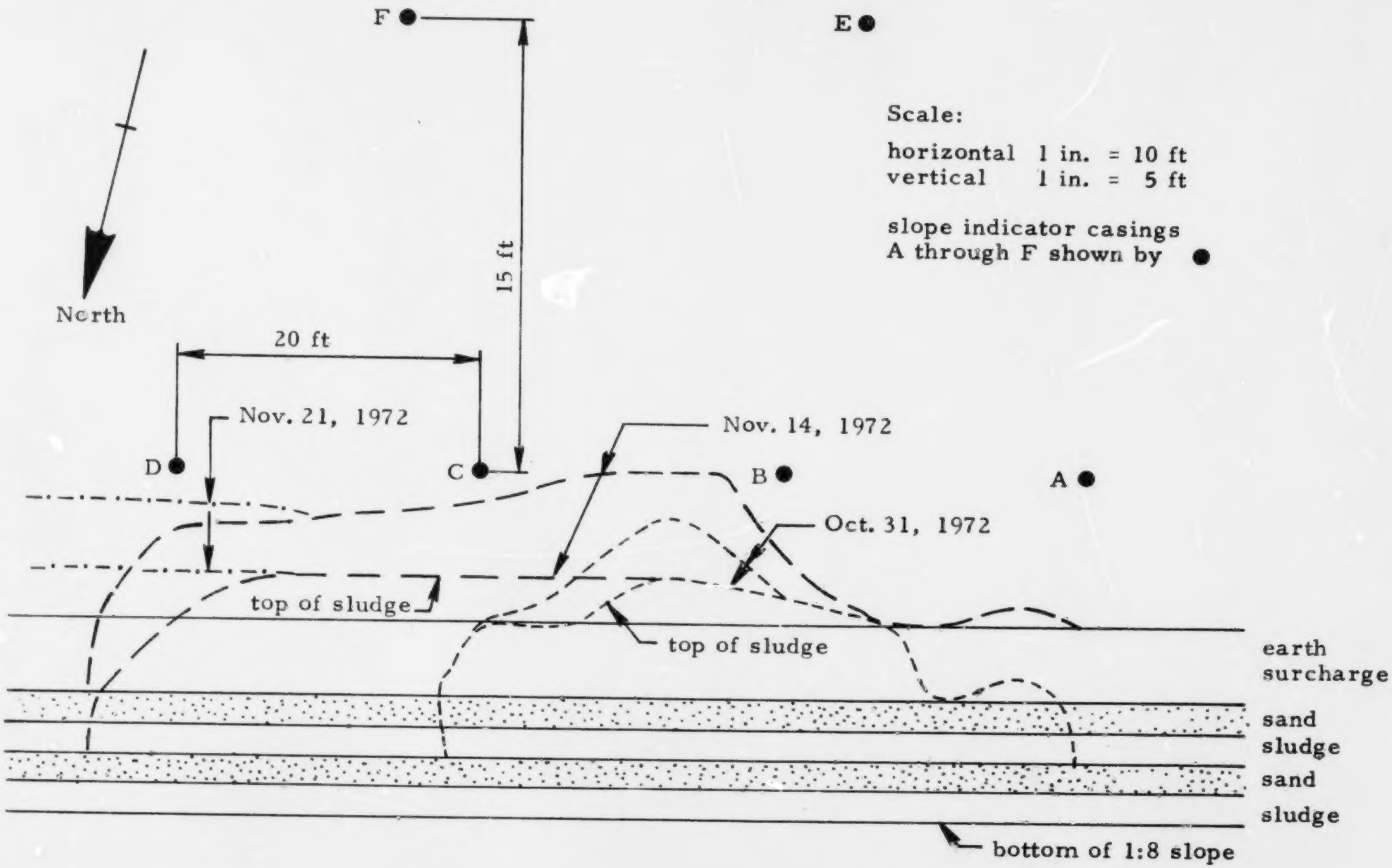
F
E
Scale:
horizontal 1 in. = 10 ft
vertical 1 in. = 5 ft
slope indicator casings
A through F shown by ●
North
15 ft
20 ft
Nov. 21, 1972
Nov. 14, 1972
Oct. 31, 1972
D
C
B
A
top of sludge
top of sludge
earth
surcharge
sand
sludge
sand
sludge
bottom of 1:8 slope

Figure A-1. Slope failure areas, plan view.

APPENDIX B

TABLE B-1. SLOPE INDICATOR DATA, September 25, 1972

Casing movement, north, inches

Casing	A		B		C		D	
Elev., ft.	North	East	North	East	North	East	North	East
94.6	-0.102		0.060		0.084		0.102	
92.6	-0.192		0.036		0.078		0.084	
90.6	-0.246		0.006		0.072		0.066	
88.6	-0.258		-0.012		0.060		0.048	
86.6	-0.252		-0.018		0.054		0.030	
84.6	-0.204		-0.024		0.030		0.012	
82.6	-0.126		-0.024		0.030		0.012	
80.6	-0.072		-0.012		0.006		0.012	
78.6	-0.030		-0.006		0.000		0.012	
76.6	-0.012		0.000		0.000		0.006	
75.6	0.000		0.000		0.000		0.000	

Casing	E		F		G		Remarks
Elev., ft.	North	East	North	East	North	East	
94.6							Two days after trench cut
92.6							
90.6							
88.6							
86.6							
84.6							
82.6							
80.6							
78.6							
76.6							
75.6							

TABLE B-2. SLOPE INDICATOR DATA, October 3, 1972

Casing movement, north or east*, inches

Casing	A		B		C		D	
Elev., ft.	North	East	North	East	North	East	North	East
94.6	-0.006	0.246	0.222	0.246	0.264	-0.042	0.252	-0.108
92.6	-0.158	0.336	0.174	0.204	0.264	-0.006	0.216	-0.132
90.6	-0.258	0.366	0.120	0.174	0.210	0.024	0.186	-0.132
88.6	-0.300	0.336	0.072	0.156	0.162	0.036	0.150	-0.108
86.6	-0.306	0.258	0.036	0.132	0.114	0.042	0.102	-0.078
84.6	-0.258	0.162	0.006	0.096	0.060	0.048	0.060	-0.042
82.6	-0.168	0.114	-0.006	0.060	0.042	0.036	0.042	-0.030
80.6	-0.096	0.072	0.000	0.030	0.012	0.018	0.024	-0.024
78.6	-0.048	0.036	0.006	0.006	0.000	0.012	0.018	-0.024
76.6	-0.018	0.012	0.006	-0.006	-0.006	0.006	0.000	-0.006
75.6	0.000	0.000	0.000	0.000	0.000	0.000	0.000	0.000

Casing	E		F		G		Remarks
Elev., ft.	North	East	North	East	North	East	
94.6	0.072		0.114		0.150		*minus sign indicates movement south or west East end of north dike excavated to toe
92.6	0.072		0.096		0.120		
90.6	0.072		0.066		0.108		
88.6	0.054		0.048		0.096		
86.6	0.042		0.042		0.078		
84.6	0.036		0.036		0.042		
82.6	0.018		0.118		0.042		
80.6	0.006		0.012		0.024		
78.6	0.000		0.006		0.006		
76.6	0.000		0.000		0.000		
75.6	0.000		0.000		0.000		

TABLE B-3. SLOPE INDICATOR DATA, October 4, 1972

Casing movement, north*, inches

Casing	A		B		C		D	
Elev., ft.	North	East	North	East	North	East	North	East
94.6	0.078		0.162		0.510		0.348	
92.6	-0.078		0.126		0.468		0.318	
90.6	-0.180		0.096		0.408		0.294	
88.6	-0.234		0.072		0.324		0.264	
86.6	-0.258		0.042		0.246		0.216	
84.6	-0.222		0.012		0.156		0.150	
82.6	-0.138		0.000		0.108		0.108	
80.6	-0.072		0.000		0.048		0.072	
78.6	-0.036		0.000		0.018		0.036	
76.6	-0.012		0.006		0.000		0.012	
75.6	0.000		0.000		0.000		0.000	

Casing	E		F		G		Remarks
Elev., ft.	North	East	North	East	North	East	
94.6							*minus sign indicates movement south
92.6							
90.6							
88.6							
86.6							
84.6							
82.6							
80.6							
78.6							
76.6							
75.6							

TABLE B-4. SLOPE INDICATOR DATA, October 7, 1972

Casing movement, north*, inches

Casing	A		B		C		D	
Elev., ft.	North	East	North	East	North	East	North	East
94.6	0.138		0.324		0.684		0.558	
92.6	-0.006		0.300		0.660		0.516	
90.6	-0.108		0.264		0.660		0.480	
88.6	-0.162		0.210		0.504		0.432	
86.6	-0.204		0.162		0.396		0.360	
84.6	-0.180		0.114		0.270		0.270	
82.6	-0.102		0.084		0.186		0.198	
80.6	-0.042		0.060		0.096		0.120	
78.6	-0.018		0.030		0.036		0.054	
76.6	-0.006		0.012		0.000		0.012	
75.6	0.000		0.000		0.000		0.000	

Casing	E		F		G		Remarks
Elev., ft.	North	East	North	East	North	East	
94.6	0.132		0.318				*minus sign indicates movement south Part of west end of north dike remaining to be excavated.
92.6	0.126		0.270				
90.6	0.114		0.222				
88.6	0.096		0.180				
86.6	0.072		0.144				
84.6	1.060		0.114				
82.6	0.030		0.084				
80.6	0.012		0.054				
78.6	0.000		0.024				
76.6	-0.006		0.006				
75.6	0.000		0.000				

TABLE B-5. SLOPE INDICATOR DATA, October 11, 1972

Casing movement, north*, inches

Casing	A		B		C		D	
Elev., ft.	North	East	North	East	North	East	North	East
94.6	0.300		0.396		0.792		0.588	
92.6	0.174		0.394		0.780		0.522	
90.6	0.078		0.342		0.726		0.522	
88.6	0.012		0.282		0.630		0.474	
86.6	-0.048		0.216		0.498		0.402	
84.6	-0.066		0.150		0.354		0.306	
82.6	-0.024		0.102		0.240		0.126	
80.6	-0.006		0.060		0.120		0.126	
78.6	0.000		0.030		0.048		0.054	
76.6	0.000		0.012		0.006		0.012	
75.6	0.000		0.000		0.000		0.000	

Casing	E		F		G		Remarks
Elev., ft.	North	East	North	East	North	East	
94.6	0.234		0.342		0.282		*minus sign indicates movement south
92.6	0.222		0.288		0.240		
90.6	0.204		0.234		0.198		
88.6	0.174		0.192		0.162		
86.6	0.138		0.144		0.126		
84.6	0.108		0.108		0.072		
82.6	0.066		0.072		0.066		
78.6	0.006		0.024		0.012		
76.6	0.000		0.006		0.000		
75.6	0.000		0.000		0.000		

TABLE B-6. SLOPE INDICATOR DATA, October 14, 1972

Casing Movement, North or East*, inches

Casing	A		B		C		D	
Elev., ft.	North	East	North	East	North	East	North	East
94.6	0.480	0.252	0.606	0.246	0.870	-0.076	0.666	-0.216
92.6	0.396	0.342	0.624	0.204	0.912	-0.228	0.660	-0.252
90.6	0.318	0.378	0.606	0.174	0.888	-0.180	0.642	-0.252
88.6	0.240	0.348	0.528	0.150	0.786	-0.138	0.600	-0.222
86.6	0.150	0.270	0.432	0.132	0.624	-0.102	0.528	-0.180
84.6	0.096	0.174	0.324	0.096	0.438	-0.078	0.420	-0.132
82.6	0.096	0.126	0.220	0.066	0.300	-0.060	0.306	-0.096
80.6	0.078	0.078	0.144	0.042	0.156	-0.036	0.192	-0.066
78.6	0.042	0.042	0.072	0.012	0.066	-0.024	0.084	-0.042
76.6	0.018	0.018	0.024	0.000	0.006	0.000	0.018	-0.018
75.6	0.000	0.000	0.000	0.000	0.000	0.000	0.000	0.000

Casing	E		F		G		Remarks
Elev., ft.	North	East	North	East	North	East	
94.6	0.330	0.114	0.378	-0.102	0.312	0.096	*Minus sign indicates movement South or West 3:4 slope
92.6	0.300	0.156	0.312	-0.126	0.264	0.096	
90.6	0.270	0.168	0.252	-0.114	0.222	0.084	
88.6	0.228	0.150	0.204	-0.108	0.180	0.066	
86.6	0.186	0.120	0.156	-0.078	0.144	0.048	
84.6	0.150	0.078	0.114	-0.060	0.078	0.024	
82.6	0.096	0.054	0.072	-0.054	0.072	0.012	
80.6	0.054	0.018	0.036	-0.030	0.042	0.018	
78.6	0.012	0.006	0.012	-0.018	0.012	0.006	
76.6	0.000	0.000	0.006	-0.006	-0.006	-0.006	

TABLE B-7. SLOPE INDICATOR DATA, October 29, 1972

Casing Movement, North or East, inches

Casing	A		B		C		D	
Elev., ft.	North	East	North	East	North	East	North	East
94.6	0.558		0.648		0.894		0.720	
92.6	0.492		0.690		0.984		0.732	
90.6	0.420		0.684		0.984		0.726	
88.6	0.336		0.606		0.882		0.684	
86.6	0.228		0.492		0.708		0.594	
84.6	0.156		0.366		0.504		0.468	
82.6	0.140		0.252		0.342		0.354	
80.6	0.108		0.156		0.180		0.210	
78.6	0.066		0.084		0.078		0.030	
76.6	0.024		0.036		0.012		0.018	
75.6	0.000		0.000		0.000		0.000	

Casing	E		F		G		Remarks
Elev., ft.	North	East	North	East	North	East	
94.6	0.420		0.444		0.420		3:4 slope
92.6	0.372		0.366		0.366		
90.6	0.336		0.300		0.312		
88.6	0.270		0.246		0.252		
86.6	0.216		0.192		0.204		
84.6	0.168		0.144		0.132		
82.6	0.108		0.096		0.114		
80.6	0.054		0.066		0.072		
78.6	0.012		0.036		0.030		
76.6	0.000		0.012		0.006		
75.6	0.000		0.000		0.000		

TABLE B-8. SLOPE INDICATOR DATA, October 23, 1972

Casing Movement, North or East, inches

Casing	A		B		C		D	
Elev., ft.	North	East	North	East	North	East	North	East
94.6	0.606		0.684		0.990		0.750	
92.6	0.540		0.744		1.08		0.768	
90.6	0.474		0.750		1.08		0.768	
88.6	0.390		0.672		0.966		0.720	
86.6	0.270		0.546		0.774		0.630	
84.6	0.186		0.408		0.546		0.498	
82.6	0.156		0.282		0.366		0.372	
80.6	0.120		0.174		0.192		0.222	
78.6	0.072		0.090		0.073		0.096	
76.6	0.030		0.036		0.006		0.018	
75.6	0.000		0.000		0.000		0.000	

Casing	E		F		G		Remarks
Elev., ft.	North	East	North	East	North	East	
94.6	0.440		0.516		0.408		3:4 slope
92.6	0.390		0.426		0.354		
90.6	0.348		0.342		0.300		
88.6	0.294		0.282		0.240		
86.6	0.240		0.222		0.186		
84.6	0.186		0.168		0.114		
82.6	0.120		0.114		0.096		
80.6	0.060		0.072		0.054		
78.6	0.018		0.036		0.024		
76.6	0.000		0.012		0.006		
75.6	0.000		0.000		0.000		

TABLE B-9. SLOPE INDICATOR DATA, October 25, 1972

Casing Movement, North or East, inches

Casing	A		B		C		D	
Elev., ft.	North	East	North	East	North	East	North	East
94.6	1.368		1.854		2.124		1.494	
92.6	1.188		1.722		2.028		1.410	
90.6	1.008		1.506		1.842		1.314	
88.6	0.810		1.224		1.536		1.176	
86.6	0.594		0.924		1.188		0.996	
84.6	0.420		0.642		0.834		0.780	
82.6	0.318		0.426		0.552		0.552	
80.6	0.216		0.252		0.282		0.324	
78.6	0.114		0.120		0.114		0.138	
76.6	0.042		0.048		0.018		0.030	
75.6	0.000		0.000		0.000		0.000	

Casing	E		F		G		Remarks
Elev., ft.	North	East	North	East	North	East	
94.6	0.576		0.666		0.498		1:8 slope
92.6	0.516		0.558		0.438		
90.6	0.456		0.456		0.372		
88.6	0.390		0.378		0.306		
86.6	0.312		0.294		0.240		
84.6	0.240		0.216		0.156		
82.6	0.162		0.144		0.126		
80.6	0.090		0.090		0.078		
78.6	0.030		0.048		0.036		
76.6	0.006		0.018		0.006		
75.6	0.000		0.000		0.000		

TABLE B-10. SLOPE INDICATOR DATA, October 26, 1973

Casing Movement, North or East*, inches

Casing	A		B		C		D	
Elev., ft.	North	East	North	East	North	East	North	East
94.6	1.602	0.432	2.388	0.372	2.766	-0.438	1.830	-0.444
92.6	1.392	0.462	2.166	0.270	2.562	-0.336	1.710	-0.438
90.6	1.170	0.450	0.842	0.204	2.262	-0.240	1.560	-0.396
88.6	0.836	0.384	1.452	0.162	1.848	-0.162	1.368	-0.330
86.6	0.678	0.282	1.068	0.132	1.398	-0.096	1.134	-0.252
84.6	0.474	0.168	0.708	0.096	0.966	-0.048	0.864	-0.174
82.6	0.348	0.120	0.468	0.054	0.618	-0.030	0.600	-0.114
80.6	0.228	0.072	0.270	0.030	0.330	-0.018	0.348	-0.066
78.6	0.114	0.036	0.126	0.006	0.138	-0.006	0.150	-0.042
76.6	0.042	0.018	0.042	0.000	0.024	0.006	0.036	-0.018
75.6	0.000	0.000	0.000	0.000	0.000	0.000	0.000	0.000

Casing	E		F		G		Remarks
Elev., ft.	North	East	North	East	North	East	
94.6	0.606		0.726		0.498		1:8 slope *Minus sign indicates movement South or West
92.6	0.540		0.606		0.438		
90.6	0.480		0.504		0.372		
88.6	0.402		0.408		0.300		
86.6	0.324		0.318		0.228		
84.6	0.246		0.240		0.144		
82.6	0.168		0.156		0.114		
80.6	0.090		0.090		0.060		
78.6	0.030		0.048		0.030		
76.6	0.006		0.018		0.006		
75.6	0.000		0.000		0.000		

TABLE B-11. SLOPE INDICATOR DATA, October 28, 1972

Casing movement, north, inches

Casing	A		B		C		D	
Elev., ft.	North	East	North	East	North	East	North	East
94.6	1.920		3.090		3.426		2.238	
92.6	1.662		2.736		3.096		2.064	
90.6	1.398		2.274		2.676		1.878	
88.6	1.110		1.746		2.136		1.614	
86.6	0.804		1.236		1.566		1.320	
84.6	0.546		0.774		1.026		0.996	
82.6	0.384		0.516		0.660		0.684	
80.6	0.240		0.300		0.348		0.390	
78.6	0.114		0.138		0.144		0.168	
76.6	0.036		0.048		0.024		0.042	
75.6	0.000		0.000		0.000		0.000	

Casing	E		F		G		Remarks
Elev., ft.	North	East	North	East	North	East	
94.6	0.666		0.762				
92.6	0.594		0.642				
90.6	0.528		0.534				
88.6	0.444		0.438				
86.6	0.360		0.336				
84.6	0.276		0.246				
82.6	0.192		0.156				
80.6	0.108		0.090				
78.6	0.048		0.036				
76.6	0.012		0.012				
75.6	0.000		0.000				

TABLE B-12. SLOPE INDICATOR DATA, November 1, 1972

Casing movement, north, inches

Casing	A		B		C		D	
Elev., ft.	North	East	North	East	North	East	North	East
94.6	2.328		3.678		4.224		2.766	
92.6	2.034		3.174		3.732		2.556	
90.6	1.716		2.592		3.174		2.298	
88.6	1.368		1.980		2.514		1.968	
86.6	0.984		1.392		1.812		1.584	
84.6	0.654		0.834		1.134		1.176	
82.6	0.456		0.588		0.744		0.792	
80.6	0.288		0.366		0.414		0.444	
78.6	0.138		0.186		0.174		0.186	
76.6	0.042		0.072		0.036		0.042	
75.6	0.000		0.000		0.000		0.000	

Casing	E		F		G		Remarks
Elev., ft.	North	East	North	East	North	East	
94.6							
92.6							
90.6							
88.6							
86.6							
84.6							
82.6							
80.6							
78.6							
76.6							
75.6							

TABLE B-13. SLOPE INDICATOR DATA, November 3, 1972

Casing Movement, North or East*, inches

Casing	A		B		C		D	
Elev., ft.	North	East	North	East	North	East	North	East
94.6	2.502	0.672	3.774	0.540	4.530	-0.768	3.186	-0.756
92.6	2.184	0.666	3.276	0.450	3.372	-0.606	2.898	-0.696
90.6	1.848	0.606	2.700	0.360	3.360	-0.444	2.556	-0.600
88.6	1.470	0.486	2.076	0.282	2.640	-0.300	2.154	-0.474
86.6	1.056	0.342	1.464	1.210	1.890	-0.186	1.698	-0.336
84.6	0.696	0.198	0.894	0.156	1.164	-0.096	1.236	-0.216
82.6	0.474	0.138	0.636	0.096	0.756	-0.066	0.828	-0.138
80.6	0.282	0.090	0.402	0.054	0.402	-0.042	0.468	-0.072
78.6	0.138	0.048	0.210	0.012	0.168	-0.012	0.198	-0.036
76.6	0.042	0.018	0.078	0.000	0.030	0.006	0.048	-0.006
75.6	0.000	0.000	0.000	0.000	0.000	0.000	0.000	0.000

Casing	E		F		G		Remarks
Elev., ft.	North	East	North	East	North	East	
94.6	0.828		0,900		0.618		1:8 slope
92.6	0.738		0.762		0.546		
90.6	0.648		0.636		0.468		
88.6	0.540		0.510		0.378		*Minus sign indicates movement South or West
86.6	0.432		0.390		0.282		
84.6	0.336		0.282		0.192		
82.6	0.228		0.180		0.144		
80.6	0.132		0.102		0.084		
78.6	0.054		0.048		0.036		
76.6	0.018		0.018		0.006		
75.6	0.000		0.000		0.000		

TABLE B-14. SLOPE INDICATOR DATA, November 8, 1972

Casing Movement, North or East, inches

Casing	A		B		C		D	
Elev., ft.	North	East	North	East	North	East	North	East
94.6	2.880		3.990		5.442		4.116	
92.6	2.508		3.468		4.614		3.648	
90.6	2.118		2.868		3.786		3.126	
88.6	1.686		2.220		2.922		2.568	
86.6	1.230		0.578		2.064		2.004	
84.6	0.828		0.954		1.254		1.434	
82.6	0.570		0.684		0.816		0.948	
80.6	0.348		0.426		0.438		0.528	
78.6	0.174		0.216		0.180		0.222	
76.6	0.054		0.078		0.030		0.054	
75.6	0.000		0.000		0.000		0.000	

Casing	E		F		G		Remarks
Elev., ft.	North	East	North	East	North	East	
94.6	0.890		0.966		0.642		1:8 slope
92.6	0.798		0.828		0.564		
90.6	0.708		0.696		0.486		
88.6	0.600		0.570		0.390		
86.6	0.486		0.438		0.294		
84.6	0.372		0.312		0.192		
82.6	0.252		0.216		0.144		
80.6	0.138		0.126		0.084		
78.6	0.060		0.060		0.036		
76.6	0.018		0.024		0.006		
75.6	0.000		0.000		0.000		

TABLE B-15. SLOPE INDICATOR DATA, November 14, 1972

Casing Movement, North or East, inches

Casing	A		B		C		D	
Elev., ft.	North	East	North	East	North	East	North	East
94.6	3.054		4.146		5.490		4.800	
92.6	2.670		3.642		4.656		4.158	
90.6	2.262		3.042		3.870		3.504	
88.6	1.812		2.382		3.054		2.826	
86.6	1.332		1.722		2.214		2.154	
84.6	0.906		1.086		1.386		1.500	
82.6	0.624		0.762		0.948		1.020	
80.6	0.378		0.480		0.558		0.588	
78.6	0.186		0.246		0.270		0.264	
76.6	0.060		0.090		0.084		0.072	
75.6	0.000		0.000		0.000		0.000	

Casing	E		F		G		Remarks
Elev., ft.	North	East	North	East	North	East	
94.6	0.954		1.05		0.684		1:8 slope
92.6	0.852		0.900		0.612		
90.6	0.756		0.756		0.528		
88.6	0.648		0.618		0.426		
86.6	0.522		0.486		0.324		
84.6	0.408		0.354		0.216		
82.6	0.276		0.234		0.167		
80.6	0.156		0.144		0.096		
78.6	0.072		0.072		0.042		
76.6	0.024		0.024		0.006		
75.6	0.000		0.000		0.000		

TABLE B- 16. SLOPE INDICATOR DATA, November 21, 1972

Casing Movement, North or East*, inches

Casing	A		B		C		D	
Elev., ft.	North	East	North	East	North	East	North	East
94.6	3.108	0.786	4.158	0.594	5.508	-0.708	4.698	-1.236
92.6	2.730	0.756	3.660	0.528	4.698	-0.546	4.104	-1.050
90.6	2.328	0.690	3.072	0.444	3.924	-0.402	3.486	-0.858
88.6	1.872	0.558	2.424	0.360	3.126	-0.288	2.844	-0.660
86.6	1.380	0.402	1.758	0.276	2.292	-0.186	2.844	-0.462
84.6	0.948	0.240	1.116	0.198	1.452	-0.102	1.560	-0.294
82.6	0.654	0.180	0.780	0.114	1.002	-0.084	1.062	-0.192
80.6	0.402	0.114	0.486	0.054	0.594	-0.060	0.612	-0.102
78.6	0.198	0.060	0.246	0.018	0.282	-0.036	0.264	-0.048
76.6	0.066	0.024	0.090	0.000	0.078	-0.006	0.072	-0.012
75.6	0.000	0.000	0.000	0.000	0.000	0.000	0.000	0.000

Casing	E		F		G		Remarks
Elev., ft.	North	East	North	East	North	East	
94.6	1.002	0.276	1.044	-0.192	0.726	0.054	
92.6	0.900	0.312	0.900	-0.216	0.636	0.066	
90.6	0.798	0.318	0.768	-0.192	0.546	0.060	1:8 slope
88.6	0.678	0.282	0.642	-0.150	0.444	0.042	
86.6	0.552	0.228	0.504	-0.096	0.342	0.018	
84.6	0.420	0.162	0.366	-0.066	0.228	-0.006	
82.6	0.276	0.114	0.240	-0.042	0.168	0.000	*minus sign indicates movement south or west
80.6	0.162	0.054	0.144	-0.018	0.096	0.006	
78.6	0.072	0.018	0.072	-0.006	0.036	0.000	
76.6	0.018	0.000	0.030	0.000	0.000	0.000	
75.6	0.000	0.000	0.000	0.000	0.000	0.000	

TABLE B-17. SLOPE INDICATOR DATA, December 12, 1972

Casing movement, north or east*, inches

Casing	A		B		C		D	
Elev., ft.	North	East	North	East	North	East	North	East
94.6	3.384	0.828	4.302		5.616		4.644	-1.206
92.6	2.970	0.792	3.828		4.830		4.122	-1.044
90.6	2.562	0.708	3.270		4.080		3.576	-0.864
88.6	2.094	0.570	2.628		3.294		2.982	-0.672
86.6	1.572	0.408	1.950		2.454		2.352	-0.480
84.6	1.104	0.240	1.266		1.596		1.710	-0.312
82.6	0.768	0.174	0.882		1.110		1.176	-0.204
80.6	0.468	0.108	0.546		0.660		0.684	-0.114
78.6	0.228	0.054	0.276		0.318		0.300	-0.054
76.6	0.272	0.018	0.102		0.096		0.084	-0.012
75.6	0.000	0.000	0.000		0.000		0.000	0.000

Casing	E		F		G		Remarks
Elev., ft.	North	East	North	East	North	East	
94.6	1.134		1.134		0.864		*minus sign indicates movement south or west
92.6	1.014		0.984		0.762		
90.6	0.900		0.840		0.654		
88.6	0.780		0.702		0.534		
86.6	0.642		0.558		0.414		
84.6	0.492		0.408		0.294		
82.6	0.342		0.276		0.204		
80.6	0.198		0.168		0.114		
78.6	0.084		0.084		0.048		
76.6	0.024		0.030		0.012		
75.6	0.000		0.000		0.000		

TABLE B-18. SLOPE INDICATOR DATA, December 29, 1972

Casing Movement, North or East*, inches

Casing	A		B		C		D	
Elev., ft.	North	East	North	East	North	East	North	East
94.6	3.468	0.936	4.422		5.718		4.662	-1.242
92.6	3.090	0.888	3.948		4.914		4.176	-1.086
90.6	2.676	0.798	3.390		4.158		3.642	-0.912
88.6	2.202	0.642	2.748		3.372		3.072	-0.726
86.6	1.668	0.462	2.070		2.532		2.454	-0.528
84.6	1.182	0.204	1.380		1.680		1.812	-0.348
82.6	0.828	0.210	0.972		1.164		1.248	-0.228
80.6	0.510	0.138	0.606		0.690		0.726	-0.132
78.6	0.252	0.072	0.312		0.330		0.324	-0.066
76.6	0.090	0.030	0.114		0.102		0.096	-0.018
75.6	0.000	0.000	0.000		0.000		0.000	0.000

Casing	E		F		G		Remarks
Elev., ft.	North	East	North	East	North	East	
94.6	1.224		1.188		0.912		1:8 slope *Minus sign indicates movement South or West
92.6	1.092		1.020		0.786		
90.6	0.978		0.870		0.672		
88.6	0.846		0.732		0.552		
86.6	0.702		0.588		0.432		
84.6	0.540		0.438		0.312		
82.6	0.372		0.204		0.222		
80.6	0.216		0.180		0.126		
78.6	0.096		0.090		0.054		
76.6	0.030		0.036		0.012		
75.6	0.000		0.000		0.000		

TABLE B-19. SLOPE INDICATOR DATA, February 10, 1973

Casing Movement, North or East, inches

Casing	A		B		C		D	
Elev., ft.	North	East	North	East	North	East	North	East
94.6			4.440		5.934			
92.6			3.996		5.088			
90.6			3.486		4.302			
88.6			2.880		3.504			
86.6			2.214		2.670			
84.6			1.512		1.818			
82.6			1.056		0.284			
80.6			0.660		0.780			
78.6			0.336		0.396			
76.6			0.132		0.132			
75.6			0.000		0.000			

Casing	E		F		G		Remarks
Elev., ft.	North	East	North	East	North	East	
94.6	1.320		1.356		0.126		
92.6	1.170		1.170		0.888		
90.6	1.032		1.002		0.756		1:8 slope
88.6	0.888		0.846		0.624		
86.6	0.726		0.684		0.492		
84.6	0.558		0.522		0.360		
82.6	0.384		0.360		0.246		
80.6	0.216		0.228		0.132		
78.6	0.084		0.120		0.048		
76.6	0.024		0.048		0.000		
75.6	0.000		0.000		0.000		

TABLE B-20. SLOPE INDICATOR DATA, April 7, 1973

Casing Movement, North or East*, inches

Casing	A		B		C		D	
Elev., ft.	North	East	North	East	North	East	North	East
94.6	3.624	1.080	4.572	0.726	6.288	-0.588	4.770	-1.272
92.6	3.324	1.026	4.170	0.642	5.394	-0.480	4.338	-1.104
90.6	2.970	0.924	3.684	0.558	4.542	-0.366	3.852	-0.930
88.6	2.502	0.756	3.078	0.450	3.690	-0.276	3.300	-0.744
86.6	1.956	0.570	2.376	0.354	2.814	-0.198	2.694	-0.546
84.6	1.422	0.390	1.620	0.264	1.920	-0.108	2.064	-0.354
82.6	1.002	0.282	1.152	0.168	1.380	-0.090	1.446	-0.234
80.6	0.630	0.186	0.732	0.102	0.876	-0.066	0.876	-0.126
78.6	0.330	0.108	0.390	0.048	0.480	-0.030	0.426	-0.048
76.6	0.132	0.048	0.156	0.018	0.192	0.000	0.150	-0.006
75.6	0.000	0.000	0.000	0.000	0.000	0.000	0.000	0.000

Casing	E		F		G		Remarks
Elev., ft.	North	East	North	East	North	East	
94.6	1.452	0.282	1.458	-0.192	1.074	0.048	1:8 slope 10 ft water in trench *Minus sign indicates movement South or West
92.6	1.302	0.324	0.248	-0.228	0.942	0.072	
90.6	1.152	0.348	1.062	-0.228	0.804	0.072	
88.6	0.984	0.336	0.894	-0.192	0.654	0.060	
86.6	0.810	0.294	0.720	-0.126	0.516	0.030	
84.6	0.630	0.222	0.546	-0.078	0.396	0.006	
82.6	0.450	0.138	0.384	-0.048	0.258	-0.006	
80.6	0.270	0.066	0.246	-0.024	0.138	0.006	
78.6	0.120	0.024	0.132	-0.012	0.054	-0.006	
76.6	0.036	0.006	0.060	-0.006	0.006	-0.012	
75.6	0.000	0.000	0.000	0.000	0.000	0.000	

TABLE B-21. SLOPE INDICATOR DATA, June 14, 1973

Casing Movement, North East, inches

Casing	A		B		C		D	
Elev., ft.	North	East	North	East	North	East	North	East
94.6	3.054		3.876		5.628		4.182	
92.6	2.562		3.258		4.494		3.654	
90.6	2.082		2.652		3.528		3.114	
88.6	1.608		2.052		2.712		2.550	
86.6	1.134		1.452		1.974		1.962	
84.6	0.714		0.840		1.254		1.386	
82.6	0.462		0.582		0.966		1.002	
80.6	0.264		0.378		0.690		0.660	
78.6	0.132		0.222		0.480		0.378	
76.6	0.054		0.108		0.192		0.168	
75.6	0.000		0.000		0.000		0.000	

Casing	E		F		G		Remarks
Elev., ft.	North	East	North	East	North	East	
94.6	1.278		1.260		1.032		
92.6	1.116		1.056		0.894		
90.6	0.960		0.870		0.756		1:8 slope
88.6	0.804		0.720		0.606		
86.6	0.636		0.564		0.462		Readings taken about 2 months after trench filled with fresh sludge.
84.6	0.450		0.402		0.354		
82.6	0.318		0.300		0.216		
80.6	0.180		0.210		0.108		
78.6	0.078		0.126		0.048		
76.6	0.030		0.060		0.012		
75.6	0.000		0.000		0.000		

APPENDIX C

TABLE C-1. SETTLEMENT PLATE ELEVATIONS AT THE BOTTOM SAND BLANKET

Date	Plate Elevation, ft.							
mo-da-yr	G1-1	G2-1	G3-1	G4-1	G5-1	G6-1	G7-1	G8-1
8-1-72	78.27	78.05	77.71	77.43	77.65	77.92	78.26	77.72
9-11-72	78.27	78.04	77.70	77.42	77.65	77.91	78.26	77.71
9-25-72[a]	78.27	78.05	77.71	77.43	77.65	77.91	78.26	77.72
9-30-72[b]	78.25	78.04	77.70	77.41	77.64	77.90	78.25	77.70
10-3-72	78.27	78.04	77.66	77.42	77.65	77.89	78.25	77.71
10-5-72	78.25	78.03	77.66	77.40	77.64	77.89	78.24	77.69
10-7-72	78.25	78.02	77.68	77.41	77.62	77.88	78.22	77.70
10-10-72	78.27	78.03	77.70	77.42	77.65	77.90	78.25	77.71
10-13-72[c]	78.26	78.04	77.71	77.41	77.65	77.90	78.25	77.71
10-19-72	78.25	78.04	77.70	77.41	77.64	77.91	78.25	77.71
10-23-72	78.27	78.04	77.71	77.42	77.65	77.90	78.25	77.71
10-25-72[d]	78.26	78.04	77.70	77.41	77.63	77.88	78.24	77.70
10-26-72	78.26	78.04	77.70	77.40	77.64	77.89	78.24	77.70
11-1-72	78.27	78.05	77.71	77.40	77.65	77.88	78.25	77.71
11-13-72	-	-	-	77.40	77.64	77.87	-	77.70
11-8-72	78.27	78.05	77.70	77.40	77.64	77.87	78.25	77.71
11-14-72	78.26	78.04	77.70	77.40	77.64	77.87	78.25	77.69
11-21-72	78.26	78.05	77.70	77.40	77.64	77.87	78.25	77.71
12-12-72	78.26	78.04	77.70	77.40	77.65	77.87	78.25	77.71
12-29-72	-	-	-	77.38	77.63	77.87	-	77.70
2-10-73	78.25	78.05	77.70	77.38	77.64	77.87	78.25	77.70
4-7-73	78.26	78.05	77.71	77.39	77.64	77.87	78.25	77.70
6-14-73[e]	78.26	78.03	77.70	77.38	77.62	77.88	78.24	77.70

[a] Two days after test trench was dug and middle sand blanket drained.

[b] After six days rain.

[c] 3:4 slope completed.

[d] 1:8 slope completed.

[e] About two months after trench filled with fresh papermill sludge.

TABLE C-2. SETTLEMENT PLATE ELEVATIONS AT THE MIDDLE SAND BLANKET

Date	Plate Elevation, ft.							
mo-da-yr	G1-3	G2-3	G3-3	G4-3	G5-3	G6-3	G7-3	G8-3
8-1-72	85.61	85.87	85.54	85.69	85.67	85.71	85.69	85.51
9-11-72	85.60	85.85	85.52	85.67	86.65	85.69	85.67	85.48
9-25-72[a]	85.59	85.84	85.48	85.67	85.65	85.68	85.66	85.47
9-30-72[b]	85.58	85.82	85.49	85.63	85.63	85.65	85.63	85.44
10-3-72	85.57	85.82	85.51	85.64	85.60	85.66	85.64	85.45
10-5-72	85.57	85.51	85.48	85.63	85.61	85.64	85.63	85.44
10-7-72	85.56	85.81	85.49	85.62	85.61	85.64	85.63	85.44
10-10-72	85.57	85.82	85.49	85.64	85.62	85.65	85.64	85.46
10-13-72[c]	85.56	85.82	85.50	85.62	85.63	85.64	85.64	85.44
10-19-72	85.56	85.82	85.49	85.62	85.61	85.64	85.63	85.44
10-23-72	85.56	85.81	85.48	85.62	85.62	85.64	85.63	85.43
10-25-72[d]	85.55	85.80	85.47	85.59	85.60	85.61	85.62	85.42
10-26-72	85.55	85.80	85.47	85.58	85.60	85.60	85.61	85.42
11-1-72	85.55	85.80	85.48	85.58	85.60	85.58	85.62	85.42
11-3-72	-	-	-	85.57	85.60	85.57	-	85.39
11-8-72	85.54	85.80	85.47	85.58	85.60	85.57	85.62	85.40
11-14-72	85.53	85.78	85.46	85.58	85.59	85.56	85.61	85.39
11-21-72	85.53	85.79	85.46	85.56	85.59	85.57	95.61	85.39
12-12-72	85.52	85.76	85.45	85.56	85.58	85.54	85.59	85.37
12-29-72	-	-	-	85.56	85.56	85.53	-	85.36
2-10-73	85.48	85.74	85.41	85.54	85.55	85.52	85.57	85.34
4-7-73	85.45	85.74	85.39	85.55	85.54	85.51	85.55	85.33
6-14-73[e]	85.42	85.72	85.38	85.54	85.53	85.52	85.54	85.32

[a] Two days after test trench was dug and middle sand blanket drained.

[b] After six days rain.

[c] 3:4 slope completed.

[d] 1:8 slope completed.

[e] About two months after trench filled with fresh papermill sludge.

TABLE C-3. SETTLEMENT PLATE ELEVATIONS AT THE TOP SAND BLANKET

Date	Plate Elevation, ft.							
mo-da-yr	G1-5	G2-5	G3-5	G4-5	G5-5	G6-5	G7-5	G8-5
8-1-72	95.06	94.94	95.06	94.83	94.94	94.84	94.80	94.73
9-11-72	94.98	94.87	94.99	94.72	94.88	94.75	94.73	94.64
9-25-72[a]	94.95	94.84	94.95	94.68	94.80	94.72	94.70	94.63
9-30-72[b]	94.92	94.81	94.93	94.66	94.81	94.67	94.67	94.59
10-3-72	94.90	94.81	94.92	94.65	94.81	94.68	94.66	94.60
10-5-72	94.89	94.78	94.90	94.64	94.78	94.66	94.64	94.57
10-7-72	94.88	94.79	94.90	94.61	94.78	94.65	94.64	94.58
10-10-72	94.89	94.78	94.90	94.62	94.78	94.65	94.64	94.57
10-13-72[c]	94.87	94.78	94.90	94.59	94.77	94.63	94.63	94.56
10-19-72	94.85	94.75	94.86	94.56	94.75	94.60	94.60	94.53
10-23-72	94.82	94.74	94.85	94.54	94.75	94.58	94.60	94.51
10-25-72[d]	94.81	94.72	94.82	94.48	94.72	94.54	94.57	94.47
10-26-72	94.80	94.72	94.82	94.46	94.71	94.53	94.58	94.47
11-1-72	94.79	94.70	94.80	94.42	94.70	94.50	94.56	94.44
11-3-72	-	-	-	94.41	94.68	94.48	-	94.43
11-8-72	94.77	94.69	94.79	94.41	94.69	94.49	94.54	94.43
11-14-72	94.75	94.68	94.78	94.39	94.66	94.47	94.53	94.41
11-21-72	94.74	94.67	94.77	94.39	94.67	94.46	94.52	94.41
12-12-72	94.71	94.63	94.74	94.38	94.63	94.43	94.49	94.37
12-29-72	-	-	-	94.33	94.60	94.39	-	94.34
2-10-73	94.63	94.57	94.67	94.29	94.56	94.34	94.41	94.29
4-7-73	94.61	94.54	94.64	94.25	94.53	94.31	94.39	94.25
6-14-73[e]	94.58	94.53	94.62	94.24	94.53	94.31	94.38	94.25

[a] Two days after test trench was dug and middle sand blanket drained.

[b] After six days rain.

[c] 3:4 slope completed.

[d] 1:8 slope completed.

[e] About two months after trench filled with fresh papermill sludge.

TABLE C-4. SETTLEMENT PLATE ELEVATIONS AT THE MID-POINTS OF THE LOWER AND UPPER SLUDGE LAYERS

Date	Plate Elevations, ft.						
mo-da-yr	G5-2	G6-2	G7-2	G8-2	G5-4	G6-4	G7-4
8-1-72	81.36	81.53	81.88	80.88	90.30	90.18	89.95
9-11-72	81.35	81.51	81.88	80.86	90.28	90.14	89.91
9-25-72[a]	81.32	81.51	81.86	80.85	90.25	90.12	89.88
9-30-72[b]	81.31	81.48	81.85	80.83	90.22	90.06	89.88
10-3-72	81.32	81.51	81.87	80.82	90.21	90.08	89.87
10-5-72	81.27	81.48	81.86	80.83	90.20	90.07	89.86
10-7-72	81.31	81.48	81.85	80.81	90.19	90.06	89.85
10-10-72	81.33	81.50	81.86	80.83	90.20	90.06	89.85
10-13-72[c]	81.33	81.50	81.86	80.83	90.19	90.05	89.85
10-19-72	81.31	81.50	81.85	80.85	90.18	90.03	89.84
10-23-72	81.33	81.50	81.86	80.85	90.17	90.02	89.83
10-25-72[d]	81.31	81.48	81.85	80.82	90.16	89.99	89.82
10-26-72	81.32	81.46	81.85	80.82	90.14	90.00	89.82
11-1-72	81.32	81.45	81.85	80.83	-	89.98	89.82
11-3-72	81.31	81.42	-	80.81	90.14	89.98	-
11-8-72	81.32	81.46	81.84	80.83	90.14	89.96	89.80
11-14-72	81.32	81.48	81.84	80.82	90.13	89.95	89.79
11-21-72	81.31	81.47	81.85	80.83	90.12	89.84	89.78
12-12-72	81.30	81.45	81.84	80.83	90.11	89.92	89.86
12-29-72	81.30	81.46	-	80.78	90.08	89.89	-
2-10-73	81.28	81.45	81.82	80.81	90.05	89.86	89.70
4-7-73	81.29	81.45	81.81	80.81	90.03	89.84	89.69
6-14-73[e]	81.29	81.47	81.81	80.80	90.03	89.85	89.68

[a] Two days after test trench was dug and middle sand blanket drained.

[b] After six days rain.

[c] 3:4 slope completed.

[d] 1:8 slope completed.

[e] About two months after trench filled with fresh papermill sludge.

APPENDIX D

TABLE D-1. PORE WATER PRESSURES FOR THE LOWER AND UPPER 1/4 POINTS OF THE LOWER AND UPPER SLUDGE LAYERS

Date mo-da-yr	Time	Pore water pressure in psi for piezometer							
		G4-2	G5-2	G4-6	G5-6	G4-4	G5-4	G4-8	G5-8
8-1-72	-	-	1.90	-	2.00	-	3.10	-	0.25
9-11-72	-	3.55	2.00	2.10	1.77	2.25	3.15	0.35	0.05
9-19-72	-	3.60	-	1.30	-	2.30	-	0.40	-
9-25-72	-	2.80	1.75	1.70	1.22	1.95	2.85	-	0.10
9-30-72[a]	-	2.75	1.90	1.75	1.40	2.00	2.85	0.75	0.10
10-2-72	-	2.90	1.90	1.85	1.45	2.00	2.75	0.65	0.20
10-3-72	2 pm	2.85	1.95	1.75	1.50	2.00	2.75	0.40	0.25
10-3-72	6 pm	2.80	-	1.70	-	2.00	-	0.60	-
10-4-72	2 pm	2.85	1.95	1.75	1.50	2.00	2.75	0.75	0.25
10-4-72	6 pm	2.80	-	1.75	-	1.95	-	0.70	-
10-5-72	7 pm	2.75	-	1.80	-	2.00	-	0.45	-
10-7-72	9 am	2.65	1.75	1.80	1.50	1.85	2.75	0.25	0.10
10-7-72	2 pm	2.50	1.80	1.80	1.60	1.85	2.85	0.25	0.20
10-10-72	3 pm	2.40	1.40	1.75	1.10	1.65	2.50	0.20	0.15
10-11-72	7 pm	2.40	1.45	1.80	1.30	1.65	2.55	0.40	0.05
10-13-72[b]	7 pm	2.40	1.20	0.75	1.35	1.45	2.60	0.15	0.15
10-19-72	10 am	2.10	0.50	1.60	1.00	1.15	2.25	0.05	0.00
10-23-72	2 pm	2.05	0.10	1.25	1.30	1.20	2.50	2.00	0.05
10-24-72	10 am	1.70	0.25	1.05	1.20	1.10	2.30	0.00	0.00
10-24-72	5 pm	1.55	0.35	0.95	1.15	1.00	2.30	0.00	0.05
10-25-72[c]	11 am	-	-	-	-	0.90	2.30	0.00	0.00
10-25-72	7 pm	-	-	-	-	0.95	2.30	0.00	0.00
10-26-72	11 pm	1.90	0.20	0.85	1.15	0.95	2.30	0.00	0.05
10-28-72	12 noon	2.05	0.00	1.05	1.00	1.05	2.30	0.00	0.00
11-1-72	3 pm	1.50	0.15	1.30	1.00	1.15	2.35	0.15	0.00
11-2-72	3 pm	1.75	0.35	1.40	1.30	1.30	2.50	0.15	0.10
11-3-72	3 pm	1.85	0.20	1.20	1.15	1.10	2.30	0.30	0.00
11-8-72	2 pm	1.85	0.20	1.70	1.05	0.25	2.30	0.35	0.00
11-14-72	4 pm	1.75	0.40	1.75	1.05	1.40	2.30	0.20	0.05
11-21-72	2 pm	1.50	0.70	1.65	0.95	1.15	2.20	0.30	0.05
12-12-72	12 noon	0.85	0.65	1.20	0.85	1.05	2.10	0.35	0.00
12-29-72	3 pm	0.70	0.80	1.10	0.80	0.95	2.25	0.30	0.00
2-10-73	-	0.60	0.80	1.15	0.55	0.70	1.95	0.40	0.00
4-7-73[d]	-	1.10	1.25	1.05	0.95	0.85	1.95	0.40	0.00
6-14-73[e]	-	0.00	1.90	2.05	2.15	3.00	3.00	0.50	0.05

[a] After six days rain.

[b] 3:4 slope completed.

[c] 1:8 slope completed.

[d] Ten feet water in trench.

[e] Two months after trench filled with fresh papermill sludge.

TABLE D-2. PORE WATER PRESSURES FOR THE CENTER OF THE LOWER AND UPPER SLUDGE LAYERS

Date mo-dy-yr	Time	Pore water pressure in psi for piezometer							
		G4-3	G5-3	G6-3	G7-3	G4-7	G5-7	G6-7	G7-7
8-1-72	-	-	2.25	2.30	2.25	-	1.10	0.90	1.60
9-6-72	-	-	2.25	2.25	2.25	-	1.85[a]	0.90	1.60
9-11-72	-	2.95	2.30	2.45	2.35	1.30	1.25	1.00	1.70
9-19-72	-	2.70	-	-	-	1.35	-	-	-
9-25-72	-	2.00	2.15	2.30	2.10	1.20	-	0.85	1.40
9-30-72[b]		2.15	2.35	2.50	2.20	1.45	-	1.05	1.70
10-2-72	-	2.20	2.20	2.35	2.10	1.60	-	1.00	1.50
10-3-72	2 pm	2.15	2.20	2.40	2.20	1.60	-	1.00	1.50
10-3-72	6 pm	2.10	-	-	-	1.55	-	-	-
10-4-72	2 pm	2.10	2.25	2.40	2.20	1.50	-	1.00	1.65
10-4-72	6 pm	2.00	-	-	-	1.45	-	-	-
10-5-72	7 am	2.05	-	-	-	1.50	-	-	-
10-7-72	9 pm	1.75	2.25	2.40	2.25	1.45	-	1.00	1.45
10-7-72	2 pm	1.65	2.30	2.45	2.35	1.50	-	1.15	1.70
10-10-72	3 pm	1.45	2.00	2.10	2.05	1.20	0.75	0.75	1.30
10-11-72	7 pm	1.40	2.05	2.20	2.15	1.35	0.70	0.90	1.50
10-13-72[c]	7 pm	1.15	2.10	2.30	2.15	1.15	0.80	0.95	1.45
10-19-72	10 am	1.15	1.30	1.90	1.75	0.55	-	0.50	0.90
10-23-72	2 pm	1.30	1.75	2.10	2.15	0.45	0.80	0.60	1.30
10-24-72	10 am	1.15	1.55	2.05	2.00	0.55	0.55	0.45	1.20
10-24-72	5 pm	1.05	1.45	2.00	2.00	0.45	0.65	0.45	1.20
10-25-72[d]	11 am	1.00	1.50	2.00	2.00	0.35	0.50	0.45	1.15
10-25-72	7 pm	1.05	1.55	2.00	2.05	0.40	0.60	0.50	1.20
10-28-72	11 am	1.05	1.50	2.00	2.00	0.40	0.70	0.40	1.15
10-28-72	12 noon	1.20	1.55	2.05	1.80	-	0.65	0.30	1.00
11-1-72	3 pm	1.00	1.35	1.80	1.95	1.25	0.95	0.40	0.95
11-2-72	3 pm	1.10	1.70	2.10	2.15	1.35	1.55	0.70	1.35
11-3-72	3 pm	1.00	1.50	2.05	2.05	1.25	1.30	0.60	1.15
11-8-72	2 pm	1.20	1.35	1.80	1.85	1.30	0.65	0.55	1.10
11-14-72	4 pm	1.00	1.40	1.90	1.85	1.15	0.60	0.65	1.10
11-21-72	2 pm	1.15	1.30	1.85	1.80	1.25	0.50	0.45	0.85
12-12-72	12 noon	0.60	1.15	1.80	1.65	1.10	0.55	0.35	0.95
12-29-72	3 pm	0.35	1.30	1.95	1.90	0.90	0.40	0.35	1.00
2-10-73	-	0.15	0.90	1.70	1.60	1.10	0.30	0.20	0.40
4-7-73[e]	-	0.75	1.20	1.90	1.80	1.15	0.55	0.75	0.75
6-14-73[f]	-	2.75	2.15	2.40	2.15	1.65	1.05	1.45	2.00

[a] Drilling rig near G5-7 at time of reading.

[b] After six days rain.

[c] 3:4 slope completed.

[d] 1:8 slope completed.

[e] Ten feet water in trench.

[f] Two months after trench filled with fresh papermill sludge.

TABLE D-3. PORE WATER PRESSURES FOR THE LOWER AND MIDDLE SAND BLANKETS

Date mo-dy-yr	Time	Pore water pressure in psi for piezometer			
		G5-1	G7-1	G5-5	G7-5
8-1-72	-	0.30	0.30	1.50	1.10
9-11-72	-	0.50	0.35	1.90	1.50
9-19-72	-	-	0.35	-	-
9-25-72	-	0.32	-	0.55	0.45
9-30-72[a]	-	0.35	-	0.90	0.65
10-2-72	-	0.45	-	1.00	0.60
10-3-72	2 pm	0.32	-	1.00	0.70
10-3-72	6 pm	-	-	-	-
10-4-72	2 pm	0.10	-	1.05	0.60
10-4-72	6 pm	-	-	-	-
10-5-72	7 pm	-	-	-	-
10-7-72	9 am	0.20	0.15	0.70	0.40
10-7-72	2 pm	0.30	-	0.75	0.45
10-10-72	3 pm	0.35	-	0.55	-
10-11-72	7 pm	0.40	-	0.50	-
10-13-72[b]	7 pm	0.30	-	0.30	-
10-19-72	10 am	0.25	-	0.20	-
10-23-72	2 pm	0.40	-	0.25	-
10-24-72	10 am	0.00	-	0.35	-
10-24-72	5 pm	0.20	-	0.30	-
10-25-72[c]	11 am	0.10	-	0.30	-
10-25-72	7 pm	0.35	-	0.35	-
10-26-72	11 am	0.15	-	0.30	-
10-28-72	12 noon	0.20	-	0.25	-
11-1-72	3 pm	0.60	-	0.30	-
11-2-72	3 pm	0.55	-	0.35	-
11-3-72	3 pm	0.30	0.10	0.35	-
11-8-72	2 pm	0.30	-	0.30	-
11-14-72	4 pm	0.30	-	0.25	-
11-21-72	2 pm	0.20	-	0.35	-
12-12-72	12 noon	0.35	0.25	0.25	-
12-29-72	3 pm	0.40	-	0.15	-
2-6-73	-	0.40	0.00	0.00	
4-7-73[d]	-	0.51	0.00	0.20	-
6-14-73[e]	-	0.50	0.10	2.15	-

[a] After six days rain.

[b] 3:4 slope completed.

[c] 1:8 slope completed.

[d] Ten feet water in trench.

[e] Two months after trench filled with fresh papermill sludge.

APPENDIX E

TABLE E-1. TEMPERATURE DATA FOR THE PAPERMILL SLUDGE LANDFILL

Thermistor No. 1			2		3		4		5	
Elevation, ft. 95.43			93.43		91.43		89.43		87.43	
Date mo-da-yr	I[a]	T[b]	I	T	I	T	I	T	I	T
9- 6-72	2.16	26.0	malfunction		2.36	23.9	2.72	20.7	2.90	19.3
9-11-72	2.52	23.5			2.50	23.7	2.74	20.6	2.89	19.3
10- 7-72	2.81	20.0			2.53	22.4	2.71	20.8	2.86	19.6
10-19-72	3.33	16.3			2.71	20.8	2.75	20.5	2.82	20.0
11- 3-72	3.70	14.0			3.04	18.2	2.91	19.2	2.87	19.5
11-21-72	4.86	8.3			3.40	15.9	3.08	17.9	2.95	18.9
12-12-72	5.79	4.7			3.93	12.7	3.37	16.1	3.10	17.8
2-10-73	6.02	4.0			4.84	8.4	4.13	11.6	3.60	14.6
4- 7-73	4.76	8.8			4.55	9.6	4.35	10.6	3.97	12.4
6-14-73	2.52	23.5			3.55	15.0	3.95	12.6	3.94	12.7
Thermistor No. 6			7		8		9		0	
Elevation, ft. 85.43			83.43		81.43		69.43		77.43	
Date mo-da-yr	I	T	I	T	I	T	I	T	I	T
9- 6-72	3.10	17.8	3.10	17.8	3.19	17.2	3.28	16.0	3.48	15.4
9-11-72	3.09	17.9	3.12	17.7	3.24	16.8	3.35	16.2	3.50	15.3
10- 7-72	3.04	18.2	3.06	18.1	3.19	17.2	3.13	16.5	3.51	15.2
10-19-72	3.01	18.5	3.06	18.1	3.19	17.2	3.32	16.4	3.51	15.2
11- 3-72	3.02	18.4	3.07	18.0	3.21	17.1	3.34	16.3	3.51	15.2
11-21-72	3.03	18.3	3.06	18.1	3.20	17.2	3.33	16.3	3.53	15.0
12-12-72	3.10	17.8	3.08	17.9	3.19	17.2	3.33	16.3	3.54	15.0
2-10-73	3.39	15.9	3.28	16.6	3.28	16.6	3.35	16.2	3.55	14.9
4- 7-73	3.74	13.8	3.54	15.0	3.49	15.3	3.39	16.0	3.55	14.9
6-14-73	3.94	12.7	3.83	13.3	3.79	13.5	3.76	13.7	3.95	12.6

[a] Instrument reading (K - ohms)

[b] Temperature (degrees Centigrade)

APPENDIX F

TABLE F-1. VANE SHEAR STRENGTH DATA, September 7, 1972

Elevation (ft)	Undisturbed		Remolded	
	Torque (kg-cm)	Shear strength (T/m^2)	Torque (kg-cm)	Shear strength (T/m^2)
93.3	210	6.11	140	4.07
92.5	220	6.40	110	3.20
91.5	230	6.69	200	5.82
90.5	255	7.42	180	5.23
89.5	275	8.00	210	6.12
88.5	305	8.87	240	6.98
87.5	360	10.47	245	7.12
86.5	380	11.05	310	9.01
85.5	455	13.23	220	6.40
84.5	420	12.21	335	9.74
83.5	420	12.21	320	9.31
82.5	480	13.96	340	9.89
81.5	560	16.28	380	11.05
80.5	600	17.45	300	8.72
79.5	680	19.77	320	9.31
78.5	610	17.74	380	11.05

2-in. O. D. Acker vane; hole augered to within 6-in. of test depth using hollow stem augers; vane pushed to test depth and rotated 360-degrees for maximum torque; vane rotated 25-times before reading remolded maximum torque.

TABLE F-2. VANE SHEAR STRENGTH DATA, October 6, 1972

Elev. ft.	Undisturbed				Remolded			
	Vertical		Horizontal		Vertical		Horizontal	
	Torque kg-cm	Shear strength T/m^2	Torque kg-cm	Shear strength T/m^2	Torque kg-cm	Shear strength T/m^2	Torque kg-cm	Shear strength T/m^2
92. 0	310	6. 20	330	6. 60	120	2. 40	100	2. 00
90. 5	310	6. 20	320	6. 40	170	3. 40	140	2. 80
89. 9	280	5. 60	305	6. 10				
87. 9	330	6. 60	350	7. 00				
87. 5*	350	7. 00	395	7. 90	160	3. 20	180	3. 60
83. 4	440	8. 80	455	9. 10				
83. 4	440	8. 80	475	9. 50			255	5. 10

60. 0-mm diameter Geonor vane; tests conducted within 2-to 3-ft from 3:4 slope surface, 1- to 2-days after completion of slope excavation.

*Adjacent to block sample C.

TABLE F-3. DUTCH CONE PENETRATION RESULTS, September 7, 1972

Elevation (ft)	Average load (kg)	Cone resistance (kg/cm^2)
93.3	83.91	8.39
92.5	59.42	5.94
91.5	59.87	5.99
90.5	60.33	6.03
89.5	60.78	6.08
88.5	61.23	6.12
87.5	93.44	9.34
86.5	80.29	8.03
85.5	105.69	10.57
84.5	101.60	10.16
83.5	95.25	9.53
82.5	107.05	10.70
81.5	121.11	12.11
80.5	166.92	16.69
79.5	167.38	16.74
78.5	113.40	11.34

10-sq cm, 60-degree Dutch cone; hole augered to within 1-ft of test elevation with hollow stem auger; cone and casing pushed to test elevation; cone tip pushed 2-in, independently of casing, with average load recorded.

APPENDIX G

TABLE G-1. TOTAL PRESSURE CELL DATA

Total pressure cell No.	G7-1 Horizontal			G7-2 Vertical			G7-3 Vertical		
Date mo-da-yr	I[a]	W[b]	S[c]	I	W	S	I	W	S
9- 6-72	17.3	12.7	14.3	14.9	10.3	11.6	9.75	5.2	5.9
9-30-72	17.25	12.6	14.2	15.0	10.4	11.7	9.5	5.0	5.6
10- 7-72	17.25	12.6	14.2	15.0	10.4	11.7	8.5	4.0	4.5
10-19-72	17.25	12.6	14.2	15.75	11.1	12.6	8.9	4.4	4.9
11- 3-72	17.25	12.6	14.2	15.0	10.4	11.7	9.0	4.5	5.0
11-21-72	17.25	12.6	14.2	16.0	11.4	12.8	8.75	4.2	4.7
2-10-73	17.60	13.0	14.6	see note			9.40	4.9	5.5
4- 7-73	17.6	13.0	14.6				9.40	4.9	5.5
6-14-73	17.40	12.8	14.4				9.4	4.9	5.5

[a] Instrument reading.

[b] W - total pressure, water calibration, psi.

[c] S - total pressure, sand calibration, psi.

Cell G7-2 gave erratic data beginning about 12-15-71.

Piezometer G7-3 was located adjacent to the total pressure cells.

APPENDIX H

TABLE H-1. UNDISTURBED CONSOLIDATION DATA, RAPID LOAD INCREMENTS

Block B test No. 1 initial water content 237% initial void ratio 4.65 weight dry specimen 29.5 gms load applied every 25 minutes October 12, 1972		Block B test No. 2 initial water content 234% initial void ratio 4.65 weight dry specimen 29.5 gms load applied every 15 minutes October 17, 1972	
load kg/cm^2	dial reading in. x 10^{-4}	load kg/cm^2	dial reading in. x 10^{-4}
0	0	0	0
0.1	296	0.05	126
0.2	548	0.075	192
0.3	792	0.1	255
0.4	1002	0.15	409
0.6	1382	0.20	500
0.8	1714	0.25	649
1.0	1974	0.30	806
1.5	2450	0.35	919
2.0	2775	0.40	1025
3.0	3213	0.50	1226
4.5	3602	0.60	1396
		0.80	1712
		1.0	1959
		1.5	2422
		2.0	2733
		1.0	2654
		0.40	2427
		1.04	2554
		1.75	2727
		2.24	2893
		3.24	3240
		4.24	3513
		0.4	3000
		0.1	2638

TABLE H-1. UNDISTURBED CONSOLIDATION DATA, RAPID LOAD INCREMENTS (continued)

Block F test No. 1 initial water content 165% initial void ratio 3.50 weight dry specimen 39.4 gms load applied every 15 minutes November 9, 1972		Block F test No. 2 initial water content 168% initial void ratio 3.52 weight dry specimen 38.8 gms load applied every 15 minutes November 15, 1972	
load kg/cm^2	dial reading in. x 10^{-4}	load kg/cm^2	dial reading in. x 10^{-4}
0	0	0	0
0.05	65	0.05	58
0.10	132	0.1	121
0.20	261	0.2	233
0.30	408	0.3	357
0.40	517	0.4	449
0.50	607	0.5	536
0.60	707	0.6	615
0.70	816	0.7	699
0.80	919	0.8	796
1.0	1093	1.0	993
1.5	1497	1.5	1414
2.0	1838	2.0	1735
3.0	2272	3.0	2192
4.5	2691	4.5	2625
1.0	2412	1.0	2335
0.10	1904	0.10	1799

TABLE H-2. UNDISTURBED CONSOLIDATION DATA, SAMPLE B-3

Initial water content 230%
Weight dry specimen 30.4 gms
October 23, 1972

time min.	dial reading in. x 10^{-4}
load 0.05 kg/cm^2	
0.0	0
0.1	43
0.25	54
0.50	66
1.00	78
2.25	90
4.30	96
6.25	99
12.25	103
36.0	111
750.0	132
load 0.10 kg/cm^2	
0.0	0
0.10	32
0.25	45
0.50	60
1.00	78
2.25	99
4.00	111
6.50	120
9.00	125
12.25	130
100.0	158
700.0	185
load 0.20 kg/cm^2	
0.0	0
0.10	48
0.25	68
0.50	92
1.0	122
2.25	158
4.0	180
6.25	194
9.00	204
12.25	212
36.0	235
190.0	270
710.0	296
load 0.40 kg/cm^2	
0.0	0
0.1	74
0.25	107
0.50	145
1.00	195
2.25	259
4.00	300
6.25	329
9.00	350
12.25	364
16.0	373
36.0	405
100.0	443
720.0	514
load 0.80 kg/cm^2	
0.0	0
0.10	95
0.25	133
0.50	180
1.00	248
2.25	352
4.00	430
6.25	485
9.00	520
12.25	540
20.0	591
100.0	664
310.0	720
730.0	749
load 1.6 kg/cm^2	
0.0	0
0.1	93
0.25	133
0.50	178
1.00	245
2.25	351
4.00	431
6.25	488
12.25	559
24.0	620
50.0	655
100.0	690
720.0	780
load 3.2 kg/cm^2	
0.0	0
0.10	91
0.25	126
0.50	166
1.00	225
2.25	322
4.00	410
6.25	466
9.00	510
12.25	542
20.0	583
40.0	630
100.0	660
300.0	706
700.0	738
load 18 kg/cm^2	
0.0	0
720.0	-259
load 0.1 kg/cm^2	
0.0	0
375.0	-575

TABLE H-3. UNDISTURBED CONSOLIDATION DATA, SAMPLE B-4

Initial water content 196%
Weight dry specimen 34.7 gms
November 1, 1972

time min.	dial reading in. x 10^{-4}	time min.	dial reading in. x 10^{-4}	time min.	dial reading in. x 10^{-4}
load 0.05 kg/cm^2		load 0.4 kg/cm^2		load 1.6 kg/cm^2	
0.0	0	0.0	0	0.0	0
0.1	33	0.1	48	0.10	77
0.25	44	0.25	66	0.25	106
0.50	55	0.50	87	0.50	138
1.00	69	1.00	104	1.00	183
2.25	85	2.25	122	2.25	260
4.00	96	4.00	139	4.00	331
7.00	106	6.25	154	6.25	393
9.00	109	12.25	167	9.00	446
12.25	113	16.0	173	15.0	542
16.0	116	66.0	203	25.0	603
27.0	121	100.0	214	55.0	680
100.0	133	300.0	226	100.0	720
300.0	142	675.0	236	300.0	770
730.0	149	(bad load increment)		685.0	782
load 0.1 kg/cm^2		load 0.8 kg/cm^2		load 3.2 kg/cm^2	
0.0	0	0.0	0	0.0	0
0.10	12	0.1	100	0.10	72
0.25	20	0.25	140	0.25	44
0.50	27	0.50	185	0.50	132
1.00	38	1.00	256	1.00	170
2.25	52	2.25	352	2.25	239
4.00	65	4.00	429	4.00	298
6.25	75	6.50	506	6.25	350
9.00	81	9.00	553	9.00	397
16.0	90	12.25	602	15.0	464
30.0	98	16.0	638	25.0	520
100.0	115	25.0	693	55.0	588
710.0	138	54.0	765	100.0	623
		100.0	810	300.0	691
load 0.2 kg/cm^2		300.0	862	720.0	708
		735.0	758		
0.0	0			load 0.8 kg/cm^2	
0.1	22				
0.25	33			0.0	0
0.50	41			745.0	-228
1.00	65				
2.25	87			load 0.1 kg/cm^2	
4.00	100				
6.25	112			0.0	0
9.00	122			670.0	-503
15.0	133				
30.0	142				
100.00	153				
300.0	164				
775.0	173				

TABLE H-4. UNDISTURBED CONSOLIDATION DATA, SAMPLE F-3

Initial water content 170%
Weight dry specimen 39.0 gms
November 27, 1972

time min.	dial reading in. x 10^{-4}
load 0.05 kg/cm^2	
0.0	0
0.1	30
0.25	38
0.50	46
1.00	57
2.25	68
4.00	74
6.25	78
9.00	80
12.25	82
100.0	90
830.0	99
load 0.1 kg/cm^2	
0.0	0
0.1	18
0.25	23
0.50	29
1.00	36
2.25	45
4.00	50
6.25	54
9.00	56
100.0	73
600.0	86
load 0.2 kg/cm^2	
0.0	0
0.1	26
0.25	34
0.50	44
1.00	56
2.25	72
4.00	82
6.25	90
12.25	99
113.0	127
740.0	152
load 0.4 kg/cm^2	
0.0	0
0.1	45
0.25	61
0.50	80
1.00	107
2.25	141
4.00	165
6.25	180
9.00	190
12.25	198
32.0	218
100.0	242
700.0	281
load 0.8 kg/cm^2	
0.0	0
0.1	67
0.25	92
0.50	119
1.00	154
2.25	206
4.00	242
6.25	268
9.00	287
12.25	302
40.0	360
100.0	385
200.0	405
720.0	435
load 1.6 kg/cm^2	
0.0	0
0.1	75
0.25	102
0.50	134
1.00	182
2.35	258
4.00	325
6.25	379
9.00	423
12.25	451
20.0	500
40.0	545
100.0	597
300.0	650
730.0	683
load 3.2 kg/cm^2	
0.0	0
0.1	79
0.25	108
0.50	143
1.00	196
2.25	287
4.00	368
6.25	437
9.00	493
12.25	534
30.0	635
50.0	670
110.0	720
275.0	750
750.0	783
load 0.8 kg/cm^2	
0.0	0
660.0	-277
load 0.1 kg/cm^2	
0.0	0
650.0	-593

TABLE H-5. UNDISTURBED CONSOLIDATION DATA, SAMPLE F-4

Initial water content 163%
Weight dry specimen 40.1 gms
December 6, 1972

load 0.05 kg/cm^2

time min.	dial reading in. x 10^{-4}
0.0	0
0.1	28
0.25	34
0.50	40
1.00	47
2.25	57
4.00	63
6.25	67
9.00	70
12.25	71
16.0	73
175.0	82
710.0	87

load 0.1 kg/cm^2

time min.	dial reading in. x 10^{-4}
0.0	0
0.1	16
0.25	20
0.50	25
1.00	30
2.25	38
4.00	43
6.25	46
9.00	49
12.25	51
16.0	52
100.0	64
725.0	77

load 0.2 kg/cm^2

time min.	dial reading in. x 10^{-4}
0.0	0
0.1	23
0.25	29
0.50	36
1.00	45
2.25	58
4.00	67
6.25	73
9.00	78
16.0	84
67.0	99
360.0	117
710.0	127

load 0.4 kg/cm^2

time min.	dial reading in. x 10^{-4}
0.0	0
0.1	28
0.25	37
0.50	48
1.00	62
2.25	84
4.00	100
6.25	112
9.00	121
12.25	127
32.0	145
100.0	163
300.0	180
660.0	192

load 0.8 kg/cm^2

time min.	dial reading in. x 10^{-4}
0.0	0
0.1	70
0.25	90
0.50	113
1.00	146
2.25	198
4.00	239
6.25	267
9.00	291
12.25	309
32.0	350
100.0	391
300.0	421
740.0	446

load 1.6 kg/cm^2

time min.	dial reading in. x 10^{-4}
0.0	0
0.1	75
0.25	99
0.50	126
1.00	167
2.25	239
4.00	305
6.25	354
9.00	395
12.25	426
16.0	450
32.0	500
70.0	548
134.0	581
414.0	624
1200.0	668

load 3.2 kg/cm^2

time min.	dial reading in. x 10^{-4}
0.0	0
0.1	76
0.25	99
0.50	130
1.00	175
2.25	251
4.00	323
6.25	388
9.00	442
12.25	482
16.0	515
32.0	593
100.0	665
400.0	725
970.0	757

load 0.8 kg/cm^2

time min.	dial reading in. x 10^{-4}
0.0	0
430.0	-264

load 0.1 kg/cm^2

time min.	dial reading in. x 10^{-4}
0.0	0
930.0	-558

APPENDIX I

TABLE I-1. TRIAXIAL TEST DATA, SAMPLE U-1-10

Axial consolidation pressure = 0.703 kg/cm^2 with K_o = 1

σ_{1_f} = 3.146 kg/cm^2	Initial water content = 182.9%
σ_{3_f} = 2.109 kg/cm^2	Final water content = 116.2%
u_f = 2.123 kg/cm^2	Initial dry density = 25.91 pcf
A_f = 0.69	c_u = 0.519 kg/cm^2

Load (kg)	Displacement (cm)	Pore pressure (kg/cm^2)	Axial strain	$\bar{\sigma}_1$ (kg/cm^2)	$\bar{\sigma}_3$ (kg/cm^2)
0.0000	0.0000	1.4061	0.0000	0.7031	0.7031
3.4474	0.0737	1.5116	0.0124	1.0211	0.5976
4.3546	0.1473	1.7787	0.0248	0.8586	0.3304
4.5814	0.2256	1.8631	0.0380	0.7943	0.2461
5.2164	0.2972	1.9053	0.0501	0.8203	0.2039
5.4432	0.3734	1.9334	0.0629	0.8102	0.1758
5,8968	0.4470	1.9615	0.0753	0.8259	0.1476
6.3050	0.5207	1.9861	0.0877	0.8385	0.1230
6.3504	0.5944	2.0037	0.1001	0.8163	0.1055
6.8040	0.6706	2.0213	0.1130	0.8386	0.0879
7.2576	0.7442	2.0389	0.1254	0.8599	0.0703
7.6205	0.8179	2.0529	0.1378	0.8735	0.0562
8.1648	0.8941	2.0740	0.1506	0.8978	0.0352
8.7091	0.9677	2.0881	0.1630	0.9278	0.0211
9.1174	1.0414	2.1022	0.1754	0.9421	0.0070
9.8431	1.1176	2.1092	0.1883	0.9938	0.0000
10.4328	1.1913	2.1232	0.2007	1.0232	-0.0141

$\bar{\sigma}_1$ and $\bar{\sigma}_3$ equal the major and minor effective principal stresses, respectively. Failure taken at maximum deviator stress or at 20 percent axial strain.

TABLE I-3. TRIAXIAL TEST DATA, SAMPLE U-1-11

Axial consolidation pressure = 1.406 kg/cm^2 with K_o = 1

σ_{1_f}	=	4.479 kg/cm^2	Initial water content	=	200.0%
σ_{3_f}	=	2.812 kg/cm^2	Final water content	=	101.2%
u_f	=	2.714 kg/cm^2	Initial dry density	=	26.53 pcf
A_f	=	0.78	c_u = 0.833 kg/cm^2		

Load (kg)	Displacement (cm)	Pore pressure (kg/cm^2)	Axial strain	$\bar{\sigma}_1$ (kg/cm^2)	$\bar{\sigma}_3$ (kg/cm^2)
0.0000	0.0000	1.4061	0.0000	1.4062	1.4062
5.4432	0.0737	1.6241	0.0133	1.8385	1.1882
8.2555	0.1473	1.9264	0.0266	1.8589	0.8859
8.9813	0.2256	2.1092	0.0407	1.7463	0.7031
9.1627	0.2972	2.2146	0.0536	1.6476	0.5976
10.0699	0.3734	2.2920	0.673	1.6575	0.5203
10.8864	0.4470	2.3623	0.0806	1.6619	0.4500
11.5668	0.5207	2.4256	0.0939	1.6558	0.3867
11.9750	0.5944	2.4678	0.1071	1.6391	0.3445
12.7008	0.6706	2.5170	0.1209	1.6472	0.2953
13.5173	0.7442	2.5521	0.1342	1.6773	0.2601
14.0162	0.8179	2.5873	0.1474	1.6719	0.2250
14.6059	0.8941	2.6154	0.1612	1.6803	0.1969
15.4224	0.9677	2.6506	0.1745	1.7033	0.1617
16.3296	1.0414	2.6857	0.1877	1.7326	0.1266
17.2368	1.1176	2.7138	0.2015	1.7650	0.0984

$\bar{\sigma}_1$ and $\bar{\sigma}_3$ equal the major and minor effective principal stresses, respectively. Failure taken at maximum deviator stress or at 20 percent axial strain.

TABLE I-3. TRIAXIAL TEST DATA, SAMPLE U-1-12

Axial consolidation pressure = 2.109 kg/cm^2 with K_o = 1

σ_{1_f} = 5.919 kg/cm^2

σ_{3_f} = 3.515 kg/cm^2

u_f = 3.452 kg/cm^2

A_f = 0.85

Initial water content = 194.4%

Final water content = 94.3%

Initial dry density = 25.75 pcf

c_u = 1.265 kg/cm^2

Load (kg)	Displacement (cm)	Pore pressure (kg/cm^2)	Axial strain	$\bar{\sigma}_1$ (kg/cm^2)	$\bar{\sigma}_3$ (kg/cm^2)
0.0000	0.0000	1.4061	0.0000	2.1092	2.1092
7.2576	0.0737	1.6170	0.0147	2.7554	1.8983
10.7957	0.1473	1.9404	0.0294	2.8308	1.5749
12.2472	0.2256	2.2428	0.0450	2.6744	1.2726
13.6080	0.2972	2.4678	0.0592	2.5819	1.0476
14.6059	0.3734	2.6506	0.0744	2.4850	0.8648
15.7399	0.4470	2.7982	0.0891	2.4355	0.7171
16.6471	0.5207	2.9177	0.1038	2.3857	0.5976
17.7811	0.5944	3.0232	0.1185	2.3707	0.4922
18.9605	0.6706	3.1076	0.1337	2.3764	0.4078
19.9584	0.7442	3.1990	0.1484	2.3535	0.3164
21.3192	0.8179	3.2693	0.1630	2.3846	0.2461
22.5893	0.8941	3.3396	0.1782	2.4006	0.1758
23.6779	0.9677	3.3958	0.1929	2.4099	0.1195
25.3109	1.0414	3.4521	0.2076	2.4670	0.0633

$\bar{\sigma}_1$ and $\bar{\sigma}_3$ equal the major and minor effective principal stresses, respectively. Failure taken at maximum deviator stress or at 20 percent axial strain.

TABLE I-4. TRIAXIAL TEST DATA, SAMPLE U-1-13

Axial consolidation pressure = 3.515 kg/cm^2 with K_o = 1

σ_{1_f} = 8.768 kg/cm^2	Initial water content	=	180.2%
σ_{3_f} = 4.921 kg/cm^2	Final water content	=	84.2%
u_f = 4.668 kg/cm^2	Initial dry density	=	27.47 pcf
A_f = 0.85	c_u = 1.923 kg/cm^2		

Load (kg)	Displacement (cm)	Pore pressure (kg/cm^2)	Axial strain	$\overline{\sigma}_1$ (kg/cm^2)	$\overline{\sigma}_3$ (kg/cm^2)
0.0000	0.0000	1.4061	0.0000	3.5154	3.5154
15.4224	0.0762	2.0389	0.0157	4.7638	2.8826
18.8244	0.1524	2.6576	0.0314	4.5234	2.2639
20.8656	0.2286	3.0865	0.0471	4.2990	1.8350
22.7707	0.3048	3.4099	0.0628	4.1562	1.5116
24.4944	0.3810	3.6560	0.0785	4.0626	1.2655
26.3088	0.4572	3.8528	0.0943	4.0217	1.0687
27.7603	0.5334	4.0075	0.1100	3.9759	0.9140
29.2572	0.6096	4.1581	0.1257	3.9434	0.7734
30.9355	0.6858	4.2747	0.1414	3.9385	0.6468
31.8881	0.7620	4.3590	0.1571	3.8934	0.5625
34.8365	0.8382	4.4926	0.1728	4.0000	0.4289
36.7416	0.9144	4.5770	0.1885	4.0394	0.3445
39.0096	0.9906	4.6684	0.2042	4.1001	0.2531

$\overline{\sigma}_1$ and $\overline{\sigma}_3$ equal the major and minor effective principal stresses, respectively. Failure taken at maximum deviator stress or at 20 percent axial strain.

TABLE I-5. TRIAXIAL TEST DATA, SAMPLE U-2-21

Axial consolidation pressure = 3.515 kg/cm^2 with K_o = 1

σ_{1_f} = 9.086 kg/cm^2

σ_{3_f} = 4.921 kg/cm^2

u_f = 4.711 kg/cm^2

A_f = 0.79

Initial water content = 215.0%

Final water content = 94.2%

Initial dry density = 23.86 pcf

c_u = 2.082 kg/cm^2

Load (kg)	Displacement (cm)	Pore pressure (kg/cm^2)	Axial strain	$\bar{\sigma}_1$ (kg/cm^2)	$\bar{\sigma}_3$ (kg/cm^2)
0.0000	0.0000	1.4061	0.0000	3.5154	3.5154
15.1956	0.0762	1.9826	0.0156	4.9064	2.9389
19.0512	0.1524	2.6295	0.0311	4.7198	2.2920
21.3192	0.2286	3.1005	0.0467	4.4941	1.8210
23.5872	0.3048	3.4380	0.0622	4.3927	1.4835
25.4016	0.3810	3.6911	0.0778	4.3114	1.2304
26.9892	0.4572	3.8739	0.0934	4.2659	1.0476
28.4407	0.5334	4.0427	0.1089	4.2121	0.8789
30.1644	0.6096	4.1833	0.1245	4.2117	0.7382
31.7520	0.6858	4.3028	0.1401	4.2100	0.6187
33.5664	0.7620	4.4153	0.1556	4.2341	0.5062
35.2901	0.8382	4.4997	0.1712	4.2689	0.4218
37.1952	0.9144	4.6051	0.1867	4.2950	0.3164
39.6900	0.9906	4.7106	0.2023	4.3751	0.2109

$\bar{\sigma}_1$ and $\bar{\sigma}_3$ equal the major and minor effective principal stresses, respectively. Failure taken at maximum deviator stress or at 20 percent axial strain.

TABLE I-6. TRIAXIAL TEST DATA, SAMPLE U-3-1

Axial consolidation pressure = 0.703 kg/cm^2 with K_o = 1

σ_{1_f} = 3.017 kg/cm^2		Initial water content	= 310.0%
σ_{3_f} = 2.109 kg/cm^2		Final Water content	= 150.9%
u_f = 2.109 kg/cm^2		Initial dry density	= 18.94 pcf
A_f = 0.77		c_u = 0.454 kg/cm^2	

Load (kg)	Displacement (cm)	Pore pressure (kg/cm^2)	Axial strain	$\bar{\sigma}_1$ (kg/cm^2)	$\bar{\sigma}_3$ (kg/cm^2)
0.0000	0.0000	1.4061	0.0000	0.7031	0.7031
2.9484	0.0483	1.5678	0.0106	0.8242	0.5414
4.1278	0.1194	1.7014	0.0262	0.7975	0.4078
4.8989	0.1753	1.8139	0.0385	0.7520	0.2953
5.3525	0.2337	1.8842	0.0514	0.7173	0.2250
5.5339	0.2921	1.9053	0.0642	0.7060	0.2039
6.2143	0.3505	1.9545	0.0770	0.7108	0.1547
6.6679	0.4089	1.9721	0.0899	0.7256	0.1371
7.0308	0.4674	2.0037	0.1027	0.7172	0.1055
7.5298	0.5258	2.0389	0.1156	0.7161	0.0703
7.9380	0.5817	2.0459	0.1278	0.7346	0.0633
8.5277	0.6401	2.0730	0.1407	0.7456	0.0352
9.0720	0.6985	2.0811	0.1535	0.7727	0.0281
9.5256	0.7315	2.0951	0.1608	0.7892	0.0141
10.3421	0.8153	2.0986	0.1792	0.8337	0.0105
11.1132	0.8738	2.1057	0.1921	0.8742	0.0035
11.7029	0.9093	2.1092	0.1999	0.9080	0.0000
12.8369	0.9906	2.1092	0.2177	0.9737	0.0000

$\bar{\sigma}_1$ and $\bar{\sigma}_3$ equal the major and minor effective principal stresses, respectively. Failure taken at maximum deviator stress or at 20 percent axial strain.

TABLE I-7. TRIAXIAL TEST DATA, SAMPLE U-3-2

Axial consolidation pressure = 0.703 kg/cm^2 with K_o = 1

σ_{1_f} = 3.351 kg/cm^2		Initial water content	= 306.0%
σ_{3_f} = 2.109 kg/cm^2		Final water content	= 147.4%
u_f = 2.151 kg/cm^2		Initial dry density	= 18.39 pcf
A_f = 0.60		c_u = 0.621 kg/cm^2	

Load (kg)	Displacement (cm)	Pore pressure (kg/cm^2)	Axial strain	$\bar{\sigma}_1$ (kg/cm^2)	$\bar{\sigma}_3$ (kg/cm^2)
0.0000	0.0000	1.4061	0.0000	0.7031	0.7031
3.8556	0.0686	1.7506	0.0161	0.7349	0.3586
5.4432	0.1499	1.8701	0.0352	0.7600	0.2390
6.4411	0.2134	1.9475	0.0501	0.7686	0.1617
7.2576	0.2819	2.0037	0.0662	0.7777	0.1055
8.1648	0.3632	2.0459	0.0853	0.8041	0.0633
9.0720	0.4293	2.0775	0.1008	0.8408	0.0316
9.7524	0.4978	2.1057	0.1169	0.8578	0.0035
10.8864	0.5791	2.1232	0.1360	0.9190	-0.0141
11.5668	0.6375	2.1373	0.1497	0.9475	-0.0281
12.7008	0.7087	2.1443	0.1664	1.0150	-0.0352
14.2884	0.7798	2.1479	0.1832	1.1191	-0.0387
15.6492	0.8509	2.1514	0.1999	1.1999	-0.0422

$\bar{\sigma}_1$ and $\bar{\sigma}_3$ equal the major and minor effective principal stresses, respectively. Failure taken at maximum deviator stress or at 20 percent axial strain.

TABLE I-8. TRAIXIAL TEST DATA, SAMPLE U-3-3

Axial consolidation pressure = 1.406 kg/cm^2 with K_o = 1

σ_{1_f} = 5.781 kg/cm^2	Initial water content	=	276.2%
σ_{3_f} = 2.81 kg/cm^2	Final water content	=	118.8%
u_f = 2.755 kg/cm^2	Initial dry density	=	19.23 pcf
A_f = 0.45	c_u = 1.485 kg/cm^2		

Load (kg)	Displacement (cm)	Pore pressure (kg/cm^2)	Axial strain	$\bar{\sigma}_1$ (kg/cm^2)	$\bar{\sigma}_3$ (kg/cm^2)
0.0000	0.0000	1.4061	0.0000	1.4062	1.4062
8.6184	0.0584	1.8701	0.0135	1.9213	0.9421
12.2018	0.1168	2.2568	0.0270	1.9227	0.5554
14.5152	0.1753	2.3553	0.0406	2.0609	0.4570
16.2389	0.2337	2.4607	0.0541	2.1206	0.3515
17.6904	0.2921	2.5592	0.0676	2.1528	0.2531
18.9605	0.3480	2.6124	0.0805	2.1976	0.1898
20.4120	0.4064	2.6716	0.0941	2.2703	0.1406
21.7728	0.4648	2.7068	0.1076	2.3433	0.1055
23.5872	0.5232	2.7244	0.1211	2.4754	0.0879
24.9480	0.5817	2.7420	0.1346	2.5568	0.0703
26.3088	0.6401	2.7420	0.1481	2.6514	0.0703
28.1232	0.6960	2.7490	0.1611	2.7805	0.0633
29.4840	0.7569	2.7490	0.1752	2.8641	0.0633
30.8448	0.8153	2.7550	0.1887	2.9383	0.0562
32.2056	0.8611	2.7550	0.1993	3.0262	0.0562

$\bar{\sigma}_1$ and $\bar{\sigma}_3$ equal the major and minor effective principal stresses, respectively. Failure taken at maximum deviator stress or at 20 percent axial strain.

TABLE I-9. TRIAXIAL TEST DATA, SAMPLE U-3-5

Axial consolidation pressure = 3.515 kg/cm^2 with K_o = 1

σ_{1_f} = 7.966 kg/cm^2	Initial water content	=	255.0%
σ_{3_f} = 4.921 kg/cm^2	Final water content	=	97.5%
u_f = 4.696 kg/cm^2	Initial dry density	=	20.32 pcf
A_f = 1.08	c_u = 1.522 kg/cm^2		

Load (kg)	Displacement (cm)	Pore pressure (kg/cm^2)	Axial strain	$\bar{\sigma}_1$ (kg/cm^2)	$\bar{\sigma}_3$ (kg/cm^2)
0.0000	0.0000	1.4061	0.0000	3.5154	3.5154
7.3483	0.0762	2.0334	0.0163	3.9938	2.9881
10.7957	0.1524	2.4010	0.0327	3.9736	2.5205
12.6101	0.2261	2.8826	0.0485	3.7085	2.0389
14.3791	0.3023	3.2341	0.0648	3.5585	1.6874
15.4224	0.3759	3.5294	0.0806	3.3650	1.3921
16.4203	0.4572	3.7403	0.0980	3.2420	1.1812
18.1440	0.5258	3.9583	0.1127	3.2032	0.9632
19.2780	0.6020	4.1481	0.1291	3.1095	0.7734
21.0924	0.6756	4.2747	0.1449	3.1565	0.6468
22.9068	0.7544	4.4504	0.1617	3.1428	0.4711
23.8140	0.8280	4.5418	0.1775	3.1049	0.3797
26.3088	0.9017	4.6543	0.1933	3.2201	0.2672
27.2160	0.9144	4.6965	0.1961	3.2694	0.2250

$\bar{\sigma}_1$ and $\bar{\sigma}_3$ equal the major and minor effective principal stresses, respectively. Failure taken at maximum deviator stress or at 20 percent axial strain.

TABLE I-10. TRIAXIAL TEST DATA, SAMPLE U-3-6

Axial consolidation pressure = 2.109 kg/cm^2 with K_o = 1

σ_{1_f} = 4.531 kg/cm^2	Initial water content = 285.8%
σ_{3_f} = 2.109 kg/cm^2	Final water content = 122.8%
u_f = 2.189 kg/cm^2	Initial dry density = 18.63 pcf
A_f = 0.90	c_u = 1.200 kg/cm^2

Load (kg)	Displacement (cm)	Pore pressure (kg/cm^2)	Axial strain	$\bar{\sigma}_1$ (kg/cm^2)	$\bar{\sigma}_3$ (kg/cm^2)
0.0000	0.0000	1.4061	0.0000	2.1092	2.1092
7.1669	0.0737	1.7928	0.0158	2.6145	1.7225
9.8431	0.1473	2.1936	0.0316	2.5272	1.3218
11.5668	0.2256	2.4748	0.0483	2.4325	1.0406
12.7008	0.2972	2.6857	0.0637	2.3334	0.8296
13.6987	0.3734	2.8474	0.0800	2.2616	0.6679
15.0595	0.4470	2.9870	0.0958	2.2492	0.5273
16.2842	0.5207	3.1146	0.1146	2.2302	0.4008
17.2368	0.5944	3.2201	0.1274	2.1973	0.2953
18.2347	0.6706	3.3044	0.1437	2.1854	0.2109
19.5955	0.7442	3.3958	0.1595	2.2022	0.1195
20.8656	0.8179	3.4732	0.1753	2.2182	0.0422
22.4532	0.8941	3.5294	0.1916	2.2812	-0.0141
23.9501	0.9677	3.5716	0.2074	2.3442	-0.0562

$\bar{\sigma}_1$ and $\bar{\sigma}_3$ equal the major and minor effective principal stresses, respectively.
Failure taken at maximum deviator stress or at 20 percent axial strain.

TABLE I-11. TRIAXIAL TEST DATA, SAMPLE U-3-7

Axial consolidation pressure = 1.406 kg/cm^2 with K_o = 1

σ_{1_f} = 4.693 kg/cm^2	**Initial water content = 289.6%**
σ_{3_f} = 2.812 kg/cm^2	**Final water content = 127.0%**
u_f = 2.777 kg/cm^2	**Initial dry density = 18.30 pcf**
A_f = 0.73	**c_u = 0.940 kg/cm^2**

Load (kg)	Displacement (cm)	Pore pressure (kg/cm^2)	Axial strain	$\bar{\sigma}_1$ (kg/cm^2)	$\bar{\sigma}_3$ (kg/cm^2)
0.0000	0.0000	1.4061	0.0000	1.4062	1.4062
1.8144	0.0152	1.4413	0.0032	1.6028	1.3710
3.6288	0.0305	1.5116	0.0063	1.7627	1.3007
4.5360	0.0432	1.5819	0.0090	1.8064	1.2304
5.4432	0.0584	1.6522	0.0121	1.8491	1.1601
6.1236	0.0737	1.7225	0.0153	1.8624	1.0896
6.4411	0.0889	1.7858	0.0185	1.8366	1.0265
7.1215	0.1041	1.8385	0.0216	1.8666	0.9738
7.6205	0.1245	1.9264	0.0259	1.8371	0.8859
8.1648	0.1473	1.9861	0.0305	1.8403	0.8261
9.2988	0.2256	2.1584	0.0469	1.7895	0.6539
10.2060	0.2972	2.2779	0.0618	1.7613	0.5343
11.1132	0.3734	2.3693	0.0776	1.7564	0.4429
12.0204	0.4479	2.4467	0.0929	1.7627	0.3656
12.7462	0.5207	2.5170	0.1082	1.7518	0.2953
13.6080	0.5944	2.5731	0.1236	1.7673	0.2390
14.5152	0.6706	2.6295	0.1394	1.7835	0.1828
15.4224	0.7442	2.6787	0.1547	1.8041	0.1336
16.3296	0.8179	2.7138	0.1700	1.8351	0.0984
17.2368	0.8941	2.7560	0.1859	1.8544	0.0562
18.3708	0.9677	2.7771	0.2012	1.9156	0.0352

$\bar{\sigma}_1$ and $\bar{\sigma}_3$ equal the major and minor effective principal stresses, respectively. Failure taken at maximum deviator stress or at 20 percent axial strain.

TABLE I-12. TRIAXIAL TEST DATA, SAMPLE U-3-8

Axial consolidation pressure = 3.515 kg/cm^2 with K_o = 1

σ_{1_f} = 9.127 kg/cm^2

σ_{3_f} = 4.921 kg/cm^2

u_f = 4.844 kg/cm^2

A_f = 0.82

Initial water content = 293.6%

Final water content = 111.0%

Initial dry density = 18.22 pcf

c_u = 2.102 kg/cm^2

Load (kg)	Displacement (cm)	Pore pressure (kg/cm^2)	Axial strain	$\bar{\sigma}_1$ (kg/cm^2)	$\bar{\sigma}_3$ (kg/cm^2)
0.0000	0.0000	1.4061	0.0000	3.5154	3.5154
12.6554	0.0762	2.1443	0.0170	4.4755	2.7772
16.3750	0.1499	2.8474	0.0334	4.2349	2.0741
19.0512	0.2261	3.2622	0.0504	4.1290	1.6593
21.0924	0.2997	3.5716	0.0669	4.0370	1.3499
23.1336	0.3759	3.8317	0.0839	3.9832	1.0898
25.3109	0.4521	4.0637	0.1008	3.9648	0.8578
26.8531	0.5258	4.2325	0.1173	3.9251	0.6890
28.8036	0.6020	4.3942	0.1343	3.9316	0.5273
30.8448	0.6782	4.5629	0.1513	3.9326	0.3586
33.3396	0.7518	4.6965	0.1677	4.0133	0.2250
35.8344	0.8280	4.7668	0.1847	4.1433	0.1547
38.5560	0.9017	4.8442	0.2011	4.2824	0.0773

$\bar{\sigma}_1$ and $\bar{\sigma}_3$ equal the major and minor effective principal stresses, respectively. Failure taken at maximum deviator stress or at 20 percent axial strain.

TABLE I-13. TRIAXIAL TEST DATA, SAMPLE G-3

Axial consolidation pressure = 1.173 kg/cm^2 with K_o = 0.3

Angle between direction of compression and horizontal = 90 degrees

σ_{1_f} = 4.566 kg/cm^2	Initial water content = 159.1%
σ_{3_f} = 3.164 kg/cm^2	Final water content = 142.0%
u_f = 3.123 kg/cm^2	Initial dry density = 20.45 pcf
A_f = 0.45	c_u = 0.701 kg/cm^2

Load (kg)	Displacement (cm)	Pore pressure (kg/cm^2)	Axial strain	$\overline{\sigma}_1$ (kg/cm^2)	$\overline{\sigma}_3$ (kg/cm^2)
15.4200	0.0000	2.8123	0.0000	1.0641	0.3515
16.3296	0.0102	2.8264	0.0013	1.0913	0.3375
17.4636	0.0178	2.8615	0.0022	1.1077	0.3023
18.1440	0.0279	2.8756	0.0035	1.1240	0.2883
18.5976	0.0305	2.8826	0.0038	1.1375	0.2812
19.0512	0.0381	2.8896	0.0047	1.1506	0.2742
21.0099	0.0787	2.9178	0.0098	1.2260	0.2461
22.9975	0.1295	2.9529	0.0161	1.2568	0.2109
24.4944	0.1778	3.0513	0.0221	1.2196	0.1125
25.4016	0.2388	3.0738	0.0296	1.2292	0.0900
26.3088	0.2997	3.0935	0.0372	1.2411	0.0703
27.2160	0.3581	3.1090	0.0444	1.2568	0.0548
28.8036	0.4521	3.1287	0.0561	1.2917	0.0352
29.4840	0.5461	3.1391	0.0678	1.2950	0.0246
30.3912	0.6401	3.1463	0.0794	1.3107	0.0176
31.2984	0.7366	3.1484	0.0914	1.3298	0.0155
31.8427	0.8331	3.1477	0.1034	1.3358	0.0162
33.5664	1.0287	3.1392	0.1276	1.3780	0.0246
35.3808	1.2217	3.1287	0.1516	1.4225	0.0352
36.2880	1.3208	3.1231	0.1639	1.4431	0.0408

$\overline{\sigma}_1$ and $\overline{\sigma}_3$ equal the major and minor effective principal stresses, respectively. Failure taken at maximum deviator stress or at 20 percent axial strain.

TABLE I-14. TRIAXIAL TEST DATA, SAMPLE G-4

Axial consolidation pressure = 1.173 kg/cm^2 with K_o = 0.3

Angle between direction of compression and horizontal = 90 degrees

σ_{1_f} = 4.983 kg/cm^2	Initial water content = 157.7%
σ_{3_f} = 3.164 kg/cm^2	Final water content = 134.0%
u_f = 3.155 kg/cm^2	Initial dry density = 24.58 pcf
A_f = 0.30	c_u = 0.910 kg/cm^2

Load (kg)	Displacement (cm)	Pore pressure (kg/cm^2)	Axial strain	$\bar{\sigma}_1$ (kg/cm^2)	$\bar{\sigma}_3$ (kg/cm^2)
15.6500	0.0000	2.8123	0.0000	1.0333	0.3515
15.6492	0.0102	2.8123	0.0010	1.0327	0.3515
17.6904	0.0203	2.8404	0.0021	1.0928	0.3234
19.9584	0.0381	2.8756	0.0039	1.1547	0.2883
21.5460	0.0559	2.8932	0.0057	1.2043	0.2707
22.4532	0.0737	2.9079	0.0075	1.2271	0.2559
25.8552	0.1676	2.9599	0.0171	1.3113	0.2039
27.6696	0.2616	2.9965	0.0268	1.3409	0.1673
29.1211	0.3556	3.0303	0.0364	1.3565	0.1336
30.7541	0.4521	3.0584	0.0462	1.3837	0.1055
31.7520	0.5512	3.0795	0.0564	1.3901	0.0844
32.8860	0.6477	3.0978	0.0662	1.4043	0.0661
34.3375	0.7442	3.1090	0.0761	1.4374	0.0548
35.3808	0.8407	3.1202	0.0860	1.4529	0.0436
36.5148	0.9373	3.1273	0.0958	1.4753	0.0366
37.6488	1.0363	3.1322	0.1060	1.4985	0.0316
38.9642	1.1328	3.1371	0.1159	1.5280	0.0267
41.6405	1.4275	3.1427	0.1460	1.5709	0.0211
44.4528	1.5240	3.1484	0.1559	1.6508	0.0155
47.6280	1.7221	3.1498	0.1761	1.7241	0.0141
50.8032	1.9202	3.1533	0.1964	1.7898	0.0105
52.6176	2.0193	3.1547	0.2065	1.8287	0.0091

$\bar{\sigma}_1$ and $\bar{\sigma}_3$ equal the major and minor effective principal stresses, respectively.

Failure taken at maximum deviator stress or at 20 percent axial strain.

TABLE I-15. TRIAXIAL TEST DATA, SAMPLE G-5

Axial consolidation pressure = 1.173 kg/cm^2 with K_o = 0.3

Angle between direction of compression and horizontal = 90 degrees

σ_{1_f} = 5.073 kg/cm^2

σ_{3_f} = 3.164 kg/cm^2

u_f = 3.149 kg/cm^2

A_f = 0.30

Initial water content = 153.7%

Final water content = 130.0%

Initial dry density = 21.95 pcf

c_u = 0.954 kg/cm^2

Load (kg)	Displacement (cm)	Pore pressure (kg/cm^2)	Axial strain	$\bar{\sigma}_1$ (kg/cm^2)	$\bar{\sigma}_3$ (kg/cm^2)
15.6500	0.0000	2.8123	0.0000	1.1543	0.3515
20.8656	0.0305	2.8791	0.0032	1.3532	0.2847
23.6779	0.0864	2.9389	0.0092	1.4303	0.2250
25.4016	0.1372	2.9726	0.0146	1.4772	0.1912
26.5356	0.1905	2.9965	0.0203	1.5030	0.1673
27.3067	0.2388	3.0162	0.0254	1.5149	0.1476
30.7541	0.4978	3.0809	0.0530	1.5793	0.0830
33.4757	0.7518	3.1153	0.0800	1.6308	0.0485
36.2880	1.0084	3.1322	0.1073	1.6959	0.0316
39.2364	1.2824	3.1406	0.1343	1.7682	0.0232
42.6384	1.5215	3.1442	0.1619	1.8557	0.0197
45.8136	1.7755	3.1491	0.1889	1.9239	0.0148
45.2693	2.0295	3.1385	0.2159	1.8489	0.0253

$\bar{\sigma}_1$ and $\bar{\sigma}_3$ equal the major and minor effective principal stresses, respectively. Failure taken at maximum deviator stress or at 20 percent axial strain.

TABLE I-16. TRIAXIAL TEST DATA, SAMPLE G-6

Axial consolidation pressure = 2.343 kg/cm^2 with K_o = 0.3

Angle between direction of compression and horizontal = 90 degrees

σ_{1_f}	= 7.694 kg/cm^2	Initial water content	= 157.2%
σ_{3_f}	= 3.504 kg/cm^2	Final water content	= 115.0%
u_f	= 3.469 kg/cm^2	Initial dry density	= 23.53 pcf
A_f	= 0.24	c_u	= 2.095 kg/cm^2

Load (kg)	Displacement (cm)	Pore pressure (kg/cm^2)	Axial strain	$\bar{\sigma}_1$ (kg/cm^2)	$\bar{\sigma}_3$ (kg/cm^2)
33.5680	0.0000	2.8123	0.0000	2.1508	0.7030
49.4424	0.0406	3.0303	0.0052	2.6070	0.4851
55.3392	0.0914	3.1709	0.0117	2.7039	0.3445
58.5144	0.1372	3.2412	0.0176	2.7542	0.2742
60.7824	0.1905	3.2904	0.0244	2.7832	0.2250
62.5968	0.2438	3.3291	0.0313	2.8024	0.1863
70.7616	0.5029	3.4155	0.0645	2.9557	0.0998
79.3800	0.7366	3.4451	0.0945	3.1714	0.0703
86.1840	0.9601	3.4556	0.1231	3.3201	0.0598
92.0808	1.1862	3.4605	0.1521	3.4231	0.0548
114.3072	1.4326	3.4662	0.1837	4.0747	0.0492
123.8328	1.6891	3.4732	0.2166	4.2274	0.0422

$\bar{\sigma}_1$ and $\bar{\sigma}_3$ equal the major and minor effective principal stresses, respectively.
Failure taken at maximum deviator stress or at 20 percent axial strain.

TABLE I-17. TRIAXIAL TEST DATA, SAMPLE G-7

Unconfined compression test

Angle between direction of compression and horizontal = 90 degrees

σ_{1_f} = 0.637 kg/cm^2

σ_{3_f} = 0 kg/cm^2

c_u = 0.318 kg/cm^2

Initial water content = 158.6%

Final water content = 158.6%

Initial dry density = 27.52 pcf

Load (kg)	Displacement (cm)	Pore pressure (kg/cm^2)	Axial strain	σ_1 (kg/cm^2)	σ_3 (kg/cm^2)
0.0000	0.0000	--	0.0000	0.0000	0.0000
2.1773	0.0457		0.0036	0.1062	
3.1752	0.0914		0.0073	0.1543	
3.9917	0.1321		0.0105	0.1899	
4.8989	0.1829		0.0145	0.2293	
5.6246	0.2337		0.0185	0.2632	
8.6184	0.4851		0.0385	0.3916	
10.9318	0.7391		0.0587	0.4896	
12.6101	0.9957		0.0790	0.5544	
13.5173	1.2522		0.0994	0.5818	
13.6987	1.5062		0.1196	0.5763	
13.6987	1.7602		0.1397	0.5698	
13.5173	1.9990		0.1587	0.5567	
13.1544	2.2327		0.1772	0.5298	
15.6492	2.4663		0.1958	0.6160	
16.3296	2.5603		0.2032	0.6368	

σ_1 and σ_3 equal the major and minor total principal stresses, respectively. Failure taken at maximum deviator stress or at 20 percent axial strain.

TABLE I-18. TRIAXIAL TEST DATA, SAMPLE G-8

Unconfined compression test

Angle between direction of compression and horizontal = 90 degrees

σ_{1_f} = 0.644 kg/cm^2

σ_{3_f} = 0 kg/cm^2

c_u = 0.322 kg/cm^2

Initial water content = 158.6%

Final water content = 158.6%

Initial dry density = 24.15 pcf

Load (kg)	Displacement (cm)	Pore pressure (kg/cm^2)	Axial strain	σ_1 (kg/cm^2)	σ_3 (kg/cm^2)
0.0000	0.0000	--	0.0000	0.0000	0.0000
2.1773	0.457		0.0038	0.1128	
2.9484	0.0940		0.0079	0.1520	
3.7422	0.1321		0.0111	0.1923	
4.3546	0.1829		0.0153	0.2228	
5.0803	0.2337		0.0196	0.2568	
8.4823	0.4851		0.0406	0.4229	
10.8864	0.7391		0.0619	0.5307	
12.6554	0.9957		0.0833	0.6028	
13.8348	1.2522		0.1048	0.6435	
13.5173	1.5062		0.1261	0.6138	
9.8885	1.7602		0.1473	0.4381	
10.4328	1.9990		0.1673	0.4514	
9.0720	2.2327		0.1869	0.3833	
9.2988	2.4663		0.2064	0.3834	

σ_1 and σ_3 equal the major and minor total principal stresses, respectively. Failure taken at maximum deviator stress or at 20 percent axial strain.

TABLE I-19. TRIAXIAL TEST DATA, SAMPLE G-9

Axial consolidation pressure = 0.696 kg/cm^2 with K_o = 0.3

Angle between direction of compression and horizontal = 90 degrees

σ_{1_f} = 3.992 kg/cm^2 Initial water content = 157.2%

σ_{3_f} = 3.023 kg/cm^2 Final water content = 153.0%

u_f = 3.002 kg/cm^2 Initial dry density = 26.92 pcf

A_f = 0.40 c_u = 0.484 kg/cm^2

Load (kg)	Displacement (cm)	Pore pressure (kg/cm^2)	Axial strain	$\bar{\sigma}_1$ (kg/cm^2)	$\bar{\sigma}_3$ (kg/cm^2)
9.9547	0.0000	2.8123	0.0000	0.6943	0.2109
12.9276	0.0508	2.8756	0.0041	0.7986	0.1476
13.8348	0.0965	2.8967	0.0077	0.8206	0.1266
14.5152	0.1321	2.9107	0.0106	0.8386	0.1125
14.9688	0.1905	2.9220	0.0153	0.8465	0.1012
15.2863	0.2388	2.9318	0.0191	0.8494	0.0914
16.7832	0.4928	2.9607	0.0395	0.8776	0.0626
18.0533	0.7442	2.9782	0.0596	0.9033	0.0450
19.0966	1.0058	2.9895	0.0806	0.9214	0.0337
20.4120	1.2649	2.9986	0.1013	0.9520	0.0246
21.3192	1.5240	3.0021	0.1221	0.9673	0.0211
22.2264	1.7831	3.0028	0.1428	0.9836	0.0204
22.9068	2.0422	3.0021	0.1636	0.9897	0.0211
23.4058	2.2911	2.9881	0.1835	1.0013	0.0352
23.6779	2.5425	0.29670	0.2037	1.0095	0.0562

$\bar{\sigma}_1$ and $\bar{\sigma}_3$ equal the major and minor effective principal stresses, respectively. Failure taken at maximum deviator stress or at 20 percent axial strain.

TABLE I-20. TRIAXIAL TEST DATA, SAMPLE G-10

Axial consolidation pressure = 0.703 kg/cm^2 with K_o = 1.0

Angle between direction of compression and horizontal = 0 degrees

σ_{1_f} = 4.413 kg/cm^2	Initial water content	=	157.0%
σ_{3_f} = 3.515 kg/cm^2	Final water content	=	145.0%
u_f = 3.325 kg/cm^2	Initial dry density	=	22.53 pcf
A_f = 0.57	c_u = 0.449 kg/cm^2		

Load (kg)	Displacement (cm)	Pore pressure (kg/cm^2)	Axial strain	$\bar{\sigma}_1$ (kg/cm^2)	$\bar{\sigma}_3$ (kg/cm^2)
0.0000	0.0000	2.8123	0.0000	0.7030	0.7030
4.0824	0.0330	2.9529	0.0030	0.7985	0.5625
6.4411	0.0864	3.0162	0.0079	0.8698	0.4992
7.9380	0.1372	3.0549	0.0125	0.9151	0.4605
8.8452	0.1880	3.0830	0.0171	0.9366	0.4324
9.6163	0.2388	3.1076	0.0218	0.9533	0.4078
12.2472	0.5004	3.1849	0.0456	1.0083	0.3304
13.6080	0.7620	3.2271	0.0695	1.0226	0.2883
14.7420	1.0211	3.2552	0.0931	1.0355	0.2601
15.8760	1.2802	3.2763	0.1167	1.0523	0.2390
16.8739	1.5392	3.2974	0.1404	1.0592	0.2180
17.9172	1.7958	3.3150	0.1637	1.0693	0.2004
19.0512	2.0549	3.3255	0.1874	1.0877	0.1898
19.2780	2.1590	3.3326	0.1969	1.0807	0.1828

$\bar{\sigma}_1$ and $\bar{\sigma}_3$ equal the major and minor effective principal stresses, respectively. Failure taken at maximum deviator stress or at 20 percent axial strain.

TABLE I-21. TRIAXIAL TEST DATA, SAMPLE G-11

Axial consolidation pressure = 2.109 kg/cm^2 with K_o = 1.0

Angle between direction of compression and horizontal = 0 degrees

σ_{1_f} = 7.151 kg/cm^2 Initial water content = 160.0%

σ_{3_f} = 4.920 kg/cm^2 Final water content = 114.0%

u_f = 4.492 kg/cm^2 Initial dry density = 23.74 pcf

A_f = 0.75 c_u = 1.115 kg/cm^2

Load (kg)	Displacement (cm)	Pore pressure (kg/cm^2)	Axial strain	$\bar{\sigma}_1$ (kg/cm^2)	$\bar{\sigma}_3$ (kg/cm^2)
0.0000	0.0000	2.8123	0.0000	2.1092	2.1092
12.7008	0.0533	3.0935	0.0047	2.6795	1.8280
16.3296	0.0183	3.3045	0.0072	2.7091	1.6171
19.0512	0.1600	3.4802	0.0141	2.7064	1.4413
20.8656	0.2108	3.5857	0.0186	2.7151	1.3359
22.5893	0.2616	3.6912	0.0231	2.7168	1.2304
27.2160	0.5232	3.9794	0.0462	2.6905	0.9421
30.3912	0.7849	4.1411	0.0694	2.6855	0.7804
32.2056	1.0465	4.2325	0.0925	2.6577	0.6890
34.2468	1.3081	4.2888	0.1156	2.6729	0.6328
36.0612	1.5697	4.3591	0.1387	2.6545	0.5625
37.8756	1.8313	4.4153	0.1618	2.6445	0.5062
39.9168	2.0930	4.4645	0.1849	216484	0.4570
42.1848	2.3520	4.5067	0.2078	2.6657	0.4148

$\bar{\sigma}_1$ and $\bar{\sigma}_3$ equal the major and minor effective principal stresses, respectively. Failure taken at maximum deviator stress or at 20 percent axial strain.

TABLE I-22. TRIAXIAL TEST DATA, SAMPLE G-12

Unconfined compression test

Angle between direction of compression and horizontal = 0 degrees

σ_{1_f} = 0.404 kg/cm^2 Initial water content = 158.6%

σ_{3_f} = 0 kg/cm^2 Final water content = 158.6%

c_u = 0.202 kg/cm^2 Initial dry density = 19.92 pcf

Load (kg)	Displacement (cm)	Pore pressure (kg/cm^2)	Axial strain	σ_1 (kg/cm^2)	σ_3 (kg/cm^2)
0.0000	0.0000	--	0.0000	0.0000	0.0000
1.9958	0.0406		0.0043	0.0973	
3.0391	0.0965		0.0103	0.1473	
3.6742	0.1473		0.0157	0.1771	
4.3092	0.1905		0.0203	0.2067	
4.7628	0.2388		0.0254	0.2272	
6.8040	0.4928		0.0524	0.3156	
8.0741	0.7442		0.0792	0.3639	
8.9359	1.0033		0.1068	0.3907	
9.5256	1.2624		0.1343	0.4036	
9.5256	1.5189		0.1616	0.3909	
8.7091	1.7780		0.1892	0.3456	
7.4844	1.9329		0.2057	0.2910	

σ_1 and σ_3 equal the major and minor total principal stresses, respectively.
Failure taken at maximum deviator stress or at 20 percent axial strain.

TABLE I-23. TRIAXIAL TEST DATA, SAMPLE G-20

Axial consolidation pressure = 2.341 kg/cm^2 with K_o = 0.3

Undrained test with σ_1 constant and σ_3 decreasing.

Initial water content = 159.0%

Final water content = 122.0%

Initial dry density = 24.37 pcf

σ_1 (kg/cm^2)	σ_3 (kg/cm^2)	pore pressure (kg/cm^2)	Axial strain	$\bar{\sigma}_1$ (kg/cm^2)	$\bar{\sigma}_3$ (kg/cm^2)
5.135	3.5154	2.8123	0.000	2.3412	0.7031
5.1535	3.4893	2.8123	0.001	2.3412	0.6770
5.1535	3.4429	2.8123	0.001	2.3412	0.6306
5.1535	3.3965	2.7947	0.001	2.3588	0.6018
5.1535	3.3501	2.7772	0.002	2.3763	0.5729
5.1535	3.2580	2.7420	0.003	2.4115	0.5160
5.1535	3.1666	2.7068	0.005	2.4467	0.4598
5.1535	3.0745	2.6506	0.006	2.5029	0.4239
5.1535	2.9986	2.7420	0.035	2.4115	0.2566
5.1535	2.9185	2.7772	0.048	2.3763	0.1413
5.1535	2.8362	2.7772	0.057	2.3763	0.0590
5.1535	2.8158	2.7596	0.085	2.3939	0.0562
5.2027	2.8123	2.8123[a]	0.087	2.3904	0.0000
5.2630[b]	2.8123	2.8123	0.091	2.4507	0
5.3504[b]	2.8123	2.8123	0.094	2.5381	0
5.5051[b]	2.8123	2.8123	0.127	2.6928	0
5.5683[b]	2.8123	2.8123	0.136	2.7560	0

[a] Pore pressure increased to initial backpressure.

[b] Small increases in axial stress.

Deformation rate approximately zero when test was terminated.

TABLE I-24. TRIAXIAL TEST DATA, SAMPLE G-21

Axial consolidation pressure = 0.703 kg/cm^2 with K_o = 0.3

Undrained test with σ_1 constant and σ_3 decreasing.

Initial water content =

Final water content = 135.0%

Initial dry density = 31.26 pcf

σ_1 (kg/cm^2)	σ_3 (kg/cm^2)	pore pressure (kg/cm^2)	axial strain	$\bar{\sigma}_1$ (kg/cm^2)	$\bar{\sigma}_3$ (kg/cm^2)
3.5153	3.0232	2.8123	0.000	0.7030	0.2109
3.5153	2.9628	2,7807	0.003	0.7346	0.1821
3.5153	2.9121	2.7561	0.007	0.7592	0.1560
3.5153	2.8622	2.7279	0.009	0.7874	0.1343
3.5153	2,8158	2.7139	0.024	0.8014	0.1019
3.5153	2.8123	2.8123[a]	0.025	0.7030	0.0000
3.5153	2.8123	2.8123[a]	0.101	0.7030	0.0000

---

[a] Pore pressure increased to initial backpressure.

Deformation rate approximately zero when test was terminated.

TABLE I-25. TRIAXIAL TEST DATA, SAMPLE C-2

Unconfined compression test

Angle between direction of compression and horizontal = 90 degrees

σ_{1_f} = 0.268 kg/cm^2	Initial water content = 162%
σ_{3_f} = 0 kg/cm^2	Final water content = 162%
c_u = 0.134 kg/cm^2	Initial dry density = 28.17 pcf

Load (kg)	Displacement (cm)	Pore pressure (kg/cm^2)	Axial strain	σ_1 (kg/cm^2)	σ_3 (kg/cm^2)
0.0000	0.0025	--	0.0000	0.0000	0.0000
1.8144	0.0813		0.0086	0.0800	
2.4494	0.1321		0.0141	0.1074	
2.9484	0.1829		0.0195	0.1286	
3.4474	0.2337		0.0249	0.1495	
3.8556	0.2896		0.0308	0.1662	
5.3525	0.5334		0.0567	0.2246	
6.2143	0.7849		0.0835	0.2534	
6.7586	1.0414		0.1108	0.2673	
6.8494	1.1430		0.1216	0.2676	
6.3504	1.2954		0.1378	0.2436	

σ_1 and σ_3 equal the major and minor total principal stresses, respectively.
Failure taken at maximum deviator stress or at 20 percent axial strain.

TABLE I-26. TRIAXIAL TEST DATA, SAMPLE C-3

Unconfined compression test

Angle between direction of compression and horizontal = 90 degrees

σ_{1_f} = 0.311 kg/cm^2 Initial water content = 157%

σ_{3_f} = 0 kg/cm^2 Final water content = 157%

c_u = 0.156 kg/cm^2 Initial dry density = 28.83 pcf

Load (kg)	Displacement (cm)	Pore pressure (kg/cm^2)	Axial strain	σ_1 (kg/cm^2)	σ_3 (kg/cm^2)
0.0000	0.0025	--	0.0000	0.0000	0.0000
1.2701	0.0813		0.0073	0.0709	
1.7464	0.1321		0.0119	0.0970	
2.1773	0.1829		0.0164	0.1203	
2.5402	0.2337		0.0210	0.1397	
2.9030	0.2896		0.0260	0.1589	
4.2638	0.5334		0.0479	0.2281	
5.1710	0.7849		0.0705	0.2701	
5.7154	1.0414		0.0935	0.2911	
6.1690	1.2954		0.1163	0.3064	
6.3504	1.4224		0.1277	0.3113	
6.3958	1.5494		0.1391	0.3094	
6.3050	1.6510		0.1482	0.3018	

σ_1 and σ_3 equal the major and minor total principal stresses, respectively. Failure taken at maximum deviator stress or at 20 percent axial strain.

TABLE I-27. TRIAXIAL TEST DATA, SAMPLE C-4

Unconfined compression test

Angle between direction of compression and horizontal = 90 degrees

σ_{1_f} = 0.204 kg/cm^2 Initial water content = 163%

σ_{3_f} = 0 kg/cm^2 Final water content = 163%

c_u = 0.102 kg/cm^2 Initial dry density = 27.64 pcf

Load (kg)	Displacement (cm)	Pore pressure (kg/cm^2)	Axial strain	σ_1 (kg/cm^2)	σ_3 (kg/cm^2)
0.0000	0.0025	--	0.0000	0.0000	0.0000
1.2247	0.0813		0.0069	0.0637	
1.6330	0.1321		0.0113	0.0846	
1.9505	0.1829		0.0156	0.1006	
2.1773	0.2337		0.0200	0.1118	
2.4494	0.2896		0.0247	0.1251	
3.4020	0.5334		0.0456	0.1701	
3.9917	0.7849		0.0670	0.1951	
4.2638	1.0414		0.0889	0.2035	
4.2185	0.1684		0.0998	0.1989	
3.9917	1.2954		0.1106	0.1860	

σ_1 and σ_3 equal the major and minor total principal stresses, respectively.
Failure taken at maximum deviator stress or at 20 percent axial strain.

TABLE I-28. TRIAXIAL TEST DATA, SAMPLE C-5

Unconfined compression test

Angle between direction of compression and horizontal = 0 degrees

σ_{1_f}	=	0.189 kg/cm^2	Initial water content	=	169%
σ_{3_f}	=	0 kg/cm^2	Final water content	=	169%
c_u	=	0.094 kg/cm^2	Initial dry density	=	27.73 pcf

Load (kg)	Displacement (cm)	Pore pressure (kg/cm^2)	Axial strain	σ_1 (kg/cm^2)	σ_3 (kg/cm^2)
0.0000	0.0025	--	0.0000	0.0000	0.0000
1.4969	0.0813		0.0079	0.0736	
1.9051	0.1321		0.0129	0.0932	
2.1773	0.1829		0.0178	0.1059	
2.4041	0.2337		0.0228	0.1164	
2.6309	0.2896		0.0282	0.1266	
3.4474	0.5334		0.0519	0.1619	
3.9463	0.7849		0.0764	0.1805	
4.2412	1.0414		0.1014	0.1888	
4.2638	1.1684		0.1138	0.1872	
4.1731	1.2954		0.1261	0.1806	

σ_1 and σ_3 equal the major and minor total principal stresses, respectively. Failure taken at maximum deviator stress or at 20 percent axial strain.

TABLE I-29. TRIAXIAL TEST DATA, SAMPLE C-6

Unconfined compression test

Angle between direction of compression and horizontal = 0 degrees

σ_{1_f} = 0.152 kg/cm^2 Initial water content = 169%

σ_{3_f} = 0 kg/cm^2 Final water content = 169%

c_u = 0.076 kg/cm^2 Initial dry density = 27.75 pcf

Load (kg)	Displacement (cm)	Pore pressure (kg/cm^2)	Axial strain	σ_1 (kg/cm^2)	σ_3 (kg/cm^2)
0.0000	0.0025	--	0.0000	0.0000	0.0000
0.9072	0.0813		0.0075	0.0483	
1.3608	0.1321		0.0122	0.0722	
1.5876	0.1829		0.0169	0.0838	
1.7690	0.2337		0.0216	0.0929	
1.9505	0.2896		0.0267	0.1019	
2.5402	0.5334		0.0493	0.1297	
2.9030	0.7849		0.0725	0.1446	
3.1298	1.0414		0.0962	0.1519	
3.1298	1.1684		0.1079	0.1499	
2.9030	1.2954		0.1196	0.1372	

σ_1 and σ_3 equal the major and minor total principal stresses, respectively. Failure taken at maximum deviator stress or at 20 percent axial strain.

TABLE I-30. TRIAXIAL TEST DATA, SAMPLE C-7

Unconfined compression test

Angle between direction of compression and horizontal = 45 degrees

σ_{1_f} = 0.208 kg/cm^2	Initial water content = 170%
σ_{3_f} = 0 kg/cm^2	Final water content = 170%
c_u = 0.104 kg/cm^2	Initial dry density = 28.35 pcf

Load (kg)	Displacement (cm)	Pore pressure (kg/cm^2)	Axial strain	σ_1 (kg/cm^2)	σ_3 (kg/cm^2)
0.0000	0.0025	--	0.0000	0.0000	0.0000
1.2701	0.0813		0.0069	0.0648	
1.6330	0.1321		0.0113	0.0829	
1.8824	0.1829		0.0156	0.0951	
2.1092	0.2337		0.0199	0.1061	
2.3360	0.2896		0.0247	0.1170	
3.0845	0.5334		0.0455	0.1512	
3.6515	0.7849		0.0669	0.1749	
3.9917	1.0414		0.0888	0.1867	
4.3546	1.2954		0.1104	0.1989	
4.6721	1.5494		0.1321	0.2082	
4.6948	1.6510		0.1408	0.2071	
4.4453	1.8034		0.1537	0.1931	

σ_1 and σ_3 equal the major and minor total principal stresses, respectively. Failure taken at maximum deviator stress or at 20 percent axial strain.

TABLE I-31. TRIAXIAL TEST DATA, SAMPLE C-8

Unconfined compression test

Angle between direction of compression and horizontal = 45 degrees

σ_{1_f}	= 0.249 kg/cm^2	Initial water content	= 169%
σ_{3_f}	= 0 kg/cm^2	Final water content	= 169%
c_u	= 0.124 kg/cm^2	Initial dry density	= 27.75 pcf

Load (kg)	Displacement (cm)	Pore pressure (kg/cm^2)	Axial strain	σ_1 (kg/cm^2)	σ_3 (kg/cm^2)
0.0000	0.0025	--	0.0000	0.0000	0.0000
0.7258	0.0813		0.0074	0.0374	
1.3608	0.1321		0.0120	0.0699	
1.8144	0.1829		0.0166	0.0927	
2.2000	0.2337		0.0212	0.1119	
2.5402	0.2896		0.0263	0.1285	
3.9917	0.5334		0.0485	0.1974	
4.8082	0.7849		0.0714	0.2320	
5.2618	1.0414		0.0947	0.2475	
5.3525	1.1684		0.1062	0.2486	
5.2618	1.2954		0.1178	0.2412	

σ_1 and σ_3 equal the major and minor total principal stresses, respectively. Failure taken at maximum deviator stress or at 20 percent axial strain.

TABLE I-32. TRIAXIAL TEST DATA, SAMPLE C-9

Unconfined compression test

Angle between direction of compression and horizontal = 90 degrees

σ_{1_f} = 0.265 kg/cm^2

σ_{3_f} = 0 kg/cm^2

c_u = 0.132 kg/cm^2

Initial water content = 178%

Final water content = 178%

Initial dry density = 25.72 pcf

Load (kg)	Displacement (cm)	Pore pressure (kg/cm^2)	Axial strain	σ_1 (kg/cm^2)	σ_3 (kg/cm^2)
0.0000	0.0025	--	0.0000	0.0000	0.0000
0.9072	0.0559		0.0056	0.0445	
1.5196	0.1118		0.0113	0.0741	
1.9732	0.1626		0.0164	0.0958	
2.3587	0.2134		0.0216	0.1139	
2.8123	0.2667		0.0269	0.1350	
3.6742	0.3988		0.0403	0.1740	
4.2638	0.5334		0.0539	0.1990	
4.8082	0.6604		0.0667	0.2214	
5.2618	0.7849		0.0793	0.2390	
5.8968	1.0363		0.1047	0.2605	
6.0782	1.1633		0.1175	0.2646	
6.1690	1.2903		0.1303	0.2647	
6.1690	1.3411		0.1355	0.2631	
5.5793	1.5519		0.1568	0.2321	
5.3525	1.6002		0.1616	0.2214	

σ_1 and σ_3 equal the major and minor total principal stresses, respectively.
Failure taken at maximum deviator stress or at 20 percent axial strain.

TABLE I-33. TRIAXIAL TEST DATA, SAMPLE C-10

Axial consolidation pressure = 0.7030 kg/cm^2 with K_o = 0.3

Undrained test with σ_1 constant and σ_3 decreasing.

Initial water content = 177.0%

Final water content = 150.0%

Initial dry density = 26.94 pcf

σ_1 (kg/cm^2)	σ_3 (kg/cm^2	pore pressure (kg/cm^2)	axial strain	$\bar{\sigma}_1$ (kg/cm^2)	$\bar{\sigma}_3$ (kg/cm^2)
3.5153	3.0232	2.8123	0.0000	0.703	0.2109
3.5153	2.9881	2.7982	0.0005	0.7171	0.1899
3.5153	2.9620	2.7912	0.0019	0.7241	0.1708
3.5153	2.9360	2.7877	0.0045	0.7276	0.1483
3.5153	2.9107	2.7912	0.0059	0.7241	0.1195
3.5153	2.8854	2.7912	0.0091	0.7241	0.0942
3.5153	2.8594	2.7912	0.0147	0.7241	0.0682
3.5153	2.8341	2.7771	0.0249	0.7382	0.0570
3.5153	2.8123	2.7560	0.0340	0.7593	0.0563
3.5153	2.8123	2.8123[a]	0.2591	0.7030	0.0000

---

[a] Pore pressure increased to initial backpressure.

Deformation rate approximately zero when test was terminated.

TABLE I-34. TRIAXIAL TEST DATA, SAMPLE C-11

Axial consolidation pressure = 0.9350 kg/cm^2 with K_o = 0.3

Undrained test with σ_1 constant and σ_3 decreasing.

Initial water content = 174.5%

Final water content = 133.5%

Initial dry density = 27.30 pcf

σ_1 (kg/cm^2)	σ_3 (kg/cm^2)	pore pressure (kg/cm^2)	axial strain	$\bar{\sigma}_1$ (kg/cm^2)	$\bar{\sigma}_3$ (kg/cm^2)
3.7474	3.0935	2.8123	0.0000	0.9351	0.2812
3.7474	3.0626	2.7982	0.0003	0.9490	0.2644
3.7474	3.0373	2.7912	0.0011	0.9561	0.2461
3.7474	3.0113	2.7631	0.0023	0.9631	0.2482
3.7474	2.9859	2.7560	0.0043	0.9701	0.2299
3.7474	2.9606	2.7490	0.0057	0.9772	0.2116
3.7474	2.9353	2.7476	0.0094	0.9997	0.1877
3.7474	2.9107	2.7279	0.0114	1.0193	0.1715
3.7474	2.8854	2.7139	0.0143	1.0334	0.1715
3.7474	2.8608	2.6998	0.0174	1.0475	0.1610
3.7474	2.8376	2.6963	0.0209	1.0509	0.1413
3.7474	2.8123	2.7174[a]	0.0437	1.0298	0.0949
3.7474	2.8123	2.8123[b]	0.0509	0.9351	0.000

[a] Small leak permitted dissipation of reduced pore pressure.

[b] Pore pressure increased to initial backpressure.

Deformation rate approximately zero when test was terminated.

TABLE I-35. TRIAXIAL TEST DATA, SAMPLE C-14

Axial consolidation pressure = 2.3430 kg/cm^2 with K_o = 0.3

Undrained test with σ_1 constant and σ_3 decreasing.

Initial water content = 174.3%

Final water content = 104.3%

Initial dry density = 27.26 pcf

σ_1 (kg/cm^2)	σ_3 (kg/cm^2)	pore pressure (kg/cm^2)	axial strain	$\bar{\sigma}_1$ (kg/cm^2)	$\bar{\sigma}_3$ (kg/cm^2)
5.1553	3.5153	2.8123	0.0000	2.343	0.703
5.1553	3.4873	2.8113	0.0004	2.344	0.676
5.1553	3.4313	2.7983	0.0007	2.357	0.633
5.1553	3.3743	2.7843	0.0012	2.371	0.590
5.1553	3.3253	2.7633	0.0014	2.392	0.562
5.1553	3.2763	2.7353	0.0018	2.420	0.541
5.1553	3.2203	2.7173	0.0025	2.438	0.503
5.1553	3.1633	2.6793	0.0032	2.476	0.484
5.1553	3.1143	2.6643	0.0035	2.491	0.450
5.1553	3.0583	2.6433	0.0046	2.512	0.415
5.1553	3.0093	2.6123	0.0053	2.543	0.397
5.1553	2.9603	2.6013	0.0065	2.554	0.359
5.1553	2.9033	2.5733	0.0081	2.582	0.330
5.1553	2.8543	2.5483	0.0098	2.607	0.306
5.1553	2.8123	2.5313	0.0109	2.624	0.281
5.1553	2.8123	2.8123[a]	0.1193	2.343	0.0000

[a] Pore pressure increased to initial backpressure.

Deformation rate approximately zero when test was terminated.

TABLE J-1. AVERAGE DAILY TEMPERATURE AND PRECIPITATION

Date	Average temp. (°F)	Pre-cipitation (in.)	Date	Average temp. (°F)	Pre-cipitation (in.)	Date	Average temp. (°F)	Pre-cipitation (in.)
September 1971			October 1971			November 1971		
1	73	0	1	76	0	1	59	0
2	73	.25	2	74	0	2	59	.16
3	72	1.24	3	75	0	3	49	T
4	76	T	4	69	0	4	40	0
5	77	0	5	63	T	5	49	0
6	75	.80	6	61	T	6	43	.22
7	75	0	7	51	0	7	26	0
8	75	0	8	54	T	8	28	0
9	75	0	9	56	.67	9	34	.06
10	75	0	10	48	.03	10	38	0
11	67	.05	11	57	0	11	41	0
12	66	0	12	53	0	12	47	0
13	63	0	13	62	.32	13	52	0
14	64	0	14	58	0	14	57	0
15	67	.02	15	65	0	15	63	0
16	63	T	16	65	.60	16	52	0
17	63	0	17	65	0	17	57	0
18	63	0	18	66	0	18	61	T
19	65	T	19	64	0	19	51	.41
20	58	.97	20	68	0	20	43	T
21	55	0	21	65	.10	21	36	T
22	60	0	22	66	.14	22	29	0
23	62	0	23	65	.10	23	26	.01
24	57	0	24	64	.21	24	31	.02
25	57	.36	25	64	0	25	34	0
26	68	.09	26	63	0	26	34	.05
27	75	0	27	65	0	27	41	.23
28	78	0	28	63	0	28	35	0
29	79	0	29	65	0	29	41	.36
30	77	0	30	65	0	30	33	.03
			31	62	0			

Source: Local climatological data from Dayton, Ohio, municipal airport
T = trace of precipitation.

TABLE J-1. AVERAGE DAILY TEMPERATURE AND PRECIPITATION (continued)

Date	Average temp. (°F)	Pre-cipitation (in.)	Date	Average temp. (°F)	Pre-cipitation (in.)	Date	Average temp. (°F)	Pre-cipitation (in.)
December 1971			January 1972			February 1972		
1	28	0	1	36	.01	1	27	0
2	28	0	2	35	.19	2	34	.01
3	26	0	3	35	0	3	26	.19
4	33	0	4	31	.38	4	9	.03
5	41	.13	5	17	.05	5	15	0
6	50	.69	6	18	0	6	25	.25
7	47	.39	7	28	0	7	9	T
8	45	0	8	28	0	8	7	T
9	48	T	9	42	.21	9	11	.04
10	59	.05	10	43	T	10	14	0
11	42	0	11	36	0	11	29	T
12	40	0	12	37	0	12	37	.03
13	36	0	13	35	.16	13	35	.08
14	43	.86	14	12	0	14	37	0
15	55	.21	15	- 6	0	15	38	.03
16	43	0	16	- 1	0	16	32	0
17	27	.04	17	27	0	17	37	.01
18	19	T	18	43	.07	18	31	.09
19	31	.18	19	41	.01	19	23	.03
20	38	.05	20	44	.01	20	22	0
21	35	0	21	35	0	21	40	0
22	30	0	22	47	.19	22	27	T
23	37	0	23	39	.07	23	29	.04
24	40	0	24	47	.02	24	34	0
25	41	.01	25	24	0	25	34	.01
26	52	.05	26	21	0	26	31	.01
27	54	.07	27	17	.10	27	33	0
28	35	.03	28	12	T	28	48	0
29	29	.04	29	11	0	29	53	0
30	47	1.00	30	11	0			
31	30	0	31	15	0			

Source: Local climatological data from Dayton, Ohio, municipal airport.
T = trace of precipitation.

TABLE J-1. AVERAGE DAILY TEMPERATURE AND PRECIPITATION (continued)

Date	Average temp. (°F)	Pre-cipitation (in.)	Date	Average temp. (°F)	Pre-cipitation (in.)	Date	Average temp. (°F)	Pre-cipitation (in.)
June 1972			July 1972			August 1972		
1	57	0	1	76	0	1	72	0
2	70	0	2	75	.01	2	76	.37
3	73	.03	3	68	.41	3	74	.04
4	78	0	4	62	.04	4	67	T
5	71	0	5	61	.02	5	63	0
6	70	.20	6	59	0	6	63	.06
7	67	0	7	63	0	7	66	.04
8	69	0	8	70	.04	8	65	.25
9	74	.23	9	74	0	9	63	0
10	57	0	10	77	T	10	65	0
11	56	0	11	80	.34	11	67	0
12	67	T	12	79	0	12	75	.12
13	71	1.67	13	79	0	13	75	0
14	79	T	14	82	0	14	76	.02
15	71	.43	15	76	.67	15	71	0
16	69	0	16	75	.03	16	72	0
17	64	0	17	76	0	17	82	0
18	69	0	18	82	.36	18	85	0
19	76	0	19	81	0	19	77	.36
20	72	T	20	84	0	20	75	0
21	62	T	21	86	0	21	75	0
22	55	T	22	85	0	22	77	.90
23	52	.17	23	84	T	23	79	.39
24	53	T	24	78	.16	24	77	.21
25	62	0	25	76	0	25	77	0
26	68	0	26	70	0	26	75	.32
27	71	0	27	76	0	27	68	.05
28	71	T	28	72	0	28	72	0
29	69	.31	29	70	0	29	72	0
30	70	T	30	71	0	30	73	0
			31	77	0	31	72	0

Source: Local climatological data from Dayton, Ohio, municipal airport.
T = trace of precipitation.

TABLE J-1. AVERAGE DAILY TEMPERATURE AND PRECIPITATION (continued)

Date	Average temp. (°F)	Pre-cipitation (in.)	Date	Average temp. (°F)	Pre-cipitation (in.)	Date	Average temp. (°F)	Pre-cipitation (in.)
March 1972			April 1972			May 1972		
1	58	.55	1	36	.01	1	66	.04
2	40	.41	2	35	.02	2	66	0
3	23	T	3	37	.17	3	55	0
4	29	.02	4	41	.08	4	53	T
5	20	T	5	46	0	5	56	0
6	26	0	6	57	.22	6	68	0
7	43	.09	7	33	.87	7	69	.22
8	24	T	8	23	T	8	55	1.05
9	23	0	9	34	0	9	49	.21
10	23	0	10	48	T	10	48	0
11	46	0	11	58	.01	11	55	0
12	56	0	12	60	.30	12	61	0
13	50	.35	13	67	.04	13	60	.85
14	34	T	14	58	0	14	66	.46
15	37	.04	15	67	.03	15	60	.34
16	45	.42	16	60	.80	16	58	.02
17	39	.06	17	56	0	17	62	0
18	32	0	18	60	0	18	65	0
19	35	0	19	64	.26	19	67	0
20	48	0	20	55	.22	20	66	T
21	58	.38	21	49	.43	21	67	0
22	42	.09	22	57	T	22	70	0
23	27	T	23	54	.09	23	71	0
24	27	T	24	47	0	24	70	0
25	29	0	25	41	0	25	71	0
26	33	T	26	47	0	26	66	0
27	41	T	27	50	0	27	65	0
28	39	0	28	53	0	28	66	0
29	39	.05	29	61	.10	29	68	.03
30	38	T	30	62	.12	30	60	1.10
31	40	0				31	48	.02

Source: Local climatological data from Dayton, Ohio, municipal airport.
T = trace of precipitation.

TABLE J-1. AVERAGE DAILY TEMPERATURE AND PRECIPITATION (continued)

Date	Average temp. (°F)	Pre-cipitation (in.)	Date	Average temp. (°F)	Pre-cipitation (in.)	Date	Average temp. (°F)	Pre-cipitation (in.)
September 1972			October 1972			November 1972		
1	77	T	1	50	0	1	57	.67
2	69	0	2	60	0	2	60	.90
3	60	.88	3	64	0	3	48	0
4	65	0	4	59	.86	4	44	T
5	64	T	5	62	.15	5	45	0
6	65	0	6	60	0	6	49	0
7	70	0	7	53	.02	7	51	1.10
8	69	T	8	57	0	8	41	.01
9	62	0	9	49	0	9	41	0
10	61	0	10	50	0	10	44	.18
11	71	.05	11	56	.09	11	45	.01
12	76	.99	12	59	.15	12	42	0
13	79	0	13	52	0	13	41	1.06
14	67	.26	14	52	0	14	36	.31
15	66	0	15	44	0	15	31	T
16	65	0	16	49	T	16	34	0
17	76	0	17	45	0	17	31	0
18	71	.55	18	35	.08	18	38	0
19	68	0	19	37	0	19	36	.40
20	66	0	20	40	0	20	35	T
21	65	.10	21	47	T	21	32	T
22	57	0	22	59	.06	22	34	.04
23	57	.22	23	58	.15	23	30	T
24	68	.48	24	44	.03	24	32	0
25	71	.22	25	41	0	25	34	.13
26	70	.24	26	46	0	26	34	.07
27	62	.06	27	51	.11	27	38	.10
28	62	T	28	56	.09	28	31	.02
29	57	.34	29	48	.02	29	31	0
30	45	.25	30	45	0	30	34	T
			31	44	.41			

Source: Local climatological data from Dayton, Ohio, municipal airport.
T = trace of precipitation.

TABLE J-1. AVERAGE DAILY TEMPERATURE AND PRECIPITATION (continued)

Date	Average temp. (^{o}F)	Pre-cipitation (in.)	Date	Average temp. (^{o}F)	Pre-cipitation (in.)	Date	Average temp. (^{o}F)	Pre-cipitation (in.)
December 1972			January 1973			February 1973		
1	39	T	1	31	0	1	47	.22
2	44	0	2	29	0	2	46	.09
3	40	T	3	37	.53	3	35	T
4	36	.01	4	34	T	4	43	0
5	48	T	5	23	T	5	46	T
6	40	.51	6	21	T	6	45	0
7	18	T	7	22	0	7	36	.05
8	33	.76	8	19	0	8	25	.20
9	33	.01	9	16	T	9	18	0
10	24	T	10	12	0	10	17	T
11	19	.05	11	14	T	11	19	0
12	44	.22	12	19	0	12	26	0
13	30	.04	13	28	0	13	34	.02
14	27	0	14	35	.18	14	38	.40
15	21	.35	15	34	T	15	28	.13
16	7	.02	16	41	0	16	9	T
17	10	0	17	50	0	17	11	0
18	28	0	18	53	.01	18	23	0
19	39	.31	19	42	.04	19	38	0
20	40	.02	20	29	0	20	35	.02
21	39	0	21	34	.28	21	29	.02
22	36	T	22	45	.10	22	24	T
23	38	0	23	32	T	23	29	T
24	39	0	24	34	0	24	35	0
25	35	0	25	42	0	25	42	T
26	33	.09	26	43	.07	26	35	.13
27	30	0	27	43	.07	27	31	0
28	33	0	28	35	.33	28	35	0
29	42	T	29	21	.02			
30	57	.13	30	25	0			
31	46	.29	31	34	0			

Source: Local climatological data from Dayton, Ohio, municipal airport.
T = trace of precipitation.

TABLE J-1. AVERAGE DAILY TEMPERATURE AND PRECIPITATION (continued)

Date	Average temp. (°F)	Pre-cipitation (in.)	Date	Average temp. (°F)	Pre-cipitation (in.)	Date	Average temp. (°F)	Pre-cipitation (in.)
March 1973			April 1973			May 1973		
1	49	0	1	53	.05	1	66	.03
2	52	.04	2	45	T	2	60	.27
3	53	.02	3	43	T	3	48	.02
4	55	.06	4	38	.70	4	48	T
5	60	.10	5	40	T	5	49	0
6	59	0	6	50	0	6	55	0
7	56	.19	7	49	.20	7	60	.03
8	52	0	8	46	.06	8	67	1.11
9	43	.18	9	44	.30	9	67	.01
10	62	.07	10	34	.06	10	67	T
11	62	.79	11	34	T	11	62	0
12	47	.01	12	38	.16	12	56	.01
13	54	0	13	38	0	13	51	T
14	64	.55	14	42	0	14	50	.05
15	63	0	15	55	0	15	46	0
16	48	.65	16	56	.32	16	55	.02
17	34	.39	17	51	.22	17	46	T
18	33	0	18	62	.23	18	52	T
19	34	0	19	65	.10	19	58	.68
20	33	0	20	71	T	20	59	T
21	33	0	21	72	0	21	61	0
22	33	0	22	67	.01	22	68	.02
23	36	0	23	58	.33	23	69	T
24	47	0	24	59	0	24	62	0
25	51	.80	25	50	T	25	66	.25
26	44	.19	26	52	0	26	63	.24
27	44	0	27	47	.56	27	66	.27
28	48	T	28	47	0	28	67	.02
29	56	.41	29	52	T	29	65	.07
30	53	T	30	63	.15	30	61	T
31	55	.19				31	59	0

Source: Local climatological data from Dayton, Ohio, municipal airport.
T = trace of precipitation.

APPENDIX K

COMPUTER PROGRAM FOR THE SOLUTION TO THE EQUATIONS IN THE THEORY OF GIBSON AND LO (1961)

```
       PROGRAM GIBSON (INPUT. OUTPUT)
       REAL LAMI
       DIMENSION S (90)
C
C      I = NO. OF TIMES DESIRED FOR SETTLEMENT COMPUTATION.
C      Q0 = APPLIED LOAD (PSI)
C      A = PRIMARY COMPRESSIBILITY (SQ. IN . /LB. )
C      B = SECONDARY COMPRESSIBILITY (SQ.  IN. /LB. )
C      LAM1 = VISCOSITY ( LB. /SQ. IN. /MIN. )
C      H1 = LAYER THICKNESS (IN. )
C      CV = COEFFICIENT OF CONSOLIDATION (SQ. IN. /MIN. )
C      T = TIME (HOURS)
C
C      READ PRIMARY DATA
C
       READ 3,I,Q0,A,B,LAM1,H1,CV
     3 FORMAT   (I5. 6F10. 0)
       L =0
       J = 0
       S(0) = 0. 0
    50 CONTINUE
       M = 0
       IF(J. EQ. 1) GO TO 40
       H=H1/2. 0
       H=H-S (J)/2. 0
C
C      READ TIME FOR SETTLEMENT COMPUTATION
C
       READ 4. T
     4 FORMAT (F10. 0)
       J = J+1
       XM=1. 0+R/A
       XN=(H**2)/(B*CV*LAM1 )
       T1=T*60.
       ULTS=(A+B)*Q0*H1
C
C      CALCULATE SETTLEMENT AT TIME = T
C
       SUM=0. 0
       D0 20 N=1. 25. 2
       YN=N
       XK1=(N**2*3. 1416**2*CV)/(4. 0*H**2)
       ALPHA=(1. 0/A+1. 0/B)/LAM1
       BETA=1. 0 /(LAM1 *B)
       XT1=((ALPHA+XK1)**2-(4. 0*BETA*XR1))
       T2=SQRT (XI1)
       R1=ALPHA+XK1
```

```
      X11=(R1+T2)/2.0
      X22=(R1-T2)/2.0
      V3=-1.0*X11*T1
      V4=-1.0*X22*T1
      V5=EXP(V3)
      V6=EXP(V4)
      XK2=A/(A+B)*XK1
      E=XK2-X11)/(X11-X22)
      E1=E*V6
      E2=(XK2-X22)/(X11-X22)
      E3=E2*V5
      G=(E1-E3)/YN**2
      SUM=SUM+G
   20 CONTINUE
      R=1.0+((8.0/3.1416**2)*SUM)
      S(J)=ULTS*R
      XT=4.0/3.1416*((A+B)/A)*Q0
      Z=H/4.0
   18 CONTINUE
C
C     CALCULATE PORE PRESSURES AT TIME = T
C
      SUM1=0.0
      DO 22 N=1.51.2
      ZN=N
      XK1=(N**2*3.1416**2*CV)/(4.0*H**2)
      ALPHA=(1.0/A+1.0/B)/LAM1
      BETA=1.0/(LAM1*B)
      XT1=((ALPHA+XK1)**2-(4.0*BETA*XK1))
      T2=SQRT(XT1)
      R1=ALPHA+XK1
      X11=(R1+T2)/2.0
      X22=(R1-T2)/2.0
      V1=A/(A+B)-X22/XR1
      V2=A/(A+B)-X11/XK1
      V3=-1.0*X11*T1
      V4=-1.0*X22*T1
      V5=EXP(V3)
      V6=EXP(V4)
      W1=(X11*V1)/(X11-X22)*V5
      W2=(X22*V2)/(X11-X22)*V6
      W3=(N*3.1416*7)/(2.*H)
      W4=SIN(W3)
      Y=(W1-W2)*W4
      Y1=Y/ZN
      SUM1=SUM1+Y1
   22 CONTINUE
      U=X1*SUM1
      L=L+1
      IF(L.GT.1)GO TO 7
```

```
 6   PRINT 80
80   FORMAT(*1*,*TIME (HOURS)*. 10X,*SETTLEMENT (INCHES)*,
     10X,*DEPTH (IN 1. )*,10X,*PORE PRESSURE (PSI)*,10X,*SUM*,
     10X,*SUM1*)
 7   PZ=H/4. 0
     IF(Z. EQ. PZ)8. 10
 8   PRINT 90,T,S(J), Z, U,SUM,SUM1
90   FORMAT (*0*,3X. F6. 0,16X,F10. 2,14X,F10. 1,13X. F10. 2,13X,
     F10. 4. 6X,F10.14)
 9   IF(Z. EQ. PZ)GO TO 11
10   PRINT 91,Z, U
91   FORMAT(*0*,48X,F10. 1. 13X,F10. 2)
11   M=M+1
     IF(M. EQ. 4) GO TO 50
     Z=Z+H/4. 0
     GO TO 18
40   CONTINUE
     END
```